UNIVERSITY OF SOUTHAMPTON
FACULTY OF PHYSICAL SCIENCES AND ENGINEERING
SCHOOL OF ELECTRONICS AND COMPUTER SCIENCE

Noncoherent Successive Relaying for Multi-User Wireless Systems

by

Li Li
B. Eng., M.Sc.

A doctoral thesis submitted in partial fulfilment of the
requirements for the award of Doctor of Philosophy
at the University of Southampton

May 2013

SUPERVISOR:
Professor Lajos Hanzo
FREng, FIEEE, FIEE, DSc, EIC of IEEE Press
Chair of Communications, Signal Processing and Control Group
School of Electronics and Computer Science
University of Southampton
Southampton SO17 1BJ
United Kingdom

Dedicated to my family

UNIVERSITY OF SOUTHAMPTON

ABSTRACT

FACULTY OF PHYSICAL SCIENCES AND ENGINEERING
SCHOOL OF ELECTRONICS AND COMPUTER SCIENCE

Doctor of Philosophy

Noncoherent Successive Relaying for Multi-User Wireless Systems

by Li Li

A noncoherent detection based successive relaying aided network (SRAN) is proposed and investigated in the context of a multi-user, multi-relay assisted scenario. The potentially excessive complexity of multiple-antenna based power-hungry channel estimation is avoided by replacing the classic coherent detection by multiple-symbol-based noncoherent detection. Then, as the benefit of forming a virtual antenna array (VAA) in a distributed fashion, the proposed cooperative network becomes capable of achieving a substantial spatial diversity gain in the uplink. Furthermore, the 50% throughput loss incurred by the conventional single relay-aided two-phase cooperative network, which is caused by the half-duplex transmit/receive constraint of practical transceivers is recovered by designing a spectral efficient successive relaying protocol. Hence the proposed noncoherent successive relaying aided multi-user wireless system becomes capable of significantly improving the system's performance.

We demonstrate that multiple-symbol differential detection (MSDD) is capable of eliminating the error floor of the conventional differential detection (CDD), when experiencing severely time-selective Rayleigh fading associated with a high Doppler frequency, since the MSDD algorithm benefits from a higher time-diversity than CDD. However, this is achieved at a potentially excessive complexity, which is unaffordable in many practical applications. As a remedy, the sphere decoding principle is incorporated into the MSDD algorithm. The resultant multiple-symbol differential sphere detection (MSDSD) strikes an attractive trade-off between the achievable BER performance and the complexity imposed. In order to improve the energy-efficiency, the hard-decision-based MSDSD algorithm is further developed to its soft-decision-based version, namely to the soft-input soft-output MSDSD (SISO-MSDSD). Furthermore, for the sake of exploiting the benefits of cooperative communications, we devise a new multiple-path propagation-aided MSDSD algorithm as a beneficial variant of the conventional MSDSD algorithm, which is further developed to the relay-aided MSDSD algorithm.

However, relay-assisted transmissions increase the amount of interference imposed. Hence, in order to suppress the successive relaying induced interference, namely both the inter-relay interference (IRI) and the co-channel interference (CCI), we invoke the DS-CDMA multiple access technique. Consequently, a noncoherent successive relaying (NC-SR) aided cooperative DS-CDMA uplink is conceived, where the typical 50% half-duplex relaying induced throughput loss is con-

verted to a potential user-load reduction for the DS-CDMA system, since the SRAN requires two - rather than a single - spreading codes for each user. First, the AF protocol is invoked for the successive AF relaying aided DS-CDMA uplink, where initially a simple single-user scenario and then a realistic multi-user scenario are investigated. The evaluation of the associated noncoherent discrete-input continuous-output memoryless channel (DCMC) capacity indicates that our AF based SRAN is capable of significantly outperforming both the conventional AF relaying and the single-link direct-transmission. Then, as a counterpart, the successive DF relaying aided DS-CDMA uplink is also conceived, where a multi-user scenario is considered. The noncoherent DCMC capacity of the DF based SRAN reveals that the DF based SRAN may outperform the AF based SRAN, especially in the low SNR region. Furthermore, a relay-aided SISO-MSDSD assisted three-stage iterative transceiver is designed for supporting the operation of the proposed DF based SRAN, which is capable of operating close to the system's capacity, while halving the system complexity imposed by the conventional single-path SISO-MSDSD aided distributed turbo decoder.

As a further advance, we also consider a multi-user multi-relay DS-CDMA uplink. In order to efficiently organize the cooperation among the multiple nodes of this large-scale wireless network, we further develop the concept of adaptive network coded cooperation (ANCC) to its generalized version, namely to our "GANC" regime, which allows arbitrary channel coding schemes to serve as the cross-layer network coding, while still adapting to both network topology changes and to link failures. Upon incorporating the proposed GANC regime into the SRAN, we construct the GANC aided SRAN. In the spirit of the joint network-channel coding (JNCC) scheme, we devise a generalized iterative detection based three-stage transceiver architecture for the proposed GANC aided SRAN. The proposed transceiver is also adaptive to both network topology changes as well as to link failures. We demonstrate that combining two DF based SRANs and operating them under the proposed GANC regime is capable of attaining a significant power gain with respect to operating them independently, i.e. without any cooperative between them.

Employing the DS-CDMA technique for suppressing the successive relaying-induced interference may lead to a potential user-load reduction for the DS-CDMA system. In order to mitigate the interference without requiring any extra orthogonal channel resources, we proposed a new multiple-symbol differential interference suppression (MS-DIS) regime, which is a novel amalgam of the adaptive modified Newton algorithm and of our SISO-MSDSD algorithm. Consequently, a MS-DIS-assisted plus relay-aided SISO-MSDSD based three-stage concatenated turbo transceiver is designed, which is capable of efficiently suppressing the interference at the expense of imposing as little as 2% training overhead, despite experiencing severely time-selective Rayleigh fading associated with a high Doppler frequency.

Declaration of Authorship

I, **Li Li**, declare that the thesis entitled **Noncoherent Successive Relaying for Multi-User Wireless Systems** and the work presented in it are my own and has been generated by me as the result of my own original research. I confirm that:

- This work was done wholly or mainly while in candidature for a research degree at this University;
- Where any part of this thesis has previously been submitted for a degree or any other qualification at this University or any other institution, this has been clearly stated;
- Where I have consulted the published work of others, this is always clearly attributed;
- Where I have quoted from the work of others, the source is always given. With the exception of such quotations, this thesis is entirely my own work;
- I have acknowledged all main sources of help;
- Where the thesis is based on work done by myself jointly with others, I have made clear exactly what was done by others and what I have contributed myself;
- Parts of this work have been published.

Signed: ..... Date: .....

Acknowledgements

Firstly, I would like to thank my supervisor Professor Lajos Hanzo for his generous support and insightful guidance and for his wise advice that allowed this work to become reality. His guidance and encouragement have greatly benefited me and I really appreciate his invaluable friendship.

I would also like to thank all my teachers and colleagues for their supports and helps. Special thanks to Dr. Li Wang for his kindly and helpful advice on my work. It is so grateful to cooperative with Kent TK Cheung and Mohammad Ismat Kadir. Thank you both for sharing your precious knowledges with me.

Finally, My sincere thanks to my parents and my wife Wei Zheng for their endless love, support and understanding.

List of Publications

1. **L. Li and L. Hanzo**, "Multiple-Symbol Differential Sphere Detection Aided Successive Relaying in the Cooperative DS-CDMA Uplink", *in Proceedings of IEEE Wireless Communications and Networking Conference (WCNC)*, Cancun, Quintana Roo, Mexico, pp. 1875-1880, March 2011.

2. **K. Cheung, L. Li, and L. Hanzo**, "On-Demand Decode and Forward Cooperative MAC for VoIP in Wireless Mesh Networks", *in Proceedings of IEEE Vehicular Technology Conference (VTC) 2011-Fall*, San Francisco, United States, pp. 1-5, September 2011.

3. **L. Li, L. Wang, and L. Hanzo**, "The Capacity of Successive DF Relaying and Using Soft Multiple-Symbol Differential Sphere Detection", *in Proceedings of IEEE Global Telecommunications Conference (GLOBECOM)*, Houston, Texas, USA, pp. 1-5, December 2011.

4. **L. Li, L. Wang, and L. Hanzo**, "Capacity Analysis of the Successive AF Relaying Aided Cooperative DS-CDMA Uplink", *in Proceedings of IEEE Wireless Communications and Networking Conference (WCNC)*, Paris, France, pp. 3057-3062, April 2012, .

5. **L. Li, L. Wang, and L. Hanzo**, "Successive DF Relaying: MS-DIS aided Interference Suppression and Three-Stage Concatenated Architecture Design", *in Proceedings of IEEE International Conference on Communications (ICC)*, Ottawa, Canada, pp. 5958-5962, June 2012.

6. **L. Li, L. Wang, and L. Hanzo**, "Differential Interference Suppression Aided Three-Stage Concatenated Successive Relaying", *IEEE Transactions on Communications*, vol. 60, pp. 2146-2155, Aug. 2012.

7. **L. Li, L. Wang, and L. Hanzo**, "Successive AF/DF Relaying in the Cooperative DS-CDMA Uplink: Capacity Analysis and Its System Architecture", *IEEE Transactions on Vehicular Technology*, vol. 62, pp. 655-666, Feb. 2013.

8. **L. Li, L. Wang, and L. Hanzo**, "Generalized Adaptive Network Coding Aided Successive Relaying for Noncoherent Cooperation", *IEEE Transactions on Communications*, vol. 61, pp. 1750-1763, May 2013.

9. **M. I. Kadir, L. Li, S. Chen, and L. Hanzo**, "Successive Decode-and-Forward Relaying Aided Coherent versus Non-coherent Cooperative Multi-carrier Space-Time Shift Keying", *IEEE Transactions on Vehicular Technology*, vol. 62, pp. 2544-2557, July 2013.

10. **L. Wang, L. Li, C. Xu, D. D. Liang, S. X. Ng, and L. Hanzo**, "Multiple-Symbol Joint Signal Processing for Differentially Encoded Single- and Multi-Carrier Communications: Principles, Designs and Applications", *IEEE Communications Surveys & Tutorials, (In Press)*.

Contents

List of Symbols

General Conventions

- The superscript * indicates complex conjugation. Hence, X^* represents the complex conjugate of the variable X.
- The superscript ^{T} indicates transpose operation. Hence, $\mathbf{X}^T$ represents the transpose of the matrix $\mathbf{X}$.
- The superscript ^{H} indicates complex conjugate transpose operation. Hence, $\mathbf{X}^H$ represents the hermitian of the matrix $\mathbf{X}$.
- The over line of $\overline{\mathbf{X}}$ or under line of $\underline{\mathbf{X}}$ are used to indicate that the vector or matrix $\mathbf{X}$ is constituted by amalgamating multi other vectors or matrices.
- Boldface characters are used to represent the vectors and matrices.
- A physical object will be frequently represented in the form of $X_{ij}^{l}[k]$, where the superscript l and index k are time domain indices, indicating the k^{th} symbol duration of the l^{th} frame. Furthermore, the subscripts i and j represent the network nodes and imply that X is associated with them.

Mathematical Operators and Functions

$\Pr(\cdot)$	The probability density function.
$\exp(\cdot)$	The exponential operation.
$\prod$	The product operation.
$\lvert\cdot\rvert$	The absolute value of a variable.
$\lVert\cdot\rVert$	The Euclidean $\mathtt{l}_2$ norm.
$\sum$	The sum operation.

$\mathrm{diag}(\cdot)$	The diagonalizing operation.
$\mathcal{E}\{\cdot\}$	The expectation of argument.
$J_0(\cdot)$	The zero order Bessel function of first kind.
$[\cdot]_{N\times M}$	The matrix having N rows and M columns.
$\triangleq$	Defines a quantity.
$\otimes$	The Kronecker product.
$\varphi_{ab}(\kappa)$	The autocorrelation function of the fading coefficients of the channel between node a and b.
Var$[\cdot]$	The variance of a variable.
$\mathrm{mod}[\cdot]$	Modulo operation.
$\det(\cdot)$	The determinant operation.
$\mathrm{tr}(\mathbf{A})$	The trace of a square matrix $\mathbf{A}$.
$I(\mathbf{a};\mathbf{b})$	Mutual information between $\mathbf{a}$ and $\mathbf{b}$.
$H(\mathbf{a}\|\mathbf{b})$	Entropy of $\mathbf{a}$ conditioned on $\mathbf{b}$.
$H(\mathbf{a})$	Entropy of $\mathbf{a}$.
$\ln(\cdot)$	Natural logarithm.
$\log_2(\cdot)$	Logarithm to base 2.
$\min(\cdot)$	The minimum value among a number of variables.
$\max(\cdot)$	The maximum value among a number of variables.
$L(\cdot)$	*A posteriori* LLR of an information bit.
$E(\cdot)$	*Extrinsic* information.
$A(\cdot)$	*A priori* information.
$T_d(\cdot)$	The transformation operator for transforming a vector to a matrix.
$T_c(\cdot)$	The transformation operator for transforming a matrix to a vector.

Specific Symbols

s_n	n^{th} source nod.
r_i	i^{th} relay node.
L	Frame length in terms of number of symbols.
M_c	Constellation size of a PSK modulation.
$\mathcal{M}_c$	Constellation of a M_c-ary PSK modulation.
χ	A set of specific signals.
$\mathbf{C}_a$	User-specific pseudo-noise spreading sequence employed by user a (or node a).
$c_a[q]$	q^{th} chip-waveform of $\mathbf{C}_a$.
$\mathbf{c}_a$	Spread signal vector consisting of a number of signal chips and transmitted by node a.
Q	The spreading factor of a PN sequence.
P_a	Average transmit power of the node a.
$f_{AM_{r_i}}$	Amplification factor of the RN r_i.
σ_{ab}^2	Variance of the channel's complex envelop.
N_0	Variance of an AWGN noise.
u	Index of user.
U	Number of total users.
h_{ab}	Channel impulse response of the channel between the node a and node b.
$\mathbf{h}_{ab}$	CIR vector consisting of a number of h_{ab}.
h_u	Channel impulse response of the channel between the u^{th} user and DN d.
$\mathbf{H}_u$	CIR vector consisting of a number of h_u.
$\mathbf{H}_{abc}$	Equivalent CIR vector whose element is the product of h_{ab} and h_{bc}.
n_a	AWGN imposed on the node a.
$\mathbf{n}_a$	Spread AWGN vector consisting of a number of AWGN chips.
n'_a	Amplified and faded AWGN, which is originally imposed on the node a.
$\tilde{n}_a$	Amplified and faded AWGN, which is originally imposed on the node a.

N_{total}	Accumulated noise component.
I_a	Interference imposed by the transmission of node a.
I_{ab}	Interference imposed by node a on node b.
$\mathcal{I}_{ab}$	Spread interference imposed by node a on node b.
$\tilde{I}_{ab}$	Despread interference imposed by node a on node b.
M	Number of interfering users.
S	M_c-ary DPSK symbol
$\tilde{S}$	Estimation of S.
$\mathbf{S}$	Symbol vector consisting of a number of M_c-ary DPSK symbols.
$\mathbf{S}'$	Estimation of $\mathbf{S}$.
V	M_c-ary PSK information symbol.
$\mathbf{V}$	Symbol vector consisting of a number of M_c-ary PSK information symbols.
$R_{r_i d}$	Signal transmitted by the RN r_i and towards the DN d.
y_a	Signal received at node a.
y_{ab}	Signal transmitted by node a and received at node b.
$\mathbf{y}$	Signal vector consisting of a number of received signal chips.
$\mathbf{y}^A$	Signal vector $\mathbf{y}$ received in the "A" type frames.
z_a	Despread signal whose main component is received from the node a.
z_a^A	Despread signal z_a received in the "A" type frames.
$\mathbf{Z}_a$	Despread signal vector consisting of a number of z_a.
$\mathbf{I}_N$	N-dimensional identity matrix.
$\mathbf{\Phi}_{\mathbf{Z}_u\mathbf{Z}_u}$	Correlation matrix of the signal vector $\mathbf{Z}_u$.
$\mathbf{F}$	Upper triangular matrix.
$\mathbf{U}_{i,j}$	Element of a matrix $\mathbf{U}$ located in row i and column j.
$\mathbf{W}$	Equivalent noise vector, whose element takes multi noises or/and interferences into account.
N	Observation window size of a multiple-symbol joint detection algorithm.

N_{wind}	Observation window size of a multiple-symbol joint detection algorithm.
N_T	Number of transmit antennas.
N_R	Number of receive antennas.
f_d	Normalized Doppler frequency.
G_{ab}	Average path-loss reduction gain of the link from node a to node b.
α	Path-loss exponent.
D_{ab}	Straight distance between node a and node b.
γ_{ab}	Cross-correlation value of the pair of PN sequences $\mathbf{C}_a$ and $\mathbf{C}_b$.
$\bar{i}$	Complement of i.
T	Time length in terms of symbol durations.
T_b	Correlated block-fading period in terms of symbol durations.
C^{AF}	Capacity of an AF relaying aided cooperative network.
C^{DF}	Capacity of a DF relaying aided cooperative network.
$\mathbf{\Psi}$	Conditional covariance matrix.
β	Ratio of source-transmission duration to relay-transmission duration.
θ	Ratio of the SR distance to the RD distance.
λ	Ratio of the MAI imposed on RN to that imposed on DN.
$u[\mu]$	μ^{th} information bit.
b	Value of a binary bit.
I^a_{inner}	Number of inner iterations of the three-stage decoder at node a.
I^a_{outer}	Number of outer iterations of the three-stage decoder at node a.
π	The interleaver.
π^{-1}	The deinterleaver.
η	Bandwidth efficiency.
R_c	Coding rate.
$\mathcal{A}$	Area under a bit-based EXIT chart curve.

$\mathcal{C}_{\text{total}}$	Entire system complexity.
$\mathcal{C}_{\text{per}-\text{iter}}$	System complexity imposed by a single iteration.
$\mathcal{I}_{\text{iter}}$	Number of iterations for the optimally matched inner and outer decoders to approach the point of perfect convergence at $(1.0, 1.0)$ in the EXIT chart.
$\mathbf{m}$	Conditional expectation of a received signal vector.
d_i^2	Accumulated squared length used in MSDSD algorithm.
$\boldsymbol{f}_g$	Coefficient vector of an adaptive filter.
$\mathbf{R}_{rr}$	Correlation matrix of the entire received signal block.
$\mathbf{R}_{ee}$	Correlation matrix of the interference-plus-noise component.
β, μ	Forgetting factors.
ν	Memory length of a convolutional code.
p	Puncture rate.
T_{Slot}	Time length of a standard time slot.
$\mathbf{u}$	Information-bit stream.
$\mathbf{u}\{t_1\}$	Information-bit packet during t_1^{th} time slot.
$\mathbf{p}$	Parity-bit stream.
$\mathbf{p}\{t_2\}$	Parity-bit packet during t_2^{th} time slot.
$\mathbf{S}\{t_1\}$	Signal block during t_1^{th} time slot.
$\mathbf{G}$	Generator matrix of a channel code.
$\beta_{m,t_2}^{n,t1}$	Coding coefficient of a generator matrix.
$\mathcal{D}$	A set of RNs.
$\mathcal{D}(I)$	A set of information-bit packets.
D_{GANC}	Diversity order of a GANC aided network.
P_{outage}	Outage probability.
d_{free}	Free distance of a channel code.
$\mathcal{T}_{\text{ave}}$	Average throughput.
P_e	Frame error ratio.
$\triangle_i^2$	Incremental euclidean distance of the SISO-MSDSD algorithm.

Chapter 1

Introduction

1.1 Historical Perspective on Cooperative Communication and Non-coherent Detection

Conceiving high-quality wireless solutions in support of the Wireless Internet is of paramount importance. Achieving a low bit-error-ratio (BER), high system throughput, low complexity, low delay, as well as seamless connectivity across the entire coverage area are of salient significance. However, as shown in the stylized illustration of Figure 1.1, we have to strike a compromise amongst these conflicting design factors.

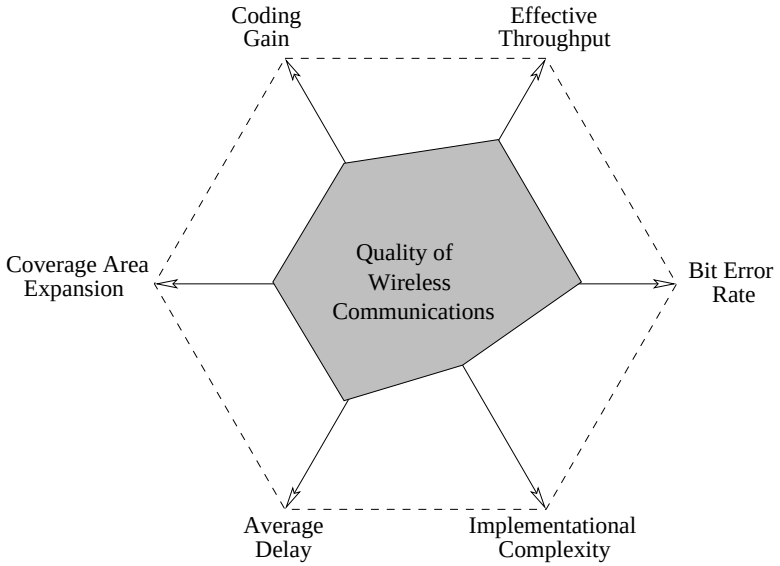

Figure 1.1: Criteria for assessing the overall quality of a wireless communication service. In this treatise, we will focus on three of them: the achievable throughput, the attainable BER, as well as the complexity imposed.

However, the detrimental impact of the hostile radio propagation severely impairs the achievable communication quality in terms of the criteria seen in the stylized Figure 1.1. One of the most detrimental phenomenon is constituted by the effects of fading. It has been demonstrated that various diversity techniques, such as temporal-diversity, frequency-diversity as well as space-diversity arrangements constitute the most effective methods of mitigating the impact of fading.

In this context, multiple-antenna aided multiple-input multiple-output (MIMO) wireless systems have attracted considerable attention in recent years [1–6]. However, the transmit antenna elements have to be sufficiently far apart to experience independent fading, which may be impractical in the uplink owing to the limited size of the mobile handset. Furthermore, even a downlink MIMO BS transmitter associated with a relatively large element separation may not benefit from independent fading, when it is subjected to shadow-fading imposed for example by large-bodied vehicles or other local shadowing paraphernalia [7].

As a remedy, cooperative communications is capable of forming a virtual antenna array (VAA) for each node (user) in a cooperative network by allowing the nodes (users) to relay the messages of other's to the destination. Hence, such a relay aided network practically constitutes a distributed MIMO system relying on the spatially distributed single antennas of the mobiles. This allow us to avoid the correlation of the antenna elements in conventional MIMO systems. The germination of the basic idea of cooperative communication can be traced back to the concept of the relay channel, which was devised by Van der Meulen in [8] and was later characterized from an information-theoretic perspective by Cover and El Gamal in [9]. Basic relaying protocols were also proposed in [9].

To elaborate a little further, cooperative communications benefits from the broadcast nature of wireless transmitters, which allows the relays to receive and retransmit all signals, leading to the concept of "cooperative diversity". Laneman *et al.* characterised both the decode-and-forward (DF) and amplify-and-forward (AF) protocols in [10,11] by evaluating both their diversity order and their outage probability. Similar concepts were investigated also by Sendonaris *et al.* in [12, 13]. These seminal paradigms [10–13] have attracted substantial research attention and inspired a number of novel contributions in the research area of cooperative communications:

a) The authors of [14–18] investigated the achievable diversity-multiplexing trade-off (DMT) of the cooperative network;

b) Relay selection regimes such as opportunistic relaying (OR) and selection cooperation (SC) were exploited in [19–23] for improving the outage performance;

c) Optimum resource allocation regimes were considered in [24–30], which are capable of improving both the power efficiency and battery recharge-period [31] of cooperative communications.

d) The combination of cooperative principles with cognitive radio concepts was considered

in [32–35] and they were also combined with orthogonal frequency division multiple access (OFDMA) in [36, 37].

e) The amalgam of cross-layer network coding and cooperative communication created the concept of network coded cooperation. It has been demonstrated in [38–42] that network coded cooperation constitutes an efficient technique of organizing a large-scale multi-user, multi-relay wireless network.

However, not with standing the above-mentioned benefits, cooperation techniques impose their own problems as well. For example, they impose a 50% throughput loss, because practical transceivers cannot transmit and receive at the same time. A beneficial technique which is capable of mitigating the half-duplex relaying induced throughput loss was advocated in [43, 44], where the successive relaying concept was proposed and analysed. However, the interference encountered both at the relays and at the destination significantly degrades the benefits of the successive relaying regime.

In order to combat this interference-related problem, a range of solutions were proposed in [45–47], where the interference was eliminated based on the idealized simplifying assumption that perfect channel state information (CSI) was available at the receiver. However, suppressing the successive relaying induced interference without requiring any CSI and any extra orthogonal channel-dimension in the time- or frequency-domain remains an open challenge. The aforementioned important issues are briefly summarized in Table 1.1.

The classic coherent detection techniques rely on the CSI for mitigating the deleterious effects of fading channels. Practical channel estimation techniques typically rely on pilot symbol assisted (PSA) training techniques [48] and on the fact that in general the consecutive channel impulse response (CIR) taps are correlated in time, as governed by the normalized Doppler frequency. However, an M-transmitter, N-receiver MIMO system has to estimate $(M \times N)$ channels, which will substantially increase the complexity of the entire system, especially at high normalized Doppler frequencies. Furthermore, in the specific scenario of a VAA-assisted cooperative network, it is unrealistic to expect that in addition to the task of relaying, the relay-station would dedicate further precious resources to the estimation of the source-to-relay channel in support of coherent detection.

Based on the above discussions, noncoherent (NC) detection schemes may be deemed to be promising solutions in the context of cooperative networks, since they are capable of providing a spatial diversity gain, while circumventing the potentially excessive burden of multiple-antenna based channel estimation. Numerous differential detection schemes have been devised for non-coherent receivers. For example, the conventional differential detection (CDD) philosophy was further developed to multiple-symbol differential detection (MSDD) [49] for the sake of achieving an improved BER performance in high-Doppler scenarios, where the CDD typically exhibits a high BER-floor. However, the detection complexity of the MSDD algorithm increases exponentially with the observation window size. In order to reduce the system's complexity, while

Year	Authors	Contributions
1971	Van der Meulen [8]	Heralded the concept of cooperative communication and established the basic three-terminal relaying model.
1979	Cover and El Gamal [9]	Analysed the capacity of the three-terminal based relaying system along with proposing some basic relaying protocols.
2003	Sendonaris *et al.* [12, 13]	Evaluated the performance of several classical cooperative protocols. The remarkable advantages of cooperative communication were quantified in terms of their large power savings, low outage probability and high diversity order.
2004	Laneman *et al.* [11]	
2005	Azarian *et al.* [14] Høst-Madsen et al. [24]	The diversity-multiplexing trade-off was quantified. Furthermore, optimal resource allocation, relay selection, as well as network coded cooperation regimes were developed for further improving the performance of cooperative communications in terms of the achievable diversity order, effective throughput, outage probability, bit error ratio, etc.
2006	Bletsas *et al.* [19] Hunter *et al.* [38]	
2007	Rankov *et al.* [43] Fan *et al.* [44]	Recovered the 50% throughput loss of the conventional half-duplex two-phase cooperative networks, where both "two-way relaying" and "successive relaying" were devised.
2009	Wicaksana *et al.* [47]	Proposed inter-relay interference cancellation for an AF based successive relaying aided network.
2011	Luo *et al.* [46]	Intelligently cancelled the interferences incurred in a DF based successive relaying aided network with the aid of the CSI knowledge.

Table 1.1: Brief history of cooperative communication.

simultaneously avoiding any BER degradation, further advanced algorithms, such as the maximum-likelihood multiple-symbol differential detection (ML-MSDD) [50] and decision-feedback differential detection (DF-DD) [51] have been conceived, while sphere decoding was advocated in [52]. In [53], sphere decoding was incorporated into the MSDD algorithm of [49], which resulted in the multiple-symbol differential sphere detection (MSDSD) technique. The MSDSD algorithm successfully mitigated the complexity of the MSDD algorithm without any BER degradation with respect to the MSDD algorithm [49]. Hence it attracted considerable attention and it was further developed to its multiple-path version in [54] in the context of cooperative communications. Then, in order to transform the hard-decision-based MSDSD algorithm [53] to a more power-efficient, soft-decision-based iterative detection scheme, the MSDSD algorithm was further developed again, in order to create the soft-input soft-output MSDSD (SISO-MSDSD) regime in [55].

1.2 Relaying Protocols: Transmission Arrangement and Diversity Order

1.2.1 Amplify-and-Forward Relaying

The third design option proposed by Cover and El Gamal in [9] for the sake of realizing cooperative communication in a three-terminal network was referred to as the "observation" scheme by Laneman *et al.* in [10]. Based on the "observation" scheme of [9] and inspired by [56, 57], Laneman *et al.* further developed and analysed a novel cooperative protocol in [10], namely the "amplify-and-forward" (AF) regime.

A. Transmission Arrangement

The typical transmission arrangement of an AF aided three-terminal cooperative network is portrayed in Figure 1.2, which consists of the source node (SN) s, relay node (RN) r and destination node (DN) d. Observe in Figure 1.2 that all the propagation paths between the nodes s, r and d are assumed to be narrowband flat Rayleigh fading channels, where the fading coefficients of the channel between node a and node b are represented by $h_{ab}[k], a, b \in \{s, r, d\}$. Furthermore, the average path-loss reduction gains of the source-to-relay (SR) link, relay-to-destination (RD) link and source-to-destination (SD) link with regard to the SD link are represented by G_{sr}, G_{rd}, and G_{sd}, respectively. Then, we denote the average transmit power of a node "a" by $P_a, a \in \{s, r\}$. Furthermore, in line with previous contributions [10, 56, 57], we also assume that the additive white Gaussian noise (AWGN) noise imposed at the different nodes has the same variance N_0. This may be deemed justified, since N_0 is determined by the noise-figure of the receiver.

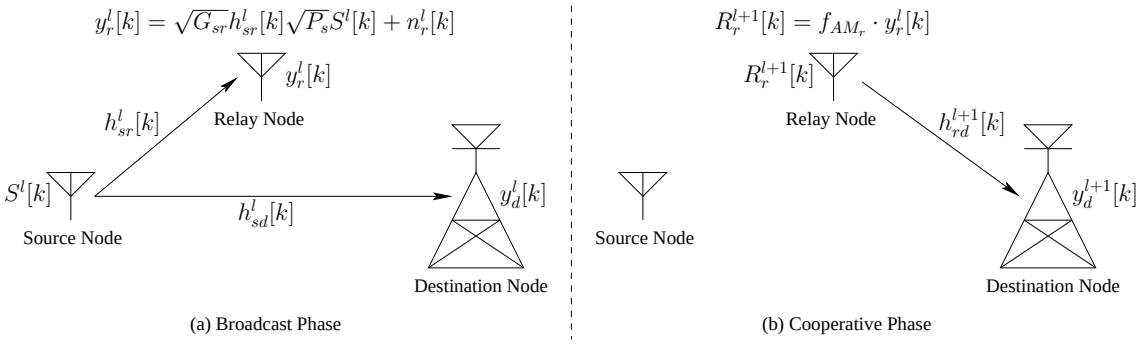

Figure 1.2: The transmission arrangements of the conventional single-relay aided half-duplex cooperative network employing the amplify-and-forward protocol.

Observe for the "(a) Broadcast Phase" in Figure 1.2 that the SN s broadcasts its information symbol $S^l[k]$ both to the RN r and to the DN d. Consequently, the signals received at the RN r and

DN d may be formulated as

$$y_r^l[k] = \sqrt{G_{sr}} h_{sr}^l[k] \sqrt{P_s} S^l[k] + n_r^l[k], \tag{1.1}$$

$$y_d^l[k] = \sqrt{G_{sd}} h_{sd}^l[k] \sqrt{P_s} S^l[k] + n_d^l[k], \tag{1.2}$$

respectively, where the superscript l is invoked for representing the phase index. Furthermore, $n_a^l[k], a \in \{r, d\}$ is the AWGN noise imposed at the node a in the l^{th} transmission phase, which obeys a distribution of $\mathcal{CN}(0, N_0)$.

In the consecutive "(b) Cooperative Phase", instead of detecting the signal $y_r^l[k]$ received during the most recent broadcast phase, the RN r simply amplifies $y_r^l[k]$ by an amplification factor f_{AM_r} according to a certain power constraint and then forwards the amplified version of $y_r^l[k]$, namely $R_r^{l+1}[k]$, to the DN d. Hence the signal received at the DN d during the $(l+1)^{st}$ transmission phase is given by

$$\begin{aligned} y_d^{l+1}[k] &= \sqrt{G_{rd}} h_{rd}^{l+1}[k] R_r^{l+1}[k] + n_d^{l+1}[k] \\ &= \sqrt{G_{rd}} h_{rd}^{l+1}[k] f_{AM_r} \left(\sqrt{G_{sr}} h_{sr}^l[k] \sqrt{P_s} S^l[k] + n_r^l[k] \right) + n_d^{l+1}[k], \end{aligned} \tag{1.3}$$

where the amplification factor f_{AM_r} is stipulated as

$$f_{AM_r} \leq \sqrt{\frac{P_r}{G_{sr} |h_{sr}^l[k]|^2 P_s + N_0}}. \tag{1.4}$$

B. Diversity Order

In the conventional single-link direct-transmission based communication systems, the receiver only receives a single representation of the original codeword transmitted by the transmitter. By contrast, as a benefit of the specific transmission arrangement portrayed in Figure 1.2, the DN d of the AF aided cooperative network always obtains two representations of the original information symbol $S^l[k]$, i.e. both $y_d^l[k]$ of (1.2) and $y_d^{l+1}[k]$ of (1.3). Intuitively, the diversity order of the AF aided cooperative network is capable of approaching "2".

In order to actually realize the diversity gain of AF protocol in practice, a well-designed DN receiver is desired. Fortunately, this design was provided by Laneman *et al.* in [58], where a maximum-ratio combiner was devised. Furthermore, its architecture was illustrated and the associated optimal weight values as well as the mapping function $f\{\cdot\}$ were derived. The BER bound of the DN's receiver was also provided[1].

The stringent theoretical evaluation of the diversity order achieved by AF relaying was also provided by Laneman *et al.* in [10], where the discussions commenced from deriving the system's outage probability. In more detail, the AF protocol produces an equivalent single-input, twin-output complex Gaussian noise channel associated with different noise levels at the outputs. Hence the

[1]In this section, we focus our attention on the diversity order of the AF protocol. We refer to [58] for more information on the maximum-ratio combiner designed for the AF protocol.

mutual information between the equivalent single input and the two outputs is given by

$$I_{\mathrm{AF}} = \frac{1}{2}\log\left(1 + \mathrm{SNR}_{sd} + \mathrm{SNR}_{eq}\right), \tag{1.5}$$

where we have

$$\begin{aligned}
&\mathrm{SNR}_{sd} = \frac{G_{sd}\left|h_{sd}^{l}[k]\right|^2 P_s}{N_0},\ \mathrm{SNR}_{sr} = \frac{G_{sr}\left|h_{sr}^{l}[k]\right|^2 P_s}{N_0},\ \mathrm{SNR}_{rd} = \frac{G_{rd}\left|h_{rd}^{l+1}[k]\right|^2 P_r}{N_0},\\
&\mathrm{SNR}_{eq}^{-1} = \mathrm{SNR}_{sr}^{-1} + \mathrm{SNR}_{rd}^{-1} + \mathrm{SNR}_{sr}^{-1}\cdot\mathrm{SNR}_{rd}^{-1}.
\end{aligned} \tag{1.6}$$

When the actual transmission rate R of the SN exceeds the system's mutual information I_{AF}, the DN can no longer correctly detect the information received. This event may be formulated as

$$\begin{aligned}
I_{\mathrm{AF}} &< R,\\
\mathrm{SNR}_{sd} + \frac{\mathrm{SNR}_{sr}\cdot\mathrm{SNR}_{rd}}{\mathrm{SNR}_{sr} + \mathrm{SNR}_{rd} + 1} &< 2^{2R} - 1.
\end{aligned} \tag{1.7}$$

The probability that the event represented by (1.7) is encountered is referred to as the outage probability. Laneman *et al.* [10] proved that the outage probability of AF relaying may be approximated for a high signal-to-noise ratio (SNR) scenario as

$$\mathrm{Pr}_{\mathrm{AF}}^{\mathrm{out}}(\mathrm{SNR},\mathrm{R}) = \Pr\left[\mathrm{I}_{\mathrm{AF}} < \mathrm{R}\right] \sim \left(\frac{2^{2\mathrm{R}} - 1}{\mathrm{SNR}}\right)^2, \tag{1.8}$$

where[2] we have $\mathrm{SNR} = \frac{P_s}{N_0} = \frac{P_r}{N_0}$. The diversity order is defined as [59]

$$D \triangleq \lim_{\mathrm{SNR}\to\infty} \frac{-\log \mathrm{Pr}^{\mathrm{out}}}{\log \mathrm{SNR}}, \tag{1.9}$$

which characterises the robustness of a communication system. When having a high diversity order, the BER of a communication system will decay fast upon increasing the SNR value of the communication system. By contrast, when having a low diversity order, the BER may decay very slowly upon increasing the SNR value, which may even lead to an error-floor event.

Substituting (1.8) into (1.9), we arrive at

$$\begin{aligned}
D &= \lim_{\mathrm{SNR}\to\infty} \frac{-\log\left(\frac{2^{2R}-1}{\mathrm{SNR}}\right)^2}{\log \mathrm{SNR}}\\
&= \lim_{\mathrm{SNR}\to\infty} \frac{\log\left(\frac{\mathrm{SNR}}{2^{2R}-1}\right)^2}{\log \mathrm{SNR}}\\
&= \lim_{\mathrm{SNR}\to\infty} \frac{2\left[\log \mathrm{SNR} - \log\left(2^{2R}-1\right)\right]}{\log \mathrm{SNR}}\\
&= \lim_{\mathrm{SNR}\to\infty} \frac{2\log \mathrm{SNR}}{\log \mathrm{SNR}} = 2.
\end{aligned} \tag{1.10}$$

According to (1.10), we can readily see that the AF protocol is indeed capable of achieving the maximum attainable diversity order of "2".

[2]We assume that the SN and RN have the same transmit power, i.e. $P_s = P_r$.

1.2.2 Decode-and-Forward Relaying

According to [9, Theorem 1], another design option was proposed by Cover and El Gamal for efficiently organizing cooperative transmissions in a three-terminal network, which was termed as the "cooperation" scheme by Laneman *et al.* in [10]. Inspired by [60,61], the "cooperation" scheme was termed later as the DF protocol [10].

A. Transmission Arrangement

In the DF aided cooperative network, the relay node attempts to decode the signals received during the broadcast phase and then re-encodes, as well as re-modulates the detected information. The RN may opt for a variety of re-encoding, re-modulating strategies. If it simply re-encodes, as well as re-modulates the detected information in the same way as the SN, this regime may be referred to as repetition-coded DF. In this section, we will briefly characterize both the transmission arrangement and diversity order of the repetition-coded DF regime.

The signals received at the RN r and DN d during "(a) Broadcast Phase" of the repetition-coded DF relaying scheme of Figure 1.3 are the same as that formulated in (1.1) and (1.2), respectively. If perfect detection is achieved at the RN during "(a) Broadcast Phase" of Figure 1.3, the signal

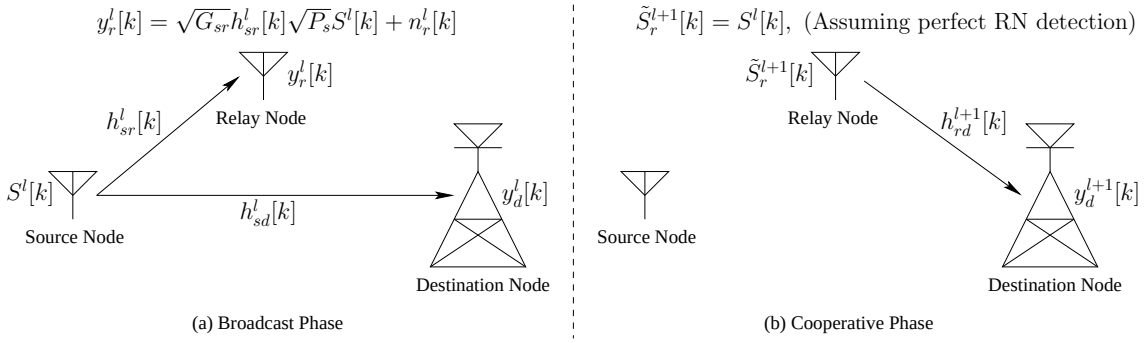

Figure 1.3: The transmission arrangements of the conventional single-relay aided half-duplex cooperative network, employing decode-and-forward protocol.

forwarded by the RN during the consecutive "(b) Cooperative Phase" of Figure 1.3 will be the same as the original source information symbol, which may be formulated as

$$\tilde{S}_r^{l+1}[k] = S^l[k]. \tag{1.11}$$

B. Diversity Order

It was indicated by Laneman *et al.* in [10] that the maximum average mutual information of the entire DF relaying system shown in Figure 1.3 can be formulated as

$$I_{\mathrm{DF}} = \frac{1}{2} \min \left\{ \log\left(1 + \mathrm{SNR}_{sr}\right), \log\left(1 + \mathrm{SNR}_{sd} + \mathrm{SNR}_{rd}\right) \right\}, \tag{1.12}$$

where the definitions of SNR_{sr}, SNR_{sd}, and SNR_{rd} are given in (1.6). In more detail, the first term in (1.12) represents the maximum error-free transmission rate of the source-to-relay link, while the

second term quantifies the maximum rate at which the DN can reliably decode the source message based on the signals received from both the SN and from the RN. Then, requiring that the RN and DN simultaneously achieve perfectly flawless detection necessitates taking the minimum of the two terms in (1.12).

According to the concept of "outage" described in Section 1.2.1, the outage event for the DF relaying regime is given by $I_{\mathrm{DF}} < R$, which is equivalent to the event of

$$\min\left\{\mathrm{SNR}_{sr}, \mathrm{SNR}_{sd} + \mathrm{SNR}_{rd}\right\} < g = \left(2^{2R} - 1\right). \tag{1.13}$$

Hence, in the presence of Rayleigh fading and assuming that we have $\mathrm{SNR} = \frac{\mathrm{P_s}}{\mathrm{N_0}} = \frac{\mathrm{P_r}}{\mathrm{N_0}} \to \infty$, the associated outage probability of DF relaying is given by

$$\begin{aligned}\mathrm{Pr}_{\mathrm{DF}}^{\mathrm{out}}(\mathrm{SNR}, \mathrm{R}) &= \mathrm{Pr}\left[I_{\mathrm{DF}} < R\right] \\ &= \mathrm{Pr}\left[\mathrm{SNR_{sr}} < \mathrm{g}\right] + \mathrm{Pr}\left[\mathrm{SNR_{sr}} \geq \mathrm{g}\right] \cdot \mathrm{Pr}[\mathrm{SNR_{sd}} + \mathrm{SNR_{rd}} < \mathrm{g}] \\ &\sim \frac{2^{2R} - 1}{\mathrm{SNR}}. \end{aligned} \tag{1.14}$$

According to (1.9), the $\frac{1}{\mathrm{SNR}}$ trend observed in (1.14) indicates that the diversity order of DF relaying is still "1". Hence it does not offer diversity gains for high SNRs, because requiring the RN to perfectly decode the source message limits the performance of DF to that of direct-transmission between the SN and RN. However, with the aid of a well designed re-encoding or re-modulation strategy, the DF protocol is still capable of achieving the maximum attainable diversity order as stated in [62].

1.2.3 Amplify-and-Forward Versus Decode-and-Forward

The major transmission arrangement difference between the amplify-and-forward protocol and decode-and-forward protocol is whether the RN detects the received signal. If the RN does not employ any detection algorithm, only amplifies the received signal and then directly forwards it to destination, it carries out amplify-and-forward relaying. Otherwise, if the RN decodes the source messages and re-encodes, as well as re-modulates them, it constitutes decode-and-forward relaying.

In the AF aided cooperative network, the RN does not have to detect the SN's information symbols, it only amplifies its received signals and forwards them to the DN. Hence the complexity imposed on the RN is lower than that incurred in DF relaying. As a result, compared to the DF protocol, the AF protocol is more suitable for a cooperative network, where the RNs only have a simple transceiver architecture and cannot afford high-complexity operations. Since the RN only amplifies the amplitude of the received signals, the AF protocol is immune to the error propagation problem potentially incurred by the DF protocol. Consequently, the AF protocol might be capable of outperforming the DF protocol, when the relay is close to the destination [63]. However, the drawback of the AF protocol is the so-called noise amplification problem, which imposes extra noise on the DN.

By contrast, the complexity of the DF protocol is typically higher than that of the AF protocol due to the decoding and re-encoding process. Again, another problem imposed by DF relaying is the "error propagation" phenomenon, because the original source message may be erroneously decoded at the RN. This typically inflicts more errors than imposed by the channel, which results in the above-mentioned error propagation. In fact, requiring the RN to perfectly decode the source information would limit the performance of the DF protocol to that of direct transmission between the SN and RN.

Hence the robustness of the RN's detector is critical for the success of the DF protocol, which should simply disable relaying in the presence of decoding errors. A range of robust detection schemes were devised in [64]. Since the quality of the source-to-relay link is critical for DF relaying, the DF protocol is recommended for those scenarios, where the RNs are in the vicinity of the SN for the sake of avoiding error propagation.

However, neither the AF protocol nor the DF protocol is capable of efficiently exploiting the degrees of freedom provided by the channel, especially not at high rates, because the RN repeats the transmission all the time. Accordingly, the incremental AF relaying was further devised in [10], where the classic automatic-repeat-request (ARQ) mechanism was incorporated into the relaying context. In more detail, in the incremental AF relaying aided cooperative network, the SN firstly transmits its information to the RN and DN. Then, the DN indicates success or failure of the SD transmission by broadcasting an acknowledgement to both the SN and RN. If the RN receives a positive acknowledgement from the DN, which indicates the success of the SD transmission, it takes no action. By contrast, if the RN receives a negative acknowledgement, it amplifies and forwards the information received from the SN. Explicitly, the incremental redundancy based AF relaying may achieve a higher bandwidth-efficiency, because it repeats the transmission of the same information only rarely.

The diversity-multiplexing trade-off struck by the direct transmission, the DF relaying, the AF relaying, as well as the incremental AF relaying is compared in Figure 1.4.

The normalized effective throughput R_{norm} used in Figure 1.4 is defined as [10]

$$R_{\text{norm}} = \frac{R}{\log\left(1+\text{SNR}\right)}, \tag{1.15}$$

where the notation R represents the actual transmission rate utilized in (1.7) and (1.8). Upon replacing R utilized in (1.7), (1.8) by R_{norm} defined in (1.15) and substituting the relevant results into (1.9), the diversity order of the AF protocol given in (1.9) may be rewritten as

$$D_{\text{AF}} = 2\left(1-2R_{\text{norm}}\right). \tag{1.16}$$

Similarly, the diversity orders of the DF protocol and of the incremental AF protocol are given by

$$\begin{aligned} D_{\text{DF}} &= 1-2R_{\text{norm}}, \\ D_{\text{Incremental-AF}} &= 2\left(1-R_{\text{norm}}\right). \end{aligned} \tag{1.17}$$

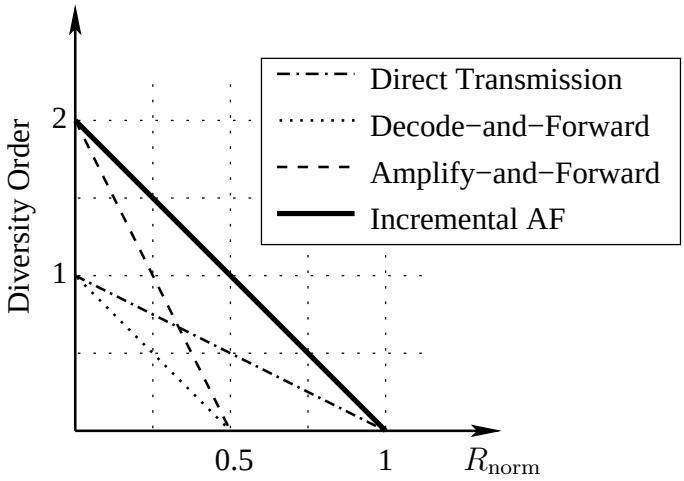

Figure 1.4: Diversity order versus the normalized effective throughput R_{norm} for direct transmission, DF, AF as well as for incremental AF, where a large SNR scenario is considered. The curves portrayed in this diagram are attained according to (1.16) and (1.17).

Explicitly, the diversity order versus normalized effective throughput curves portrayed in Figure 1.4 are attained according to (1.16) and (1.17). For example, the diversity order of the AF protocol is $D_{\text{AF}} = 2\,(1 - 2R_{\text{norm}})$ as seen in (1.16). Thus, its maximum diversity order of 2 is indeed achieved when we have $R_{\text{norm}} \to 0$, which constitutes the left-most point of the AF's curve in Figure 1.4. The resultant maximum normalized spectral efficiency of $\frac{1}{2}$ is achieved as $D_{\text{AF}} \to 0$, which constitutes the right-most point of the AF's curve in Figure 1.4.

1.2.4 Successive Relaying

The concept of successive relaying, or "two-path relaying" first occurred in [65]. Based on [65], as well as inspired by the related benefits reported in [43, 66–68], a more generalized successive relaying protocol was proposed by Fan *et al.* in [44], offering further insights into the achievable rates and into the associated diversity-multiplexing trade-off.

A. Transmission Arrangement

The transmission process of the successive relaying protocol proposed in [44] is illustrated in Figure 1.5, where we observe $(L + 1)$ number of processing phases and ignore the interference between the two RNs[3]. Instead of the single-relay aided three-terminal structure employed in conventional cooperative networks, the successive relaying regime relies on two RNs for alternately forwarding the source messages to the DN.

In more detail, the specific actions involved in every phase shown in Figure 1.5 are described as follows

[3]The successive relaying induced interferences will be discussed in Chapter 3 and Chapter 4.

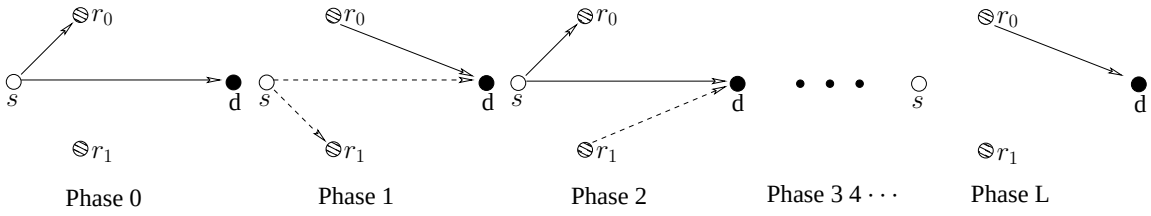

Figure 1.5: Transmission schedule of the successive relaying protocol.

Phase 0: The SN s broadcasts the message $S[0]$; the RN r_0 listens to the SN s and receives the message $S[0]$; the RN r_1 remains silent; the DN d receives the message $S[0]$.

Phase 1: The SN s continues to broadcast the message $S[1]$; the RN r_0 forwards the message $S[0]$ to the DN; the RN r_1 listens to the SN s and receives the message $S[1]$; the DN d simultaneously receives the messages $S[0]$ and $S[1]$ via the relay-to-destination link and source-to-destination link, respectively.

Phase 2: The SN s continues to broadcast the message $S[2]$; the RN r_0 listens to the SN s and receives the message $S[2]$; the RN r_1 forwards the message $S[1]$ to the DN; the DN d simultaneously receives the messages $S[1]$ and $S[2]$.

Phase 3 4 ...: The transmission options described in Phase 1 and 2 will be alternately repeated until Phase $(L-1)$.

Phase L: The SN s completes all of its transmissions and stops broadcasting; the RN r_0 or r_1 forwards the message $S[L-1]$ to the DN; another RN remains silent; the DN d receives the message $S[L-1]$.

B. Diversity Order

Fan *et al.* analysed the diversity-multiplexing trade-off of DF based successive relaying, while assuming perfect source-to-relay (SR) links. In more detail, the diversity order of the successive DF relaying is formulated as [44]

$$D_{\text{Successive-DF}} = 2\left(1 - \frac{L+1}{L} R_{\text{norm}}\right)^{+}, \tag{1.18}$$

where the operation $(x)^+$ is defined as $(x)^+ = \max\{0, x\}$. Furthermore, R_{norm} has a similar definition to that detailed in (1.15), which was also referred to as multiplexing gain in [4, 44][4]. According to the transmission process depicted in Figure 1.5, intuitively, the multiplexing gain of the successive DF relaying is limited to the region of $R_{\text{norm}} \in \left[0, \frac{L}{L+1}\right]$.

[4]The multiplexing gain in $[4, 44]$ is defined as $R_{\text{norm}} = \frac{R}{\log(\text{SNR})}$, which is slightly different from that defined in (1.15). However, this distinction caused by different definitions will not affect the characterisation of the system's diversity-multiplexing trade-off.

Similar to Figure 1.4, the diversity-multiplexing trade-off struck by the successive DF relaying associated with different number of processing phases L is visualized in Figure 1.6. The DMT achieved by the conventional DF relaying and that achieved by the incremental AF relaying are also presented in Figure 1.6 as the benchmarkers, which are directly echoed from Figure 1.4. Observe in Figure 1.6 that successive DF relaying is capable of achieving a significantly improved DMT compared to conventional DF relaying. Furthermore, the DMT of successive DF relaying is capable of gradually approaching that of incremental AF relaying upon increasing the number of processing phases L.

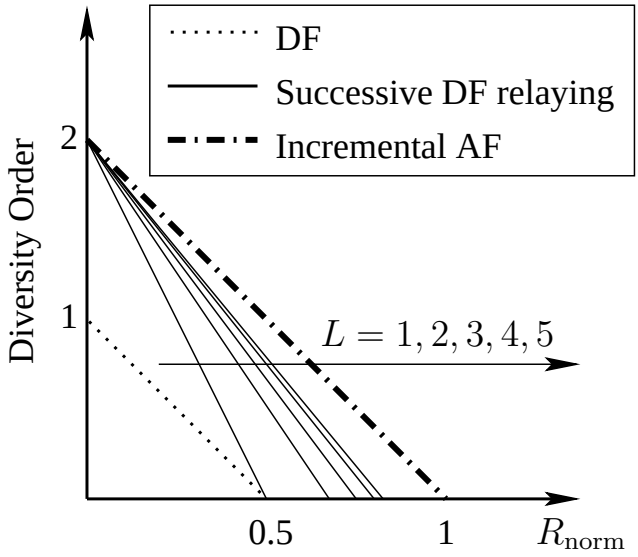

Figure 1.6: Diversity order versus multiplexing gain R_{norm} for the successive DF relaying protocol, where the number of processing phases L is increased from $L = 1$ to $L = 5$. The relevant curves are attained according to (1.18). The diversity-multiplexing trade-off (DMT) of both the conventional DF relaying and of the incremental AF relaying as portrayed in Figure 1.4 are also included here as a pair of benchmarkers.

1.3 Novel Contributions

The main contributions of this thesis are as follows:

- We conceive a novel relay-aided MSDSD algorithm for the successive relaying aided network (SRAN), which was created from the conventional single-user/single-path MSDSD algorithm of [53]. For the sake of suppressing the successive relaying induced interferences, we invoke the code division multiple access (CDMA) technique and combine it with our SRAN regime. As a benefit, we convert the typical 50% half-duplex relaying-induced throughput loss to a potential user-load reduction of the CDMA system. In order to mitigate the com-

plexity imposed on the relay node, we opt for the AF protocol at the relay node. **- These novel contributions were proposed in papers "No.1"and "No.2" in the publication list.**

- We further extend our research to a multi-user scenario relying on the AF protocol at the relay node. Correspondingly, a specific interference suppression regime is designed for this scenario, where the effects of both the successive relaying induced interference and of the multiple access interference (MAI) are evaluated. In order to analyse the performance upper bound of our system, we derive the noncoherent discrete-input continuous-output memoryless channel (DCMC) capacity of the AF based SRAN operating in multi-user scenarios. We demonstrate that the proposed successive AF relaying aided cooperative DS-CDMA uplink exhibits substantial advantages, especially in high user-load scenarios. **- These novel contributions were subjected to peer-review in papers "No.4" and "No.7" in the publication list.**

- In order to significantly improve the achievable power-efficiency at a fixed target BER, instead of employing the aforementioned hard-decision-based detection, we incorporated soft-decision-based iterative detection into our system. Furthermore, instead of AF relaying, the DF protocol is employed this time in support of more sophisticated signal processing at the relay node. Hence we conceive a noncoherent iterative detection aided DF based SRAN operating in a multi-user scenario. We also derived the noncoherent DCMC capacity of this DF based SRAN and devised an iterative three-stage MSDSD-URC-RSC transceiver. It is demonstrated that the proposed transceiver significantly reduces the system's complexity, whilst recovering much of the half-duplex relaying-induced throughput loss, and operating close to the associated system capacity. **- These novel contributions were detailed in papers "No.3", "No.7", and "No.8" in the publication list.**

- We conceived a new multiple-symbol differential interference suppression (MS-DIS) algorithm for our DF based SRAN, which is capable of cancelling the successive relaying-induced interference without estimating the channel impulse response (CIR). However, in this context we have not relied on having unique, stream-specific CDMA spreading sequences. Hence, compared to the system employing CDMA for suppressing the successive relaying-induced interference, the MS-DIS algorithm does not require any extra orthogonal channels, such as the stream-specific spreading codes of CDMA. Hence much of the half-duplex relaying-induced throughput loss is recovered with the aid of our MS-DIS algorithm without the above-mentioned penalty of potential user-load reduction, as in the CDMA system of Chapter 3. Correspondingly, a new adaptive MS-DIS filtering and MSDSD decoding assisted channel-code-aided three-stage turbo receiver architecture is designed for the DN's receiver. We demonstrate furthermore that our proposed transceiver is capable of efficiently suppressing the interference by imposing as little as 2% training overhead, despite experiencing severe time-selective Rayleigh fading. **- These novel contributions were disseminated**

in papers "No.5" and "No.6" in the publication list.

- We extended the concept of "matching code-on-graph with network-on-graph" to arbitrary channel coding schemes and conceived the required new signal processing and transmission arrangements in support of this extension. Consequently, a generalized adaptive network coding (GANC) scheme was proposed for multi-user, multi-relay scenarios. Then, we intrinsically amalgamated the successive relaying protocol with the GANC philosophy to conceive a new GANC aided SRAN based DS-CDMA system concept. As a result, the typical 50% half-duplex relaying-induced throughput loss was converted to a potential user-load reduction for the CDMA system, since the interference of the relays was avoided by invoking a pair of low-correlation spreading codes. Correspondingly, a generalized iterative detection based three-stage transceiver architecture was created for the proposed GANC aided SRAN. The GANC aided SRAN advocated is capable of adapting to both link failures and to network topology changes, while recovering much of the half-duplex relaying-induced throughput loss. We demonstrated that as a benefit of operating in a network coded cooperative manner, the GANC aided SRAN exceeds the performance of the conventional SRAN. Hence it is eminently suitable for organizing a large-scale wireless network. - **These novel contributions were detailed in paper "No.8" in the publication list.**

1.4 Outline of the Thesis

Having briefly reviewed the literature of both cooperative communication and of noncoherent detection, let us now highlight the outline of this thesis, which is organized as shown in Figure 1.7.

Chapter 2 : Noncoherent Differential Multiple-Symbol Joint Detection

In Chapter 2, we focus our attention on noncoherent differential multiple-symbol joint detection techniques. Firstly, the conventional differential detection (CDD) technique is introduced in Section 2.1, followed by the mathematical principles of the MSDD algorithm in Section 2.2. The MSDD algorithm is capable of eliminating the error floor of the CDD, when experiencing severely time-selective Rayleigh fading associated with a high Doppler frequency. However its high complexity is potentially unaffordable in many practical applications. Consequently, in Section 2.3, we conceived the MSDSD algorithm, which strikes an attractive trade-off between the achievable BER performance and the complexity imposed. We will demonstrate that the MSDSD algorithm is capable of shifting the BER curve closer to the noncoherent differential detector's optimum performance bound. In order to adapt our receiver for employment in cooperative networks, the multiple-path MSDSD algorithm was devised in Section 2.4. Finally, we further developed the hard-decision-based MSDSD to the soft-decision-based SISO-MSDSD in Section 2.5, which is the foundation of our relay-aided SISO-MSDSD scheme employed in Chapter 3.

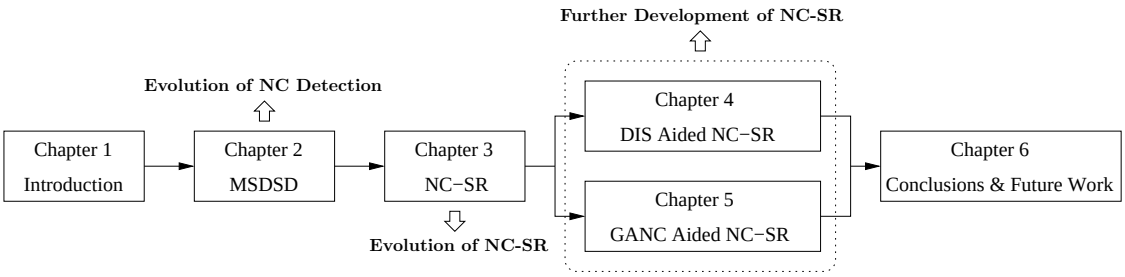

Figure 1.7: Organization of the thesis.

Chapter 3: Evolution of Noncoherent Successive Relaying

In Chapter 3, motivated by the promising advantages of both the MSDSD and of the SRAN, we propose a noncoherent successive relaying (NC-SR) aided cooperative DS-CDMA system. We strive for consistently improving the performance of the proposed NC-SR regime, which evolved from a basic prototype to a sophisticated architecture as a benefit of the techniques proposed in this chapter. In order to suppress the successive relaying induced interference, the DS-CDMA multiple access technique was then invoked. Consequently, the typical 50% half-duplex relaying induced throughput loss is converted to a potential user-load reduction for the DS-CDMA system, since the SRAN requires two spreading codes for each user. For characterising the performance bounds of the proposed systems, the associated noncoherent DCMC capacities are also derived. Furthermore, in order to beneficially incorporate the MSDSD algorithm into our cooperative system, two meritorious variants of the classical MSDSD algorithm are devised, namely the "relay-aided MSDSD" and the "relay-aided SISO-MSDSD". Finally, in Section 3.3.3, we also design an advanced three-stage iterative detection based transceiver for approaching the system's capacity.

In more detail, in Section 3.1, the successive AF relaying aided single-user DS-CDMA uplink is conceived as our basic system prototype, where we devise a new hard-decision-based relay-aided MSDSD algorithm as its noncoherent detection scheme. We will demonstrate that as a benefit of its diversity gain, our basic system prototype is capable of exceeding the BER performance of the coherent detection aided single-link based direct-transmission. Then, we further develop our prototype system from the single-user scenario to a more realistic multi-user scenario in Section 3.2. In this section, we will detail the associated noise accumulation problem imposed by the IRI in our system and design the associated DS-CDMA based interference suppression solution. The noncoherent DCMC capacity of the AF based SRAN embedded in a multi-user DS-CDMA uplink is also derived in Section 3.2.2. The related capacity results will indicate that our AF based SRAN is capable of significantly outperforming both the conventional AF relaying and the single-link direct-transmission. Finally, in Section 3.3, we develop our basic system prototype for the successive DF relaying aided multi-user DS-CDMA uplink for the sake of remarkably improving the system's power efficiency. The NC DCMC capacity of the DF based SRAN is also derived. The related

simulation results reveal that the DF based SRAN may outperform the AF based SRAN, especially in the low SNR region. In the spirit of improving the system's energy efficiency, the hard-decision-based relay-aided MSDSD is then further developed by conceiving the more powerful soft-decision-based relay-aided SISO-MSDSD algorithm. Again, in Section 3.3.3, a relay-aided SISO-MSDSD assisted three-stage iterative transceiver is designed for supporting the operation of the proposed DF based SRAN. This transceiver is capable of operating close to the system's capacity.

Chapter 4: Differential Interference Suppression Aided Noncoherent Successive Relaying

A crucial challenge incurred in the context of NC-SR is that of suppressing the successive relaying-induced interference. In Chapter 3, this problem was solved by invoking the classic DS-CDMA multiple access technique. Nevertheless, the resultant penalty is a potential user-load reduction for the DS-CDMA system. Hence, in this chapter, we attempt to tackle the challenge of interference suppression with the aid of our new MS-DIS regime, which is a novel amalgam of the adaptive modified Newton algorithm and the SISO-MSDSD algorithm.

In more detail, in order to simplify our analysis, a simplified system model is described in Section 4.1, where a DF based SRAN consisting of only four nodes (a SN, two RNs, and a DN) is considered. In Section 4.2, the basic principles of the adaptive MS-DIS regime are highlighted, including the maximum signal-to-interference-plus-noise ratio (SINR) criterion, the adaptive modified Newton algorithm, as well as the relay-aided SISO-MSDSD. Then, a MS-DIS plus relay-aided SISO-MSDSD assisted three-stage turbo transceiver is designed in Section 4.3, where the adaptive MS-DIS filter is employed as the first component of the DN for the sake of interference suppression. Since the DN relies on multiple antennas in support of the MS-DIS regime, the single-antenna scenario considered in Chapter 3 is further developed to a new multiple-antenna aided scenario. As a further contribution, the noncoherent DCMC capacity of the multiple-antenna aided DF based SRAN is derived in Section 4.4 as a benchmarker for assessing the proposed multiple-antenna aided transceiver's performance. We demonstrate in Section 4.5 that the MS-DIS filter aided transceiver is capable of efficiently suppressing the interference at the expense of imposing as little as 2% training overhead, despite experiencing severely time-selective Rayleigh fading associated with a high Doppler frequency.

Chapter 5: Generalized Adaptive Network Coded Noncoherent Successive Relaying

In Chapter 5, we revert our discourse back to the context of DS-CDMA assisted NC-SR, where a multi-user, multi-relay scenario is considered. In order to efficiently organize the cooperation among the multiple nodes of the large-scale wireless network considered, we further develop the concept of adaptive network coded cooperation (ANCC) to its generalized version, namely to our "GANC" regime. In order to improve the bandwidth efficiency of the proposed GANC scheme, we invoke the NC-SR arrangement, which results in the GANC

aided SRAN. Moreover, instead of using a pair of separate network and channel coding arrangement, we opt for conceiving a joint network-channel coding (JNCC) scheme, which is capable of achieving a further coding gain.

In more detail, in Section 5.1, we devise the above-mentioned GANC regime based on both an ANCC and a DNC regime, which allows arbitrary channel coding schemes to serve as the cross-layer network coding, while remaining flexible in terms of mitigating the effects of both network topology changes and of link failures. The transmission arrangement, the related signal processing, as well as the major advantages of the nonbinary linear block code (NBLB) coded GANC and of the RSC coded GANC are detailed in this section. Then we incorporate the proposed GANC regime into the successive DF relaying aided multi-user, multi-relay DS-CDMA uplink in Section 5.2. In the spirit of our JNCC scheme, we devise a generalized iterative detection based three-stage transceiver architecture for the proposed GANC aided SRAN in Section 5.3. The proposed transceiver is also capable of adapting to the network topology changes. The robustness of the proposed GANC aided noncoherent SRANs having different source group size to relay group size ratios is investigated in Section 5.4 with the aid of the extrinsic information transfer (EXIT) chart analysis method. We will demonstrate that combining two DF based SRANs and operating them with the aid of the proposed GANC regime is capable of attaining a significant power gain with respect to operating them independently, i.e. without any cooperation between them.

Chapter 6: Conclusions and Future Work

In Chapter 6, we summarize the main findings of the entire thesis. Specific design guidelines are provided for clarifying the rationale of our design decisions, as well as for offering further insights into the applications of the advanced solutions introduced in this thesis. Further potential research topics are also outlined for the future. For example, we may invoke some more sophisticated signal processing techniques, such as irregular convolutional codes (IrCC). Finding optimal resource allocation scheme is also attractive for further research for the sake of improving the bandwidth or energy efficiency of our system. Furthermore, we may employ some more sophisticated relaying protocols, such as soft decode-and-forward (Soft-DF) and buffer-aided relaying for further developing our cooperative systems.

Chapter 2

Noncoherent Differential Multiple-Symbol Detection

As stated in Section 1.1, the single-antenna aided mobile stations involved in cooperative communication constitute a MIMO system relying on distributed antenna elements, thereby forming a VAA for each participant. However, the channel estimation of a multi-antenna aided cooperative network imposes a high complexity, especially at high Doppler frequencies, since the channel's coherence time is short. Furthermore, it may be unrealistic to expect that in addition to the task of relaying, the RN would dedicate further precious resources to the estimation of the SR channel in support of coherent detection. Therefore, noncoherent detection becomes an attractive design alternative, which is still capable of achieving a beneficial "cooperative diversity gain", while circumventing the potentially excessive burden of MIMO channel estimation. Hence, in this chapter, we focus our attention on conceiving advanced noncoherent multiple-symbol joint-detection based differential detection algorithms. These techniques will be further exploited in the forthcoming chapters.

The conditional probability density function (PDF) of an N-dimensional Gaussian random vector was derived by Van Trees in [69], which laid the theoretical foundations for improving the decision rule of the multiple-symbol differential detection (MSDD) algorithm [49, 70–72]. In [49, 70], Divsalar *et al.* conceived the MSDD algorithm by extending the twin-symbol observation interval of the conventional differential detection (CDD) to multiple symbols, which required simultaneously making a joint decision on these multiple symbols. They also analysed the BER performance of the MSDD algorithm in AWGN channels. Based on the contributions in [49] and inspired by the derivation process of the conditional PDF of an N-dimensional Gaussian random vector provided in [69], Ho and Fung [71, 72] improved the decision matrix of the MSDD algorithm and further analysed its BER performance for transmission over correlated Rayleigh fading channels.

It has been demonstrated in [49, 70–72] that the BER performance gains of the MSDD algorithm achieved over the CDD technique will be further enhanced upon increasing the observation

interval. However, when implementing the MSDD algorithm in its maximum-likelihood (ML) sequence estimation form, the associated system's complexity grows exponentially with the observation interval size. For example, assuming that the constellation size of the modulation scheme is M_c and the observation window size is N, the MSDD algorithm has to estimate $\left(M^N\right)$ different symbol sequences for the sake of decoding $(N-1)$ information symbols. The rapidly increased decoding complexity significantly impairs the practicality of the MSDD algorithm. Consequently, several improved approaches to low-complexity MSDD were proposed in [50, 73, 74], where different compromises were struck between the attainable BER performance and the associated decoding complexity. For example, Mackenthun [50] developed an ML-MSDD for both AWGN channels and classic block-fading Rayleigh channels, which only requires a complexity of order $N\log_2(N)$ per N symbols. The decision-feedback differential detection (DF-DD) [74] proposed for time-varying Rayleigh fading channels offers substantial performance benefits, while its per-symbol complexity is only linearly increasing with the observation window size.

Then, Lampe *et al.* reformulated the decision matrix proposed in [71] and incorporated the sphere detection mechanism in the MSDD algorithm. Consequently, the MSDD algorithm was further developed to conceive the multiple-symbol differential sphere detection (MSDSD) algorithm in [53]. The MSDSD algorithm remarkably reduces the MSDD's decoding complexity, especially in the high-SNR scenarios without impairing its BER performance. Hence the trade-off between the attainable BER performance and the decoding complexity was further improved. However, the decoding complexity of the MSDSD algorithm imposed at low SNRs still grows exponentially upon decreasing the SNR. For solving this particular drawback of MSDSD, Pun *et al.* devised the Fano Multiple-Symbol Differential Detection (Fano-MSDD) algorithm in [75, 76] by further developing the Fano algorithm [77] as an efficient MSDD receiver. On the other hand, in order to transform the hard decision based MSDSD algorithm to a power-efficient, soft-decision-aided iterative detection scheme, the MSDSD algorithm was further developed to the soft-input soft-output MSDSD (SISO-MSDSD) regime in [55].

Furthermore, as a benefit of the cooperative diversity, the DN of a cooperative network will obtain multiple versions of the same codeword transmitted from the SN. Hence the receiver at the DN should be capable of simultaneously processing multiple input signal sequences. For satisfying this requirement, the MSDSD algorithm [53] was further modified by Wang *et al.* in [54, 78]. We would like to refer to this variant of the MSDSD algorithm as the multiple-path processing based MSDSD. Consequently, the application scenario of the MSDSD algorithm was extended from single-link direct transmission based systems to cooperative networks.

Based on the previous contributions on multiple-symbol differential detection, we further developed the single-user/single-path MSDSD algorithm of [53] into a novel relay-aided form in [79]. More specifically, compared to the multiple-path processing based MSDSD algorithm of [78], the size of the decision matrix in our novel relay-aided MSDSD only increases linearly with the number of entities (source nodes plus relays) and hence the system's complexity is reduced. Correspond-

ingly, we developed the soft-decision based version of our relay-aided MSDSD in [80], to create the relay-aided soft-input soft-output MSDSD (relay-adied SISO-MSDSD).

We summarize the above-mentioned history of multiple-symbol differential detection techniques in Table 2.1. Similar to [81], Figure 2.1 is provided for visualizing the evolution of the noncoherent differential detection technologies.

Year	Authors	Contributions
1968	Trees [69]	Contributed the critical theoretical foundation of the MSDD algorithm.
1990	Divsalar et al. [49, 70]	Heralded the MSDD algorithm by using a multiple-symbol observation interval during the differential detection process and analysed its BER performance in AWGN channels.
1992	Ho and Fung [71]	Reformed the decision matrix of the MSDD algorithm, and analysed its bit error performance in correlated Rayleigh fading channels.
1994	Mackenthun [50]	Developed an ML-MSDD algorithm, which only imposes a complexity order of $N\log_2(N)$ per N symbols in AWGN and block-fading Rayleigh channels.
1999	Schober et al. [74]	Devised the DF-DD algorithm, where the per-symbol complexity of the MSDD algorithm grows linearly with the observation window size. Consequently, a suboptimum trade-off between the performance attained and complexity imposed was achieved.
2005	Lampe et al. [53]	Developed the MSDD algorithm to the contemporary state-of-the-art noncoherent detection regime - MSDSD.
	Pun and Ho [75]	Proposed the Fano-MSDD algorithm as an alternative technique of MSDSD for low SNR scenarios.
2006	Pauli et al. [55]	Devised the power-efficient, soft-decision-aided SISO-MSDSD regime.
2009	Wang and Hanzo [78]	Applied the MSDSD algorithm to cooperative networks, and consequently generated the multiple-path MSDSD.
2011	Li et al. [79, 80]	Created both the hard-decision and soft-decision based relay-aided MSDSD, which was exclusively designed for combing the multiple input information streams at the DN of a cooperative network when dispensing with CSI.

Table 2.1: Contributions to multiple-symbol differential detection.

2.1 Conventional Differential Signalling and Detection

We briefly introduce the classic M_c-ary differential phase-shift keying (M_c-DPSK) signalling and detection techniques in this section. Firstly, the entire differential encoding and decoding process is illustrated in Figure 2.2. Let $\mathcal{M}_c$ denote the constellation of an M_c-ary phase-shift keying (M_c-PSK) modulation scheme, which is defined as $\mathcal{M}_c = \{e^{j2\pi m/M_c}; m = 0, 1, \ldots, M_c - 1\}$. Let

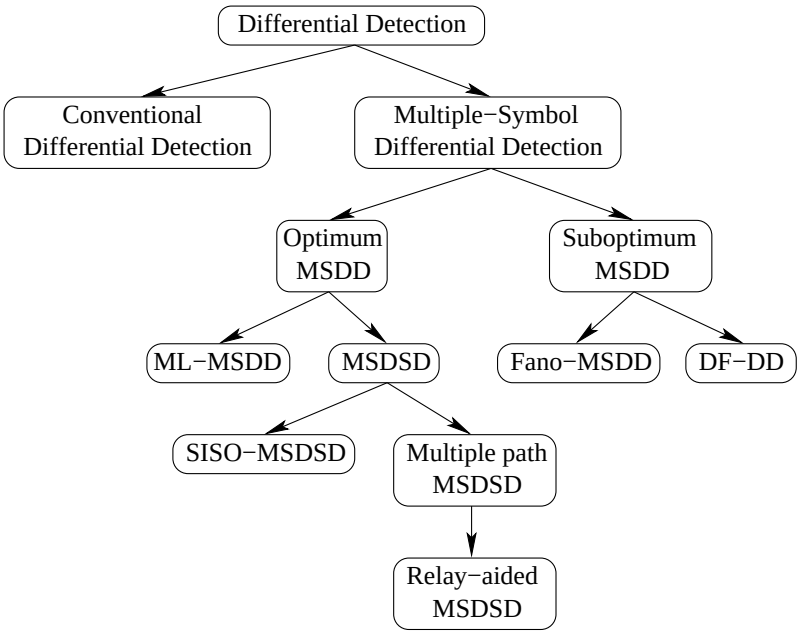

Figure 2.1: Evolution of the multiple-symbol differential detectors: CDD [82], MSDD [49,70], ML-MSDD [50], DF-DD [74], Fano-MSDD [75], MSDSD [53], SISO-MSDSD [55], Multiple-path MSDSD [78], Relay-aided MSDSD [79, 80].

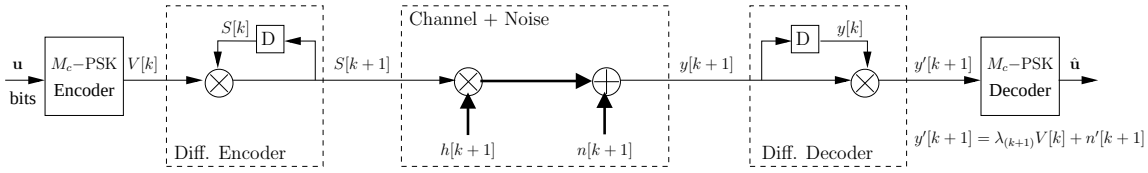

Figure 2.2: General encoding and decoding process of the M_c-DPSK scheme.

$V[k] \in \mathcal{M}_c$ denote the k^{th} information symbol. Consequently, the differentially encoded M_c-DPSK symbol transmitted in the $(k+1)^{st}$ symbol duration is given by

$$S[k+1] = S[k] \cdot V[k] \,, \qquad k = 1, 2, 3, \ldots \tag{2.1}$$

where the first reference symbol $S[1]$ is normally fixed to unity. After propagating via a narrow-band flat-fading Rayleigh channel whose fading coefficient is represented by $h[k]$, the signals received at the differential decoder may be formulated as

$$y[k] = h[k]S[k] + n[k], \tag{2.2}$$

$$y[k+1] = h[k+1]S[k+1] + n[k+1], \tag{2.3}$$

where $n[k]$ is the AWGN obeying the distribution of $\mathcal{CN}(0, N_0)$.

Assuming that the channel is a slowly fading channel, i.e. the normalized Doppler frequency f_d is low, the adjacent fading coefficients will have a high correlation, which leads to $h[k+1] \approx h[k]$.

Additionally, bearing (2.1) in mind, we may rewrite (2.3) as

$$y[k+1] \approx h[k]S[k]V[k] + n[k+1] = y[k]V[k] + n[k+1] - V[k]n[k]. \tag{2.4}$$

Hence the input of the M_c-PSK demodulator shown on the right-hand side of Figure 2.2 is given by

$$y'[k+1] = \frac{y[k+1]}{y[k]} \approx V[k] + \underbrace{\frac{1}{y[k]}n[k+1] - \frac{V[k]}{y[k]}n[k]}_{\text{Amplified Noise}}. \tag{2.5}$$

Consequently, according to (2.5), the entire DPSK system illustrated in Figure 2.2 may be equivalently treated as a system communicating over an AWGN channel, where the noise variance is approximately doubled. Owing to this noise amplification effect, the DPSK scheme will incur at least 3dB performance loss with regard to its PSK counterpart. This can be verified by comparing the BER curves of the coherent detector to those of the coherent differential detector[1] demonstrated in Figure 2.3. Furthermore, since the assumption of $h[k+1] \approx h[k]$ is readily satisfied by having $f_d = 0.001$, there is only a negligible discrepancy between the BER curves of coherent differential detection and NC differential detection as shown in the bottom-right corner of Figure 2.3.

Channel Model	Narrow-Band Flat-Fading Channel
Normalized Doppler Frequency	$f_d = 0.001$ for Slow-Rayleigh-Fading
	$f_d = 0.03$ for Fast-Rayleigh-Fading
Modulation	4-PSK for Coherent Detection
	4-DPSK for Differential Detection
Detector	Coherent Detector
	Coherent Differential Detector
	NC Differential Detector

Table 2.2: System parameters employed in Figure 2.3

However, the relative mobility of the transmitter with respect to the receiver potentially converts a slow-fading channel into a fast-fading channel. In this case, the channel envelope variation between $h[k+1]$ and $h[k]$ cannot be neglected. Correspondingly, we have to rewrite (2.3) as

$$y[k+1] = h[k+1]S[k]V[k]+n[k+1] = \frac{h[k+1]}{h[k]}y[k]V[k]+n[k+1]-\frac{h[k+1]}{h[k]}V[k]n[k]. \tag{2.6}$$

Consequently, the detailed components of the M_c-PSK demodulator's input are given by

$$y'[k+1] = \frac{y[k+1]}{y[k]} = \lambda_{(k+1)}V[k] + \underbrace{\frac{1}{y[k]}n[k+1] - \lambda_{(k+1)}\frac{V[k]}{y[k]}n[k]}_{\text{Amplified Noise}}, \tag{2.7}$$

[1] In the coherent differential detector, as a benefit of having perfect CSI, it achieves the BER lower bound of the differential detection.

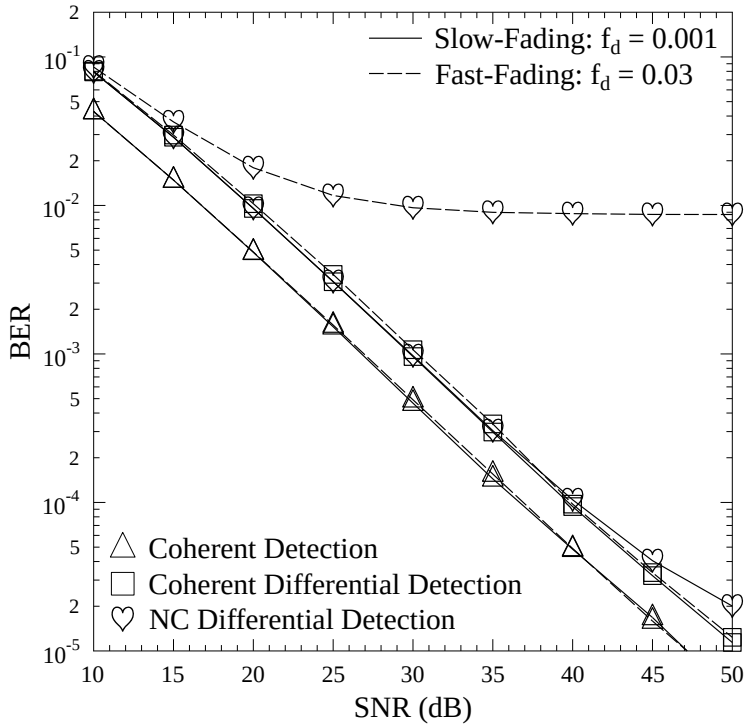

Figure 2.3: BER vs SNR performance comparison among different detection schemes, where $f_d = 0.001$ and $f_d = 0.03$ are employed for the sake of modelling both low-Doppler and high-Doppler Rayleigh-fading, respectively. The results are based on the schematic of Figure 2.2 and the system parameters of Table 2.2.

where we have $\lambda_{(k+1)} = \frac{h[k+1]}{h[k]}$. Upon Comparing (2.7) to (2.5), apparently, an additional amplification factor of $\lambda_{(k+1)}$ is imposed on $V[k]$, which may significantly distort the original information symbols. Hence an error floor will emerge for noncoherent differential detection in fast fading scenarios. This phenomenon is also demonstrated by the BER curves associated with the high-Doppler Rayleigh fading scenario of Table 2.2, as shown in Figure 2.3, where the discrepancy between the BER curves of coherent differential detection and NC differential detection becomes quite substantial.

The CDD technique is capable of achieving a competitive BER performance despite dispensing with CSI in narrow-band slowly fading channels. However, a significant performance degradation occurs, when CDD is applied for rapidly-fading channels. In order to compensate the discrepancy between the BER performance of the CDD and the attainable lower bound of the differential detection, multiple-symbol differential detection (MSDD) was advocated by Divsalar and Simon in [49], which will be discussed in the ensuing section.

2.2 Multiple-Symbol Differential Detection

As argued in Section 2.1, the CDD scheme performs adequately in AWGN and/or narrow-band slow-fading channels for the sake of guaranteeing a competitive BER performance compared to the classic coherent detection schemes. However, when encountering rapidly fading Rayleigh channels, its BER performance degrades significantly, as shown in Figure 2.3. In order to achieve a good performance over rapidly fading Rayleigh channels for NC detection, Divsalar and Simon [49] extended the twin-symbol observation window size of the CDD to multiple-symbol intervals, and made a joint decision on the multiple symbols within the detection window simultaneously. This led to the concept of multiple-symbol differential detection (MSDD) algorithm.

The MSDD algorithm benefits from achieving a higher time-diversity gain by extending the observation window size. Furthermore, the signals received in an observation block carry implicit information about the instantaneous channel gains, which may be interpreted as exploiting channel state information (CSI). Implicitly, this allow the MSDD algorithm to efficiently mitigate the effects of fast fading.

2.2.1 The General Gaussian Problem

Let $\mathbf{V}$ denote an information symbol vector, which consists of $(N-1)$ M_c-PSK information symbols $V[k]$ represented in (2.1), where the information symbol vector $\mathbf{V}$ can be differentially encoded to a DPSK symbol vector $\mathbf{S}$ having a length of N. Observe in Figure 2.2 that after $\mathbf{S}$ experiences a flat Rayleigh fading channel, the differential decoder will receive a signal vector $\mathbf{y}$, which is the distorted version of $\mathbf{S}$. Hence we have the following relationships

$$\begin{aligned}\mathbf{V} &= [V[k+1], V[k+2], \ldots, V[k+N-1]]^T, \\ \mathbf{S} &= [S[k+1], S[k+2], \ldots, S[k+N]]^T, \\ \mathbf{y} &= [y[k+1], y[k+2], \ldots, y[k+N]]^T. \end{aligned} \tag{2.8}$$

Apparently, there are $(M_c)^{N-1}$ legitimate combinations of the information symbol vector $\mathbf{V}$, which may be denoted by the set χ. Hence the challenge encountered by the differential decoder is that of finding the actually transmitted information vector $\mathbf{V}$ out of the whole set χ, when only relying on the received signal vector $\mathbf{y}$. The mathematical principle behind this problem relates to the so-called "general Gaussian problem" [69]. Before discussing it in more depth, several relevant basic mathematical theorems are listed:

1. If every variable in a set of random variables $y[1], y[2], \ldots, y[N]$ individually obeys a normal distribution and all their linear combinations are still Gaussian random variables, we declare the set of random variables $y[1], y[2], \ldots, y[N]$ to be jointly Gaussian.

2. If the elements $y[1], y[2], \ldots, y[N]$ of a vector $\mathbf{y}$ are jointly Gaussian, the vector $\mathbf{y}$ is referred

to a "Gaussian random vector".

3. If $\Pr(\mathbf{y}|\mathbf{S})$ is a Gaussian density conditioned on all hypotheses $\mathbf{S}$, the corresponding hypothesis testing problem is referred to as a general Gaussian problem.

According to the system model described in (2.2), (2.3), the received signals $y[k]$ are uniquely and unambiguously determined by the channel coefficients $h[k]$ and the AWGN noise samples $n[k]$, when the transmitted signals $S[k]$ are given. Since the communication scenario is assumed to be a narrow-band flat block Rayleigh fading channel, both the fading and noise are zero-mean complex-valued Gaussian processes. Hence, according to the theorems stated in the previous paragraph, the received signal vector $\mathbf{y}$ is a "Gaussian random vector", given the associated DPSK symbol vector $\mathbf{S}$. The conditional probability density function (PDF) of a Gaussian random vector was discussed in [69]. Hence, according to the relevant results provided in [69], the conditional PDF of the received signal vector $\mathbf{y}$ - given the transmitted DPSK symbol vector $\mathbf{S}$ - may be formulated as

$$\Pr(\mathbf{y} \mid \mathbf{S}) = \left[(2\pi)^{\frac{N}{2}} \|\mathbf{\Phi}\|^{\frac{1}{2}}\right]^{-1} \exp\left[-\frac{1}{2}\left(\mathbf{y}^T - \mathbf{m}^T\right)\mathbf{\Phi}^{-1}\left(\mathbf{y} - \mathbf{m}\right)\right], \tag{2.9}$$

where the conditional expectation $\mathbf{m}$ and the covariance matrix $\mathbf{\Phi}$ are defined as

$$\mathbf{m} = \begin{bmatrix} m[1] \\ m[2] \\ \vdots \\ m[N] \end{bmatrix} \triangleq \mathcal{E}\left[\mathbf{y} \mid \mathbf{S}\right] = \begin{bmatrix} \mathcal{E}\left(y[k+1] \mid \mathbf{S}\right) \\ \mathcal{E}\left(y[k+2] \mid \mathbf{S}\right) \\ \vdots \\ \mathcal{E}\left(y[k+N] \mid \mathbf{S}\right) \end{bmatrix}, \tag{2.10}$$

$$\mathbf{\Phi} = \mathcal{E}\left[\left(\mathbf{y} - \mathbf{m}\right)\left(\mathbf{y}^T - \mathbf{m}^T\right) \mid \mathbf{S}\right], \tag{2.11}$$

respectively.

Accordingly, the solution of the general Gaussian problem encountered at the differential decoder of Figure 2.2 is to select the optimum DPSK symbol vector $\hat{\mathbf{S}}$ out of all the $(M_c)^{N-1}$ legitimate vectors, which maximizes the conditional PDF presented in (2.9). This decision rule can be formulated as

$$\hat{\mathbf{S}} = \arg\max_{\mathbf{S}\in\chi}\{\Pr\left(\mathbf{y} \mid \mathbf{S}\right)\}. \tag{2.12}$$

2.2.2 Evolution of the MSDD Decision Rule

After extending the observation window to multiple symbols, the MSDD algorithm has to make a decision on the DPSK symbol vector $\mathbf{S}$ which consists of the N symbols $\left[S[k+1], S[k+2], \ldots, S[k+N]\right]^T$ within the observation window. As stated in Section 2.2.1, this decision belongs to the family of general Gaussian problems. Hence, according to (2.12), the crucial problem encountered in MSDD is that of choosing the optimum DPSK symbol vector $\hat{\mathbf{S}}$, which maximizes the conditional PDF, given the received signal vector $\mathbf{y}$.

However, directly implementing the MSDD algorithm according to the decision rule formulated in (2.12) will lead to the conventional brute-force research, which imposes a potentially excessive decoding complexity. Accordingly, Ho and Fung [71] rewrote the specific form of the conditional PDF given in (2.12), which constituted the foundation and inspiration for Lampe *et al.* [53] to devise the state-of-the-art MSDSD algorithm. In more detail, the generalized conditional PDF presented in (2.12) may be rewritten as

$$\Pr\left(\mathbf{y} \mid \mathbf{S}\right) = \frac{1}{(2\pi)^{\frac{N}{2}} \|\mathbf{\Phi_{yy}}\|^{\frac{1}{2}}} \exp\left(-\frac{1}{2}\mathbf{y}^H {\mathbf{\Phi_{yy}}}^{-1}\mathbf{y}\right), \tag{2.13}$$

where N denotes the observation window size, i.e the length of the DPSK symbol vector $\mathbf{S}$, which is also identical to that of the received signal vector $\mathbf{y}$. Then the correlation matrix is given by

$$\mathbf{\Phi_{yy}} \triangleq \mathrm{diag}\left\{\mathbf{S}\right\}\left\{\mathcal{E}\left\{\mathbf{H}\mathbf{H}^H\right\} + \sigma_n^2\mathbf{I}_N\right\}\mathrm{diag}\left\{\mathbf{S}^*\right\}, \tag{2.14}$$

where we have $\mathbf{H} = [h[k+1], h[k+2], \ldots, h[k+N]]^T$, $\mathbf{I}_N$ is an N-dimensional identity matrix and $\sigma_n^2 = N_0$ is the noise variance.

Let us now discuss the evaluation of the expectation $\mathcal{E}\{\mathbf{H}\mathbf{H}^H\}$ involved in (2.14), which may be formulated as

$$\begin{aligned}\mathcal{E}\left\{\mathbf{H}\mathbf{H}^H\right\} &= \mathcal{E}\left\{\begin{bmatrix} h[k+1] \\ h[k+2] \\ \vdots \\ h[k+N] \end{bmatrix}\left[h^*[k+1], h^*[k+2], \ldots, h^*[k+N]\right]\right\} \\ &= \begin{bmatrix} \varphi(0) & \varphi(1) & \cdots & \varphi(N-1) \\ \varphi(-1) & \varphi(0) & \cdots & \varphi(N-2) \\ \vdots & \vdots & \ddots & \vdots \\ \varphi(1-N) & \varphi(2-N) & \cdots & \varphi(0) \end{bmatrix}_{N\times N}, \end{aligned} \tag{2.15}$$

where, according to the widely used Clarke model [83], the channel's autocorrelation function is defined as

$$\varphi(\kappa) \triangleq \mathcal{E}\left\{h[k+\kappa]h^*[k]\right\} = J_0\left(2\pi f_d \kappa\right), \tag{2.16}$$

with $J_0(\cdot)$ representing the zero-order Bessel function of the first kind.

Based on Equations (2.14), (2.15), and (2.16), it becomes possible to obtain the exact value of the correlation matrix $\mathbf{\Phi_{yy}}$ after specifying the associated DPSK symbol vector $\mathbf{S}$. As a further step, it was demonstrated in [71] that when the amplitude of any legitimate DPSK symbol $S[k]$ is fixed to unity, the determinant $\|\mathbf{\Phi_{yy}}\|$ in (2.13) becomes independent of the DPSK symbol vector $\mathbf{S}$. Hence, when comparing the values of the conditional PDF corresponding to different DPSK symbol vectors, we only have to concentrate our attention on the $\left(\mathbf{y}^H {\mathbf{\Phi_{yy}}}^{-1}\mathbf{y}\right)$ part at the right hand size of (2.13). Since the conditional PDF $\Pr\left(\mathbf{y} \mid \mathbf{S}\right)$ in (2.13) is a monotonically decreasing function of the metric $\left(\mathbf{y}^H {\mathbf{\Phi_{yy}}}^{-1}\mathbf{y}\right)$, maximising $\Pr\left(\mathbf{y} \mid \mathbf{S}\right)$ over the entire set of $\mathbf{S}$ is equivalent

to minimising $\left(\mathbf{y}^H {\mathbf{\Phi_{yy}}}^{-1}\mathbf{y}\right)$ over the entire set of $\mathbf{S}$. Finally, the decision rule presented in (2.12) is simplified to

$$\hat{\mathbf{S}} = \arg\min_{\mathbf{S}} \left\{\mathbf{y}^H {\mathbf{\Phi_{yy}}}^{-1}\mathbf{y}\right\}. \tag{2.17}$$

2.3 Multiple-Symbol Differential Sphere Decoding

As stated at the beginning of this chapter, Mackenthun's low-complexity ML-MSDD algorithm [50] obviated the brute-force search problem incurred in Divsalar's original MSDD algorithm [49]. Correspondingly, the complexity of implementing the ML-MSDD algorithm for the DPSK symbol vector $\mathbf{S}$ consisting of N DPSK symbols is reduced to $N\log_2(N)$. However, the ML-MSDD algorithm proposed in [50] is only applicable to AWGN channels and to flat block-fading Rayleigh channels, where the Rayleigh channel gains $h[k]$ remain constant over the observation window consisting of N symbol periods. Between the consecutive observation windows, this block-fading Rayleigh channel is typically assumed to fluctuate independently from block to block. In order to overcome the high decoding complexity encountered in the context of conventional time-variant flat Rayleigh fading channels, Lampe *et al.* [53] devised the state-of-the-art NC detection philosophy, namely the MSDSD, which is based on the refined decision metric proposed in [71].

Hence, we firstly highlight and interpret the mathematical derivation of the MSDSD algorithm in Section 2.3.1. In the ensuing Section 2.3.2, we then further clarify the resultant sphere decoding regime in the context of multiple-symbol differential decoding. Finally, we present our simulation results in Section 2.3.3 for characterising the error correction capability and complexity reduction of the MSDSD algorithm.

2.3.1 Mathematical Principles of MSDSD

The correlation matrix $\mathbf{\Phi_{yy}}$ defined in (2.14) may also be represented as $\mathbf{\Phi_{yy}} \triangleq \mathrm{diag}\{\mathbf{S}\}\mathbf{C}\mathrm{diag}\{\mathbf{S}^*\}$, where we have $\mathbf{C} \triangleq \mathcal{E}\{\mathbf{H}\mathbf{H}^H\} + \sigma_n^2\mathbf{I}_N$. Correspondingly, the decision rule formulated in (2.17) may be rewritten as

$$\begin{aligned}
\hat{\mathbf{S}} &= \arg\min_{\mathbf{S}} \left\{\mathbf{y}^H {\mathbf{\Phi_{yy}}}^{-1}\mathbf{y}\right\} \\
&= \arg\min_{\mathbf{S}} \left\{\mathbf{y}^H \left[\mathrm{diag}\{\mathbf{S}\}\mathbf{C}\mathrm{diag}\{\mathbf{S}^*\}\right]^{-1}\mathbf{y}\right\} \\
&= \arg\min_{\mathbf{S}} \left\{\mathbf{y}^H \mathrm{diag}\{\mathbf{S}\}\mathbf{C}^{-1}\mathrm{diag}\{\mathbf{S}^*\}\mathbf{y}\right\} \\
&= \arg\min_{\mathbf{S}} \left\{\left(\mathrm{diag}\{\mathbf{y}\}\mathbf{S}^*\right)^H \mathbf{C}^{-1}\left(\mathrm{diag}\{\mathbf{y}\}\mathbf{S}^*\right)\right\}.
\end{aligned} \tag{2.18}$$

Then, upon applying the Cholesky factorization of the inverse matrix $\mathbf{C}^{-1}$, we arrive at $\mathbf{C}^{-1} = \mathbf{F}^H\mathbf{F}$, where $\mathbf{F}$ is a upper triangular matrix. If we define furthermore $\mathbf{U} \triangleq \left(\mathbf{F}\mathrm{diag}\{\mathbf{y}\}\right)^*$, then we

arrive at

$$\begin{aligned}\hat{\mathbf{S}} &= \arg\min_{\mathbf{S}} \left\{ \left(\mathrm{diag}\{\mathbf{y}\}\mathbf{S}^*\right)^H \mathbf{F}^H \mathbf{F} \left(\mathrm{diag}\{\mathbf{y}\}\mathbf{S}^*\right) \right\} \\ &= \arg\min_{\mathbf{S}} \left\{ \left(\mathbf{F}\mathrm{diag}\{\mathbf{y}\}\mathbf{S}^*\right)^H \left(\mathbf{F}\mathrm{diag}\{\mathbf{y}\}\mathbf{S}^*\right) \right\} \\ &= \arg\min_{\mathbf{S}} \left\{ \left(\mathbf{U}^*\mathbf{S}^*\right)^H \left(\mathbf{U}^*\mathbf{S}^*\right) \right\} \\ &= \arg\min_{\mathbf{S}} \left\{ \|\mathbf{U}\mathbf{S}\|^2 \right\}, \end{aligned} \tag{2.19}$$

where, the notation $\|\cdot\|$ denotes the euclidean norm.

Observe by scrutinising the new decision metric $\|\mathbf{U}\mathbf{S}\|^2$ in (2.19) that the MSDD can be regarded as a "shortest vector problem", which may be efficiently solved by sphere detection [52, 84]. Accordingly, the new decision rule given in (2.19) may be evaluated with the aid of the sphere detection regime. We will demonstrate that the resultant MSDSD algorithm is capable of significantly mitigating the decoding complexity without degrading the BER performance.

2.3.2 Sphere Decoding Algorithm

According to the sphere decoding strategy [84], the specific DPSK symbol vectors $\hat{\mathbf{S}}$, which are located within a sphere of radius R, for which we have $\|\mathbf{U}\hat{\mathbf{S}}\|^2 \leq R^2$ will be temporarily regarded as the potential candidates. By contrast, the DPSK symbol vectors $\hat{\mathbf{S}}$, which violate the condition of $\|\mathbf{U}\hat{\mathbf{S}}\|^2 \leq R^2$ will be excluded from the search. The above-mentioned test is repeated along with a gradually reduced sphere radius R, until only the optimum candidate vector $\hat{\mathbf{S}}$ lies within the sphere. This process is exemplified in Figure 2.4, where an observation window of $N = 5$ and a differentially-encoded 4-DPSK differential-detection aided modulation scheme are employed.

Let $u_{i,j}, 1 \leq i, j \leq N$ denote the element in the i^{th} row, and j^{th} column of the matrix $\mathbf{U}$. Correspondingly, the matrix $\mathbf{U}$ involved in (2.19) may be formulated as

$$\mathbf{U} = \begin{bmatrix} u_{1,1} & u_{1,2} & \cdots & u_{1,N} \\ 0 & u_{2,2} & \cdots & u_{2,N} \\ \vdots & \vdots & \ddots & \vdots \\ 0 & 0 & \cdots & u_{N,N} \end{bmatrix}_{N \times N}. \tag{2.20}$$

Since it has an upper triangular form, we may carry out the sphere decoding in a component-wise manner. Bearing in mind that we have $\hat{\mathbf{S}} = \left[\hat{S}[1], \hat{S}[2], \ldots, \hat{S}[N]\right]^T$, the accumulated squared distance accounting for the last $(N - i)$ components of $\hat{\mathbf{S}}$, i.e. $\left[\hat{S}[i+1], \hat{S}[i+2], \ldots, \hat{S}[N]\right]^T$ is formulated as

$$d_{i+1}^2 = \sum_{l=i+1}^{N} \left| \sum_{j=l}^{N} u_{l,j} \hat{S}[j] \right|^2, \tag{2.21}$$

which is a fraction of the total Euclidean distance $\|\mathbf{U}\hat{\mathbf{S}}\|^2$. Assuming that the last $(N - i)$ components of $\hat{\mathbf{S}}$ have already satisfied the condition of $d_{i+1}^2 \leq R^2$, the potential DPSK symbols for $\hat{S}[i]$

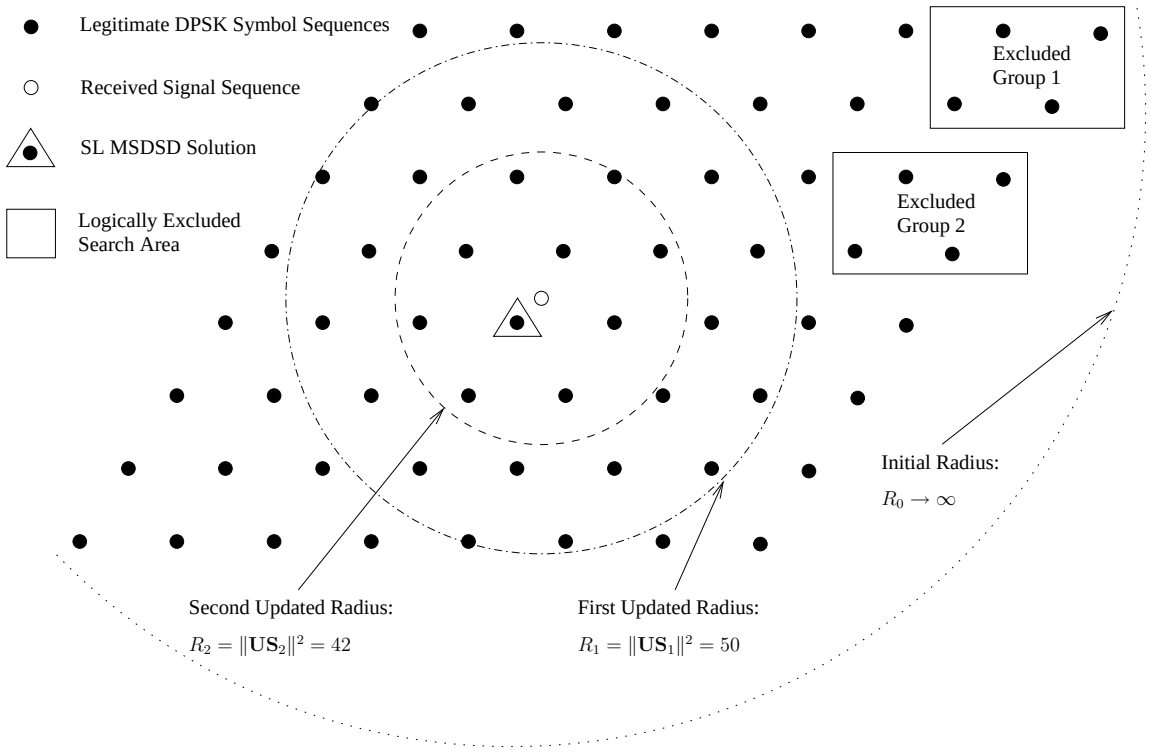

Figure 2.4: Search space of the single-link MSDSD, which is further discussed in Figure 2.5. Since we have $N = 5$, there are $M_c^{N-1} = 4^4 = 256$ legitimate DPSK symbol sequence $\hat{\mathbf{S}}$, but to avoid obfuscating details, we only depict part of them, which are explicitly labelled by 64 black dots. Then, the original signal sequence $\mathbf{S}$ will incur an amplitude attenuation and phase rotation of its component 4-DPSK symbols. Hence the received signal sequence represented by the hollow circle in the centre cannot fall on to any of the legitimate DPSK symbol sequences. Instead, it has a certain distance from the black dots. Hence, our MSDSD algorithm aims for finding the black dot, which has the minimum distance from the hollow circle, which is deemed to be the original signal sequence $\mathbf{S}$.

have to satisfy the condition

$$d_i^2 = \left| u_{i,i}\hat{S}[i] + \sum_{j=i+1}^{N} u_{i,j}\hat{S}[j] \right|^2 + d_{i+1}^2 \leq R^2. \tag{2.22}$$

Having introduced the above criterion to be tested for every component $\hat{S}[i]$, the detailed sphere decoding process may be summarised with reference to Figures 2.4 and 2.5 as follows:

1. As seen in Figure 2.4, during the first search round, the initial sphere radius R is set to infinity, i.e. we have $R_0 \to \infty$. The received 5-symbol sequence is indicated by the white spot in Figure 2.4, whose Euclidean distance with regard to a legitimate symbol sequence is evaluated on a symbol-by-symbol basis using (2.22).

The last component $\hat{S}[N]$ of $\hat{\mathbf{S}}$ is regarded as the reference symbol, which is fixed to the 4-DPSK symbol of "$\underline{00}$". A right-to-left search direction is adopted, where the sphere decoding search commences from $\hat{S}[N-1]$ next to the known reference symbol and terminates at $\hat{S}[1]$.

Once the right-to-left search approaches its last stage in Figure 2.5, i.e. i is reduced to $i = 1$, the sphere radius of the MSDSD algorithm will be updated. This process is represented by the dash-dotted line in Figure 2.5. In more detail, its reference symbol in Figure 2.5 is $\hat{S}[5]$, which is fixed to the known 4-DPSK symbol "$\underline{00}$". Observe in Figure 2.5 that when the search path approaches $\hat{S}[1]$, the temporary hypothesis of $\hat{\mathbf{S}}_1 = [\underline{00}\ \underline{00}\ \underline{11}\ \underline{10}\ \underline{00}]$ is obtained for the path marked by the dash-dotted line. Its associated Euclidean distance $\|\mathbf{U}\hat{\mathbf{S}}_1\|^2$ is utilized as the new sphere radius, which leads to $R_1 = 50$ in Figure 2.5.

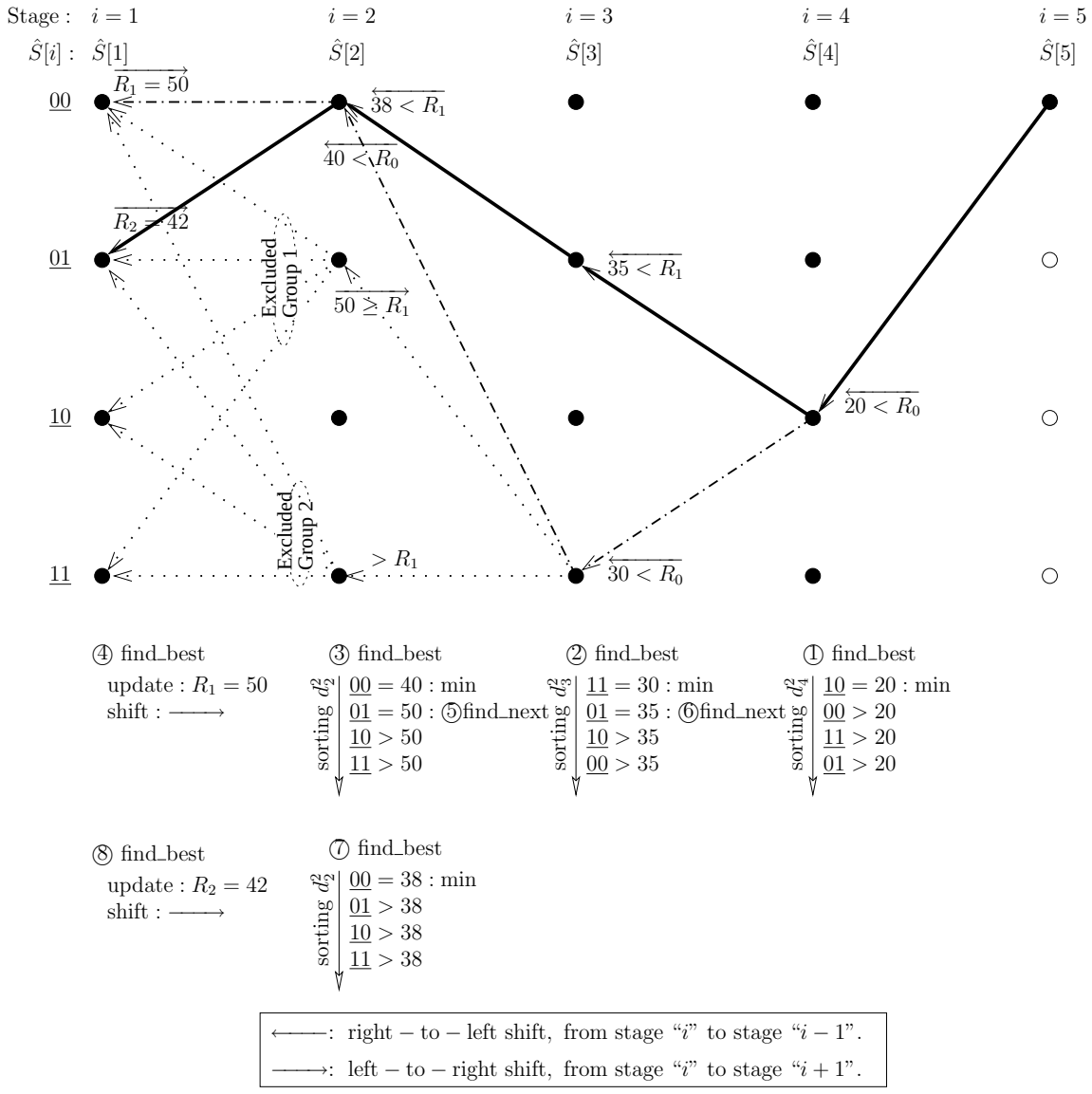

Figure 2.5: Search path of a single-link MSDSD, where an observation window of $N = 5$ and a 4-DPSK modulation scheme are employed.

When the sphere decoding process approaches the i^{th} stage, the specific legitimate DPSK

symbol, which yields the minimum accumulated squared distance of d_i^2 is recorded as the current candidate for $\hat{S}[i]$. Meanwhile, the remaining (M_c-1) legitimate DPSK symbols are arranged in an increasing order sorted according to their associated d_i^2 values as exemplified in Figure 2.5. These d_i^2 based minimization and sorting operations are represented by the "$\mathrm{find\_best}$" function, which is detailed in [53]. The "$\mathrm{find\_best}$" operation is always triggered by a right-to-left search stage shift through the search path. For example, observe at the right hand side of Figure 2.5 that the search path shifts from stage $i = 5$ to stage $i = 4$, which triggers the operation "① $\mathrm{find\_best}$". After implementing the "① $\mathrm{find\_best}$" operation, the SL MSDSD decoder finds that currently the 4-DPSK symbol "$\underline{10}$" is the best candidate for $\hat{S}[4]$, which has the minimum accumulated squared distance of $d_4^2 = 20$. All the legitimate 4-DPSK symbols are sorted in the increasing order of their accumulated squared distance of d_4^2.

2. After the first search round terminates at $\hat{S}[1]$ of Figure 2.5, the search stage shifts from left to right by one step, i.e. the symbol index i is increased from $i = 1$ to $i = 2$. This shift of search stage is represented by "$\mathrm{shift}: \longrightarrow$" under the operation label "④ $\mathrm{find\_best}$" in Figure 2.5. Consequently, $\hat{S}[2]$ is tested again. The previous candidate $\hat{S}[2] = \underline{00}$ tested during the previous search round is replaced by that specific legitimate DPSK symbol, which yields the minimum d_i^2 among the remaining legitimate DPSK symbols that have not as yet been considered as the candidate symbol for $\hat{S}[2]$. Again, this operation was referred to as "$\mathrm{find\_next}$" function in [53], which is always triggered by a left-to-right shift of the search path.

   In more detail, the above mentioned "$\mathrm{find\_next}$" operation is represented by the label that "⑤ $\mathrm{find\_next}$" in Figure 2.5. Then the single-link MSDSD decoder recognizes that the accumulated squared distance of the second candidate "$\underline{01}$" has exceeded the current sphere radius of R_1, i.e. we have $50 \geq R_1$. Since the accumulated squared distance in (2.22) increases monotonically as the search path shifts from right to left, i.e. as we reduce the symbol index i, we can anticipate that the four dotted search paths marked by the "Excluded Group 1" vertical ellipsoidal label will yield larger Euclidean distances compared to R_1. This implies that the differential symbol sequences corresponding to these four dotted search paths emerging from $\hat{S}[2] = \underline{01}$ can be reasonably excluded from the search without evaluating their Euclidean distances according to (2.22). In the same spirit, the legitimate differential symbol sequences marked by the "Excluded Group 2" vertical ellipsoidal label can also be excluded from the search without evaluating their Euclidean distances according to (2.22).

   In general, if we have $d_i^2 \geq R_{\text{current}}^2$, it is logical that regardless of the first $(i-1)$ components of $\hat{\mathbf{S}}$, i.e. regardless of $\left[\hat{S}[1], \hat{S}[2], \cdots, \hat{S}[i-1]\right]^T$, the Euclidean distance $\|\mathbf{U}\hat{\mathbf{S}}\|^2$ will exceed the current sphere radius R_{current}^2, if the current sub-vector $\left[\hat{S}[i], \hat{S}[i+1], \ldots, \hat{S}[N]\right]^T$ is employed as the last $(N-i+1)$ components of the final decision $\hat{\mathbf{S}}$. This implies that $M_c^{(i-1)}$ legitimate combinations of $\hat{\mathbf{S}}$ are justifiably excluded from the search space, hence we

dispense with evaluating their associated Euclidean distances. As a benefit, the brute-force maximum-likelihood search is obviated. Again, this benefit of sphere decoding is also visualized in Figure 2.4, where the "Excluded Group 1" and "Excluded Group 2" are explicitly emphasized.

Still considering Figure 2.5, after implementing "⑤ $\mathrm{find\_next}$", we have "$50 \geq R_1$" for $\hat{S}[2] = \underline{01}$. Hence we further shift from left to right by one stage, i.e. the symbol index i is increased to $i = 3$. Consequently, the "$\mathrm{find\_next}$" operation is triggered again, which is represented by the label "⑥ $\mathrm{find\_next}$". Since the accumulated squared distance d_3^2 associated with $\hat{S}[3] = \underline{01}$ equals to 35, which is smaller than R_1, the search path emerges from $\hat{S}[3] = \underline{01}$ and a shift from right to left by one stage takes place. Consecutively, this right-to-left search stage shift triggers the "$\mathrm{find\_best}$" operation, which is represented by the label "⑦ $\mathrm{find\_best}$", where the best candidate for $\hat{S}[2]$ relying on the tentative assumption that the sub-vector of $\left[\hat{S}[3], \hat{S}[4], \hat{S}[5]\right]$ is set to $\left[\underline{01}\ \underline{10}\ \underline{00}\right]$ is retested. We find that $\hat{S}[2] = \underline{00}$ is the best candidate, which yields an accumulated squared distance of $d_2^2 = 38$. Since the current accumulate squared distance still satisfies $38 < R_1$, the search path shifts from right to left and approaches the last stage of $i = 1$ again. After implementing "⑧ $\mathrm{find\_best}$", the 4-DPSK symbol $\underline{01}$ is considered as the best candidate for $\hat{S}[1]$ relying on the tentative assumption that the sub-vector of $\left[\hat{S}[2], \hat{S}[3], \hat{S}[4], \hat{S}[5]\right]$ is set to $\left[\underline{00}\ \underline{01}\ \underline{10}\ \underline{00}\right]$. This test yields an accumulated squared distance of $d_1^2 = 42$. The whole process described above and labelled by "⑥ $\mathrm{find\_next}$", "⑦ $\mathrm{find\_best}$", and "⑧ $\mathrm{find\_best}$" constitutes a new search path, which is represented by the solid line in Figure 2.5.

Consequently, the sphere radius R is updated by the newest d_1^2, which yields a tightened sphere radius of $R_2 = 42$. This is also shown in Figure 2.4. Simultaneously, a better differential symbol sequence of $\hat{\mathbf{S}}_2 = [\underline{01}\ \underline{00}\ \underline{01}\ \underline{10}\ \underline{00}]$ associated with the solid search path in Figure 2.5 is gained.

3. In general, if we have $d_i^2 < R_{\text{current}}^2$, the sphere decoding stage will shift from right to left by one step, i.e. i is reduced by one. Consecutively, the "$\mathrm{find\_best}$" operation is implemented for the new search stage. By contrast, if we have $d_i^2 \geq R_{\text{current}}^2$, the sphere decoding stage will shift from left to right by one step, i.e. i is increased by one. Hence, the "$\mathrm{find\_next}$" operation is implemented for the new search stage. This compare-shift-select (CSS) process is visualized in Figure 2.6.

   The compare-shift-select (CSS) search process described above will be repeated, until either all the possible combinations of $\hat{\mathbf{S}}$ are evaluated or they are excluded from the search space.

Additionally, as summarized above, we have to order the legitimate DPSK symbols for $\hat{S}[i]$ according to their d_i^2 values during the sphere decoding process. A plausible method is that of calculating d_i^2 for every legitimate DPSK symbol and then comparing them. However, this imposes a high complexity owing to its brute-force search style. Fortunately, an intelligent ordering method

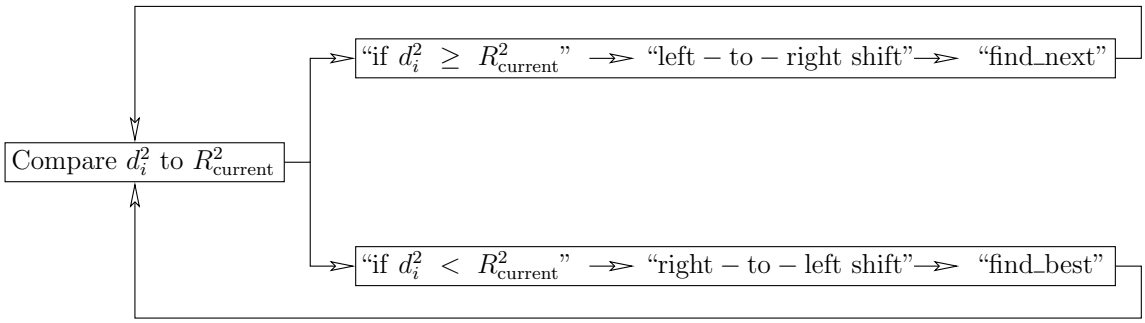

Figure 2.6: Compare-shift-select (CSS) operation of the sphere decoding process.

was proposed in [53], which is capable of directly finding the optimum candidate $\hat{S}[i]$, and then accomplishing the ordering by simply "zigzagging" through the M_c-ary DPSK constellation. Hence the decoding complexity of MSDSD is further mitigated.

In more detail, we provide the pseudo-codes of the functions "$\mathrm{find\_best}$" and "$\mathrm{find\_next}$" in Table 2.3, where k_i is given by the component $\sum_{j=i+1}^{N} u_{i,j}\hat{S}[j]$ of (2.22) and $u_{i,i}$ has the same definition as that involved in (2.22). The constellation of the i^{th} M_c-ary DPSK symbol may be defined as

$$\mathcal{M}_c \in \left\{ e^{j\frac{2\pi}{M_c}m_i}; \quad m_i = 0, 1, \ldots, M_c - 1 \right\}. \tag{2.23}$$

Hence, m_i is used for indicating the index of the selected symbol and step_i determines the action to be adopted by the next candidate. Furthermore, the function $\mathrm{angle}(\cdot)$ returns the angle of a variable, while the function $\mathrm{sign}(\cdot)$ returns the sign of a variable, which is defined as

$$\mathrm{sign}(x) = \begin{cases} 1, & \text{if } x \geq 0 \\ -1, & \text{if } x < 0. \end{cases} \tag{2.24}$$

Then, we detail the "zigzagging" process implemented during the action labelled by "① $\mathrm{find\_best}$"

$$\begin{aligned}
[m_i, \mathrm{step}_i] &= \mathrm{find_best}(k_i, u_{i,i}) \\
k_i &= \sum_{j=i+1}^{N} u_{i,j}\hat{S}[j] && \text{——①} \\
p &= \frac{M_c}{2\pi}\left(\mathrm{angle}\left(-\frac{k_i}{u_{i,i}}\right)\right) && \text{——②} \\
m_i &= \lfloor p \rceil && \text{——③} \\
\mathrm{step}_i &= \mathrm{sign}(p - m_i) && \text{——④}
\end{aligned}$$

$$\begin{aligned}
[m_i^{\mathrm{new}}, \mathrm{step}_i^{\mathrm{new}}] &= \mathrm{find_next}\left(m_i^{\mathrm{old}}, \mathrm{step}_i^{\mathrm{old}}\right) \\
m_i^{\mathrm{new}} &= m_i^{\mathrm{old}} + \mathrm{step}_i^{\mathrm{old}} && \text{——⑤} \\
\mathrm{step}_i^{\mathrm{new}} &= -\mathrm{step}_i^{\mathrm{old}} - \mathrm{sign}(\mathrm{step}_i^{\mathrm{old}}) && \text{——⑥}
\end{aligned}$$

Table 2.3: Pseudo-codes of the "find_best" and "find_next" functions.

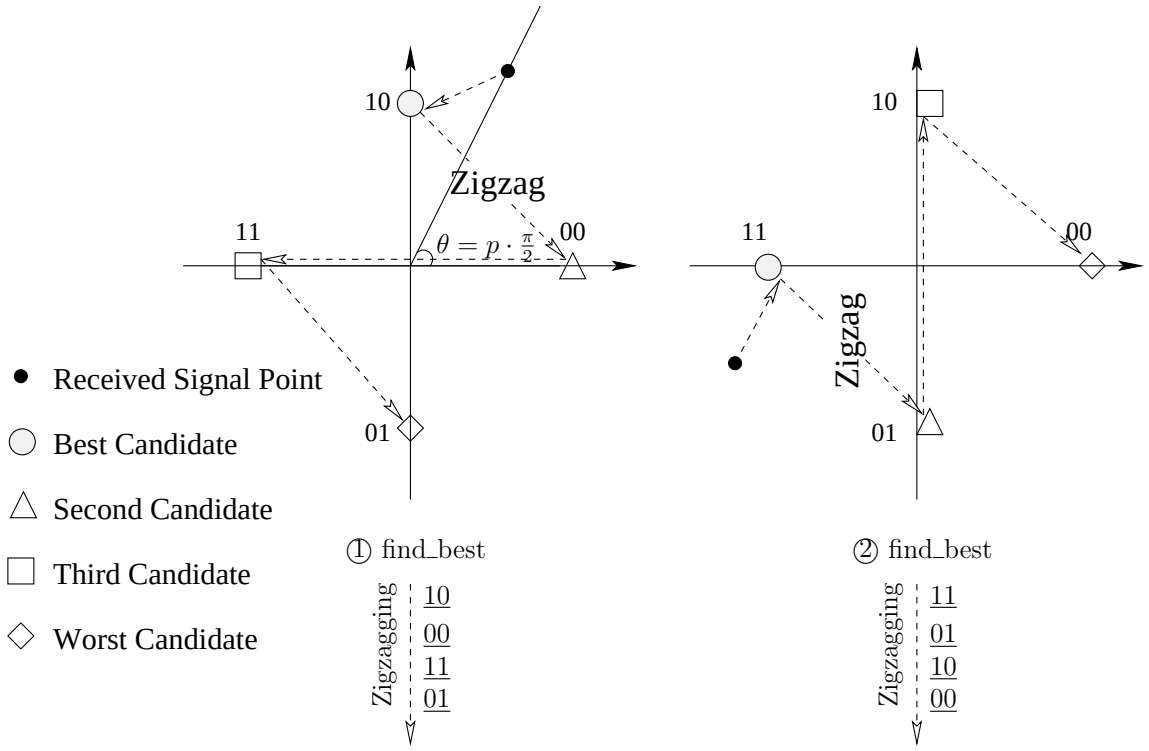

Figure 2.7: Zigzagging process involved in the "① find_best" and "② find_best" of Figure 2.5.

in Figure 2.5 as an example. Observe in Figure 2.5 that when focusing on "① find_best", the symbol index is fixed to $i = 4$. Meanwhile, we assume that the related variables k_4 and $u_{4,4}$ have the values of $k_4 = 1.2\mathrm{e}^{j2\pi 0.175}$ and $u_{4,4} = -1\mathrm{e}^{j0}$, respectively. Consequently, the optimization and sorting process may be summarized as follows:

1 Substituting $k_4 = 1.2\mathrm{e}^{j2\pi 0.175}$ and $u_{4,4} = -1\mathrm{e}^{j0}$ into the function $\mathrm{find\_best}(k_i, u_{i,i})$ of Figure 2.5 and executing the code labelled by ② in Table 2.3, we obtain $p = 0.7$. The value of p may be regarded as the degree of the received signal point in the constellation. Hence the variable p indicates the geometric relationship between the received signal and the legitimate DPSK symbols, which is also illustrated in Figure 2.7 by the labelling $\theta = p \cdot \frac{\pi}{2}$. After implementing the pseudo-code labelled by ③ in Table 2.3, we arrive at $m_4 = 1$. According to (2.23), the best candidate for $\hat{S}[4]$ is the DPSK symbol "$\underline{10}$". Meanwhile, the adjustment required for approaching the second-best candidate, which has the second-best Euclidean distance from the received signal point is $\mathrm{step}_4 = -1$. This is obtained according to the pseudo-code labelled by ④ in Table 2.3.

2 In order to find the next candidate, namely the one which has the second-best minimum Euclidean distance from the received signal point, the values of $m_4 = 1$ and $\mathrm{step}_4 = -1$ obtained during the above step are substituted into the function "$\mathrm{find\_next}\left(m_i^{\mathrm{old}}, \mathrm{step}_i^{\mathrm{old}}\right)$" as m_i^{old} and $\mathrm{step}_i^{\mathrm{old}}$, respectively. According to the pseudo-code labelled by ⑤ in Table 2.3,

the second-best candidate is given by $m_4^{\text{new}} = m_4^{\text{old}} + \text{step}_4^{\text{old}} = 1 + (-1) = 0$. According to (2.23), $m_4^{\text{new}} = 0$ corresponds to the DPSK symbol "$\underline{00}$", which is labelled by the triangle in Figure 2.7. This process is equivalent to the sorting path's zigzag-route from the circle-"$\underline{10}$" to the triangle-"$\underline{00}$" as shown at the left hand side of Figure 2.7. Meanwhile, the pseudo-code labelled by ⑥ in Table 2.3 indicates that the adjustment required for approaching the third-best candidate when departing from the second-best candidate is $\text{step}_4^{\text{new}} = -(-1) - \text{sign}(-1) = 2$.

3 Repeating the function "$\text{find\_next}\left(m_i^{\text{old}}, \text{step}_i^{\text{old}}\right)$" of Figure 2.5 again, we substitute $m_4^{\text{new}} = 0$ and $\text{step}_4^{\text{new}} = 2$ obtained during the preceding step into it as m_4^{old} and $\text{step}_4^{\text{old}}$, respectively. Similarly, implementing the pseudo-code labelled by ⑤ in Table 2.3 again, the third-best candidate is given by $m_4^{\text{new}} = m_4^{\text{old}} + \text{step}_4^{\text{old}} = 0 + 2 = 2$. This process is equivalent to the event, when the sorting path further zigzags from the triangle-"$\underline{00}$" to the square-"$\underline{11}$", which is also shown at the left hand side of Figure 2.7. Meanwhile, relying on the pseudo-code labelled by ⑥ in Table 2.3 again, the adjustment required for approaching the last candidate is $\text{step}_4^{\text{new}} = -(2) - \text{sign}(2) = -3$.

4 Similarly, implementing the function "$\text{find\_next}\left(m_i^{\text{old}}, \text{step}_i^{\text{old}}\right)$" of Figure 2.5 again, the sorting path will zigzag from the square-"$\underline{11}$" to the last legitimate symbol "$\underline{01}$", which is represented by the diamond at the left hand side of Figure 2.7.

2.3.3 BER versus Complexity of the MSDSD

As mentioned at the beginning of Section 2.2, owing to its time-diversity effect and as a benefit of its action reminiscent of blind-channel-estimation, the MSDSD algorithm is capable of mitigating the impact of fast fading. In order to visualize these effects, the BER versus SNR performance of different decoding strategies are compared in Figure 2.8, where the normalized Doppler frequency and modulation scheme are fixed to $f_d = 0.03$ and 4-DPSK, respectively, for the sake of a fair comparison. The significant discrepancy between the BER curve of conventional noncoherent differential detection and the lower bound of the differential detection constituted by coherent differential detection is mitigated by employing the MSDSD algorithm. For instance, the BER curve of the MSDSD having an observation window of $N = 10$ gets quite close to that of the coherent differential detection.

Furthermore, it was commented by Lampe *et al.* in [53] that "since with growing observation window size N the memory of the fading process is more completely taken into account, the performance of MSDSD shall improve with increasing N". This is confirmed by the fact that around 2dB performance gain is obtained upon increasing the observation window size in Figure 2.8 from 6 to 10 at a target BER 10^{-4}. However, the performance gain obtained upon increasing N will become more and more negligible, whilst the associated decoding complexity increases significantly. Hence, a trade-off has to be struck between the BER performance and associated system

Channel Model	Narrow-Band Flat-Fading Channel
Normalized Doppler Frequency	$f_d = 0.03$ for Fast-Rayleigh-Fading
Modulation	4-PSK for Coherent Detection
	4-DPSK for Differential Detection
Detector	Coherent Detector
	Coherent Differential Detector
	NC Differential Detector
	SL DT based MSDSD
Window Size of MSDSD	$N = 6, 10$

Table 2.4: System parameters employed in Figures 2.8 and 2.9. The parameters that are different from Table 2.2 are shown in bold font.

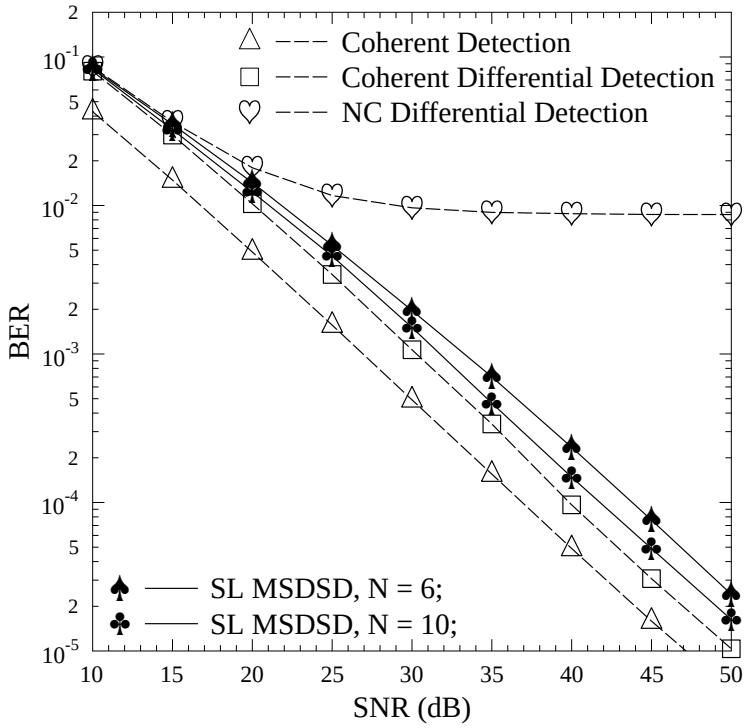

Figure 2.8: BER performance of the single-link (SL) direct-transmission (DT) based MSDSD in a flat Rayleigh fading channel. The BER performance of coherent detection, coherent differential detection, and NC differential detection is also portrayed. The results are based on the system parameters of Table 2.4.

complexity.

The complexity of differential detection is dominated by the evaluation of the Euclidean distance d_i^2 given in (2.22). Hence, in order to quantify the decoding complexity, the average number of Euclidean distance calculation (EDC) required for decoding a single differential symbol sequence $\mathbf{S}$ given in (2.8) is employed as our complexity metric[2]. In more detail, as a reference symbol, the magnitude of the last differential symbol of the observation interval is always fixed to unity and the symbol "$\underline{00}$" may be used for 4-DPSK. Hence there are M_c^{N-1} legitimate combinations of the differential symbol sequence $\mathbf{S}$, which have to be tested by the MSDD algorithm. Correspondingly, the MSDD algorithm has to implement M_c^{N-1} EDC for making a decision for each observation window. In this spirit, the CDD may be treated as a particular MSDD scheme, where the observation interval is fixed to two-symbol durations. Consequently, its EDC metric based complexity is given by $M_c^{N-1} = 4$, when employing a 4-DPSK modulation scheme. Finally, the complexity of our MSDSD algorithm configured for different observation window sizes is characterized in Figure 2.9.

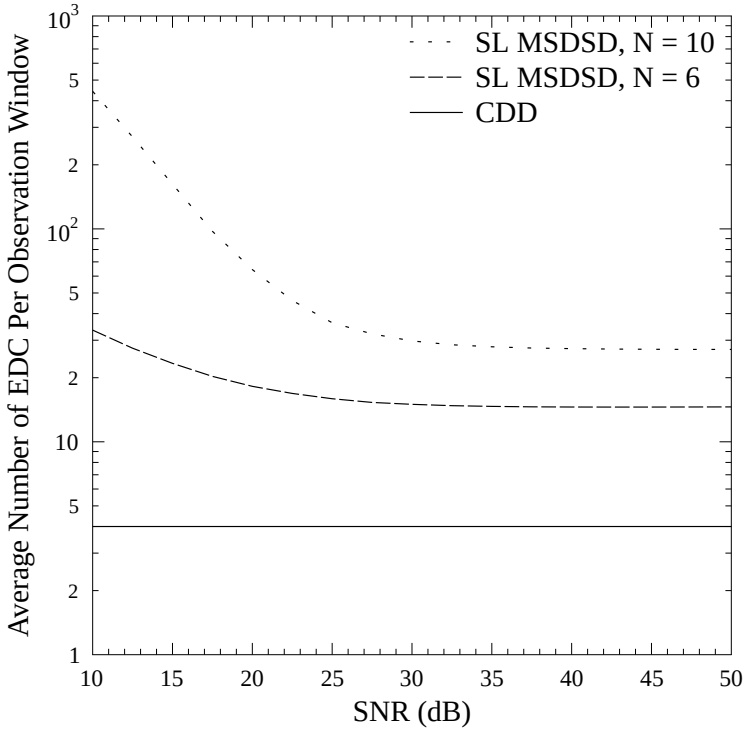

Figure 2.9: Average number of EDC required by the single-link direct-transmission based MSDSD for decoding a single observation interval, where the observation window sizes of $N = 6$ and $N = 10$ are investigated. The corresponding ML search complexities are $M_c^{N-1} = 4^5$ and $M_c^{N-1} = 4^9$, respectively. The results are based on the system parameters of Table 2.4.

[2]The complexity imposed by the sorting operation during the differential decoding process is ignored for the sake of simplifying the complexity comparison among CDD, MSDD, and MSDSD.

Finally, observe in Figure 2.8 that there is still an approximately 3dB gap between the coherent detection and coherent differential detection, which is caused by the noise amplification problem of differential detection, as revealed in (2.7). Hence this performance loss spurs us to further develop the NC differential detection philosophy for compensating this 3dB gap and for the sake of mitigating its performance degradation at high Doppler frequencies. Having characterized the single-link MSDSD, in the next section we consider its multi-link counterpart.

2.4 Multiple-Path Multiple-Symbol Differential Sphere Decoding

In this section we introduce the concept of "multi-path" MSDSD and contrast it to the conventional single-link version of Section 2.3. Explicitly, we refer to it as the "multi-path" MSDSD, because instead of processing a single received signal stream, the multi-path MSDSD is capable of simultaneously processing multiple received signal streams, which are associated with the same original source signal stream and making a joint decision. This is beneficial for example, when combing the signals received both form the source and the relay in cooperative communications.

As reported in Section 2.3.3, we have a performance discrepancy between the BER curve of coherent detection and that of classical MSDSD. Then, the SNR required by the classical MSDSD algorithm for approaching a target BER of 10^{-4} is beyond 40dB when encountering a fast-fading scenario, which is excessive for a practical system. Hence, in order to mitigate the performance gap between coherent detection and MSDSD, as well as to efficiently exploit the attainable spatial diversity, the MSDSD algorithm is considered in the important context of a practical multiple-path propagation scenario.

Transplanting the classical MSDSD algorithm into multiple-path communication scenarios, as exemplified in the relay aided cooperative network of Figure 2.10, was primarily advocated by Wang and Hanzo in [54, 78]. Consequently, the multiple-path Multiple-Symbol Differential Sphere Decoding algorithm was conceived. A remarkable performance gain was achieved, which will be demonstrated in Section 2.4.3.

The system model conceived for the multiple-path MSDSD algorithm is described in Section 2.4.1. Then we focus our attention on the mathematical characterization of the multiple-path MSDSD algorithm in Section 2.4.2, where the final decision rule and its efficient implementation are introduced. Finally, our simulation results are provided in Section 2.4.3.

2.4.1 Typical Application Scenario

A multiple RN aided cooperative communication network is illustrated in Figure 2.10, where the solid lines represent the transmissions during the broadcast phase and the dashed lines indicate the transmissions during the cooperative phase. The AF protocol introduced in Section 1.2.1 is em-

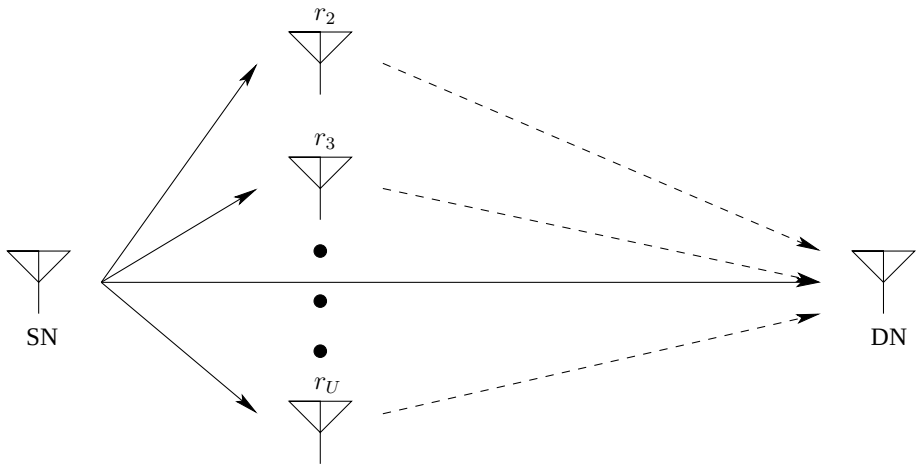

Figure 2.10: Uplink of a multiple relay aided cooperative communication network, where the solid lines represent the transmissions during the broadcast phase and the dashed lines indicate the transmissions during the cooperative phase.

ployed for supporting cooperative communication. Furthermore, we assume that perfectly orthogonal transmissions are supported by the system shown in Figure 2.10 by utilizing any of the classical multiple access techniques, such as time division multiple access (TDMA) relying on time-domain (TD) orthogonality, frequency division multiple access (FDMA) using frequency-domain (FD) orthogonality, or CDMA employing orthogonal spreading codes. Moreover, let $P_a, a \in \{s, r_i\}$ denote the transmit power of node a.

Observe in Figure 2.10 that the DN will receive multiple replicas of the same M_c-ary DPSK symbol $S[k]$ via the orthogonal source-to-destination (SD) and relay-to-destination (RD) links. Assuming that we appoint $(U-1)$ RNs $\{r_i\}_{i=2}^{U}$, the signals received at the DN corresponding to the same source symbol $S[k]$ may be formulated as

$$\mathbf{Y}[k] = \mathbf{S}[k]\mathbf{H}[k] + \mathbf{N}[k], \tag{2.25}$$

where the DPSK source symbol matrix, the Rayleigh flat-fading gain vector and the AWGN vector

are given by

$$\mathbf{S}[k] = \begin{bmatrix} S[k] & 0 & \cdots & 0 \\ 0 & S[k] & \cdots & 0 \\ \vdots & \vdots & \ddots & \vdots \\ 0 & 0 & \cdots & S[k] \end{bmatrix}_{U\times U}, \tag{2.26}$$

$$\mathbf{H}[k] = \begin{bmatrix} \sqrt{P_s}h_{sd}[k] \\ \sqrt{P_s}f_{AM_{r_2}}h_{sr_2}[k]h_{r_2d}[k] \\ \vdots \\ \sqrt{P_s}f_{AM_{r_U}}h_{sr_U}[k]h_{r_Ud}[k] \end{bmatrix}_{U\times 1}, \tag{2.27}$$

$$\mathbf{N}[k] = \begin{bmatrix} n_{sd}[k] \\ f_{AM_{r_2}}h_{r_2d}[k]n_{sr_2}[k] + n_{r_2d}[k] \\ \vdots \\ f_{AM_{r_U}}h_{r_Ud}[k]n_{sr_U}[k] + n_{r_Ud}[k] \end{bmatrix}_{U\times 1}, \tag{2.28}$$

where $S[k]$ was defined in (2.1). Furthermore, $h_{ab}[k], a, b \in \{s, r_i, d\}$ denotes the fading coefficients of the channel between node a and node b while $n_{ab}[k], a, b \in \{s, r_i, d\}$ is the AWGN noise imposed on node b associated with the transmissions from node a to node b, where $n_{ab}[k]$ obeys the distribution of $\mathcal{CN}(0, N_0)$. The amplification factor of the i^{th} RN is defined as $f_{AM_{r_i}} = \sqrt{\frac{P_{r_i}}{P_s\sigma^2_{sr_i}+N_0}}$, which constrains the transmit power of the i^{th} RN to P_{r_i}.

Again, (2.25) describes the single-symbol system model of the network shown in Figure 2.10. When simultaneously observing N consecutively transmitted source symbols, the associated multiple-symbol system model may be formulated as

$$\underline{\mathbf{Y}} = \underline{\mathbf{S}}\mathbf{H} + \underline{\mathbf{N}}, \tag{2.29}$$

where the equivalent channel block vector $\underline{\mathbf{H}}$ and the AWGN block vector $\underline{\mathbf{N}}$ are constituted by vertically stacking N channel gain vectors $\mathbf{H}[k]$ obeying (2.27) and AWGN noise vectors $\mathbf{N}[k]$ formulated in (2.28), respectively, which are further detailed as

$$\underline{\mathbf{H}} = \begin{bmatrix} \mathbf{H}[k+1] \\ \mathbf{H}[k+2] \\ \vdots \\ \mathbf{H}[k+N] \end{bmatrix}_{N\times 1}, \tag{2.30}$$

$$\underline{\mathbf{N}} = \begin{bmatrix} \mathbf{N}[k+1] \\ \mathbf{N}[k+2] \\ \vdots \\ \mathbf{N}[k+N] \end{bmatrix}_{N\times 1}. \tag{2.31}$$

Correspondingly, the equivalent transmitted signal block matrix of (2.29) is given by $\underline{\mathbf{S}} = \mathrm{diag}\{\mathbf{S}[k+1], \mathbf{S}[k+2], \ldots, \mathbf{S}[k+N]\}$. Hence, the received signal block vector $\underline{\mathbf{Y}}$ may also be represented as

$$\underline{\mathbf{Y}} = \left[\mathbf{Y}^T[k+1], \mathbf{Y}^T[k+2], \ldots, \mathbf{Y}^T[k+N]\right]^T, \tag{2.32}$$

where $\mathbf{S}[k]$ and $\mathbf{Y}[k]$ are given in (2.26) and (2.25), respectively.

Example 2.1: Signal Arrangement of the Multiple-Path MSDSD: $U = 2$, $N = 3$

Here, we illustrate the signal arrangement of a specific multiple-path MSDSD application scenario, where we have $U = 2$, $N = 3$. When $U = 2$, the general AF relaying aided twin-phase based cooperative network shown in Figure 2.10 is simplified to the single-relay assisted twin-phase based AF relaying scenario of Figure 1.2. The corresponding general single-symbol system model of (2.25) is simplified to

$$\begin{bmatrix} Y_{sd}[k] \\ Y_{sr_2d}[k] \end{bmatrix} = \begin{bmatrix} S[k] & 0 \\ 0 & S[k] \end{bmatrix} \times \begin{bmatrix} \sqrt{P_s} h_{sd}[k] \\ \sqrt{P_s} f_{AM_{r_2}} h_{sr_2}[k] h_{r_2d}[k] \end{bmatrix} + \begin{bmatrix} n_{sd}[k] \\ f_{AM_{r_2}} h_{r_2d}[k] n_{sr_2}[k] + n_{r_2d}[k] \end{bmatrix}. \tag{2.33}$$

Since $N = 3$, we will amalgamate the DN's signal vectors represented in (2.33) and received during three consecutive time slots, when k increased from $k = 1$ to $k = 3$ according to the method stipulated in (2.29), which is visualized in Figure 2.11.

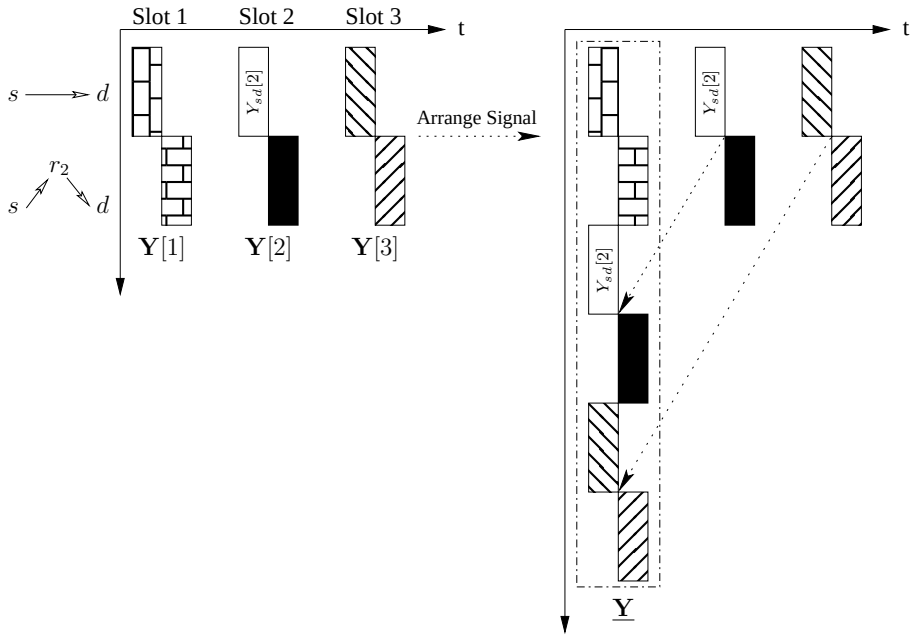

Figure 2.11: The process of combining the DN's signal vectors $\mathbf{Y}[1], \mathbf{Y}[2], \mathbf{Y}[3]$ given in (2.33) into a single vector $\underline{\mathbf{Y}}$ according to the method stipulated by (2.29).

To elaborate a little further, the detailed $\underline{\mathbf{S}}$, $\underline{\mathbf{H}}$, $\underline{\mathbf{N}}$ matrices of (2.29) associated with the

particular instance portrayed in Figure 2.11 are given by

$$\underline{\mathbf{S}} = \begin{bmatrix} S[1] & 0 & 0 & 0 & 0 & 0 \\ 0 & S[1] & 0 & 0 & 0 & 0 \\ 0 & 0 & S[2] & 0 & 0 & 0 \\ 0 & 0 & 0 & S[2] & 0 & 0 \\ 0 & 0 & 0 & 0 & S[3] & 0 \\ 0 & 0 & 0 & 0 & 0 & S[3] \end{bmatrix}, \tag{2.34}$$

$$\underline{\mathbf{H}} = \begin{bmatrix} \sqrt{P_s} h_{sd}[1] \\ \sqrt{P_s} f_{AM_{r_2}} h_{sr_2}[1] h_{r_2 d}[1] \\ \sqrt{P_s} h_{sd}[2] \\ \sqrt{P_s} f_{AM_{r_2}} h_{sr_2}[2] h_{r_2 d}[2] \\ \sqrt{P_s} h_{sd}[3] \\ \sqrt{P_s} f_{AM_{r_2}} h_{sr_2}[3] h_{r_2 d}[3] \end{bmatrix}, \tag{2.35}$$

$$\underline{\mathbf{N}} = \begin{bmatrix} n_{sd}[1] \\ f_{AM_{r_2}} h_{r_2 d}[k] n_{sr_2}[1] + n_{r_2 d}[1] \\ n_{sd}[2] \\ f_{AM_{r_2}} h_{r_2 d}[k] n_{sr_2}[2] + n_{r_2 d}[2] \\ n_{sd}[3] \\ f_{AM_{r_2}} h_{r_2 d}[k] n_{sr_2}[3] + n_{r_2 d}[3] \end{bmatrix}. \tag{2.36}$$

As shown in Figure 2.2, the component $y[k]$ of (2.8) only consists of a single signal sample received at the DN via the single SD link. By contrast, the component $\mathbf{Y}[k]$ in (2.32) consists of multiple replicas of the same original codeword received via independently fading multiple paths, as demonstrated in Figure 2.10. Hence we cannot directly employ the classical single-link MSDSD algorithm introduced in Section 2.3 for realizing the multiple-symbol based differential detection of $\underline{\mathbf{Y}}$ seen in (2.32). In order to extend the multiple-symbol based differential detection technique to the multiple-path scenario shown in Figure 2.10, the multiple-path MSDSD algorithm was devised by Wang and Hanzo in [78].

2.4.2 Mathematical Characterization of the Multiple-Path MSDSD

Our approach in further developing the single-link MSDSD to the multiple-path MSDSD is based on organizing the DN's received signals spanning an observation window in a form similar to that represented in (2.8), as formulated in (2.32). The only potential problem is that the fundamental prerequisite of employing multiple-symbol differential detection, namely that the received signal vector should be a Gaussian vector is not strictly satisfied in the context of the multiple relay aided AF assisted cooperative network considered. This is because, as revealed in (2.27), the equivalent channel fading coefficients involve the multiplications of two Gaussian variables, which are hence

non-Gaussian. However, fortunately, it has been demonstrated in [78, Figure 2] that the components of $\mathbf{H}[k]$ and $\mathbf{N}[k]$ in (2.27) and (2.28) exhibit a near-Gaussian distribution, hence the penalty imposed by this approximation is negligible. Consequently, we can directly substitute the received signal block vector $\underline{\mathbf{Y}}$ of (2.29) into the conditional PDF defined in (2.13). Upon transforming the original ML decision rule defined in (2.17) according to the operations stipulated in (2.18), we arrive at the ML decision rule of the multiple-path MSDSD, which is given by

$$\hat{\mathbf{S}} = \arg\min_{\mathbf{S}} Tr\left\{\underline{\mathbf{Y}}^H \underline{\mathbf{S}}\, \underline{\mathbf{C}}^{-1} \underline{\mathbf{S}}^H \underline{\mathbf{Y}}\right\}. \tag{2.37}$$

The notation $\underline{\mathbf{C}}$ in (2.37) can be evaluated as

$$\underline{\mathbf{C}} \triangleq \mathcal{E}\left\{\underline{\mathbf{H}}\underline{\mathbf{H}}^H\right\} + \mathcal{E}\left\{\underline{\mathbf{N}}\underline{\mathbf{N}}^H\right\}. \tag{2.38}$$

For facilitating the evaluation of $\underline{\mathbf{C}}$, the calculation of $\mathcal{E}\left\{\underline{\mathbf{H}}\underline{\mathbf{H}}^H\right\}$ is explicitly detailed below

$$\begin{aligned}\mathcal{E}\left\{\underline{\mathbf{H}}\underline{\mathbf{H}}^H\right\} &= \mathcal{E}\left\{\begin{bmatrix}\mathbf{H}[k+1]\\ \mathbf{H}[k+2]\\ \vdots \\ \mathbf{H}[k+N]\end{bmatrix}[\mathbf{H}^*[k+1], \mathbf{H}^*[k+2], \ldots, \mathbf{H}^*[k+N]]\right\} \\ &= \begin{bmatrix}\Gamma(0) & \Gamma(1) & \cdots & \Gamma(N-1)\\ \Gamma(-1) & \Gamma(0) & \cdots & \Gamma(N-2)\\ \vdots & \vdots & \ddots & \vdots \\ \Gamma(1-N) & \Gamma(2-N) & \cdots & \Gamma(0)\end{bmatrix}_{UN\times UN},\end{aligned} \tag{2.39}$$

where the notation $\Gamma(\kappa)$ is defined as

$$\Gamma(\kappa) \triangleq \begin{bmatrix} P_s\varphi_{sd}(\kappa) & 0 & \cdots & 0 \\ 0 & P_s\frac{P_{r_2}}{P_s\sigma^2_{sr_2}+N_0}\varphi_{sr_2}(\kappa)\varphi_{r_2d}(\kappa) & \cdots & 0 \\ \vdots & \vdots & \ddots & \vdots \\ 0 & 0 & \cdots & P_s\frac{P_{r_U}}{P_s\sigma^2_{sr_U}+N_0}\varphi_{sr_U}(\kappa)\varphi_{r_Ud}(\kappa)\end{bmatrix}_{U\times U}, \tag{2.40}$$

where the autocorrelation function $\varphi_{ab}(\kappa), a, b \in \{s, r_i, d\}$ of the fading coefficients of the channel between node a and b is given in (2.16). Furthermore, the component $\mathcal{E}\left\{\underline{\mathbf{N}}\underline{\mathbf{N}}^H\right\}$ of (2.38) may be calculated as

$$\mathcal{E}\left\{\underline{\mathbf{N}}\underline{\mathbf{N}}^H\right\} = \mathbf{I}_N \otimes \begin{bmatrix} N_0 & 0 & \cdots & 0 \\ 0 & \left(\frac{P_{r_2}\sigma^2_{r_2d}}{P_s\sigma^2_{sr_2}+N_0}+1\right)N_0 & \cdots & 0 \\ \vdots & \vdots & \ddots & \vdots \\ 0 & 0 & \cdots & \left(\frac{P_{r_U}\sigma^2_{r_Ud}}{P_s\sigma^2_{sr_U}+N_0}+1\right)N_0\end{bmatrix}. \tag{2.41}$$

Hence, upon substituting (2.39) and (2.41) into (2.38), we arrive at $\underline{\mathbf{C}}$ of (2.38).

Before further transforming the decision rule presented in (2.37), we would like to introduce some of the relevant transformation operators. The operator $T_d(\cdot)$ is provided for transforming a vector to a matrix in a particular form. In more detail, let $\mathbf{B}$ denote a vector consisting of N U-element sub-vectors $\mathbf{B}_n$, which can be written as:

$$\mathbf{B} = [\mathbf{B}_1, \mathbf{B}_2, \ldots, \mathbf{B}_N], \tag{2.42}$$

where we have $\mathbf{B}_n = [b_1, b_2, \ldots, b_U]$. When the transformation operator $T_d(\cdot)$ is applied to $\mathbf{B}$, it yields

$$T_d(\mathbf{B}) = \begin{bmatrix} \boldsymbol{\Upsilon}_1 & 0 & \cdots & 0 \\ 0 & \boldsymbol{\Upsilon}_2 & \cdots & 0 \\ \vdots & \vdots & \ddots & \vdots \\ 0 & 0 & \cdots & \boldsymbol{\Upsilon}_N \end{bmatrix}_{UN \times U^2 N}, \tag{2.43}$$

where

$$\boldsymbol{\Upsilon}_n \triangleq \begin{bmatrix} \mathbf{B}_n & 0 & \cdots & 0 \\ 0 & \mathbf{B}_n & \cdots & 0 \\ \vdots & \vdots & \ddots & \vdots \\ 0 & 0 & \cdots & \mathbf{B}_n \end{bmatrix}_{U \times U^2}. \tag{2.44}$$

Then the transformation operator $T_c(\cdot)$ is provided for transforming a matrix to a vector. In more detail, let $\mathbf{A}$ denote a square matrix, which is given by

$$\mathbf{A} = \begin{bmatrix} a_1 & a_{U+1} & \cdots & a_{(U-1)U+1} \\ a_2 & a_{U+2} & \cdots & a_{(U-1)U+2} \\ \vdots & \vdots & \ddots & \vdots \\ a_U & a_{2U} & \cdots & a_{U^2} \end{bmatrix}_{U \times U}. \tag{2.45}$$

Upon applying $T_c(\cdot)$ to the squared matrix $\mathbf{A}$, it yields

$$T_c(\mathbf{A}) = [a_1, \ldots, a_U, a_{U+1}, \ldots, a_{2U}, \ldots, a_{U^2-U+1}, \ldots, a_{U^2}]^T. \tag{2.46}$$

Consequently, given the operators $T_d(\cdot)$ and $T_c(\cdot)$ defined in (2.43) and (2.46), respectively, the metric of (2.37) can be reformulated as

$$\begin{aligned} \hat{\mathbf{S}} &= \arg\min_{\mathbf{S}} Tr\left\{ \left(T_d(\underline{\mathbf{Y}})\, \overline{\mathbf{S}}^* \right)^H \underline{\mathbf{C}}^{-1} T_d(\underline{\mathbf{Y}})\, \overline{\mathbf{S}}^* \right\} \\ &= \arg\min_{\mathbf{S}} Tr\left\{ \overline{\mathbf{S}}^T T_d(\underline{\mathbf{Y}})^H \underline{\mathbf{C}}^{-1} T_d(\underline{\mathbf{Y}})\, \overline{\mathbf{S}}^* \right\}, \end{aligned} \tag{2.47}$$

where we have

$$\begin{aligned} \overline{\mathbf{S}} &= \left[\overline{\mathbf{S}}[k+1], \overline{\mathbf{S}}[k+2], \ldots, \overline{\mathbf{S}}[k+N] \right] \\ &= \left[T_c(\mathbf{S}[k+1])^T, T_c(\mathbf{S}[k+2])^T, \ldots, T_c(\mathbf{S}[k+N])^T \right]^T. \end{aligned} \tag{2.48}$$

Let us generate the $(UN \times UN)$-element upper-triangular matrix $\underline{\mathbf{F}}$, which obeys $\underline{\mathbf{F}}^H \underline{\mathbf{F}} = \underline{\mathbf{C}}^{-1}$ with the aid of Cholesky factorization. Then, by further constructing a $(UN \times U^2N)$-element upper-triangular block matrix $\underline{\mathbf{U}}$ as

$$\begin{aligned} \underline{\mathbf{U}} &\triangleq \left(\underline{\mathbf{F}} T_d\left(\underline{\mathbf{Y}}\right)\right)^* \\ &= \begin{bmatrix} \mathbf{U}_{1,1} & \mathbf{U}_{1,2} & \cdots & \mathbf{U}_{1,N} \\ 0 & \mathbf{U}_{2,2} & \cdots & \mathbf{U}_{2,N} \\ \vdots & \vdots & \ddots & \vdots \\ 0 & 0 & \cdots & \mathbf{U}_{N,N} \end{bmatrix}_{UN \times U^2 N}, \end{aligned} \tag{2.49}$$

where, we have

$$\mathbf{U}_{i,j} \triangleq \begin{bmatrix} u_{U(i-1)+1,U^2(j-1)+1} & u_{U(i-1)+1,U^2(j-1)+2} & \cdots & u_{U(i-1)+1,U^2 j} \\ u_{U(i-1)+2,U^2(j-1)+1} & u_{U(i-1)+2,U^2(j-1)+2} & \cdots & u_{U(i-1)+2,U^2 j} \\ \vdots & \vdots & \ddots & \vdots \\ u_{Ui,U^2(j-1)+1} & u_{Ui,U^2(j-1)+2} & \cdots & u_{Ui,U^2 j} \end{bmatrix}_{U \times U^2}, \tag{2.50}$$

we finally arrive at

$$\hat{\mathbf{S}} = \arg\min_{\mathbf{S}} \left\| \underline{\mathbf{U}} \overline{\mathbf{S}} \right\|. \tag{2.51}$$

Example 2.2: Transforming the ML Decision Metric to the Multiple-Path MSDSD: $U = 2$, $N = 2$

Here, we exemplify the transformation of the ML decision metric given in (2.37) to the multiple-path MSDSD of a specific application scenario, where we have $U = 2$, $N = 2$.

Below we exploit the diagonal structure of both $\Gamma(\kappa)$ in (2.40) and of $\mathcal{E}\left\{\underline{\mathbf{N}}\underline{\mathbf{N}}^H\right\}$ in (2.41). Then the correlation matrix $\underline{\mathbf{C}}$ involved in (2.37) also has a particular diagonal format, which may be represented for the case of $U = 2$, $N = 2$ as

$$\underline{\mathbf{C}} = \left[\begin{array}{c|c} \underline{\mathbf{C}}_{\text{sub}}[0] & \underline{\mathbf{C}}_{\text{sub}}[1] \\ \hline \underline{\mathbf{C}}_{\text{sub}}[-1] & \underline{\mathbf{C}}_{\text{sub}}[-0] \end{array}\right] = \left[\begin{array}{cc:cc} \underline{\mathbf{C}}_{1,1} & 0 & \underline{\mathbf{C}}_{1,3} & 0 \\ 0 & \underline{\mathbf{C}}_{2,2} & 0 & \underline{\mathbf{C}}_{2,4} \\ \hdashline \underline{\mathbf{C}}_{3,1} & 0 & \underline{\mathbf{C}}_{3,3} & 0 \\ 0 & \underline{\mathbf{C}}_{4,2} & 0 & \underline{\mathbf{C}}_{4,4} \end{array}\right]. \tag{2.52}$$

Then, according to the Cholesky factorization of $\underline{\mathbf{F}}^H \underline{\mathbf{F}} = \underline{\mathbf{C}}^{-1}$, where $\underline{\mathbf{F}}$ is an upper-triangular matrix, the matrix $\underline{\mathbf{F}}$ associated with $\underline{\mathbf{C}}$ in (2.52) has the following format as

$$\underline{\mathbf{F}} = \left[\begin{array}{cc:cc} \underline{\mathbf{F}}_{1,1} & 0 & \underline{\mathbf{F}}_{1,3} & 0 \\ 0 & \underline{\mathbf{F}}_{2,2} & 0 & \underline{\mathbf{F}}_{2,4} \\ \hdashline 0 & 0 & \underline{\mathbf{F}}_{3,3} & 0 \\ 0 & 0 & 0 & \underline{\mathbf{F}}_{4,4} \end{array}\right], \tag{2.53}$$

where $\underline{\mathbf{F}}_{i,j}$ represents the non-zero coefficients of the matrix.

Recalling our system model introduced in Section 2.4.1, the received signal block vector $\underline{\mathbf{Y}}$ may be represented for the case of $U = 2$, $N = 2$ as

$$\underline{\mathbf{Y}} = \big[\mathbf{Y}[1], \mathbf{Y}[2]\big] = \big[\,[Y_{1,1}\; Y_{1,2}]\,, [Y_{2,1}\; Y_{2,2}]\,\big]. \tag{2.54}$$

Upon applying the vector-to-matrix transformation operator $T_d(\cdot)$ defined in (2.43) to $\underline{\mathbf{Y}}$, we arrive at

$$T_d\left(\underline{\mathbf{Y}}\right) = \left[\begin{array}{c:c} \boldsymbol{\Upsilon}_1 & \text{NULL} \\ \hdashline \text{NULL} & \boldsymbol{\Upsilon}_2 \end{array}\right] = \left[\begin{array}{cccc:cccc} Y_{1,1} & Y_{1,2} & 0 & 0 & 0 & 0 & 0 & 0 \\ 0 & 0 & Y_{1,1} & Y_{1,2} & 0 & 0 & 0 & 0 \\ \hdashline 0 & 0 & 0 & 0 & Y_{2,1} & Y_{2,2} & 0 & 0 \\ 0 & 0 & 0 & 0 & 0 & 0 & Y_{2,1} & Y_{2,2} \end{array}\right]. \tag{2.55}$$

Then the $(UN \times U^2N)$-element upper-triangular block matrix $\underline{\mathbf{U}}$ involved in the decision metric of (2.51) is given by

$$\begin{aligned} \underline{\mathbf{U}} &\triangleq \left(\underline{\mathbf{F}} T_d\left(\underline{\mathbf{Y}}\right)\right)^* \\ &= \left[\begin{array}{cc:cc} \underline{\mathbf{F}}_{1,1} & 0 & \underline{\mathbf{F}}_{1,3} & 0 \\ 0 & \underline{\mathbf{F}}_{2,2} & 0 & \underline{\mathbf{F}}_{2,4} \\ \hdashline 0 & 0 & \underline{\mathbf{F}}_{3,3} & 0 \\ 0 & 0 & 0 & \underline{\mathbf{F}}_{4,4} \end{array}\right]^* \times \left[\begin{array}{cccc:cccc} Y_{1,1} & Y_{1,2} & 0 & 0 & 0 & 0 & 0 & 0 \\ 0 & 0 & Y_{1,1} & Y_{1,2} & 0 & 0 & 0 & 0 \\ \hdashline 0 & 0 & 0 & 0 & Y_{2,1} & Y_{2,2} & 0 & 0 \\ 0 & 0 & 0 & 0 & 0 & 0 & Y_{2,1} & Y_{2,2} \end{array}\right]^* \\ &= \left[\begin{array}{c:c} \mathbf{U}_{1,1} & \mathbf{U}_{1,2} \\ \hdashline \text{NULL} & \mathbf{U}_{2,2} \end{array}\right] \\ &= \left[\begin{array}{cccc:cccc} u_{1,1} & u_{1,2} & 0 & 0 & u_{1,5} & u_{1,6} & 0 & 0 \\ 0 & 0 & u_{2,3} & u_{2,4} & 0 & 0 & u_{2,7} & u_{2,8} \\ \hdashline 0 & 0 & 0 & 0 & u_{3,5} & u_{3,6} & 0 & 0 \\ 0 & 0 & 0 & 0 & 0 & 0 & u_{4,7} & u_{4,8} \end{array}\right]. \end{aligned} \tag{2.56}$$

Hence, the final decision metric of the multiple-path MSDSD given in (2.51) can be formulated for the case of $U = 2, N = 2$ as

$$\|\underline{\mathbf{U}}\overline{\mathbf{S}}\| = \left[\begin{array}{c:c} \mathbf{U}_{1,1} & \mathbf{U}_{1,2} \\ \hdashline \text{NULL} & \mathbf{U}_{2,2} \end{array}\right] \times \left[\begin{array}{c} \overline{\mathbf{S}}[1] \\ \hdashline \overline{\mathbf{S}}[2] \end{array}\right], \tag{2.57}$$

where after omitting the zero coefficients, the multiplication of $\mathbf{U}_{i,j}$ and $\overline{\mathbf{S}}[k+1]$ always yields a two-element vector in the following form

$$\begin{aligned} \mathbf{U}_{i,j} \times \overline{\mathbf{S}}[k+1] &= \left[\begin{array}{cccc} u_{2i-1,4j-3} & u_{2i-1,4j-2} & 0 & 0 \\ 0 & 0 & u_{2i,4j-1} & u_{2i,4j} \end{array}\right] \times \left[\begin{array}{c} S[k+1] \\ 0 \\ 0 \\ S[k+1] \end{array}\right] \\ &= \left[\begin{array}{c} u_{2i-1,4j-3} S[k+1] \\ u_{2i,4j} S[k+1] \end{array}\right]. \end{aligned} \tag{2.58}$$

Observe at the right-hand side of (2.57) that the matrix structure of the multiple-path MSDSD's final decision metric $\|\underline{\mathbf{U}}\overline{\mathbf{S}}\|$ is the same as that of the single-link MSDSD's decision

metric introduced in Section 2.3.1. Hence the multiple-path MSDSD also relies on solving a "shortest vector problem", which can be efficiently solved by employing the sphere decoding (SD) algorithm introduced in Figures 2.4, 2.5, as well as 2.6 of Section 2.3.2.

The only difference is that in the decision metric of the single-link MSDSD both the $u_{i,j}$ component defined in (2.20) and the $S[k+1]$ component defined in (2.8) are constituted by a single scalar variable. Their multiplication also yields a single scalar value. Hence, the associated accumulated squared distance $d_l^2 = \sum_{i=l}^{N} \left\{ \left| \sum_{j=i}^{N} u_{i,j} \hat{S}[j] \right|^2 \right\}$ defined in (2.21) is based on the sum of terms $u_{l,j}\hat{S}[j]$. By contrast, in the decision metric of the multiple-path MSDSD, the $\mathbf{U}_{i,j}$ component defined in (2.50) and the $\overline{\mathbf{S}}[k+1]$ component defined in (2.48) are multiple-element matrices. Their multiplication will generate two products. Owing to the specific structure of $\mathbf{U}_{i,j}$ and $\overline{\mathbf{S}}[k+1]$ as shown in (2.58), these two products are always generated by multiplying the first and last coefficient of $\mathbf{U}_{i,j}$, i.e. $u_{2i-1,4j-3}$ and $u_{2i,4j}$ to $\hat{S}[j]$, respectively. Consequently, the accumulated squared distance of a twin-path MSDSD having an arbitrary observation window width of N is rewritten as

$$d_l^2 = \sum_{i=l}^{N} \left\{ \left| \sum_{j=i}^{N} u_{2i-1,4j-3} \hat{S}[j] \right|^2 + \left| \sum_{j=i}^{N} u_{2i,4j} \hat{S}[j] \right|^2 \right\}, \tag{2.59}$$

where we have two different types of products, namely $u_{2i-1,4j-3}\hat{S}[j]$ and $u_{2i,4j}\hat{S}[j]$ into account.

As shown in Example 2.2, based on the final decision metric of (2.51), the multiple-path MSDSD can be implemented following the same process as in Section 2.3.2. The only difference is that the evaluation of the accumulated squared distance has to be modified. In more detail, this modification required for the twin-path MSDSD was demonstrated in (2.59), where the following two types of terms $\left| \sum_{j=i}^{N} u_{2i-1,4j-3} \hat{S}[j] \right|^2$ and $\left| \sum_{j=i}^{N} u_{2i,4j} \hat{S}[j] \right|^2$ were taken into account, where the two different types of terms relied on two different types of products. By contrast, for a U-path MSDSD, U different types of terms are involved in the evaluation of the accumulated squared distance, as detailed in [54]. The resultant complication is that the multiple types of products involved in the accumulated squared distance calculation of a multiple-path MSDSD will violate the convenient geometric relationship between the received signal point and the legitimate DPSK symbols, which previously obeyed in Figure 2.7. Hence the zigzagging method introduced in the end of Section 2.3.2 for directly finding the optimum candidate $\hat{S}[i]$ becomes invalid. Hence we have to resort to a brute-force search style for implementing the "$\mathrm{find\_best}$" function involved in the MSDSD decoding process. Therefore, the decoding complexity is inevitably increased.

2.4.3 Performance of the Multiple-Path MSDSD

The properties of the multiple-path MSDSD algorithm are characterized in the context of the multiple-relay aided AF protocol assisted cooperative uplink of Figure 2.10. Specifically, we con-

sider two cooperative systems, a single-relay aided cooperative system, namely the "twin-path" system, which employs the twin-path MSDSD and a twin-relay aided cooperative system, namely the "triple-path" system, which employs the triple-path MSDSD. The schematics of the single link MSDSD based system and that of the "twin-path" system, as well as that of the "triple-path" system are portrayed in Figures 2.12, 2.13, as well as 2.14, respectively. All the channels involved in the transmission are assumed to be Rayleigh flat-fading channels. The classic TDMA scheme is employed as our multiple access technique. Furthermore, 4-DPSK modulation is used. In order to approach a fair comparison with the single-link direct-transmission based system, we explicitly stipulate that the transmit power of every node obeys the relationships that $P_s + \sum_{i=2}^{U} P_{r_i} = 1$ and $P_s = P_{r_i}, i \in \{2, 3, \ldots, U\}$.

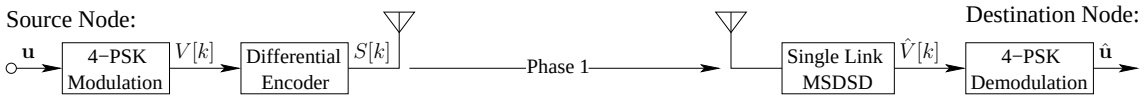

Figure 2.12: Schematic of single link MSDSD.

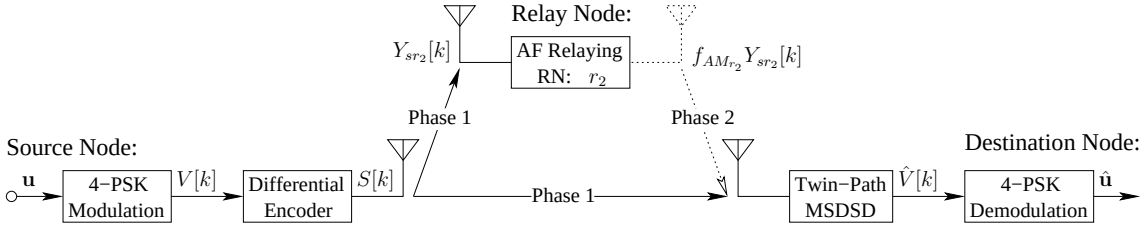

Figure 2.13: Schematic of twin-path MSDSD.

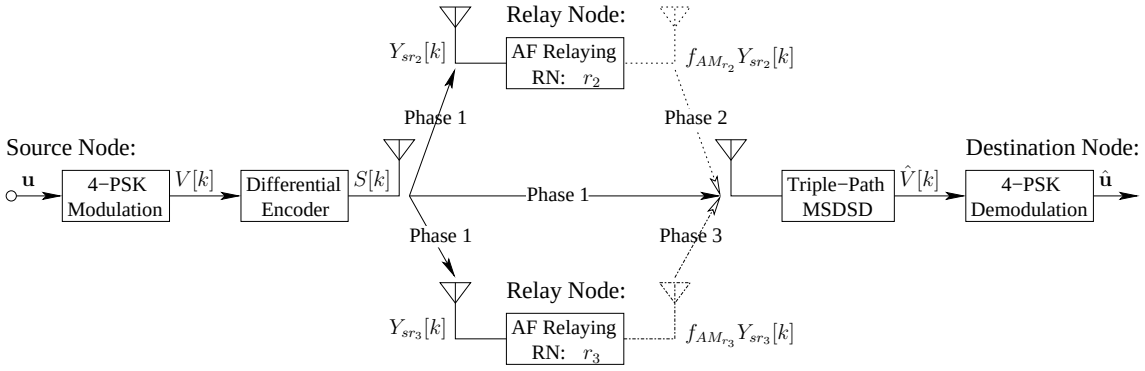

Figure 2.14: Schematic of triple-path MSDSD.

As revealed in Section 2.3.3, the observation window size N_{wind} is a critical parameter of the MSDSD algorithm, which significantly affects the error correction capability and computational complexity of the MSDSD algorithm. Hence, the effect of the observation window size is investigated in Figure 2.15, where the BER performance of various window sizes spanning from 3 to

System Model	single-link direct-transmission
	single-relay aided cooperation
	twin-relay aided cooperation
Channel Model	Narrow-Band Flat-Fading Channel
Normalized Doppler Frequency	$f_d = 0.05, 0.03, 0.01$ for Fast-Rayleigh-Fading
	$f_d = 10^{-3}, 10^{-4}$ for Slow-Rayleigh-Fading
Modulation	4-DPSK for Differential Detection
Detector	single link MSDSD
	twin − path MSDSD
	triple − path MSDSD
Window Size of MSDSD	$N = 3, 4, \ldots, 10$

Table 2.5: System parameters employed in this section.

10 are demonstrated. In line with the simulation result demonstrated in Figure 2.8, a valuable performance gain is achieved upon increasing the window size, which is achieved at a moderate complexity increase as shown in Figure 2.16. For example, we save approximately 2.5dB power at the target BER of 10^{-4} by increasing the observation window size from $N_{\text{wind}} = 3$ to $N_{\text{wind}} = 4$. However, it is also indicated in Figure 2.15 that the performance gain achieved upon increasing the observation window size N_{wind} gradually becomes marginal upon increasing the value of N_{wind}. Simultaneously, the associated complexity keeps growing as shown in Figure 2.16. Then, as a benefit of higher diversity order, the multiple-path MSDSD outperforms its single-link counterpart, which may be verified by comparing the dashed line marked by triangle labels with the solid line marked by triangle labels. This BER improvement is achieved at the cost of imposing higher complexity again, which is characterised in Figure 2.17. It is delighted to observe in Figure 2.15 that the multiple-path MSDSD algorithm even surpasses the single-link direct-transmission based coherent detection during the high SNR region.

Since the multiple-path MSDSD algorithm based systems benefit from an increased spatial diversity, let us embark on quantifying these gains. Accordingly, we compare the twin-path MSDSD based system, which is portrayed in Figure 2.13 to the triple-path MSDSD based system seen in Figure 2.14, where the observation window size is fixed to $N_{\text{wind}} = 6$. Consequently, the BER performance of these two systems experiencing different Doppler frequencies is illustrated in Figure 2.18.

It is shown in Figure 2.18 that the "triple-path" cooperative network always significantly outperforms its "twin-path" counterpart, regardless of the normalized Doppler frequencies. In more detail, the benefit of increasing the spatial diversity order is that an approximately 5dB performance gain is achieved at a target BER of 10^{-4} by adding an extra independently fading propagation path,

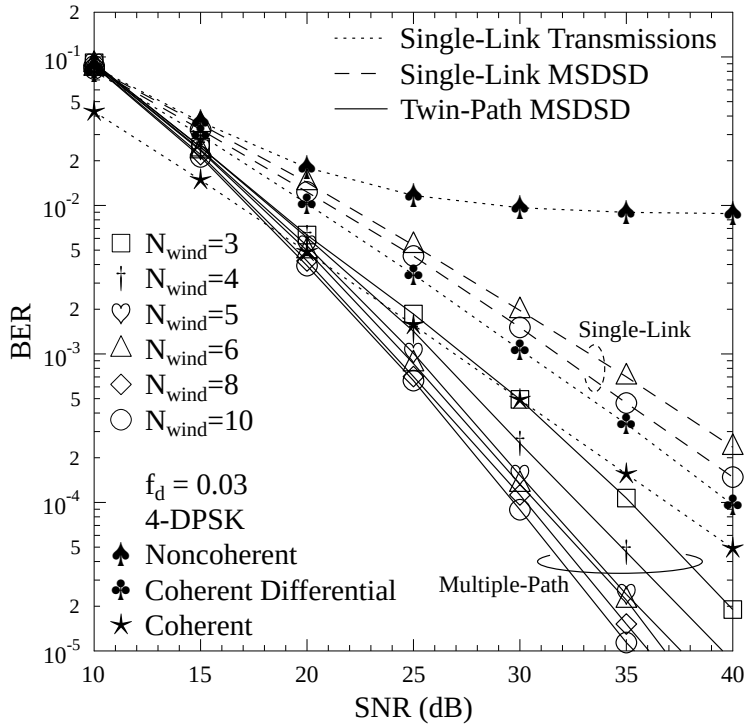

Figure 2.15: BER performance of the multiple-path MSDSD algorithm in flat Rayleigh fading channels having a normalized Doppler frequency of $f_d = 0.03$. The effect of the observation window size N_{wind} is investigated, where N_{wind} increases from 3 to 10. Furthermore, the BER performance of conventional differential detection and of coherent differential detection, as well as of coherent detection is also portrayed as a benchmarker. The BER curves of the classic single-link MSDSD algorithm having $N_{\text{wind}} = 6, 10$ is also provided. Naturally, the BER performance improvement is achieved at an increased complexity, as quantified in Figure 2.16 and Figure 2.17. The results for twin-path MSDSD algorithm are based on the schematic of Figure 2.13 and the parameters of Table 2.5.

as seen at the bottom-right corner of Figure 2.18. The spatial diversity gain remains similar for the different normalized Doppler frequency values. Hence, again, spatial diversity constitutes an efficient method of improving the attainable system performance. On the other hand, it can also be observed in Figure 2.18 that the "triple-path" system encounters a worse BER performance than the "twin-path" system, when the SNR value is below about 10dB. The reason is that in the low-SNR region the reliability of the independently fading signals contributed by the relay nodes is too low to correct errors. However, the relay nodes still share the same total system power as the direct-transmission based system. Nevertheless, this low-SNR drawback of the "triple-path" system is negligible owing to the fact that in the low-SNR region the attainable BER performance of the "twin-path" system is also inadequate for practical applications. The slope of the BER curves in the "triple-path" system is more sharp than that of the "twin-path" system, which confirms again

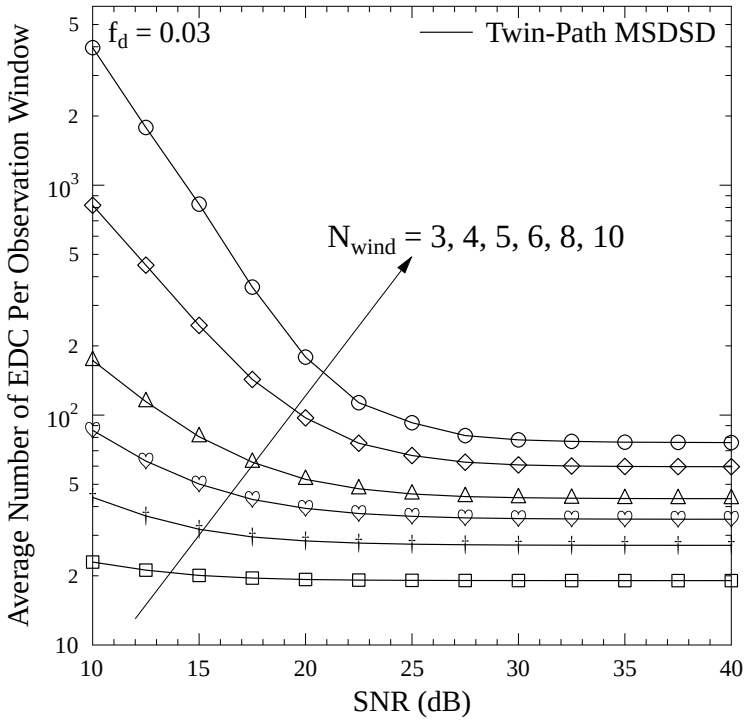

Figure 2.16: Detection complexity versus SNR characteristics, where the complexity increases upon increasing the observation window size of the multiple-path MSDSD. The average number of EDC per observation window metric was introduced in Section 2.3.3, which is employed again as our complexity metric. These results are based on the schematic of Figure 2.13 and the parameters of Table 2.5.

that the "triple-path" system exhibits a higher spatial diversity order. Finally, the complexity imposed by increasing the number of path and the normalized Doppler frequency is demonstrated in Figure 2.19.

The observation window size N_{wind} and the number of independent propagation paths constitute important characteristics of the multiple-path processing based MSDSD algorithm. Hence, as shown in Figures 2.15 and 2.18, they dominate the system's performance. However, the Doppler frequency also has a substantial impact on the system's performance.

In our investigations, we simply assume that all the independent channels involved in the system characterized in Figure 2.10 have the same normalized Doppler frequency. Upon varying the common normalized Doppler frequency, the associated results are portrayed in Figure 2.20. As expected, the system's BER performance is improved upon reducing the normalized Doppler frequency. Meanwhile, the complexity imposed by multiple-path MSDSD algorithm is also mitigated as shown in Figure 2.21. However, this BER performance gain also depends on the target BER. Observe in Figure 2.20 for example that at a target BER of 10^{-3} a performance gain of about 3dB is attained upon reducing the normalized Doppler frequency from $f_d = 0.05$ to 0.01. However, any further performance gains remain negligible, when the normalized Doppler frequency f_d is further

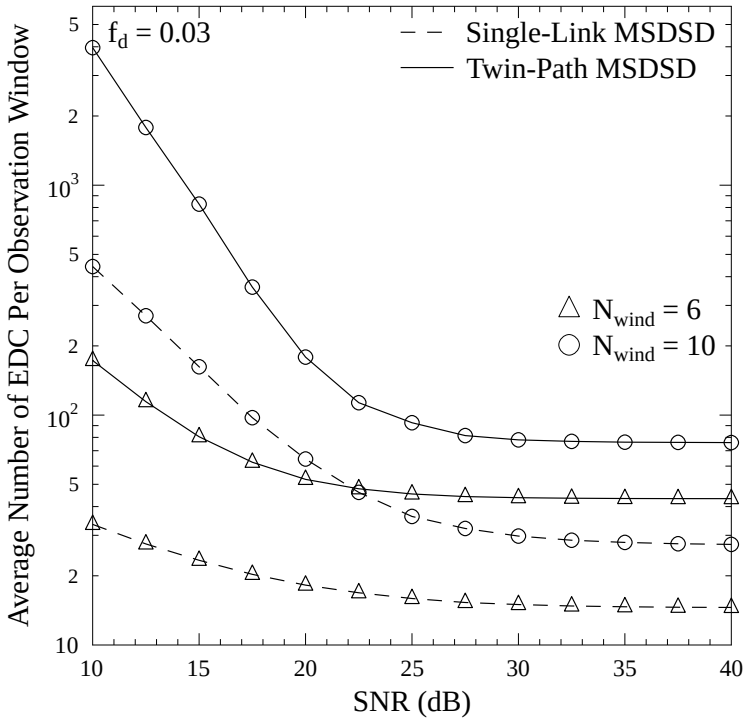

Figure 2.17: Detection complexity versus SNR characteristics, where the classic single link MSDSD and the twin-path MSDSD are compared. The scenario of $N_{\text{wind}} = 6$ and $N_{\text{wind}} = 10$ are investigated. The results for single link MSDSD are based on the schematic of Figure 2.12. The results for twin-path MSDSD are based on the schematic of Figure 2.13. The parameters of Table 2.5 are employed again.

reduced from $f_d = 0.01$ to 10^{-3}. This implies that the increased complexity of the multiple-path processing based MSDSD algorithm is more justified for rapidly fading communication environments. When the fading depth is reduced owing to experiencing more benign Rice fading, or when the paths become correlated, the advantage of employing the multiple-path MSDSD algorithm is not so significant. In fact, in the light of its extra complexity it becomes unjustified. We also observe in Figure 2.20 that the performance gain increases again, when the normalized Doppler frequency is approaching $f_d = 10^{-4}$, because the channel can be regarded as a slow fading when having $f_d = 10^{-4}$ and it is demonstrated in Figure 2.3 that even the CDD is capable of approaching the optimum performance bound in a slow fading scenario.

In Figure 2.20, all the propagation paths are assumed to obey the same fading parameters. However, in a more practical scenario, the system may experience different fading effects for the different independently fading paths. Hence, it is more practical to investigate a system, which has different fading parameters for the different propagation paths. For a single-relay aided cooperative system, the definitions of the fading scenarios considered are listed in Table 2.6, where the notations $f_{d_{sd}}$ and $f_{d_{sr}}$ as well as $f_{d_{rd}}$ represent the normalized Doppler frequency values of the SD link,

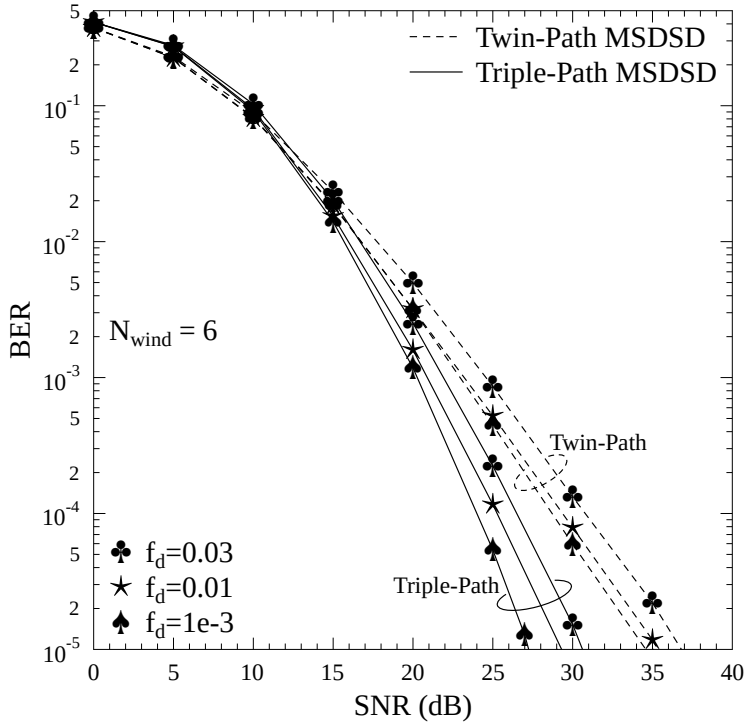

Figure 2.18: BER performance comparison between the single-relay aided and twin-relay aided cooperative systems, where the multiple-path MSDSD algorithm is employed and its observation window size is fixed to $N_{\text{wind}} = 6$. Flat Rayleigh fading channels having different normalized Doppler frequency values are used. The results for single-relay aided cooperative system are based on the schematic of Figure 2.13, meanwhile the results for twin-relay aided cooperative system are based on the schematic of Figure 2.14.

of the SR link as well as of the RD link, respectively. Furthermore, the idealized scenarios that all the paths involved have the same common f_d of 0.03 and 0.001 characterize the lower and upper performance bounds. Consequently, the BER simulation results corresponding to the above-mentioned scenarios are portrayed in Figure 2.22.

Observe in Figure 2.22 that all the scenarios defined in Table 2.6 yield a better BER performance than the idealized scenario having $f_d = 0.03$ for all the paths involved. This implies that any improvement of the sub-channels, namely of the SR link, or RD link will result in an improved overall system performance. Then, the BER performance of "Scenario II" is better than that of "Scenario I" or of "Scenario III". This implies that the quality of the SD link dominates the overall system performance, since the SD link avoids the noise amplification problem incurred by the AF relay links.

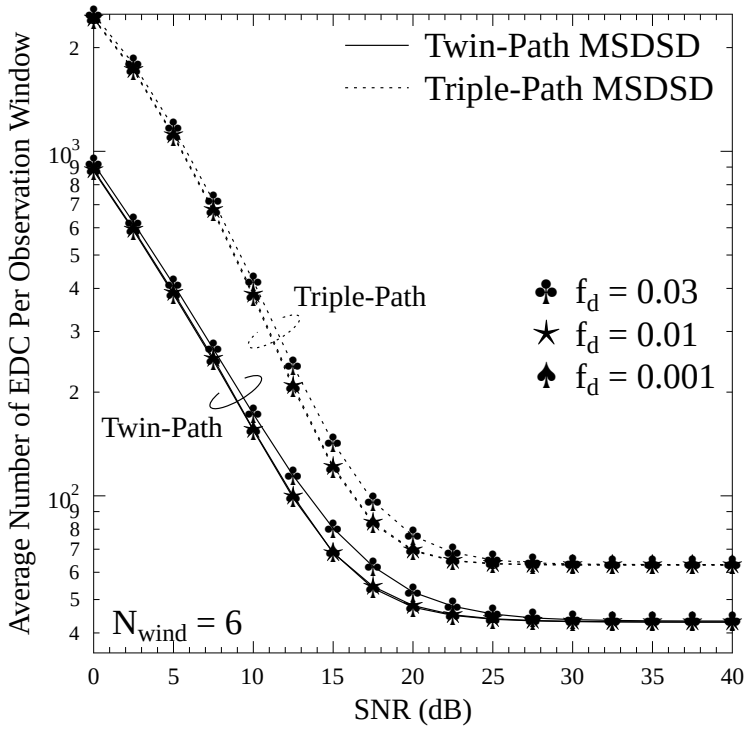

Figure 2.19: Detection complexity versus SNR characteristics upon increasing the number of path of the multiple-path MSDSD algorithm. The results for "twin-path" system are based on the schematic of Figure 2.13, meanwhile the results for "triple-path" system are based on the schematic of Figure 2.14. System parameters are referred to Table 2.5.

	$f_{d_{sd}}$	$f_{d_{sr}}$	$f_{d_{rd}}$
Scenario I	0.03	0.03	0.001
Scenario II	0.001	0.03	0.03
Scenario III	0.03	0.001	0.03

Table 2.6: Definitions of various fading scenarios.

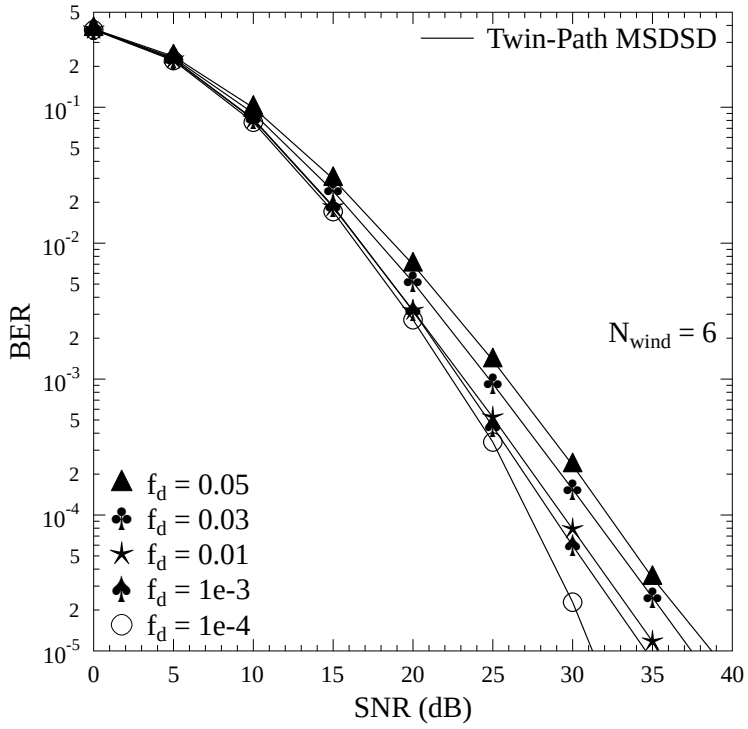

Figure 2.20: BER versus SNR performance of the multiple-path MSDSD assisted single relay aided cooperative system, where various normalized Doppler frequency values are considered for modelling different communication environments. The results are based on the schematic of Figure 2.13 and the parameters of Table 2.5.

2.5 Soft-Input Soft-Output Multiple-Symbol Differential Sphere Decoding

Having introduced the family of hard-decision based multiple-symbol differential detection schemes in the previous sections, let us now consider the corresponding soft-detection schemes, since the later are capable of achieving substantial performance improvements as detailed in [85–90]. Let us hence embark on transforming the hard-decision-based MSDSD algorithm to a power-efficient soft-decision-based iterative detection scheme. This contribution was proposed by Pauli *et al.* in [55], where the maximum *a posteriori* (MAP) algorithm was invoked by the MSDSD and the soft-output generation of the MSDSD was conceived, as detailed in this section.

2.5.1 Maximum a Posteriori MSDSD

Upon recalling the generalized conditional PDF of a Gaussian random vector given in (2.13) and the critical property that the determinant $\|\mathbf{\Phi_{yy}}\|$ in (2.13) is independent of the transmitted symbol vector $\mathbf{S}$, we arrive at

$$-\ln\left(\Pr\left(\mathbf{y} \mid \mathbf{S}\right)\right) \propto \mathbf{y}^H \mathbf{\Phi_{yy}}^{-1} \mathbf{y}. \tag{2.60}$$

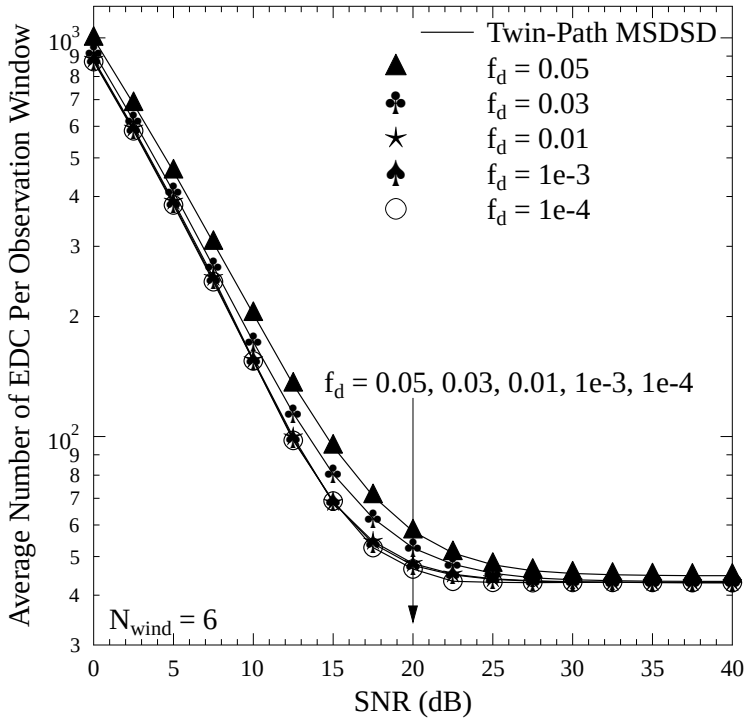

Figure 2.21: Detection complexity versus SNR for different normalized Doppler frequencies. The results are based on the schematic of Figure 2.13 and the parameters of Table 2.5.

According to the derivation provided in Section 2.3.1, (2.60) can be equivalently expressed as

$$-\ln\left(\Pr\left(\mathbf{y} \mid \mathbf{S}\right)\right) \propto \|\mathbf{US}\|^2, \tag{2.61}$$

where the matrix $\mathbf{U}$ is identical to that involved in (2.19).

According to the differential encoding scheme formulated in (2.1), once the DPSK symbol vector $\mathbf{S}$ is fixed, the associated PSK information symbol vector $\mathbf{V}$ is also determined. However, when the PSK information symbol vector $\mathbf{V}$ is fixed, the associated DPSK symbol vector $\mathbf{S}$ is not unique. For example, a common phase shift assigned to each and every component of $\mathbf{S}$ will not result in a different $\mathbf{V}$. In order to establish a unique relationship between the DPSK symbol vector and its associated PSK symbol vector, we introduce the new DPSK symbol vector $\mathbf{a} = [a[1], a[2], \ldots, a[N]]^T$, which is defined as

$$a_i = \begin{cases} \prod_{l=i}^{N-1} V^*[l], & 1 \leq i \leq N-1 \\ 1, & i = N. \end{cases} \tag{2.62}$$

According to (2.62), the vector $\mathbf{a}$ may be treated as a particular variant of the vector $\mathbf{S}$, where the last component of $\mathbf{S}$, i.e. $S[N]$ is always unity. Correspondingly, the DPSK symbol vectors $\mathbf{a}$ and $\mathbf{S}$ become interchangeable. Similarly, the DPSK symbol vector $\mathbf{a}$ and the PSK information symbol vector $\mathbf{V}$ also become interchangeable. Accordingly, (2.61) is equivalent to

$$-\ln\left[\Pr\left(\mathbf{y} \mid \mathbf{V}\right)\right] \propto \|\mathbf{Ua}\|^2. \tag{2.63}$$

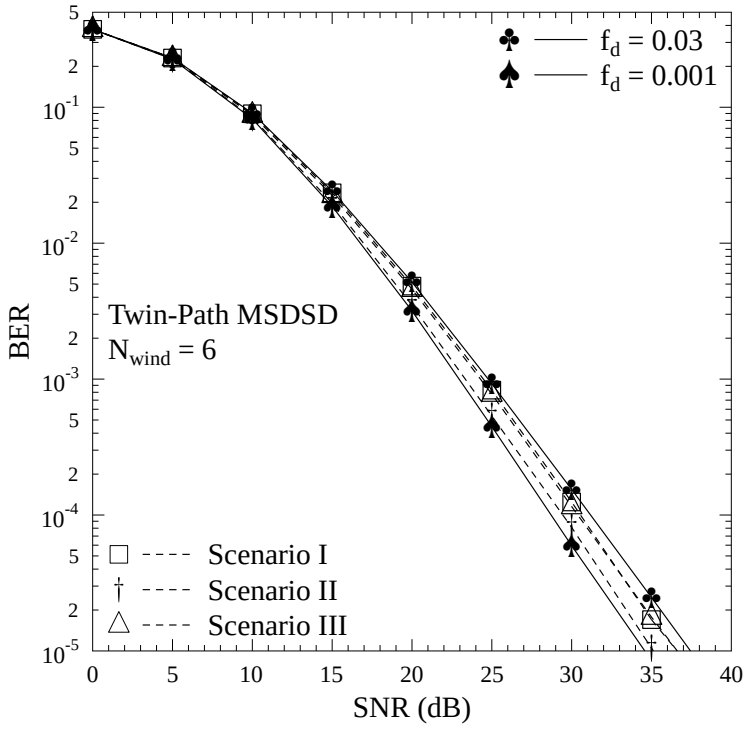

Figure 2.22: BER versus SNR performance of the multiple-path MSDSD assisted single-relay aided cooperative system, where the different independently fading paths have different fading parameters. The exact definitions of the various fading scenarios can be found in Table 2.6. Furthermore, the BER performance associated with the idealized scenarios, when all the channels involved have the same f_d of 0.03 and of 0.001 are employed as the benchmarks. The results are based on the schematic of Figure 2.13.

Both the single-link hard-decision-based MSDSD algorithm introduced in Section 2.3 and the multiple-path MSDSD algorithm introduced in Section 2.4 aim for maximizing the *a priori* conditional PDF $\Pr(\mathbf{y}|\mathbf{V})$. Alternatively, we may opt for maximizing the *a posteriori* conditional PDF $\Pr(\mathbf{V}|\mathbf{y})$ as the optimization criterion of the MSDSD algorithm, which may be expressed as

$$\hat{\mathbf{V}}_{\mathrm{MAP}} = \arg\min_{\mathbf{V}} \left\{ -\ln\left[\Pr(\mathbf{V} \mid \mathbf{y})\right] \right\}. \tag{2.64}$$

Upon involving Bayes' theorem in the context of (2.63), we arrive at

$$\begin{aligned} -\ln\left[\Pr(\mathbf{V} \mid \mathbf{y})\right] &= -\ln\left(\frac{\Pr(\mathbf{y} \mid \mathbf{V})\Pr(\mathbf{V})}{\Pr(\mathbf{y})}\right) \\ &\propto -\ln\left[\Pr(\mathbf{y} \mid \mathbf{V})\right] - \ln\left[\Pr(\mathbf{V})\right] \\ &\propto \|\mathbf{U}\mathbf{a}\|^2 - \ln\left[\Pr(\mathbf{V})\right]. \end{aligned} \tag{2.65}$$

Then, upon exploiting the independence of the components of $\mathbf{V}$, we arrive at

$$\ln\left[\Pr(\mathbf{V})\right] = \sum_{i=1}^{N-1} \ln\left[\Pr(V[i])\right]. \tag{2.66}$$

Substituting (2.65) and (2.66) into (2.64), the decision rule of the maximum a posteriori multiple-symbol differential sphere detection (MAP-MSDSD) may be reformulated as

$$\hat{\mathbf{V}}_{\mathrm{MAP}} = \arg\min_{\mathbf{V}} \left\{ \|\mathbf{U}\mathbf{a}\|^2 - \sum_{i=1}^{N-1} \ln\left[\Pr(V[i])\right] \right\}. \tag{2.67}$$

For the sake of solving the "shortest vector problem" formulated in (2.67) in a sphere decoding context, we invoke again the accumulated squared distance concept introduced in Section 2.3.2. Similar to (2.21), the accumulated squared distance of the vector $\mathbf{a}$ is given by

$$d_1^2 = \|\mathbf{U}\mathbf{a}\|^2 - \sum_{i=1}^{N-1} \ln\left[\Pr(V[i])\right] = \sum_{i=1}^{N-1} \left(\left| \sum_{l=i}^{N} u_{i,l} a[l] \right|^2 - \ln\left[\Pr(V[i])\right] \right) + |u_{N,N}|^2, \tag{2.68}$$

where the notation $u_{i,l}, 1 \leq i,l \leq N$ denotes the element in the i^{th} row, and l^{th} column of the matrix $\mathbf{U}$. To elaborate a little further, (2.68) reveals that a valid PSK symbol candidate for $V[i]$ has to satisfy

$$d_i^2 \triangleq \left\{ \left| u_{i,i} a[i+1] V^*[i] + \sum_{l=i+1}^{N} u_{i,l} a[l] \right|^2 - \ln\left[\Pr(V[i])\right] \right\} + d_{i+1}^2 \leq R^2, \tag{2.69}$$

where R is the radius of the sphere.

Example 2.3: Decomposition of the Decision Metric of MAP-MSDSD: $N = 4$

Here, for the sake of exemplifying the relationship between the accumulated squared distance d_i^2 defined in (2.69) and the components of the decision metric defined in (2.67), we decompose the decision metric of a MAP-MSDSD having $N = 4$ into accumulated squared distances.

As stated previously in this section, the matrix $\mathbf{U}$ of (2.67) is identical to that involved in (2.19) and the vector $\mathbf{a}$ of (2.67) has a form of $\mathbf{a} = \left[a[1], a[2], \ldots, 1\right]^T$. Hence, for $N = 4$, we have

$$\begin{aligned} \mathbf{U}\mathbf{a} &= \begin{bmatrix} u_{1,1} & u_{1,2} & u_{1,3} & u_{1,4} \\ 0 & u_{2,2} & u_{2,3} & u_{2,4} \\ 0 & 0 & u_{3,3} & u_{3,4} \\ 0 & 0 & 0 & u_{4,4} \end{bmatrix} \times \begin{bmatrix} a[1] \\ a[2] \\ a[3] \\ 1 \end{bmatrix} \\ &= \begin{bmatrix} u_{1,1} \cdot a[1] + u_{1,2} \cdot a[2] + u_{1,3} \cdot a[3] + u_{1,4} \cdot 1 \\ u_{2,2} \cdot a[2] + u_{2,3} \cdot a[3] + u_{2,4} \cdot 1 \\ +u_{3,3} \cdot a[3] + u_{3,4} \cdot 1 \\ + u_{4,4} \cdot 1 \end{bmatrix}. \end{aligned} \tag{2.70}$$

Correspondingly, the decision metric of the MAP-MSDSD algorithm formulated in (2.67)

may be detailed for the case of $N = 4$ as

$$\begin{aligned}
\|\mathbf{Ua}\|^2 - \sum_{i=1}^{3} \ln\left[\Pr(V[i])\right] = \\
\left\{\left|u_{1,1}\cdot a[1] + u_{1,2}\cdot a[2] + u_{1,3}\cdot a[3] + u_{1,4}\cdot 1\right|^2 - \ln\left[\Pr(V[1])\right]\right\} \\
+ \left\{\left|u_{2,2}\cdot a[2] + u_{2,3}\cdot a[3] + u_{2,4}\cdot 1\right|^2 - \ln\left[\Pr(V[2])\right]\right\} \\
+ \left\{\left|u_{3,3}\cdot a[3] + u_{3,4}\cdot 1\right|^2 - \ln\left[\Pr(V[3])\right]\right\} \\
+ \left\{\left|u_{4,4}\cdot 1\right|^2 - \qquad \text{null}\right\}, \qquad (2.71)
\end{aligned}$$

which can be directly generalized to the formulation seen in (2.68).

With the aid of (2.71), the relationship between the accumulated squared distance and the final decision metric of the MAP-MSDSD may be visualized as in Figure 2.23

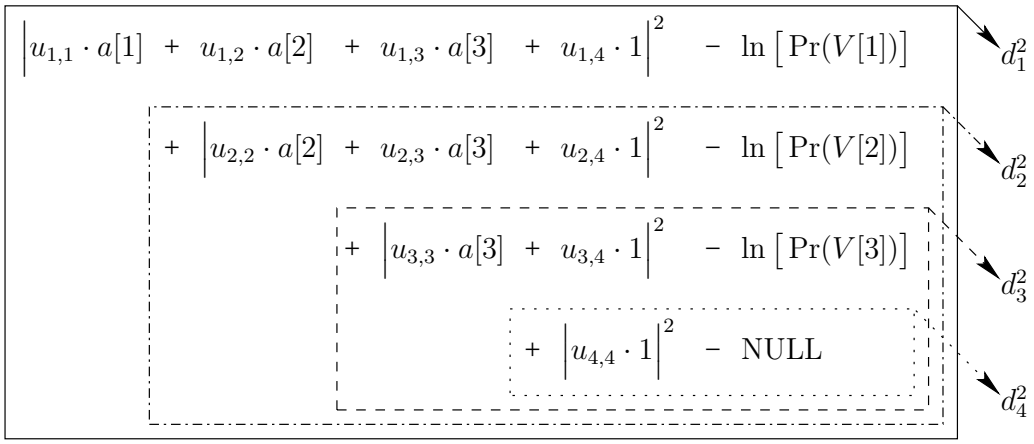

Figure 2.23: Decomposing the entire decision metric of the MAP-MSDSD algorithm having $N = 4$ into accumulated squared distances.

Based on the similarity between (2.69) and (2.22), the sphere decoding mechanism introduced in Section 2.3.2 is still valid for the MAP-MSDSD algorithm. The only difference is that in the original MSDSD algorithm of [53], we select the best candidate $\hat{S}[i]$, which minimizes the i^{th} accumulated squared distance d_i^2 given in (2.22) and then reorder the remaining $(M_c - 1)$ candidates simply by zigzagging through the M_c-ary DPSK constellation, as illustrated early in Figure 2.7. By contrast, we cannot employ the above-mentioned Schnorr-Euchner strategy [91] in the sphere decoding process of the MAP-MSDSD algorithm, because the incorporation of the *a priori* information of $\ln\left[\Pr(V[i])\right]$ in (2.69) destroys the regular geometry of the M_c-ary DPSK constellation. The distortion of the regular geometry of the M_c-ary DPSK constellation imposed by $\ln\left[\Pr(V[i])\right]$ is illustrated in Figure 2.24.

The regular geometry of the M_c-ary DPSK constellation and the sorting process of the hard-decision-based single-link MSDSD is portrayed at the left-hand side of Figure 2.24. Observe at

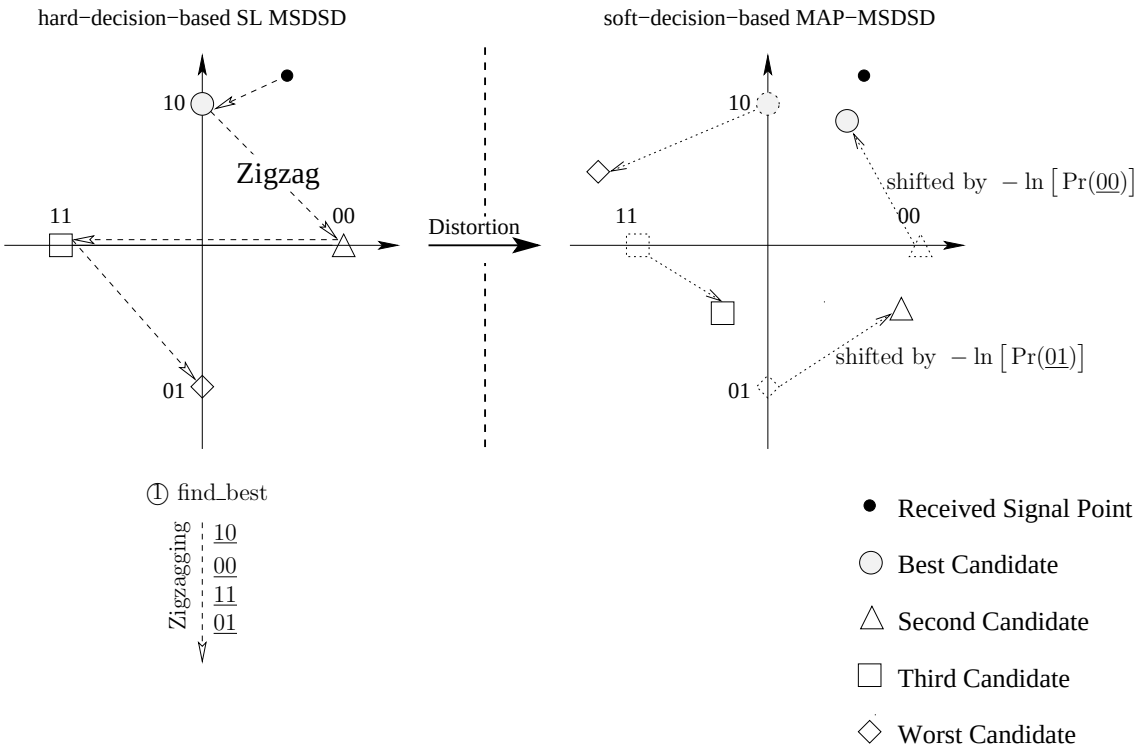

Figure 2.24: Distortion of the regular geometry of the M_c-ary DPSK constellation imposed by the MAP-MSDSD algorithm, when taking into account the a priori information.

the right-hand side of Figure 2.24 that after invoking the *a priori* information of $-\ln\left[\Pr(\underline{00})\right]$, the previous second candidate $\underline{00}$ becomes the optimum candidate for $V[i]$ in the MAP-MSDSD algorithm. Similarly, the previous worst candidate $\underline{01}$ becomes the second-best candidate in the MAP-MSDSD algorithm.

Hence we have to estimate d_i^2 of all the legitimate M_c candidates for $V[i]$, and then order the candidates according to their associated d_i^2 values. In fact, a similar situation has been encountered in the multiple-path MSDSD algorithm discussed in the context of Example 2.2, as well as at the end of Section 2.4.2.

2.5.2 Soft-Output Generation of MAP-MSDSD

The MAP-MSDSD introduced in Section 2.5.1 became capable of exploiting soft-information, where the *a priori* information $\ln\left[\Pr(V[i])\right]$ is taken into account during the sphere decoding process as the soft-input. Hence, in this section, we will now concentrate our attention on the generation of soft-outputs for the SISO-MSDSD algorithm.

Let $u[\mu]$ denote the μ^{th} information bit carried by the information symbol vector $\mathbf{V}$. Hence, according to [92] and with the aid of Bayes' theorem, the *a posteriori* log log-likelihood ratio (LLR)

of the μ^{th} information bit $u[\mu]$ may be expressed as

$$\begin{aligned} L(u[\mu]) &= \ln\left(\frac{\Pr\{u[\mu]=b|\mathbf{y}\}}{\Pr\{u[\mu]=\bar{b}|\mathbf{y}\}}\right) \\ &= \ln\frac{\sum_{\mathbf{V}\in\chi_{:u[\mu]=b}}\Pr\left(\mathbf{y}\mid\mathbf{V}\right)\Pr(\mathbf{V})}{\sum_{\mathbf{V}\in\chi_{:u[\mu]=\bar{b}}}\Pr\left(\mathbf{y}\mid\mathbf{V}\right)\Pr(\mathbf{V})}, \quad b\in\{0,1\} \end{aligned} \tag{2.72}$$

where $\chi_{:u[\mu]=b}$ represents the set of $M_c^{N-1}/2$ legitimate potentially transmitted information symbol vectors $\mathbf{V}$, whose μ^{th} information bit is $u[\mu]=b$ and similarly, $\chi_{:u[\mu]=\bar{b}}$ is defined as the set corresponding to $u[\mu]=\bar{b}$. Based on (2.65) and invoking the "sum-max" approximation[3] [93], the *a posteriori* LLR of $u[\mu]$ given in (2.72) is further approximated by

$$\begin{aligned} L(u[\mu]) &\approx \ln\left(\frac{\max_{\mathbf{V}\in\chi_{:u[\mu]=b}}\left\{\exp\left(-\|\mathbf{U}\mathbf{a}\|^2+\ln\Pr(\mathbf{V})\right)\right\}}{\max_{\mathbf{V}\in\chi_{:u[\mu]=\bar{b}}}\left\{\exp\left(-\|\mathbf{U}\mathbf{a}\|^2+\ln\Pr(\mathbf{V})\right)\right\}}\right) \\ &= -\left\{\underbrace{\|\mathbf{U}\hat{\mathbf{a}}^b_{\mathrm{MAP}}\|-\ln\Pr\left(\hat{\mathbf{V}}^b_{\mathrm{MAP}}\right)}_{\mathrm{MAP-MSDSD}\in\chi_{:u[\mu]=b}}\right\}+\left\{\underbrace{\|\mathbf{U}\hat{\mathbf{a}}^{\bar{b}}_{\mathrm{MAP}}\|-\ln\Pr\left(\hat{\mathbf{V}}^{\bar{b}}_{\mathrm{MAP}}\right)}_{\mathrm{MAP-MSDSD}\in\chi_{:u[\mu]=\bar{b}}}\right\}, \end{aligned} \tag{2.73}$$

where the estimate $\hat{\mathbf{V}}_{\mathrm{MAP}}$ given in (2.67) is always employed as $\hat{\mathbf{V}}^b_{\mathrm{MAP}}$, i.e. we have $\hat{\mathbf{V}}^b_{\mathrm{MAP}}=\hat{\mathbf{V}}_{\mathrm{MAP}}$, because $\hat{\mathbf{V}}_{\mathrm{MAP}}$ given in (2.67) is the globally optimum candidate for $\mathbf{V}$, hence the associated μ^{th} bit of $\hat{\mathbf{V}}_{\mathrm{MAP}}$ is also the most likely value for $u[\mu]$. By contrast, its opposite, i.e. $\bar{b}$ becomes the most unlikely value for $u[\mu]$. Then $\hat{\mathbf{V}}^{\bar{b}}_{\mathrm{MAP}}$ is the optimum estimate of the constrained MAP-MSDSD, where we constrain the MAP-MSDSD search to the set $\chi_{:u[\mu]=\bar{b}}$.

The constrained MAP-MSDSD may be conceived by slightly modifying the MAP-MSDSD algorithm by ensuring that the vectors corresponding to $u[\mu]=b$ are excluded from the search space.

Hence the evaluation of the *a posteriori* LLR of $u[\mu]$ may be summarized as follows

1. Implement the MAP-MSDSD algorithm according to its decision rule given in (2.67). Correspondingly, the globally optimum estimate $\hat{\mathbf{V}}_{\mathrm{MAP}}$ is obtained. This may be achieved in the same process as described in Section 2.3.2. The only difference is the realization of the "$\mathrm{find\_best}$" function, which has been portrayed in Figure 2.24.

2. Set $\hat{\mathbf{V}}_{\mathrm{MAP}}$ to $\hat{\mathbf{V}}^b_{\mathrm{MAP}}$. Correspondingly, the detected value of the μ^{th} bit of $\hat{\mathbf{V}}_{\mathrm{MAP}}$ is assigned to the variable b involved in (2.73), i.e. the constrained search space $\chi_{:u[\mu]=\bar{b}}$ is determined, which is represented by the black circles in Figure 2.25.

[3]The "sum-max" approximation may be formulated as

$$\ln\left(\sum_i \mathrm{e}^{x_i}\right)\approx\max_i(x_i),$$

where $\max_i(x_i)$ means the maximum value of x_i.

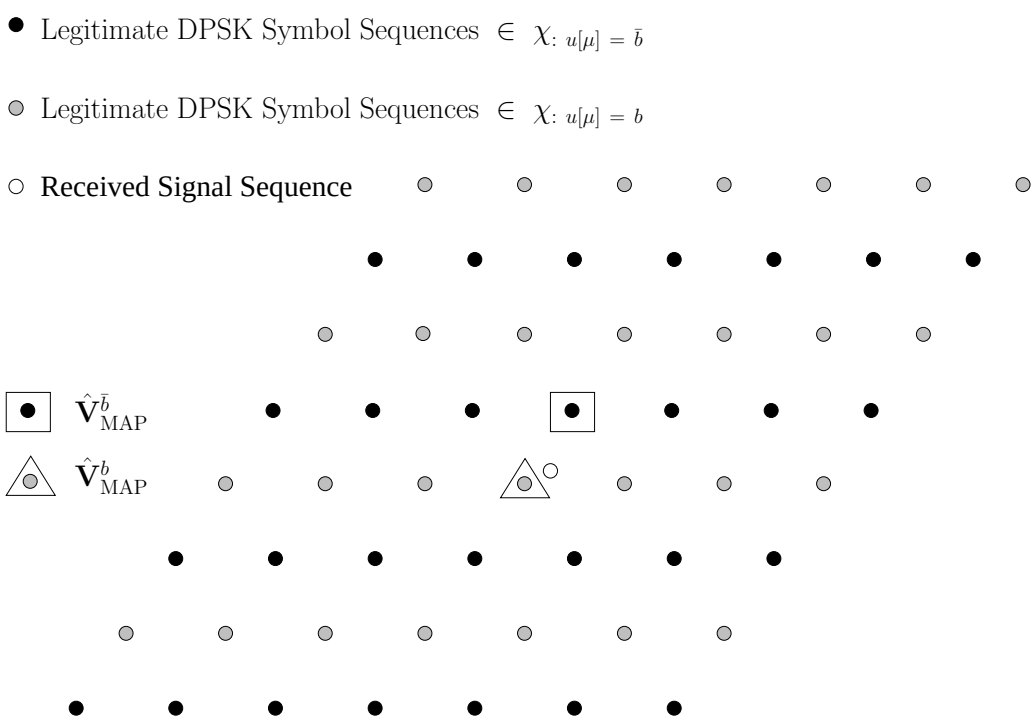

Figure 2.25: Constrained search space of the SISO-MSDSD.

3. Implement the constrained MAP-MSDSD algorithm, whose search space is constrained to $\chi_{:u[\mu]=\bar{b}}$. Correspondingly, the associated $\hat{\mathbf{V}}^{\bar{b}}_{\mathrm{MAP}}$ has to be selected from the set of black circles, which is explicitly labelled in Figure 2.25.

4. Substituting the obtained $\hat{\mathbf{V}}^{b}_{\mathrm{MAP}}$ and $\hat{\mathbf{V}}^{\bar{b}}_{\mathrm{MAP}}$ into (2.73). Finally, the *a posteriori* LLR of $u[\mu]$ is obtained.

2.6 Chapter Summary

In this chapter, we extended the observation window size from two symbols to multiple symbols. As a result, the conventional differential detection was developed further in Section 2.2 to multiple-symbol differential detection. Consequently, a substantial BER versus SNR performance gain was obtained in Figure 2.8 with regard to the CDD. As detailed in Section 2.2.2, the solution of the MSDD problem is equivalent to maximizing the conditional PDF of a Gaussian random vector, given the transmitted information symbols. With the aid of appropriately modifying the decision metric of the MSDD problem, we revealed in Section 2.3.1 that the MSDD problem may be treated as a "shortest vector problem". Accordingly, sphere decoding was invoked in Section 2.3.2 for the sake of significantly mitigating the complexity of the ML MSDD algorithm, which leads to the state-of-the-art MSDSD algorithm of Section 2.3. Then, some further evolved versions of the MSDSD algorithm were conceived for satisfying specific design requirements. For example, the multiple-path MSDSD concept was devised in Section 2.4 for adapting the multiple-symbol

noncoherent detection technique to a multiple access network. The SISO-MSDSD algorithm was devised in Section 2.5 for transforming the hard-decision-based MSDSD to a power-efficient soft-decision-based iterative detection scheme.

Naturally, the BER performance improvements of the noncoherent detection schemes introduced in this chapter are achieved at the cost of imposing an increased complexity. In order to clarify the trade-off between the power gain attained and the extra system's complexity imposed, we summarize the associated trade-offs for different NC detection schemes in Table 2.7. Furthermore,

Scheme	N_{wind}	Power Gain	Complexity
Single-Link MSDSD	6	0 dB	14.6 EDC
	10	2 dB	27.3 EDC
Twin-Path MSDSD	3	8.7 dB	19.1 EDC
	4	11.2 dB	27.2 EDC
	5	12.7 dB	35.4 EDC
	6	13.3 dB	43.7 EDC
	8	13.9 dB	60.7 EDC
	10	14.3 dB	78.1 EDC
Triple-Path MSDSD	3	14.2 dB	27.03 EDC
	4	16.0 dB	39.2 EDC
	5	17.0 dB	51.6 EDC
	6	17.5 dB	64.9 EDC
	8	18.1 dB	92.1 EDC
	10	18.4 dB	130.0 EDC

Table 2.7: Summary of power gain versus complexity trade-off for multi schemes, where the power gain is in terms of SNR, the normalized Doppler frequency is fixed to $f_d = 0.03$, the target BER is at BER $= 10^{-4}$, the SNR required by the single-link MSDSD algorithm having $N_{\text{wind}} = 6$ for approaching the target BER of 10^{-4} is regarded as the benchmark.

the power gain versus complexity of the multiple-path MSDSD is visualized in Figure 2.26. It is demonstrated in Figure 2.26 that the benefit of investing an increased system complexity becomes more and more marginal upon increasing the observation window size N_{wind}.

However, the size of the critical matrix $\underline{\mathbf{U}} \in \mathbb{C}^{UN \times U^2 N}$ involved in the multiple-path MSDSD algorithm of Section 2.4 still grows exponentially upon increasing the number of paths U. Hence its employment becomes unrealistic in scenarios, which have a high number of paths. However, the discussions of the SISO-MSDSD algorithm were still constrained to single-link direct-transmission based systems in Section 2.5. Its multiple-path version had not been considered. These limitations

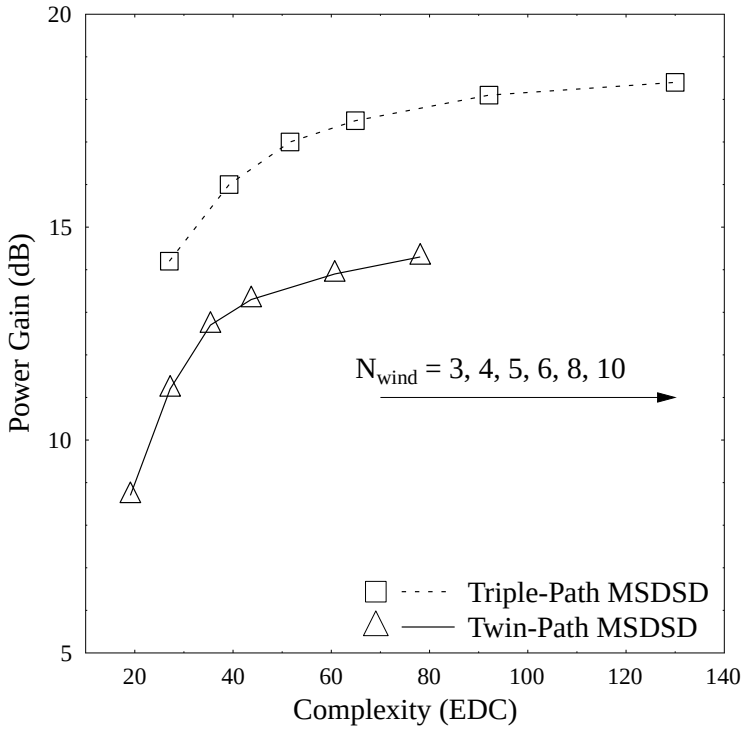

Figure 2.26: Power gain versus complexity for multiple-path MSDSD, where the power gain is in terms of SNR, the normalized Doppler frequency is fixed to $f_d = 0.03$, the target BER is at BER $= 10^{-4}$, the SNR required by the single-link MSDSD algorithm having $N_{\text{wind}} = 6$ for approaching the target BER of 10^{-4} is regarded as the benchmark. The results for "twin-path" system are based on the schematic of Figure 2.13, meanwhile the results for "triple-path" system are based on the schematic of Figure 2.14.

of the existing noncoherent detection schemes motivate us to develop an iterative-detection based multiple-path MSDSD in next chapter, whose decoding complexity will not be significantly increased upon increasing the number of paths. This novel technique will be incorporated in an attractive successive relaying aided network as a critical component of its receiver. The relevant contributions will be reported in the next chapter.

Chapter 3

Noncoherent Detection Aided Successive Relaying

Multiple-Input Multiple-Output (MIMO) techniques [94] are capable of providing a spatial diversity gain and hence efficiently mitigate the deleterious effects of hostile fading channels. However, the crucial condition for achieving a diversity gain is that the multiple co-located antenna elements are sufficiently far apart to experience independent fading. Regretfully, achieving transmit diversity in the uplink is typically impractical due to the limited size of the mobile. Fortunately, the family of cooperation techniques advocated by van der Meulen in [8] is capable of forming a virtual antenna array (VAA) for each node (user) by allowing nodes (users) to relay the messages of others to the destination. Hence, such a relay aided network practically constitutes a distributed MIMO system, where cooperative diversity is achieved [7, 10]. However, the conventional two-phase cooperative system [10] incurs a severe multiplexing loss due to the half-duplex transmit/receive constraint of practical transceivers. A beneficial technique of recovering the half-duplex relaying induced throughput loss was advocated in [43, 44, 95], where the successive relaying regime was proposed and analysed.

Most of the cooperative solutions found in the literature employ classic coherent detection. They also often assume the availability of perfect channel state information (CSI) at the receiver. However, practical pilot symbol assisted (PSA) techniques may impose a high pilot overhead, especially at high normalised Doppler frequencies. Then, the channel estimation of a M-transmitter, N-receiver MIMO system requires the estimation of $(M \times N)$ CSIs, which significantly increases the entire system's complexity and consumes considerable extra energy, especially when the Doppler frequency is high. Moreover, in a practical view, it is also hard to expect that in addition to the task of relaying, the relays could altruistically afford the complex and power-hungry task of channel estimation in support of coherent detection. Hence the employment of non-coherent detection operating without any requirement of channel estimation becomes an attractive design alternative, especially in cooperative networks in the interest of reducing the relay's complexity. As

demonstrated in Figure 2.3, they typically impose a 3dB performance loss in comparison with their perfect-channel-estimation-based counterparts in the AWGN channels or flat slow fading Rayleigh channels. Regretfully, however, it is also shown in Figure 2.3 that the noncoherent detector's performance significantly erodes at high normalized Doppler frequencies. As stated in Chapter 2, this performance degradation can be substantially mitigated with the aid of Multiple-Symbol Differential Detection (MSDD) [71]. However, along with the performance gain obtained by replacing CDD with MSDD, the associated imposed computing complexity grows exponentially with the increasing observation window size. As a remedy, the Multiple-Symbol Differential Sphere Detection (MSDSD) algorithm devised by Lampe *et al.* [53] strikes an attractive trade-off between the BER performance attained and the complexity imposed. Then, the MSDSD algorithm was considered in the context of cooperative communication systems [54, 81], and the single-user MSDSD algorithm was further developed for employment in single-user multiple-path scenarios. Resultantly, the so called "multiple-path MSDSD" algorithm introduced in Section 2.4 was created.

However, the above mentioned successive relaying regime imposes a co-channel interference at the DN, where the signals transmitted by the SN and that forwarded by the RN arrive at the DN almost simultaneously [96] and hence interfere each other[1]. This co-channel interference may significantly degrade the benefits of the successive relaying regime [43, 44]. On the other hand, as detailed in Section 2.4.2, the size of the matrix $\underline{\mathbf{U}} \in \mathbb{C}^{UN \times U^2 N}$ of (2.49) involved in the multiple-path MSDSD algorithm increases cubically upon increasing the number of paths U. Hence a further improvement of the multiple-path MSDSD algorithm is desired for the scenarios, which have a high number of propagation paths.

Against this background, we invoked the direct-sequence code division multiple access (DS-CDMA) [97] technique and designed the successive relaying aided cooperative DS-CDMA uplink. In this transmission framework, the successive relaying aided network (SRAN) is embedded into the DS-CDMA uplink for improving the communication quality of a cell-edge user. Hence, the DS-CDMA multiple-access technique is utilized for mitigating the successive relaying induced interference between the transmitted signals of the source and relay.

In more detail, for the sake of a fair comparison to the conventional two-phase cooperative system [10], we have to ensure that no extra channel-resources are required by our successive relaying aided cooperative DS-CDMA uplink. Practically, governed by a certain target BER value, there may be a strict limit to the number of active users that can be supported in a DS-CDMA system, which we denote by "$U_{\text{Threshold}}$". In general, it is realistic to assume that there are some idle users in a DS-CDMA cellular system. Hence, the preconditions of employing the proposed SRAN in support of a cell-edge user in our DS-CDMA system may be

1. We find a sufficient number of idle users between the SN and DN, willing to support the

[1]Here we ignore the propagation delay deference between the two path and set this aside for future research.

cell-edge user.

2. The sum of the number of active users and relays, namely $U_{\mathrm{ACT}} + U_{\mathrm{RN}}$ is still lower than $U_{\mathrm{Threshold}}$.

In other words, the relays employed in our SRAN are the idle users of the DS-CDMA cellular system. Moreover, since we assume that $U_{\mathrm{ACT}} + U_{\mathrm{RN}} < U_{\mathrm{Threshold}}$, the system does not run out of spreading sequences. However, when appointing idle users to serve as the relays increases the total number of active entities in the DS-CDMA cellular system, hence increasing the interference. Therefore, it may be concluded that the proposed successive relaying aided cooperative DS-CDMA uplink essentially converts the typical 50% half-duplex relaying-induced throughput loss to a potential user-load reduction of the CDMA system.

Additionally, we further develop the single-user/single-path MSDSD algorithm of [53] into a novel relay-aided form. More specifically, in Section 3.1.2, we will demonstrate that compared to the multiple-path MSDSD algorithm of [54, (26)], the size of the matrix $\mathbf{U}$ defined in (3.18) only increases linearly with the number of communicating entities (source node plus relays) in our novel relay-aided MSDSD and hence the system's complexity is reduced. Then, in Section 3.1.3, we will incorporate our relay-aided MSDSD algorithm into the successive relaying aided cooperative DS-CDMA uplink. A specific decoding arrangement will be designed in Section 3.1.3 for solving this challenge. In order to mitigate the complexity imposed on the RN, throughout Section 3.1, we opt for employing the amplify-and-forward (AF) protocol at the RN. Consequently, the successive AF relaying aided cooperative DS-CDMA system employing the proposed relay-aided MSDSD algorithm [79] will be conceived in Section 3.1 as our basic prototype system.

This prototype system simultaneously achieves several advantages: i) it has a high bandwidth-efficiency, its successive relaying regime may be capable of recovering the half-duplex relaying induced throughput loss of 50%; ii) it overcomes the successive relaying induced interference at the DN, which is another benefit of combination with the DS-CDMA design philosophy; iii) it dispenses with the power-hungry channel estimation, accordingly, the relevant pilot overhead and the associated extra complexity are avoided; iv) it exhibits an attractive performance as a benefit of its specifically designed relay-aided MSDSD algorithm.

However, our noncoherent cooperation aided prototype system proposed in Section 3.1 only concentrates on a specific cell-edge user, while the impact of the interfering users activated in the same DS-CDMA cell, i.e. the multi-user interference (MUI) is ignored. Furthermore, apart from ignoring the MUI imposed on the successive AF relaying aided cooperative DS-CDMA uplink, another impediment of the successive relaying protocol is the inter-relay interference (IRI). Moreover, as we will demonstrate in Section 3.2.1.1, the IRI may be aggravated by a noise accumulation problem in our successive AF relaying aided network. Nevertheless, the suppression of the IRI had not been considered in the prototype system proposed in Section 3.1 or in [79]. Finally, the theoretical performance bound of the prototype system proposed in Section 3.1 and in [79] is still

unknown.

For the sake of improving our basic noncoherent detection aided cooperation prototype of [79], by overcoming its drawbacks mentioned above, in Section 3.2, we will consider a general multi-user spread-spectrum scenario, where the multiple access interference (MAI) is also taken into account. More explicitly, in Section 3.2.1, we will design a DS-CDMA based interference suppression regime for mitigating the MAI as well as both the successive relaying induced CCI and the IRI, which essentially converts the typical 50% half-duplex relaying-induced throughput loss to a commensurate user-load reduction of the CDMA system. In section 3.2.2, we also derive the noncoherent discrete-input continuous-output memoryless channel (DCMC) capacity of the AF based SRAN in the context of the DS-CDMA uplink for theoretically characterizing the system considered. Consequently, an AF based SRAN operating in the context of the multi-user DS-CDMA uplink, which is decontaminated from the MUI and IRI was proposed in [98, 99] as a further improved version of our original noncoherent cooperation aided prototype [79].

As mentioned in Section 1.2, in contrast to the AF protocol, the decode-and-forward (DF) protocol may achieve a better BER performance at the cost of imposing a higher complexity on the RN. With the goal of designing an energy-efficient communication system, in Section 3.3, we will replace the AF based SRAN by the DF based SRAN. Another technique of significantly reducing the energy resources required, while maintaining a given target BER is constituted by replacing the hard-decision-based MSDSD algorithm by the more energy-efficient soft-decision-based MSDSD algorithm. However, as mentioned in the last paragraph of Section 2.6, the SISO-MSDSD algorithm [55] was still constrained to single-link direct-transmission based systems. Its multiple-path version had not been considered in Section 2.5. In more detail, the SISO-MSDSD algorithm of Section 2.5 was applied to a conventional single-relay aided two-phase cooperative network in [100], where the SISO-MSDSD operates in a classical distributed turbo decoding mode. By contrast, in order to develop it further for the multiple-path context involved in the DF based SRAN of Section 3.3.1, we specifically designed a relay-aided SISO-MSDSD decoder, which is capable of jointly decoding the different received signal streams at the destination. Hence the extra iterations imposed by the distributed turbo decoding structure employed in [100] were avoided, which remarkably reduced the system's complexity. Consequently, a sophisticated relay-aided SISO-MSDSD assisted three-stage iterative-detection architecture was devised in [80, 99] for realizing the proposed successive DF relaying aided cooperative multi-user system, which will be detailed in Section 3.3.3. As a further advance, its noncoherent DCMC capacity was also evaluated in [80, 99] in support of the theoretical analysis. Finally, in Section 3.3.4, we will demonstrate that by incorporating the relay-aided SISO-MSDSD decoder in the DF based SRAN, the resultant three-stage iterative-detection based transceiver significantly reduces the system's complexity and recovers the half-duplex relaying induced throughput loss, while operating close to the associated capacity. Nonetheless, we note again that the overall system's same rate potentially remains unchanged.

In summary, the evolution of our noncoherent successive relaying aided cooperative DS-CDMA

system from its basic version to a fully-fledged version is visualized in Figure 3.1, where the terms "System-I", "System-II", "System-III" correspond to our systems proposed in Section 3.1 [79], in Section 3.2 [98] as well as in Section 3.3 [80], respectively.

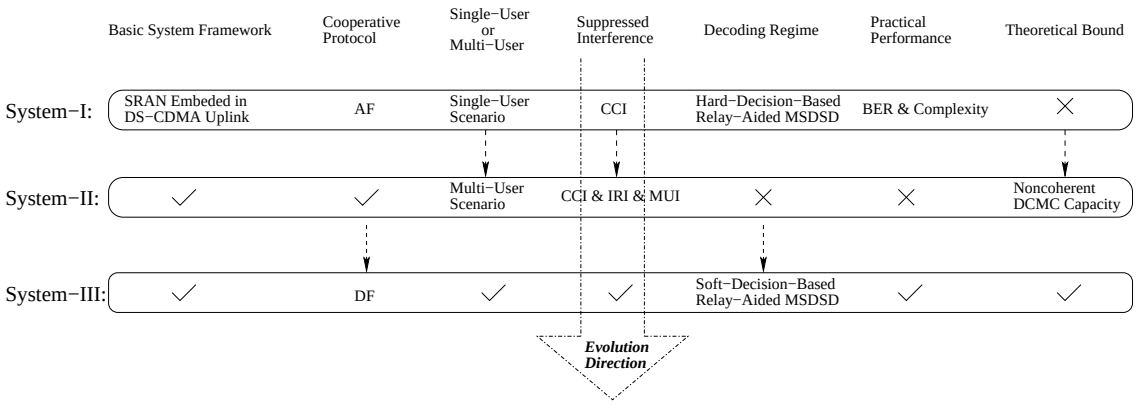

Figure 3.1: The development of our noncoherent successive relaying aided cooperative DS-CDMA system. The crosses indicate that the associated operations are not implemented in the specific system. The tick means that the associated operations of the preceding system were inherited by the current system. The dashed arrow is used to emphasize the specific change between two different systems.

3.1 Successive AF Relaying Aided Single-User DS-CDMA Uplink: Employ Relay-Aided MSDSD

As argued at the beginning of this chapter, incorporating noncoherent detection into cooperative networks constitutes a promising strategy. In more detail, in Section 3.1.2, we devised a novel relay-aided MSDSD algorithm for acting as our noncoherent detection scheme. Then, in Section 3.1.3, we embedded the hard-decision-based relay-aided MSDSD into the AF based SRAN for constituting our system's basic framework. The resultant system prototype is discussed in the Section 3.1.4 along with its BER and complexity characteristics.

The contents of this section are organised as follows. The system model of the proposed successive AF relaying aided DS-CDMA uplink is described in Section 3.1.1. Section 3.1.2 details our novel hard-decision-based relay-aided MSDSD algorithm. Then Section 3.1.3 analyses the requirement of the specific coding and decoding strategy. The associated simulation results and their discussions are provided in Section 3.1.4.

3.1.1 System Overview of the Successive AF Relaying Aided DS-CDMA Uplink

We consider the uplink of the relay aided DS-CDMA system of Figure 3.2, where s_n and $h_{s_n d}$, $n = 1, 2, \ldots, M$, represent the Mobile Stations (MSs) $\{s_n\}_{n=1}^{M}$ and the Channel Impulse Responses (CIR) spanning from the source s_n to the destination, respectively. We assume that some of the idle MSs are willing to act as relays and they exclusively assist one of the M users seen at the left hand side of Figure 3.2 based on the successive relaying protocol of [44]. Explicitly, the elements of Figure 3.2 constitute a classic successive relaying aided network (SRAN) using DS-CDMA transmissions. Let us now focus our attention on this successive relaying regime. Figure 3.3

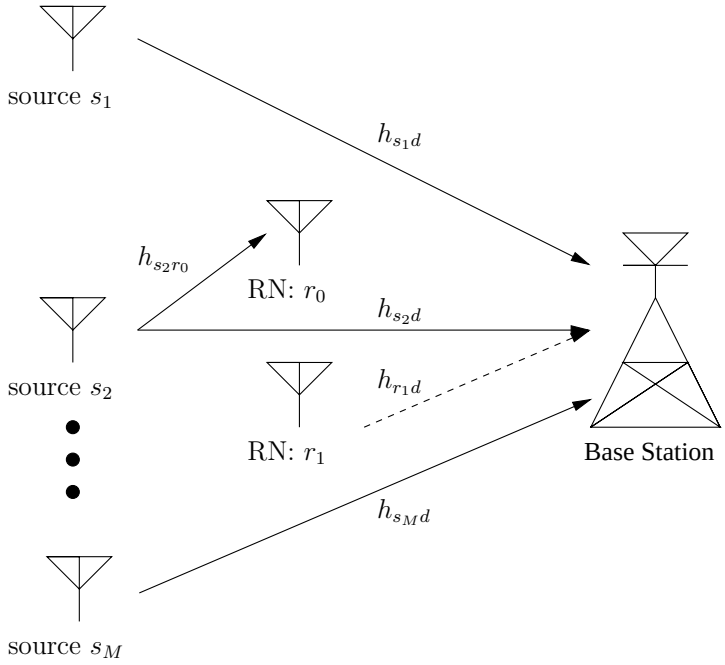

Figure 3.2: The simplified uplink diagram of the successive AF relaying aided DS-CDMA, assuming that the successive relaying aided cooperative sub-system is embedded in the middle.

further details the principles portrayed in Figure 3.2, displaying three scenarios corresponding to the different cooperative frames. We assume that the two relays are sufficiently far apart, so that the channels experienced by the different relays experience reasonably independent fading with respect to each other even in the presence of correlated shadowing and hence achieve the maximum attainable spatial diversity. We also assume that the impact of the successive relaying induced IRI reported in [44] is negligible in our scenario, in other words relay r_0 is assumed to receive no interference from relay r_1 and vice versa. The signals are supposed to be perfectly synchronised, for example using the solution of [101]. The pass-loss effects are ignored for simplicity. In order to improve the practicability of our work, classic frame-by-frame based transmissions routinely employed in realistic communication networks are considered here. According to the specific structure of the successive relaying aided cooperative network, the frame-based transmission regime delivers

a specific codeword which is forwarded by the RN and will arrive at the DN a frame period later with respect to the directly received replica transmitted by the SN. Hence the system delay is related to the frame length L. Based on these assumptions, Figure 3.3 summarizes the main properties of the SRAN.

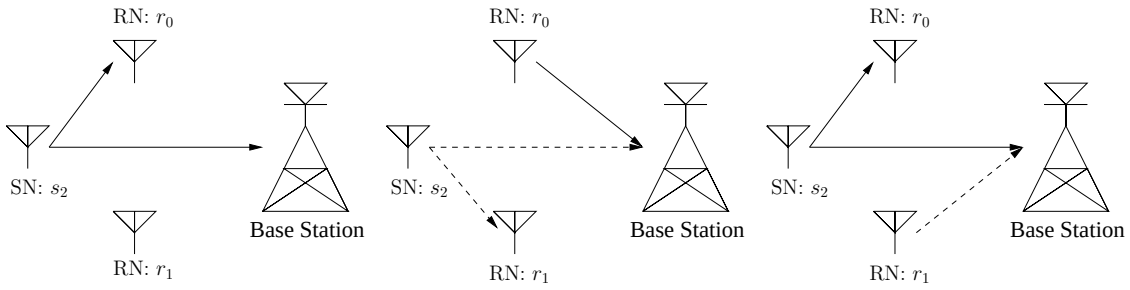

Figure 3.3: The successive relaying aided cooperative sub-system, during various cooperative frames.

In this section, we consider the successive relaying induced CCI problem reported in [43, 44]. As detailed in [102], the CCI is owing to that the signals directly transmitted by the SN and the signals forwarded by one of the two RNs are always simultaneously received at the DN. Hence, the algorithm discussed in [103] provides a feasible method of extracting the different components from the resultant composite signal with an acceptable accuracy. Inspired by [103], the DS-CDMA technique was adopted in order to avoid the potential interference between the transmitted signals of the SN and RN, which was further developed for our SRAN.

In more detail, a number of $(L-1)$ M_c-ary PSK information symbols $V[k] \in \chi = \{e^{j2\pi m/M_c}; m = 0, 1, \cdots, M_c - 1\}$ are differentially encoded at the SN according to (2.1) of Chapter 2 and consequently generate the l^{th} frame, which consists of a number of L M_c-ary DPSK modulated signals. Then, let k indicate the global index of a M_c-ary DPSK signal involved in our transmissions.

We divide all the frames into two sets, according to which specific RN receiver was activated during that frame. The frame in which relay r_0 is receiving is referred to as frame A and the frame during which relay r_1 is receiving becomes frame B. For example, frame 1 and frame 2 depicted in Figure 3.3 correspond to frame-set B and frame-set A, respectively. Then, a specific DS-CDMA spreading strategy is implemented: two different binary DS spreading waveforms, namely $\mathbf{C}_0$, $\mathbf{C}_1$ chosen from the entire spreading sequence family are employed for spreading the signals transmitted by the SN during frame A and frame B, respectively.

Furthermore, the AF relaying scheme [81] is adopted in order to impose a lower complexity compared to that of the DF scheme [81]. For the sake of a fair comparison with classic direct communications using no relays, the power allocation strategy introduced at the beginning of Section 2.4.3 is adopted here again. Hence we have $P_s + P_{r_i} = P, i \in \{0, 1\}$ and $P_s = P_{r_0} = P_{r_1}$. According to [54] and to the analysis of the delay associated with the relayed signals, the amplified

signal forwarded by the i^{th} RN may be expressed as

$$\begin{aligned} R_{r_i d}[k] &= f_{AM_{r_i}} y_{sr_i}[k-L] \\ &= f_{AM_{r_i}} \left\{ \sqrt{P_s} S[k-L] h_{sr_i}[k-L] + n_{sr_i}[k-L] \right\}, \quad i \in \{0,1\} \end{aligned} \tag{3.1}$$

where $y_{sr_i}[k-L]$ represents the source-to-relay signal received at the i^{th} RN during the last frame; $S[k-L]$ is the signal broadcast from the SN in the last frame; $h_{sr_i}[k-L]$ corresponds to the CIR between the SN and the i^{th} RN in the last frame; $n_{sr_i}[k-L]$ is the AWGN noise; as stated in (2.27) and (2.28), $f_{AM_{r_i}}$ is the amplification factor of the i^{th} relay, which should ensure that the average transmit power of the i^{th} relay equals to P_{r_i}, and is given by [104]

$$f_{AM_{r_i}} = \sqrt{\frac{P_{r_i}}{P_s \sigma_{sr_i}^2 + N_0}}, \tag{3.2}$$

where $\sigma_{sr_i}^2$ represents the variance of the channel's complex envelope between the SN and the i^{th} RN, while N_0 is the noise variance.

Let us now define

$$\begin{aligned} \mathbf{y}^A[k] &= \left[y^A[(k-1)Q+1], y^A[(k-1)Q+2], \ldots, y^A[(k-1)Q+Q] \right]^T \\ \mathbf{y}^B[k] &= \left[y^B[(k-1)Q+1], y^B[(k-1)Q+2], \ldots, y^B[(k-1)Q+Q] \right]^T \\ \mathbf{C}_0 &= \frac{1}{\sqrt{Q}} \left[c_0[1], c_0[2], \ldots, c_0[Q] \right]^T \\ \mathbf{C}_1 &= \frac{1}{\sqrt{Q}} \left[c_1[1], c_1[2], \ldots, c_1[Q] \right]^T \end{aligned} \tag{3.3}$$

where $y^A[(k-1)Q+q]$ represents the $\big((k-1)Q+q\big)^{th}$ received signal chip at the DN in a chip-duration and all the Q chips $\{y^A[(k-1)Q+q]\}_{q=1}^{Q}$ constitute the vector $\mathbf{y}^A[k]$, which represents the signal vector corresponding to the k^{th} entire symbol-duration. The variables $y^B[(k-1)Q+q]$ and $\mathbf{y}^B[k]$ have similar definitions and the same relationship with respect to $y^A[(k-1)Q+q]$ and $\mathbf{y}^A[k]$. Explicitly, $c_0[q]$ or $c_1[q]$ is one of the chip-waveforms and belongs to $\mathbf{C}_0$ or $\mathbf{C}_1$, whose spreading factor is Q. Hence, the exact components of the signal received at the DN in the A or B type frames may be formulated respectively as

$$\begin{aligned} \mathbf{y}^A[k] =& \sqrt{P_s} S[k] \mathbf{C}_0 h_{sd}[k] + \\ & f_{AM_{r_1}} \left\{ \sqrt{P_s} S[k-L] \mathbf{C}_1 h_{sr_1}[k-L] + \mathbf{n}_{r_1}[k-L] \right\} h_{r_1 d}[k] + \mathbf{n}_d[k], \end{aligned} \tag{3.4}$$

$$\begin{aligned} \mathbf{y}^B[k] =& \sqrt{P_s} S[k] \mathbf{C}_1 h_{sd}[k] + \\ & f_{AM_{r_0}} \left\{ \sqrt{P_s} S[k-L] \mathbf{C}_0 h_{sr_0}[k-L] + \mathbf{n}_{r_0}[k-L] \right\} h_{r_0 d}[k] + \mathbf{n}_d[k], \end{aligned} \tag{3.5}$$

where the notation $\mathbf{n}_a[k] = \left[n_a[(k-1)Q+1], n_a[(k-1)Q+2], \ldots, n_a[(k-1)Q+Q] \right]^T$ represent the AWGN noise vector imposing on the node $a \in \{r_i, d\}$ during the k^{th} symbol duration. Its component $n_a[(k-1)Q+q]$ obeys the distribution of $\mathcal{CN}(0, N_0)$

The specific DS-CDMA spreading strategy employed enables us to alternatively despread the signals received at the DN by reconfiguring the chip-waveform matched-filter according to the

frame type (A or B). In the l^{th} frame A, we first employ a filter matched to the waveform of $\mathbf{C}_0$. The main component of the despread signal is the source signal $S[k]$, while the component corresponding to the source signal $S[k-L]$ forwarded by relay r_1 becomes the interference. At the next step, we reconfigure the filter to match the waveform of $\mathbf{C}_1$. Consequently, the main component becomes the previous source signal $S[k-L]$, and simultaneously the current source signal $S[k]$ acts as the interference. The pair of different despread signals generated from the same received signal during frame A is described by

$$z_s^A[k] = \sqrt{P_s}S[k]h_{sd}[k] + I_{r_1}[k] + n'_{r_1}[k] + n_d[k], \tag{3.6}$$

and

$$z_{r_1}^A[k] = \sqrt{P_s}S[k-L]h_{sr_1}[k-L]f_{AM_{r_1}}h_{r_1d}[k] + I_s[k] + n'_{r_1}[k] + n_d[k], \tag{3.7}$$

where both $I_{r_1}[k] = \frac{1}{Q}\sqrt{P_s}S[k-L]h_{sr_1}[k-L]f_{AM_{r_1}}h_{r_1d}[k]$ and $I_s[k] = \frac{1}{Q}\sqrt{P_s}S[k]h_{sd}[k]$ represent the interfering components. Then the AWGN imposed on the signals received by RN r_1 will be amplified by a factor of $f_{AM_{r_1}}$ and transmitted via the channel between the RN r_1 and DN. Finally, we arrive at $n'_{r_1}[k] = \mathbf{C}_0^T\mathbf{n}_{r_1}[k-L]f_{AM_{r_1}}h_{r_1d}[k]$, which can be rewritten as $n'_{r_1}[k] = n_{r_1}[k-L]f_{AM_{r_1}}h_{r_1d}[k]$ and the AWGN noise $n_{r_1}[k]$ obeys the distribution of $\mathcal{CN}(0, N_0)$. Furthermore, $n_d[k] = \mathbf{C}_0^T\mathbf{n}_d[k] \sim \mathcal{CN}(0, N_0)$ is the AWGN imposed on the signal received at the DN. Similarly, in frame B, two differently despread signals can be obtained, which are represented by

$$z_s^B[k] = \sqrt{P_s}S[k]h_{sd}[k] + I_{r_0}[k] + n'_{r_0}[k] + n_d[k] \tag{3.8}$$

and

$$z_{r_0}^B[k] = \sqrt{P_s}S[k-L]h_{sr_0}[k-L]f_{AM_{r_0}}h_{r_0d}[k] + I_s[k] + n'_{r_0}[k] + n_d[k], \tag{3.9}$$

where the terms such as $I_{r_0}[k]$, $I_s[k]$, $n'_{r_0}[k]$, and $n_d[k]$ maintain similar properties to those mentioned before. Benefiting from the particular spreading and despreading strategies employed, the CCI imposed by successive relaying can also be successfully mitigated, when employing an amplify-and-forward relaying scheme. More explicitly, we are not constrained to the employment of decode-and-forward relaying schemes, when considering the CCI cancellation problem in the context of cooperative systems. Hence the DS-CDMA despread, decode, re-encode and re-spread operations employed at the RN in [103] are avoided, therefore, the system's complexity is reduced. Additionally, the number of spreading sequences required is also lower compared to [103].

3.1.2 Principle of Hard-Decision-Based Relay-Aided MSDSD

As introduced in Section 2.4, the MSDSD algorithm was advocated in the context of cooperative communication systems in [54]. One of the critical design issues is that of combining the multiple relay-aided received signals, which correspond to the same source symbols but are transmitted by multiple users and experience different channels. Clearly, we want to generate a single observed

signal sequence, similar to that of the single-user MSDSD operations. Consequently, the single-user MSDSD may be directly applied to process this composite signal sequence. As summarized in Section 2.6, the problem is that the extension of the single-user MSDSD to the multiple-path MSDSD of [54] is feasible, but the size of the critical matrix $\mathbf{U}$ of [54, (26)] rapidly increases and the implementation of sphere detection based on this matrix becomes a challenge, when the number of users increases. Hence, a new relay-aided MSDSD concept is introduced here. Without loss of generality, let us define

$$\begin{aligned}\mathbf{V} &= \left[V[1], V[2], \ldots, V[N-1]\right]^T \\ \mathbf{S} &= \left[S[1], S[2], \ldots, S[N]\right]^T \\ \mathbf{Z}_u &= \left[z_u[1], z_u[2], \ldots, z_u[N]\right]^T \\ \mathbf{H}_u &= \left[h_u[1], h_u[2], \ldots, h_u[N]\right]^T, \end{aligned} \tag{3.10}$$

where $\mathbf{V}$ is the original M_{ary}-PSK information symbol sequence and $\mathbf{S}$ is the differentially encoded M_{ary}-DPSK symbol sequence. Furthermore, $\mathbf{Z}_u$ is the individual symbol sequence received from the u^{th} entity (SN or RN). Finally, $\mathbf{H}_u$ is the CIR vector of the channel between the u^{th} entity and the DN, while N is the observation window size of MSDSD, which is a time domain parameter.

Similar to the situation discussed in [105], provided that the assumptions made in Section 3.1.1 are satisfied, the received sequences $\{\mathbf{Z}_u\}_{u=1}^{U}$ are independent Gaussian random vectors. Hence the corresponding conditional PDF can be written as

$$\Pr\left(\{\mathbf{Z}_u\}_{u=1}^{U}|\mathbf{S}\right) = \prod_{u=1}^{U} \Pr\left(\mathbf{Z}_u|\mathbf{S}\right), \tag{3.11}$$

where U is the number of entities involved in cooperative communication. According to [71], when an M_c-ary DPSK sequence was transmitted, the conditional PDF of the u^{th} received sequence $\mathbf{Z}_u$ is represented as

$$\begin{aligned}\Pr\left(\mathbf{Z}_u|\mathbf{S}\right) &= \frac{1}{(2\pi)^{\frac{N}{2}} \left\|\mathbf{\Phi}_{\mathbf{Z}_u\mathbf{Z}_u}\right\|^{\frac{1}{2}}} \exp\left(-\frac{1}{2}{\mathbf{Z}_u}^H \mathbf{\Phi}^{-1}_{\mathbf{Z}_u\mathbf{Z}_u}\mathbf{Z}_u\right) \\ &= \eta_u \cdot \exp\left(-\frac{1}{2}{\mathbf{Z}_u}^H \mathbf{\Phi}^{-1}_{\mathbf{Z}_u\mathbf{Z}_u}\mathbf{Z}_u\right). \end{aligned} \tag{3.12}$$

Upon substituting (3.12) into (3.11), (3.11) may be rewritten as

$$\Pr\left(\{\mathbf{Z}_u\}_{u=1}^{U}|\mathbf{S}\right) = \left(\prod_{u=1}^{U}\eta_u\right) \times \exp\left(-\frac{1}{2}\sum_{u=1}^{U}{\mathbf{Z}_u}^H \mathbf{\Phi}^{-1}_{\mathbf{Z}_u\mathbf{Z}_u}\mathbf{Z}_u\right), \tag{3.13}$$

where the factor $\prod_{u=1}^{U}\eta_u$ is independent of $\mathbf{S}$. Hence, the relay-aided MSDSD decision rule of finding the specific sequence $\mathbf{S}' = \left[S'[1], S'[2], \ldots, S'[N]\right]^T$ which maximises the conditional PDF of (3.13) is equivalent to selecting the particular transmitted source signal sequence $\mathbf{S}'$, whose matrix sum is the smallest, which is formulated as

$$\mathbf{S}' = \arg\min_{\mathbf{S}}\left\{\sum_{u=1}^{U}{\mathbf{Z}_u}^H \mathbf{\Phi}^{-1}_{\mathbf{Z}_u\mathbf{Z}_u}\mathbf{Z}_u\right\}, \tag{3.14}$$

where the correlation matrix obeys

$$\begin{aligned} \mathbf{\Phi}_{\mathbf{Z}_u\mathbf{Z}_u} &\triangleq \mathrm{diag}\{\mathbf{S}\}\mathbf{C}^{\mathrm{u}}\mathrm{diag}\{\mathbf{S}^*\}, \\ \mathbf{C}^u &\triangleq \mathcal{E}\left\{\mathbf{H}_u{\mathbf{H}_u}^H\right\} + \sigma_n^2\mathbf{I}_N, \\ \sigma_n^2 &= N_0. \end{aligned} \tag{3.15}$$

Similar to [53], the new relay-aided MSDSD decision rule can be rewritten as

$$\mathbf{S}' = \arg\min_{\mathbf{S}} \left\{ \sum_{u=1}^{U} \left\| \mathbf{U}^u\mathbf{S} \right\|^2 \right\}, \tag{3.16}$$

where we have $\mathbf{U}^u \triangleq \left(\mathbf{F}^u\mathrm{diag}\left\{\mathbf{Z}_{\mathrm{u}}\right\}\right)^*$, which is an upper triangular matrix. Then the corresponding upper triangular matrix $\mathbf{F}^u$ is defined by the Cholesky factorization of the inverse of the matrix $\mathbf{C}^u$, namely of $(\mathbf{C}^u)^{-1} = (\mathbf{F}^u)^H\mathbf{F}^u$. The more detailed version of the matrix $\mathbf{U}^u$ is formulated as

$$\mathbf{U}^u = \begin{bmatrix} \mathbf{U}^u_{1,1} & \mathbf{U}^u_{1,2} & \cdots & \mathbf{U}^u_{1,N} \\ 0 & \mathbf{U}^u_{2,2} & \cdots & \mathbf{U}^u_{2,N} \\ \vdots & \vdots & \ddots & \vdots \\ 0 & 0 & \cdots & \mathbf{U}^u_{N,N} \end{bmatrix}_{N\times N}. \tag{3.17}$$

Then, we further define a $(UN \times N)$-element matrix $\mathbf{U}$ as

$$\mathbf{U} = \begin{bmatrix} \mathbf{U}_{1,1} & \mathbf{U}_{1,2} & \cdots & \mathbf{U}_{1,N} \\ 0 & \mathbf{U}_{2,2} & \cdots & \mathbf{U}_{2,N} \\ \vdots & \vdots & \ddots & \vdots \\ 0 & 0 & \cdots & \mathbf{U}_{N,N} \end{bmatrix}_{UN\times N}, \tag{3.18}$$

and

$$\mathbf{U}_{i,j} = [\mathbf{U}^1_{i,j}, \mathbf{U}^2_{i,j}, \cdots, \mathbf{U}^U_{i,j}]^T, \tag{3.19}$$

where $\mathbf{U}_{i,j}$ is the specific vector component of $\mathbf{U}$ in row i and column j, $1 \le i,j \le N$, $\mathbf{U}^u_{i,j}$ denotes the entry of $\mathbf{U}^u$ found in row i and column j. Upon substituting (3.18) into (3.16), we finally arrive at our relay-aided MSDSD decision rule

$$\mathbf{S}' = \arg\min_{\mathbf{S}} \left\{ \left\| \mathbf{U}\mathbf{S} \right\|^2 \right\}. \tag{3.20}$$

Compared to the single-user/single-stream MSDSD of [53], to implement the proposed relay-aided MSDSD given by (3.20), the difference manifests itself in the definition of the best candidate point $S'[i]$ for the i^{th} estimated symbol in $\mathbf{S}'$, which has to satisfy

$$S'[i] = \arg\min_{\chi} \left\{ \sum_{u=1}^{U} \left| \mathbf{U}^u_{i,i}S'[i] + \sum_{j=i+1}^{N} \mathbf{U}^u_{i,j}S'[j] \right|^2 \right\}. \tag{3.21}$$

The size of the corresponding matrix $\mathbf{U}$ used in [54, (26)] is $(UN \times U^2N)$, which is cubically proportional to the number of entities U. By contrast, the size of the newly devised matrix $\mathbf{U}$ of

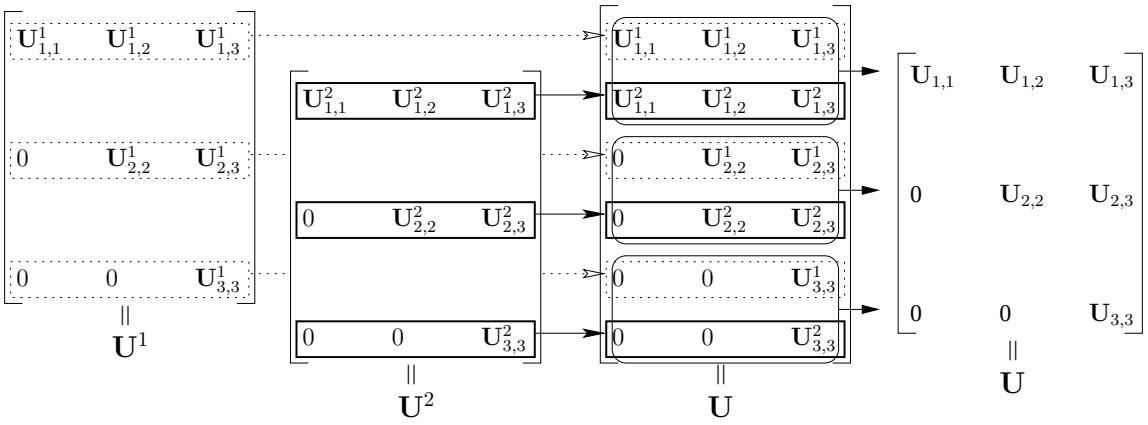

Figure 3.4: As formulated in (3.18) and (3.19), the first rows of $\mathbf{U}^1$ and $\mathbf{U}^2$ are vertically stacked to constitute the first virtual row of $\mathbf{U}$, which is represented by the rectangle having rounded corners. Similarly, the second rows of $\mathbf{U}^1$ and $\mathbf{U}^2$ are vertically stacked to constitute the second virtual row of $\mathbf{U}$, which is also represented by the rectangle associated with rounded corners. Hence an element of $\mathbf{U}$, for example $\mathbf{U}_{2,3}$ as seen at the right hand side is given by $\mathbf{U}_{2,3} = \left[\mathbf{U}^1_{2,3}, \mathbf{U}^2_{2,3}\right]^T$.

(3.18) is reduced to $(UN \times N)$, which only increases linearly with U. Furthermore, in contrast to the channel-noise autocorrelation matrix $\mathbf{C}^u$ involved in (3.14), which is computed only once during the entire detection process, the calculation of the matrix $\mathbf{U}$ is repeated in every observation window. Hence our relay-aided MSDSD proposed in this paper reduces the complexity imposed by the multiple-path MSDSD algorithm [54], especially for $U > 3$.

Our algorithm may be decomposed into two steps: first, we individually calculate each $\mathbf{U}^u$ contribution seen in (3.17) according to the conventional single-user MSDSD algorithm; then, we execute the relay-aided MSDSD based on the matrix $\mathbf{U}$ of (3.18), which is constituted by combining all the $\{\mathbf{U}^u\}_{u=1}^U$ components based on (3.19).

Example 3.1: Combining the $(N \times N)$-element matrices $\{\mathbf{U}^u\}_{u=1}^U$ into an $(UN \times N)$-element matrix $\mathbf{U}$: $U = 2$, $N = 3$

In comparison to the decision metric of the single-link MSDSD algorithm of (2.19), the decision metric of the relay-aided MSDSD algorithm formulated in (3.16) has a slightly different format, which may be regarded as a sum of the single link MSDSD decision metrics. In order to represent the decision rule of the relay-aided MSDSD algorithm in the same format as that of the single-link MSDSD algorithm, we define an $(UN \times N)$-element matrix $\mathbf{U}$ in (3.18). With the aid of the $(UN \times N)$-element matrix $\mathbf{U}$, we then rewrite the decision rule of the relay-aided MSDSD algorithm in the form of (3.20), which can be regarded as a "shortest vector problem". Hence, the sphere detection process interpreted in Section 2.3.2 becomes applicable again for solving this "shortest vector problem".

The composition of the $(UN \times N)$-element matrix $\mathbf{U}$ based on U $(N \times N)$-element matrices $\mathbf{U}^u$ is formulated according to (3.17), (3.18), (3.19). In order to exemplify this critical operation, we assume that $U = 2$ and $N = 3$. Correspondingly, there are two (3×3)-element matrices. According to (3.17), one of them associated with the transmission path from the SN to the DN is given by

$$\mathbf{U}^1 = \begin{bmatrix} \mathbf{U}^1_{1,1} & \mathbf{U}^1_{1,2} & \mathbf{U}^1_{1,3} \\ 0 & \mathbf{U}^1_{2,2} & \mathbf{U}^1_{2,3} \\ 0 & 0 & \mathbf{U}^1_{3,3} \end{bmatrix}. \tag{3.22}$$

Similarly, another (3×3)-element matrix associated with the transmission path from the RN to the DN is given by

$$\mathbf{U}^2 = \begin{bmatrix} \mathbf{U}^2_{1,1} & \mathbf{U}^2_{1,2} & \mathbf{U}^2_{1,3} \\ 0 & \mathbf{U}^2_{2,2} & \mathbf{U}^2_{2,3} \\ 0 & 0 & \mathbf{U}^2_{3,3} \end{bmatrix}. \tag{3.23}$$

Then the process of combining the two (3×3)-element matrices $\mathbf{U}^1$ and $\mathbf{U}^1$ into the (6×3)-element matrix $\mathbf{U}$ is illustrated in Figure 3.4.

3.1.3 Incorporate Relay-Aided MSDSD into the AF Based SRAN

Our motivation in this section is to incorporate the relay-aided MSDSD of Section 3.1.2 into the successive AF relaying cooperative regime of Figure 3.3, and consequently create the relay-aided MSDSD assisted successive AF relaying based cooperative DS-CDMA system. Without loss of generality, we focus our attention on a length-N M_c-ary DPSK symbol vector broadcast by the SN during frame A, namely $\mathbf{S}$, which is represented as

$$\mathbf{S} = \big[S[k+1], S[k+2], \ldots, S[k+N]\big]^T. \tag{3.24}$$

According to the analysis provided in Section 3.1.1, one of the two replicas of the observed M_c-ary DPSK symbol block $\mathbf{S}$ is generated by the source-to-destination transmission in the same frame of $\mathbf{S}$ and actually constituted by the despread signals $z^A_s[k]$ of (3.6) as

$$\mathbf{Z}^A_s = \big[z^A_s[k+1], z^A_s[k+2], \ldots, z^A_s[k+N]\big]^T. \tag{3.25}$$

The another replica of the observed M_c-ary DPSK symbol block $\mathbf{S}$ forwarded by RN r_0 will arrive at the DN L symbol periods later in the next frame and actually be constituted by the despread signals $z^B_{r_0}[k]$ of (3.9) as

$$\mathbf{Z}^B_{r_0} = \big[z^B_{r_0}[k+L+1], z^B_{r_0}[k+L+2], \ldots, z^B_{r_0}[k+L+N]\big]^T. \tag{3.26}$$

Clearly, according to the principle described in Section 3.1.2, we can directly implement the relay-aided MSDSD algorithm by utilizing $\mathbf{Z}^A_s$ and $\mathbf{Z}^B_{r_0}$ as the $\mathbf{Z}_u$ components in (3.11). The entire process is illustrated in more detail by Figure 3.5, where the exact activities of each entity in

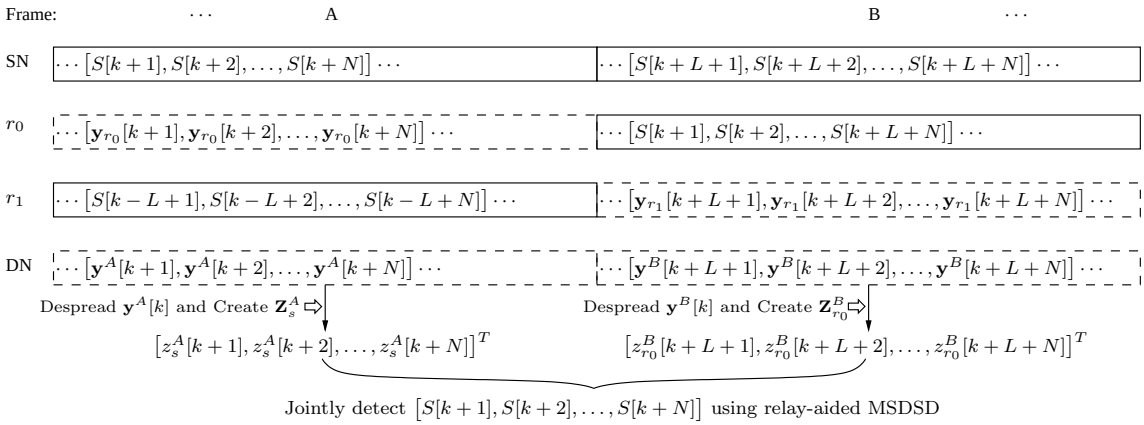

Figure 3.5: Frame structure of the relay-aided MSDSD assisted successive AF relaying based cooperative system, where the solid box represents the transmitted signals, the dashed box the received signals.

the relay-aided MSDSD assisted successive AF relaying based cooperative network are portrayed during frame A or B.

Furthermore, the vector $\mathbf{Z}_s^A$ in (3.25) may be rewritten in a more compact matrix form as

$$\mathbf{Z}_s^A = \mathbf{H}_{sd}\mathbf{S} + \mathbf{W}_s^A, \tag{3.27}$$

where $\mathbf{H}_{sd}$ and $\mathbf{W}_s^A$ are given by (3.28) and (3.29), respectively, which are the equivalent CIR matrix and the equivalent noise matrix, respectively.

$$\mathbf{H}_{sd} = \begin{bmatrix} \sqrt{P_s}h_{sd}[k+1] \\ \sqrt{P_s}h_{sd}[k+2] \\ \vdots \\ \sqrt{P_s}h_{sd}[k+N] \end{bmatrix}_{N\times 1}, \tag{3.28}$$

$$\mathbf{W}_s^A = \begin{bmatrix} \frac{\sqrt{P_s}}{Q}S[k-L+1]h_{sr_1}[k-L+1]f_{AM_{r_1}}h_{r_1d}[k+1] + n_{r_1}[k-L+1]f_{AM_{r_1}}h_{r_1d}[k+1] + n_d[k+1] \\ \frac{\sqrt{P_s}}{Q}S[k-L+2]h_{sr_1}[k-L+2]f_{AM_{r_1}}h_{r_1d}[k+2] + n_{r_1}[k-L+2]f_{AM_{r_1}}h_{r_1d}[k+2] + n_d[k+2] \\ \vdots \\ \underbrace{\frac{\sqrt{P_s}}{Q}S[k-L+N]h_{sr_1}[k-L+N]f_{AM_{r_1}}h_{r_1d}[k+N]}_{I_{r_1}} + \underbrace{n_{r_1}[k-L+N]f_{AM_{r_1}}h_{r_1d}[k+N]}_{n'_{r_1}} + n_d[k+N] \end{bmatrix} \tag{3.29}$$

Here, the interference component I_{r_1} is approximated by a noise process, hence the equivalent noise process of (3.29) is constituted by the 2nd, 3rd and 4th components of (3.6), which are the interference term I_{r_1}, the amplified and faded noise component n'_{r_1} and the AWGN n_d. Furthermore, (3.30)∼(3.31) are provided to facilitate the calculation of $\mathbf{U}^s$ of (3.17) which corresponds to $\mathbf{Z}_s^A$. Apparently, the evaluation of the correlation matrices, namely $\mathcal{E}\left\{\mathbf{H}_{sd}{\mathbf{H}_{sd}}^H\right\}$ and $\mathcal{E}\left\{\mathbf{W}_s^A{\mathbf{W}_s^A}^H\right\}$, is similar to that involved in (2.39) and (2.41), respectively. In more detail, all the links involved in

the cooperative communication session are simultaneously taken into account in (2.39) and (2.41). By contrast, when we exploit the distributed nature of our novel relay-aided MSDSD algorithm detailed in Section 3.1.2, we may concentrate on a single link in (3.30) and (3.31).

$$\mathcal{E}\left\{\mathbf{H}_{sd}\mathbf{H}_{sd}{}^{H}\right\} = P_s \times \begin{bmatrix} \varphi_{sd}(0) & \varphi_{sd}(1) & \cdots & \varphi_{sd}(N-1) \\ \varphi_{sd}(-1) & \varphi_{sd}(0) & \cdots & \varphi_{sd}(N-2) \\ \vdots & \vdots & \ddots & \vdots \\ \varphi_{sd}(1-N) & \varphi_{sd}(2-N) & \cdots & \varphi_{sd}(0) \end{bmatrix}_{N\times N}, \tag{3.30}$$

$$\mathcal{E}\left\{\mathbf{W}_s^A\mathbf{W}_s^{AH}\right\} = \mathbf{I}_N \times \left(\frac{P_s}{Q^2}\sigma_{sr_1}^2 f_{AM_{r_1}}^2\sigma_{r_1d}^2 + \left(\sigma_{r_1d}^2 f_{AM_{r_1}}^2 + 1\right)N_0\right). \tag{3.31}$$

Then, the vector $\mathbf{Z}_{r_0}^B$ in (3.26) obeys a similar relationship to $\mathbf{Z}_s^A$, yielding

$$\mathbf{Z}_{r_0}^B = \mathbf{H}_{sr_0d}\mathbf{S} + \mathbf{W}_{r_0}^B, \tag{3.32}$$

where the equivalent CIR vector $\mathbf{H}_{sr_0d}$ is defined as

$$\mathbf{H}_{sr_0d} = \begin{bmatrix} \sqrt{P_s}f_{AM_{r_0}}h_{sr_0}[k+1]h_{r_0d}[k+L+1] \\ \sqrt{P_s}f_{AM_{r_0}}h_{sr_0}[k+2]h_{r_0d}[k+L+2] \\ \vdots \\ \sqrt{P_s}f_{AM_{r_0}}h_{sr_0}[k+N]h_{r_0d}[k+L+N] \end{bmatrix}_{N\times 1}, \tag{3.33}$$

and $\mathbf{W}_{r_0}^B$ are similar to that conceived for $\mathbf{W}_s^B$. Furthermore, the $\mathbf{U}^{r_0}$ corresponding to $\mathbf{Z}_{r_0}^B$ can be attained in a similar way to the calculation of $\mathbf{U}^s$.

According to the principles outlined in Section 3.1.2, after individually calculating the matrices $\mathbf{U}^s$ and $\mathbf{U}^{r_a}$, we combine them to create the matrix $\mathbf{U}$ as detailed in (3.18) and (3.19). Finally, we invoke sphere detection according to (3.20) and (3.21), in order to complete the entire detection process of $\mathbf{S}$.

Based on the symmetry of the transmission mechanisms between frame A and B, the decoding process of the M_{ary}-DPSK symbol block broadcast by the SN during frame B is similar to that conceived for $\mathbf{S}$, as detailed above.

3.1.4 BER versus Complexity

Based on the analysis outlined in the previous sections, compared to the conventional two-phase Amplify-and-Forward (AF) cooperative procedure operations with the aid of the multiple-path MS-DSD algorithm of [54], the new scheme proposed in this section recovers the 50% throughput loss. However, this throughput improvement is achieved at the cost of imposing CCI plus the extra amplified and faded noise component $n'_{r_0}[k]$ in (3.6) on the received signals, which may erode the performance gain. Hence, the simulation results of Figure 3.6 characterize the trade-off between the achievable throughput and BER performance attained. In Figure 3.6, a time-selective communication environment is assumed, where the normalized Doppler frequency is fixed to $f_d = 0.01$

for all experiments based on our proposed systems. Then, the observation window size of MSDSD is fixed to $N = 6$ and differential QPSK (DQPSK) modulation is employed. The interpretations of the benchmark schemes employed for comparison are given in Table 3.1. The interference between

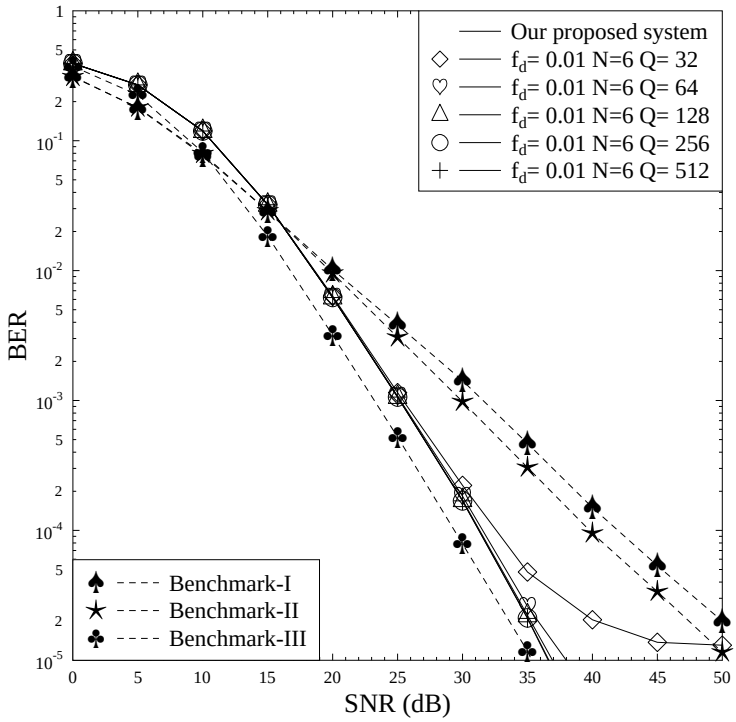

Figure 3.6: BER versus SNR performance of our relay-aided MSDSD assisted successive AF relaying based cooperative DS-CDMA uplink configured with various values of Q, when transmitting via time-selective flat Rayleigh fading channels. Three different benchmark curves are provided.

the transmitted signals of the SN and RN imposed by the successive relaying protocol significantly affects the system's performance. As shown in Figure 3.6, increasing the DS-CDMA spreading factor (SF) Q mitigates the influence of interference. Nevertheless, an error floor is encountered for a SF of 32 between BER of 10^{-4} and of 10^{-5}. No significant BER improvement can be attained upon increasing the SF beyond 64, but nevertheless a SF of 512 will be adopted in our forthcoming investigations for minimizing the influence of interference in adverse propagation conditions, as justified at a later stage in the context of Figure 3.7.

The relay-aided MSDSD assisted successive AF system using SF $= 512$ requires an approximately 2 dB higher transmit power for achieving the target BER of 10^{-4} compared to benchmark-III of Table 3.1, i.e. in comparison to its single-relay aided conventional two-phase cooperative counterpart, which employs the multi-path MSDSD algorithm of Section 2.4. The associated performance degradation is attributable to two main reasons: firstly, to the successive-relaying-induced CCI between the transmitted signals of the SN and RN; secondly, to the noise $n'_{r_i}[k]$ amplified and forwarded by the RN r_i, which is imposed on the despread source signal $z_s^A[k]$ in (3.6) or on

$z_s^B[k]$ in (3.8), but would never appear in the Source-to-Destination link of benchmark-III. In more detail, let us compare (2.28) of Chapter 2 to (3.29) of this section. It can be observed that both the interference component I_{r_1} and the amplified noise component n'_{r_1} of (3.29) are absent in the first row of (2.28), which also corresponds to the SD link. Furthermore, the interference component I_{r_1} of (3.29) is also absent in all rows of (2.28). According to the comparison of our system and benchmark-III, we may argue that our system doubles the bandwidth efficiency with regard to benchmark-III without substantially degrading the BER performance. On the other hand, our relay-aided MSDSD assisted successive AF relaying system substantially outperforms the conventional single-user direct-transmission based schemes operating without RNs. For example, observe in Figure 3.6 that our scheme results in a performance gain of about 10 dB at a target BER of 10^{-4} compared to the benchmark-**I** curve. It is also clearly seen in Figure 3.6 that our scheme maintains a performance gain of about 8 dB at a target BER of 10^{-4} compared to the benchmark-**II**. Hence our proposed system may approach the optimum trade-off between the achievable throughput and the attainable BER performance among all the schemes listed in Table 3.1.

Benchmark-I	single-user scenario dispensing with relaying	MSDSD [53]	$f_d = 0.01$ $N = 6$
Benchmark-II	single-user scenario dispensing with relaying	coherent DQPSK	$f_d = 0.01$
Benchmark-III	single relay-aided two-phase cooperation	multi-path MSDSD [54]	$f_d = 0.01$ $N = 6$
Benchmark-IV	single-user scenario dispensing with relaying	coherent DQPSK	$f_d = 0.06$

Table 3.1: Definitions of benchmarks employed in Figures 3.6 and 3.7

As stated in Section 2.3.3 and 2.4.3, apart from increasing the spatial diversity order for the sake of reducing the detrimental impact of time-selective fading channels, increasing the observation window size of the MSDSD algorithm is another beneficial method, which results in an improved time diversity. However, when the window size is extended, the complexity imposed increases rapidly. In order to assess the trade-offs between the attainable time diversity and the system's complexity, simulation results are provided in Figures 3.7 and 3.8. Other parameters, such as the normalized Doppler frequency, the spreading factor and the modulation schemes, are fixed to $f_d = 0.06$, $Q = 512$ and Differential QPSK, respectively.

As expected, an increased performance gain is attained, when the window size increases from $N = 3$ to 12, as shown in Figure 3.7. If the window size is relatively small, such as $N = 3$ or 4, the performance of the new system becomes slightly worse than that of the conventional single-user coherent DQPSK scheme dispensing with relaying with the same normalized Doppler frequency $f_d = 0.06$, but gradually improves upon increasing N. However, no further significant performance gain may be attained, once the window size reached $N = 8$, despite investing substantially increased search complexity, as quantified in terms of the number of multiplications required for decoding a single symbol. This is particularly so in the low-SNR region, as shown in Figure 3.8. In practical applications, the BER should be lower than 10^{-3}. In other words, according to Figure 3.7, the new system performs well for SNRs above 30 dB. In this SNR range of Figure 3.8, the

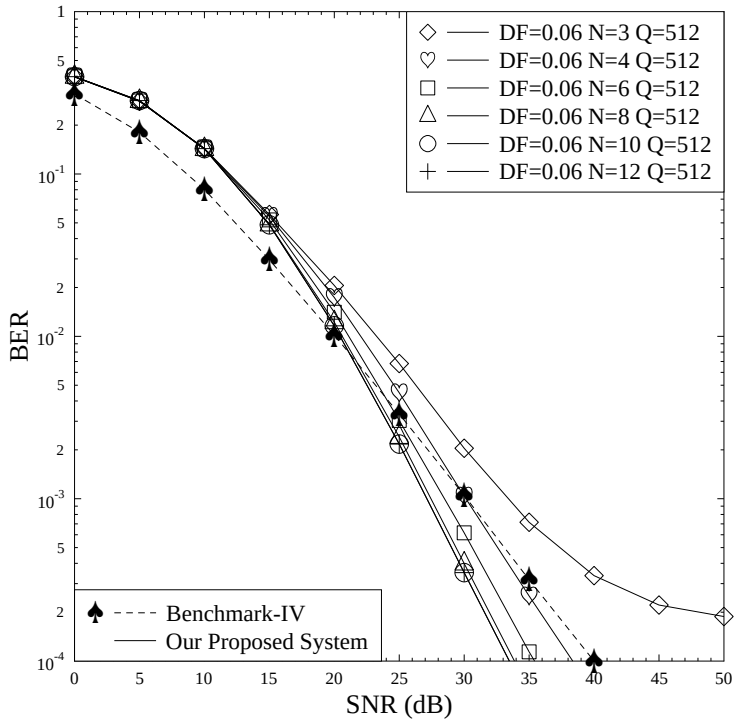

Figure 3.7: The effect of the MSDSD observation window size on the BER performance of the relay-aided MSDSD assisted successive AF relaying based DS-CDMA uplink, when experiencing time-selective flat Rayleigh fading channels and a f_d of 0.06.

complexity difference is no longer significant between the different window sizes. This justifies our previous statements, arguing that a window size of $N = 8$ could be a meritorious choice, which has a moderate complexity, whilst achieving the best BER performance in the context of the parameters considered.

3.2 Successive AF Relaying Aided Multi-User DS-CDMA Uplink: its DCMC Capacity

In this section, we further extend the prototype system introduced in Section 3.2 from the single-user scenario to a more realistic multi-user DS-CDMA uplink (UL) scenario. Both the suppression of the multiple access interference (MAI) involved in the multi-user scenario and the path-loss reduction gain accruing from employing RNs for reducing the propagation distance are taken into account in the system developed. Furthermore, in contrast to [46], and in the spirit of [79], the successive relaying induced interferences generated both at the RN, namely "IRI" and at the the DN, namely "CCI" are eliminated by directly exploiting the classic DS-CDMA principle upon assigning unique, link-specific spreading codes to the potentially interfering links. Naturally, this implies that the orthogonal time-slots used in [44] are replaced by unique, link-specific CDMA

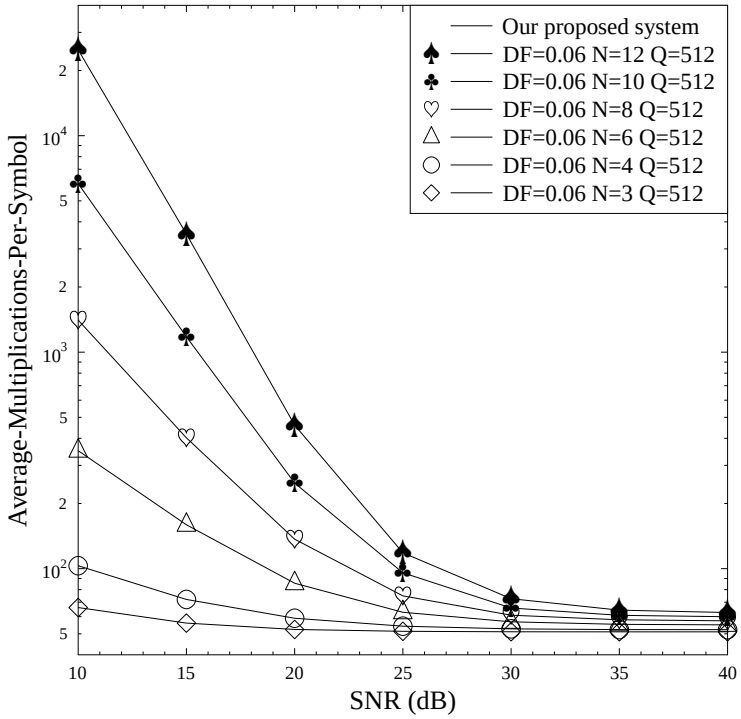

Figure 3.8: Complexity versus SNR performance of the relay-aided MSDSD assisted successive AF relaying based cooperative DS-CDMA uplink with respect to various observation window sizes.

spreading codes at the cost of imposing a soft-limit on the number of users that maybe supported, given the limited number of spreading codes.

Based on the idealized simplifying assumption that the channel state information (CSI) is perfectly known, the capacity of AF based cooperative systems was characterized in [27, 106]. However, the noncoherent DCMC capacity of the AF based SRAN is still unknown. Hence we derive the noncoherent DCMC capacity of our successive AF relaying aided multi-user DS-CDMA system in this section for providing the theoretical bounds.

In more detail, the developed system model and interference suppression regime is described in Section 3.2.1. Section 3.2.2 derives the noncoherent DCMC capacity of the AF based SRAN. In Section 3.2.3, the simulation results are provided and the benefit of embedding the AF based SRAN in DS-CDMA uplink is analysed.

3.2.1 System Overview and Interference Suppression Regime

After extending the single-user DS-CDMA uplink to the more realistic multi-user scenario, the simplified successive AF relaying aided single-user DS-CDMA uplink diagram shown in Figure 3.2 is correspondingly replaced by a more generalized network topology, which is portrayed in Figure 3.9, where the MS s roaming close to the edge of the DS-CDMA cell activates the SRAN

regime to improve its communication quality. The activated two relays r_0, r_1 and the BS d are specifically labelled in Figure 3.9. In Section 3.1, we did not consider the path-loss effect encoun-

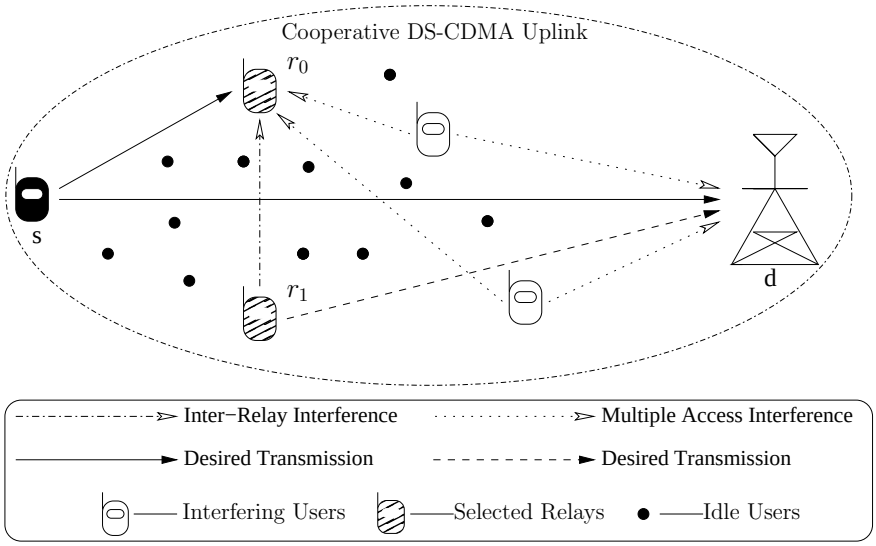

Figure 3.9: The successive AF relaying aided multi-user DS-CDMA uplink topology.

tered in the realistic telecommunication systems. By contrast, in order to improve the practicality of our investigations, the path-loss effects are also taken into account from this section. Onwards, as detailed in [107], the average path-loss reduction gain of the link spanning from node a to node b with respect to the Source-to-Destination link is given by $G_{ab} = \left(\frac{D_{sd}}{D_{ab}}\right)^{\alpha}, (a,b) \in \{s, r_0, r_1, d\}$, where the notation D_{ab} represents the distance between node a and node b. Throughout this section, the path-loss exponent is fixed to $\alpha = 3$ for representing a typical urban area. To simplify our analysis, we assume that the SRAN has a symmetric topology, which implies that D_{sr_0}, D_{r_0d}, G_{sr_0} and G_{r_0d} are identical to D_{sr_1}, D_{r_1d}, G_{sr_1} and G_{r_1d}, respectively. Then, in line with the definition stipulated in Section 2.4.3, we still utilize P_a to denote the transmit power of node a. Furthermore, $\bar{i}$ is defined as the complement of i.

In Section 3.1, transmissions via the time-selective flat Rayleigh fading channels were investigated. In order to simplify our theoretical analysis by focusing on a single transmission block, all the possible propagation paths between the s, r_i and d are assumed to be time-selective block-fading Rayleigh channels [108], where the fading coefficients $h_{ab}[k]$ of the channel between node a and node b fluctuate according to the normalized Doppler frequency within a block and change according to an independent and identical distribution (i.i.d) from one block to the next [109][2]. The correlated block-fading period of the channel is represented by T_b.

The successive relaying regime was introduced in Section 1.2.4, which was then repeated in Figure 3.3. For convenience, we would like to illustrate its typical transmission processes and the

[2]This assumption is different from the conventional scenario, where we assume that the envelope is constant in a block and then faded independently between blocks according to the Rayleigh PDF.

associated interference contributions incurred in a multi-user scenario in Figure 3.10, where the source transmissions are segmented into identical-length transmission frames of L symbols. As detailed in [44] [102], an impediment of the SRAN is the interference generated among the relays, which is also referred as the inter-relay interference (IRI). The IRI is further aggravated by the co-channel interference (CCI) between the signals transmitted from the source node (SN) and RN contaminating the signal received at the DN, as seen in Figure 3.10. As a benefit of combining DS-CDMA with the SRAN philosophy, the inherent ability of CDMA to deal with the multipath effects assists the SRAN in overcoming its interference-limited behaviour.

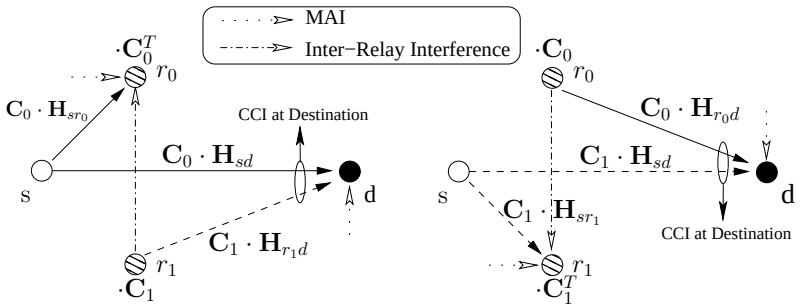

(a) Even Phase "$l \in \{0, 2, 4, \cdots\}$" (b) Odd Phase "$l \in \{1, 3, 5, \cdots\}$"

Figure 3.10: The abstract of both the successive relaying aided transmission processes and of the associated interferences induced by successive relaying or multi-user scenario.

3.2.1.1 Noise Accumulation Problem

In the scenario specified in Section 3.1.1, where the successive relaying induced IRI was not considered, we did not incur the noise accumulation problem either. However, when considering the IRI encountered by our system illustrated in Figure 3.10, the noise accumulation problem detailed in this section will occur owing to directly employing the classic AF protocol in the SRAN, where the RN simply amplifies its received signal before retransmitting it. When considering the classic DS-CDMA uplink embedded into the AF based SRAN, the transmit power of the RN r_i assigned to the k^{th} symbol of the $(l+1)^{st}$ transmission frame consists of four components received during the most recent frame: the power $P_s^l[k]$ of the SN's broadcast signal, the power $P_{r_{\bar{i}}}^l[k]$ of IRI, the power $P_{\text{MAI}}^l[k]$ of MAI and the power σ^2 of the AWGN noise, which may be simply formulated by omitting the index k, yielding

$$P_{r_i}^{l+1} = f_{AM_{r_i}}^2 \left\{ G_{sd} P_s^l + G_{r_{\bar{i}} r_i} P_{r_{\bar{i}}}^l + P_{\text{MAI}}^l + \sigma^2 \right\} \tag{3.34}$$

$$P_{r_{\bar{i}}}^l = f_{AM_{r_{\bar{i}}}}^2 \left\{ G_{sd} P_s^{l-1} + G_{r_i r_{\bar{i}}} P_{r_i}^{l-1} + P_{\text{MAI}}^{l-1} + \sigma^2 \right\} \tag{3.35}$$

$$\vdots$$

$$P_{r_1}^2 = f_{AM_{r_1}}^2 \left\{ G_{sd} P_s^1 + G_{r_0 r_1} P_{r_0}^1 + P_{\text{MAI}}^1 + \sigma^2 \right\}, \tag{3.36}$$

where the amplification factor $f_{AM_{r_i}}$ of RN r_i constrains the transmitted power of the RN r_i to P_{r_i}. Obviously, the noise component received by $r_{\bar{i}}$ in the $(l-1)^{st}$ frame will contaminate the signal of r_i transmitted in the $(l+1)^{st}$ frame, as seen by substituting (3.35) into (3.34). This process is then continued recursively.

The noise accumulation problem incurred in the successive AF relaying regime, where the RN simply amplifies its received signal before retransmitting it is visualized in Figure 3.11. In more

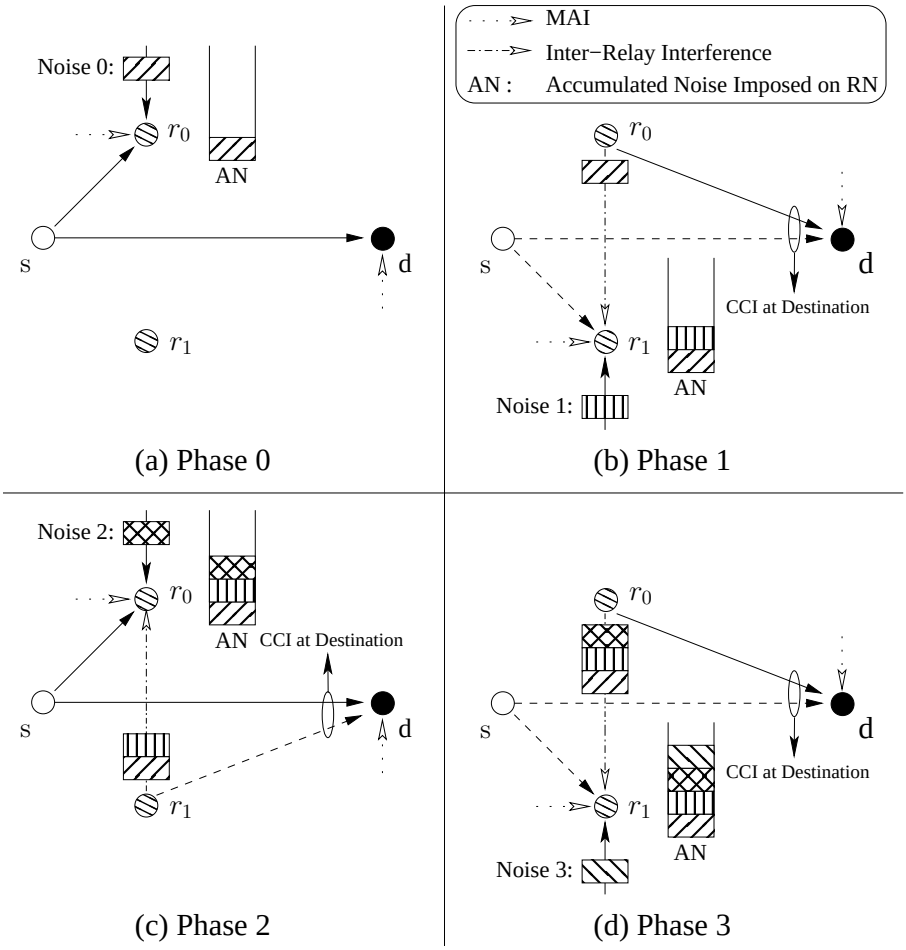

Figure 3.11: The accumulated noise (AN) imposed on the RNs during the successive AF relaying process.

detail, the noise accumulation process portrayed in Figure 3.11 may be summarized as follows

1. Observe in "Figure 3.11 (a) Phase 0" that the RN r_0 receives an AWGN noise contribution, namely "Noise 0". Hence, at this moment, the accumulated noise (AN) imposed at the RN r_0 only has a single component: "Noise 0".

2. Observe in "Figure 3.11 (b) Phase 1" that the RN r_0 simply amplifies all the signal components received during "(a) Phase 0" and then transmits them. Hence, the noise component "Noise 0" is also forwarded to the RN r_1 as part of the IRI. Simultaneously, a new AWGN noise contribution generated during "Figure 3.11 (b) Phase 1", namely "Noise 1" is further

imposed on the RN r_1. Hence, during "Figure 3.11 (b) Phase 1", the AN imposed at r_1 increases to two components: "Noise 0" and "Noise 1".

3. Observe in "Figure 3.11 (c) Phase 2" that the AN consisting of "Noise 0" and "Noise 1", which is imposed on the RN r_1 during the last phase is further forwarded to the RN r_0. Simultaneously, a new AWGN noise contribution generated during "Figure 3.11 (c) Phase 2", namely "Noise 2" is also imposed on the RN r_0. Hence, now, the AN imposed on r_0 has three components: "Noise 0", "Noise 1" and "Noise 2".

4. Owing to the same mechanism as stated above, the AN imposed on the RN r_1 will have four components during "Figure 3.11 (d) Phase 3". Apparently, the accumulated noise imposed on the RNs will continue to increase upon continuing the successive AF relaying transmissions.

Based on the assumption that P_s^l, P_{MAI}^l and the signal-to-noise-ratio (SNR) remain constant for the different frames, and proceeding backwards from the $(l+1)^{st}$ to the 2^{nd} frame, the variance of the total recursively accumulated noise component in $P_{r_i}^{l+1}$ may be approximated by

$$\begin{aligned}\mathbf{Var}[N_{\text{total}}] &= \sigma^2 f^2 \left[1 + f^2 G + \left(f^2 G\right)^2 + \cdots + \left(f^2 G\right)^{l-1}\right] \\ &\approx \sigma^2 f^2 \lim_{l\to\infty} \sum_{n=0}^{l-1} \left(f^2 G\right)^n = \frac{\sigma^2 f^2}{1 - f^2 G}, \end{aligned} \tag{3.37}$$

where f and G represent $f_{AM_{r_i}}$ and $G_{r_{\bar{i}} r_i}$, respectively. This reveals that all the noise generated in different frames at the different relays will be consistently scaled and accumulated during the transmission process of the classic AF based SRAN. Quantitatively they impose an extra noise component having a variance of $\sigma^2 f_{AM_{r_i}}^2 G_{r_i d} \cdot \frac{1}{1-f^2 G}$ on the DN, which cannot be mitigated by the single despreading operation at the DN. By contrast, in Section 3.1, owing to ignoring the IRI problem, the AWGN received at the RNs $r_i, i \in \{0,1\}$ finally only imposes an amplified and faded noise component $n'_{r_i}[k]$ on the DN's despread signals. As indicated in (3.6) and (3.7), the variance of $n'_{r_i}[k]$ is identical to $\sigma^2 f_{AM_{r_i}}^2 G_{r_i d}$.

3.2.1.2 The DS-CDMA Based Interference Suppression Regime

According to the analysis provided in Section 3.2.1.1, the scaled and accumulated noise components received at the RNs $r_i, i \in \{0,1\}$ cannot be mitigated by the single despreading operation at the DN. Hence the regime designed in Section 3.1 for suppressing the interference becomes invalid in this section. Consequently, a new interference suppression regime is desired.

Let γ_{01} denote the cross-correlation (CCL) value of the pair of pseudo-noise (PN) sequences $\mathbf{C}_i, i \in \{0,1\}$ in (3.3). Observe at RN r_0 of Figure 3.10 that the received AWGN vector $\mathbf{n}[k]$ of a symbol-duration consists of Q chip-related AWGN samples $n[(k-1)Q+q]$, which may be formulated as [97]: $\mathbf{n}[k] = \left[n[(k-1)Q+1], n[(k-1)Q+2], \cdots, n[(k-1)Q+Q]\right]$, where $n[(k-1)Q+q] \sim \mathcal{CN}(0, \sigma^2/Q)$. After despreading by $\mathbf{C}_0^T$, the corresponding term of $\mathbf{n}[k]$ is

given by

$$\eta_1 = \sum_{q_1=1}^{Q} n[(k-1)Q + q_1]c_0[q_1] \sim \mathcal{CN}(0, \sigma^2), \tag{3.38}$$

where η_1 is a Gaussian variable. If η_1 is further spread by $\mathbf{C}_0$ and then despread by $\mathbf{C}_1^T$, we obtain

$$\eta_2 = \sum_{q_2=1}^{Q} \eta_1 c_0[q_2]c_1[q_2]. \tag{3.39}$$

Observe that η_1 of (3.38) obeys a Gaussian distribution in statistical terms, but each of its realizations becomes a specific value in (3.39). Hence (3.39) may be rewritten as

$$\eta_2 = \eta_1 \sum_{q_2=1}^{Q} c_0[q_2]c_1[q_2] = \eta_1\gamma_{01}. \tag{3.40}$$

This implies that the power of the AWGN vector $\mathbf{n}[k]$ cannot be reduced by a single combined spread-despread operation, but it can definitely be mitigated by multiple spread-despread operations.

Based on the above analysis, a specifically arranged DS-CDMA regime is designed here in order to circumvent the potential noise accumulation process, and to mitigate both the successive relaying induced interferences and the MAI imposed on the cooperative DS-CDMA uplink. In more detail, at the SN s, the modulated symbols $S^l[k]$ are alternately spread by $\mathbf{C}_0$ and $\mathbf{C}_1$ from frame to frame ($l = 0, 1, \cdots$). The received signals are firstly despread by $\mathbf{C}_i^T$ in the listening mode of RN r_i, and then directly spread by $\mathbf{C}_i$ in the transmit mode of RN r_i before the amplification operation. Hence, when we employ an appropriate PN sequence to suppress the interfering signal transmitted by the RNs (e.g. the IRI) at the receiver (RN or DN), according to (3.40), the AF noise component inherent in the interference will be simultaneously suppressed. This implies that the noise accumulation process is indeed avoided. Thus our spreading scheme also guarantees that the two different components of the signal received at the DN, namely those, which correspond to the SN's transmitted signal and to the RN's forwarded signal, respectively, are always spread by different PN sequences. These operations are also illustrated in Figure 3.10.

3.2.1.3 System Model for Successive AF Relaying Aided Multi-User DS-CDMA

We assume that the channel's fading coefficients in the l^{th} frame $h_{ab}^l[k]$ maintain the same value in different chip-durations of the same symbol. Hence, the k^{th} received signal of the l^{th} frame at the DN may be formulated as

$$\mathbf{y}^l[k] = \sqrt{G_{sd}}h_{sd}^l[k]\mathbf{c}_s^l[k] + \sqrt{G_{r_id}}h_{r_id}^l[k]\mathbf{c}_{r_i}^l[k] + \mathcal{I}_{s^Md}^l[k] + \mathbf{n}_d^l[k], \tag{3.41}$$

where $i = \mod[(l+1), 2], l = (0, 1, \cdots)$. The spread AWGN vector $\mathbf{n}_d^l[k]$ obeys $\mathcal{E}\left\{\mathbf{n}_d^l[k]\ \mathbf{n}_d^{l\,H}[k]\right\} = \frac{1}{Q}\sigma^2\mathbf{I}_Q$, where $\mathbf{I}_Q$ denotes the identity matrix having a dimension of Q. We assume

having $(M+1)$ users, namely the desired user plus M interfering users. Consequently, the MAI imposed by the M interfering users on the DN is given by

$$\mathcal{I}^{l}_{s^M d}[k] = \sum_{m=1}^{M} \sqrt{G_{s_m d}} h^{l}_{s_m d}[k] \sqrt{P_{s_m}} S^{l}_{s_m}[k] \cdot \mathbf{C}_{s_m}. \tag{3.42}$$

The SN's broadcast signal is given by $\mathbf{c}^{l}_{s}[k] = \sqrt{P_s} S^{l}[k] \cdot \mathbf{C}_{\bar{i}}$ and the RN's forwarded signal of (3.41) can be detailed as

$$\mathbf{c}^{l}_{r_i}[k] = f_{AM_{r_i}} \times \left\{ \sqrt{G_{sr_i}} h^{l-1}_{sr_i}[k] \mathbf{c}^{l-1}_{s}[k] + \mathcal{I}^{l-1}_{r_{\bar{i}} r_i}[k] + \mathcal{I}^{l-1}_{s^M r_i}[k] + \tilde{\mathbf{n}}^{l-1}_{r_i}[k] \right\}. \tag{3.43}$$

The component $\mathcal{I}^{l-1}_{r_{\bar{i}} r_i}[k]$ in (3.43) captures the effect of IRI after the combined despread-spread operation of RN r_i, which can be detailed as

$$\mathcal{I}^{l-1}_{r_{\bar{i}} r_i}[k] = \gamma_{\bar{i}i} \sqrt{G_{r_{\bar{i}} r_i}} h^{l-1}_{r_{\bar{i}} r_i}[k] \sqrt{P_{r_{\bar{i}}}} R^{l-1}_{\bar{i}}[k] \cdot \mathbf{C}_i, \tag{3.44}$$

where the CCL between the PN sequence $\mathbf{C}_a$ and the PN sequence $\mathbf{C}_b$ is commonly represented by γ_{ab}. We assign a pair of PN sequences having $\gamma_{\bar{i}i} = 1/Q$ as $\mathbf{C}_{\bar{i}}$ and $\mathbf{C}_i$ in order to significantly reduce the IRI effects. Then, after the combined despread-spread operation, the MAI imposed on r_i during the $(l-1)^{st}$ frame becomes

$$\begin{aligned} \mathcal{I}^{l-1}_{s^M r_i}[k] &= \tilde{I}^{l-1}_{s^M r_i}[k] \cdot \mathbf{C}_i \\ &= \sum_{m=1}^{M} \gamma_{mi} \sqrt{G_{s_m r_i}} h^{l-1}_{s_m r_i}[k] \sqrt{P_{s_m}} S^{l-1}_{s_m}[k] \cdot \mathbf{C}_i. \end{aligned} \tag{3.45}$$

From the central limit theorem [110], the summation of M independent random variables may be modelled by the Gaussian distribution. Hence, additionally based on the Gaussian approximation method [111], the variance of $\tilde{I}^{l-1}_{s^M r_i}[k]$ may be approximated by

$$\mathbf{Var}\left[\tilde{I}^{l-1}_{s^M r_i}\right] = \sum_{m=1}^{M} \frac{1}{3Q} G_{s_m r_i} P_{s_m}. \tag{3.46}$$

Regretfully, the power of the MAI imposed on the RN is unknown, but we may utilize the MAI imposed on the DN to approximately model it. Then, based on the assumption that the DS-CDMA system has a perfect power control, we may readily derive the following relationship

$$\sum_{m=1}^{M} G_{s_m d} P_{s_m} = M P_s; \ \sum_{m=1}^{M} G_{s_m r_i} P_{s_m} = \lambda \cdot M P_s, \tag{3.47}$$

where the factor λ is determined by the ratio of the MAI imposed on the RN r_i to the MAI imposed on the BS d[3].

By substituting (3.47) to (3.46), (3.46) is rewritten as

$$\mathbf{Var}\left[\tilde{I}^{l-1}_{s^M r_i}\right] \approx \frac{\lambda}{3Q} M P_s. \tag{3.48}$$

[3]The actual value of λ will vary owing to different network topologies. As one possible value, 2.0 is assigned to λ in our simulations.

In order to constrain the transmitted power of the RN r_i to P_{r_i} [104], and invoking (3.44) as well as (3.48), we can obtain

$$f_{AM_{r_i}} = \sqrt{\frac{P_{r_i}}{G_{sr_i}P_s + \frac{1}{Q^2}G_{r_{\bar{i}}r_i}P_{r_{\bar{i}}} + \frac{\lambda}{3Q}MP_s + \sigma^2}}. \tag{3.49}$$

We also note that $\mathbf{c}^l_{r_i}[k]$ of (3.43) corresponds to the k^{th} modulated source symbol of the previous frame, namely to $S^{l-1}[k]$, instead of corresponding to $S^l[k]$ transmitted by the SN in the present frame. This particular property of the SRAN was also illustrated in Figure 3.5.

Similar to $(3.6)\sim(3.9)$ in Section 3.1.1, at the DN, the different components of the received signal $\mathbf{y}^l[k]$ can be resolved by appropriately configuring the chip-waveform matched-filter for the different spreading codes. When the filter is matched to the waveform $\mathbf{C}_{\bar{i}}$, the signal directly transmitted by the SN will contribute the main component of the despread signal, while the RN's forwarded signal and the interfering users' signals become the interference. Hence, the associated output of the chip-waveform matched-filter is given by

$$z^l_s[k] = \sqrt{G_{sd}}h^l_{sd}[k]\sqrt{P_s}S^l[k] + I^l_{r_id}[k] + I^l_{s^Md}[k] + n^l_d[k], \tag{3.50}$$

where $I^l_{r_id}[k]$ accounts for the relay's forwarded signal component after the despreading operation. Recalling the analysis of Section 3.2.1.2, according to (3.40), the noise term $\tilde{\mathbf{n}}^{l-1}_{r_i}[k]$ in (3.43) will be suppressed along with the other components of (3.43) by the CCL $\gamma_{\bar{i}i}$. Then $I^l_{s^Md}[k]$ is the despread version of $\mathcal{I}^l_{s^Md}[k]$ in (3.41), whose variance may be calculated by a process similar to (3.45), (3.48). Hence we can derive that $\mathbf{Var}\left[I^l_{r_id}\right] = \frac{1}{Q^2}G_{r_id}P_{r_i}$; $\mathbf{Var}\left[I^l_{s^Md}\right] = \frac{1}{3Q}MP_s$; $n^l_d[k] \sim \mathcal{CN}(0, \sigma^2)$. Similarly, the despread signal extracted from $\mathbf{y}^l[k]$ but dominated by the RN's forwarded signal $\mathbf{c}^l_{r_i}[k]$ can be expressed as

$$\begin{aligned} z^l_{r_i}[k] = {} & f_{AM_{r_i}}\sqrt{G_{sr_i}}\sqrt{G_{r_id}}h^{l-1}_{sr_i}[k]h^l_{r_id}[k]\sqrt{P_s}S^{l-1}[k] \\ & + I^{l-1}_{r_{\bar{i}}r_i}[k] + I^{l-1}_{s^Mr_i}[k] + I^l_{sd}[k] + I^l_{s^Md}[k] + \tilde{n}^{l-1}_{r_i}[k] + n^l_d[k], \end{aligned} \tag{3.51}$$

where $I^{l-1}_{r_{\bar{i}}r_i}[k]$, $I^{l-1}_{s^Mr_i}[k]$ and $\tilde{n}^{l-1}_{r_i}[k]$ are the amplified and faded, then despread versions of $\mathcal{I}^{l-1}_{r_{\bar{i}}r_i}[k]$, $\mathcal{I}^{l-1}_{s^Mr_i}[k]$ and $\tilde{\mathbf{n}}^{l-1}_{r_i}[k]$ in (3.43). $I^l_s[k]$ is the interference imposed by the SN's broadcast signal $\mathbf{c}^l_s[k]$. Their variances are summarized as $\mathbf{Var}\big[I^{l-1}_{r_{\bar{i}}r_i}\big] = \big(\frac{1}{Q^2}G_{r_{\bar{i}}r_i}P_{r_i}\big)f^2_{AM_{r_i}}G_{r_id}$; $\mathbf{Var}\big[I^{l-1}_{s^Mr_i}\big] = \big(\frac{\lambda}{3Q}MP_s\big)f^2_{AM_{r_i}}G_{r_id}$; $\mathbf{Var}\big[I^l_{sd}\big] = \frac{1}{Q^2}G_{sd}P_s$; $\mathbf{Var}\big[\tilde{n}^{l-1}_{r_i}\big] = (\sigma^2)f^2_{AM_{r_i}}G_{r_id}$.

3.2.1.4 Definition of Channel Capacity

In the ensuing section, we will embark on deriving the noncoherent DCMC capacity of the AF SRAN. Before this capacity derivation, we firstly clarify our definition of channel capacity.

- The maximum data rate in bits per channel use at which information can be sent with arbitrary low probability of error is referred to as the capacity $\mathbf{C}$ of the channel [112]. Hence throughout this thesis, the terminology of capacity can be equivalently regarded as the terminology of the maximum data rate at which reliable transmission is possible.

- In this spirit, for example, the capacity of the AWGN channel under the power constraint $\mathbf{P}$ and noise variance σ^2 is given by [59]

$$\mathbf{C} = \frac{1}{2}\log\left(1 + \frac{\mathbf{P}}{\sigma^2}\right). \tag{3.52}$$

- The definition of channel capacity stipulated in this section will be employed throughout the entire thesis.

3.2.2 Noncoherent DCMC Capacity of the AF SRAN in the Multi-User DS-CDMA Uplink

The transmission arrangement of the twin-relay-aided successive relaying procedure may be viewed as the superimposed transmissions of two conventional single-relay aided two-phase cooperative links [102]. This is also illustrated in Figure 3.10, where the transmissions represented by the solid lines in the even phase and odd phase constitute one of the half-duplex three-terminal cooperative networks, namely Coop-I. Similarly, the transmissions represented by the dashed lines in the even and odd phases constitute another one, namely Coop-II.

In order to further clarify the philosophy of the AF based SRAN, we illustrate its detailed transmission process in Figure 3.12, where the transmissions of the SRAN were split into 5 phases. Observe in Figure 3.12 that the transmission arrangement of the 5-phase SRAN may be treated as the superposition of the transmissions of a pair of 4-phase based half-duplex three-terminal cooperative networks, which are the above mentioned sub-networks "Coop-I" and "Coop-II". The slight difference between our sub-network "Coop-I" (or "Coop-II") and the conventional half-duplex three-terminal cooperative network is that we additionally imposed the omni-present CCI and IRI on the DN and RN of the sub-networks, respectively, because we have to assume that an equivalent amount of CCI (or IRI) is also imposed on the DN of the sub-networks, just like that happens to the AF based SRAN located in the middle of Figure 3.12. In more detail, we will demonstrate that the effect of the CCI imposed on the sub-network induces the "$\frac{G_{r_1 d}}{Q^2}$" term in (3.55), or the "$\frac{G_{sd}}{Q^2}$" term in (3.57). Then, the effect of the IRI imposed on the sub-network is modelled by the "$\frac{G_{r_1 r_0}}{Q^2}$" term in (3.57).

Hence, we can readily extend the relationship between the AF based SRAN and the pair of half-duplex three-terminal cooperative networks based on Figure 3.12 to the generalized scenario, where the transmission arrangement of an $(N+1)$-phase SRAN may be treated as a superposition of the transmissions of two N-phase half-duplex three-terminal cooperative networks[4]. Hence, assuming that $(N+1)$ is sufficiently high, we may readily conclude that the noncoherent DCMC capacity

[4]The transmission arrangements of the first and last phases in the AF based SRAN do not strictly satisfy our decomposition of the AF based SRAN. Nevertheless, when the total number of transmission phases in the AF based SRAN is sufficiently high, we may ignore the slight inaccuracy incurred in the two particular phases.

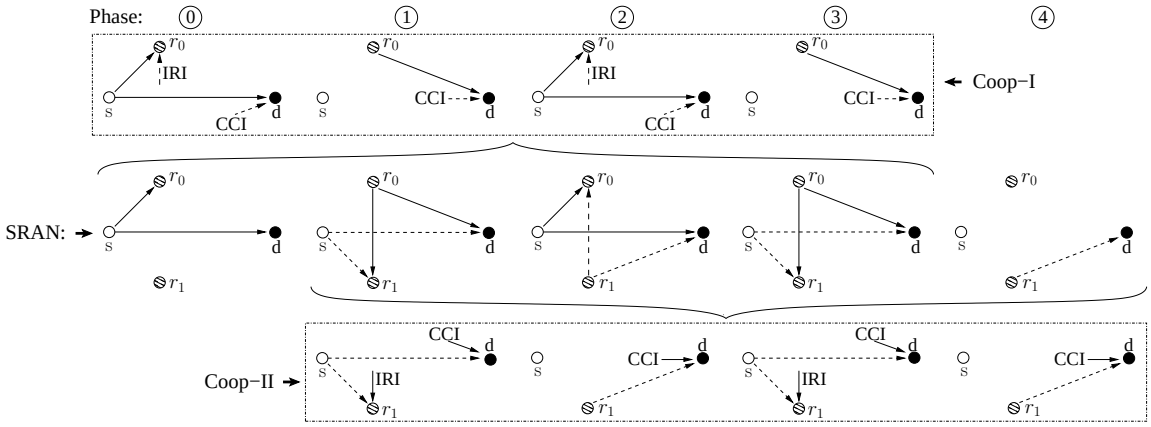

Figure 3.12: Decomposition of the AF based SRAN.

of the AF based SRAN is constituted by the sum of the capacities of the AF based sub-network "Coop-I" and "Coop-II", which is formulated as

$$C^{\mathrm{AF}}_{\mathrm{Successive}} = C^{\mathrm{AF}}_{\text{Coop-I}} + C^{\mathrm{AF}}_{\text{Coop-II}}. \tag{3.53}$$

Since the noncoherent DCMC capacity of the AF based half-duplex three-terminal cooperative network e.g. $C^{\mathrm{AF}}_{\text{Coop-I}}$ is unknown, it will be derived below.

In the sub-network Coop-I, during the broadcast interval of length T_s, a block of the modulated source symbols $\mathbf{S}^l = \left[S^l[k+1], S^l[k+2], \cdots, S^l[k+T_b]\right]^T$ is broadcast by the SN. The transmissions via the SD link generate the signal vector $\mathbf{z}_s^l = \left[z_s^l[k+1], z_s^l[k+2], \cdots z_s^l[k+T_b]\right]^T$, which is actually constituted by the associated despread signals received at the DN, as detailed in (3.50). According to [110] again, by treating the interference components in (3.50) as a Gaussian variable, the overall equivalent noise component imposed on the vector $\mathbf{z}_s^l$ may be expressed as

$$\mathbf{n}_s^l = \begin{bmatrix} I^l_{r_1 d}[k+1] + I^l_{s^M d}[k+1] + n^l_d[k+1] \\ \vdots \\ I^l_{r_1 d}[k+T_b] + I^l_{s^M d}[k+T_b] + n^l_d[k+T_b] \end{bmatrix}, \tag{3.54}$$

whose covariance matrix is given by

$$\mathbf{\Psi}_{\mathbf{n}_s^l} = \left\{ \left[\frac{G_{r_1 d}}{Q^2} + \frac{M}{3Q} \right] P + \sigma^2 \right\} \mathbf{I}_{T_b}. \tag{3.55}$$

Furthermore, the associated fading coefficients of the SD link are represented by $\mathbf{h}_{sd} = \left[h^l_{sd}[k+1], h^l_{sd}[k+2], \cdots, h^l_{sd}[k+T_b]\right]^T$. Hence, given the definitions[5] $\mathbf{\Phi}_{sd} = P\mathcal{E}\{\mathbf{h}_{sd}{\mathbf{h}_{sd}}^H\}$ and $\overline{\mathbf{S}} = \mathrm{diag}\{\mathbf{S}^l\}$, the covariance matrix $\mathbf{\Psi}_{sd}$ of the despread received signal vector $\mathbf{z}_s^l$ is given by

$$\mathbf{\Psi}_{sd} = \mathcal{E}\left\{ \mathbf{z}_s^l {\mathbf{z}_s^l}^H | \mathbf{S}^l \right\} = \overline{\mathbf{S}} \mathbf{\Phi}_{sd} \overline{\mathbf{S}}^H + \mathbf{\Psi}_{\mathbf{n}_s^l}. \tag{3.56}$$

[5]From now on, the assumption that $P_s = P_{r_i} = P$ is utilized in order to simplify the form of the equations.

where both the successive relaying induced interference and the MAI are included in the evaluation. A similar derivation procedure of (3.56) may be found in [53] and [54].

Similarly, the signal vector $\mathbf{z}_{r_0}^{l+1} = \left[z_{r_0}^{l+1}[k+1], z_{r_0}^{l+1}[k+2], \cdots, z_{r_0}^{l+1}[k+T_b]\right]^T$ represents another replica of the same modulated source symbol block $\mathbf{S}^l$, which is generated by the consecutive transmissions from the SN to the RN during the broadcast phase of duration T_s, and then to the DN during the multiple-access phase of duration T_r. The equivalent fading coefficients of the associated channels are represented by $\mathbf{h}_{sr_0d} = \left[h_{sr_0}^l[k+1]\cdot h_{r_0d}^{l+1}[k+1], \cdots, h_{sr_0}^l[k+T_b]\cdot h_{r_0d}^{l+1}[k+T_b]\right]^T$. Then the overall equivalent noise component $\mathbf{n}_{r_0}^{l+1}$ imposed on the vector $\mathbf{z}_{r_0}^{l+1}$ is composed by all the interference and noise components in (3.51). The relevant covariance matrix is formulated as

$$\mathbf{\Psi}_{\mathbf{n}_{r_0}^{l+1}} = \left\{ \frac{G_{r_0d}\left\{\left[\frac{G_{r_1r_0}}{Q^2} + \frac{\lambda M}{3Q}\right]P + \sigma^2\right\}P}{\left[G_{sr_0} + \frac{G_{r_1r_0}}{Q^2} + \frac{\lambda M}{3Q}\right]P + \sigma^2} + \left[\frac{G_{sd}}{Q^2} + \frac{M}{3Q}\right]P + \sigma^2 \right\} \times \mathbf{I}_{T_b}. \tag{3.57}$$

Similar to our previous analysis, let us define $\mathbf{\Phi}_{sr_0d} = Pf_{AM_{r_0}}^2 G_{sr_0}G_{r_0d}\mathcal{E}\{\mathbf{h}_{sr_0d}\mathbf{h}_{sr_0d}^H\}$, the covariance matrix $\mathbf{\Psi}_{sr_0d}$ of the signal vector $\mathbf{z}_{r_0}^{l+1}$ is formulated as

$$\mathbf{\Psi}_{sr_0d} = \overline{\mathbf{S}}\mathbf{\Phi}_{sr_0d}\overline{\mathbf{S}}^H + \mathbf{\Psi}_{\mathbf{n}_{r_0}^{l+1}}. \tag{3.58}$$

In the capacity analysis, the sub-network Coop-I may be equivalently modelled by a single-input-multiple-output (SIMO) system having $N_T = 1$ transmit and $N_R = 2$ receive antennas, which is visualized in Figure 3.13. Observe in Figure 3.13 that the transmissions via the SD link during the broadcast phase can be viewed as the transmissions from the single transmit antenna T_1 to one of the two receive antennas R_1 in the equivalent SIMO system. Similarly, the consecutive transmissions from the SN to the RN ensuing during the broadcast phase, and then to the DN during the multiple-access phase in Coop-I can be treated as the transmissions from the single transmit antenna T_1 to another receive antenna R_2, while experiencing the equivalent channel's fading and incurring the same interference-plus-noise impairment in the equivalent SIMO system. Hence, given the definitions $\overline{\mathbf{Z}} = \left[\mathbf{z}_s^l \;\; \mathbf{z}_{r_0}^{l+1}\right]$, $\overline{\mathbf{H}} = \left[\mathbf{h}_{sd} \;\; \mathbf{h}_{sr_0d}\right]$ and $\overline{\mathbf{N}} = \left[\mathbf{n}_s^l \;\; \mathbf{n}_{r_0}^{l+1}\right]$, the entire input-output relation of the equivalent SIMO system may be formulated by

$$\overline{\mathbf{Z}} = \overline{\mathbf{S}} \cdot \overline{\mathbf{H}} + \overline{\mathbf{N}}. \tag{3.59}$$

It was pointed out by Ding *et al.* [106] that the equivalent channel's fading coefficients - the elements of $\mathbf{h}_{sr_0d}$, involve a product of Gaussian random variables, which is no longer Gaussian. Nevertheless, Ding *et al.* further demonstrated that the ergodic channel capacity of the AF aided single-relay system based on the Gaussian assumption is still achievable, provided that the covariance matrix of the system's input signal is diagonal, and the diagonal elements may be obtained by solving the resultant optimization problems invoking multidimensional integrals. In the spirit of [106], we may approximate the capacity of the equivalent SIMO system based on the Gaussian assumption. Hence, according to [113], the PDF of $\overline{\mathbf{Z}}$ conditioned on $\overline{\mathbf{S}}$ is readily expressed as

$$\Pr(\overline{\mathbf{Z}}|\overline{\mathbf{S}}) = \frac{1}{\left[\pi^{T_b N_T}\det(\mathbf{\Psi})\right]^{N_R}} \cdot \exp\left[-\mathrm{tr}\left(\overline{\mathbf{Z}}^H\mathbf{\Psi}^{-1}\overline{\mathbf{Z}}\right)\right], \tag{3.60}$$

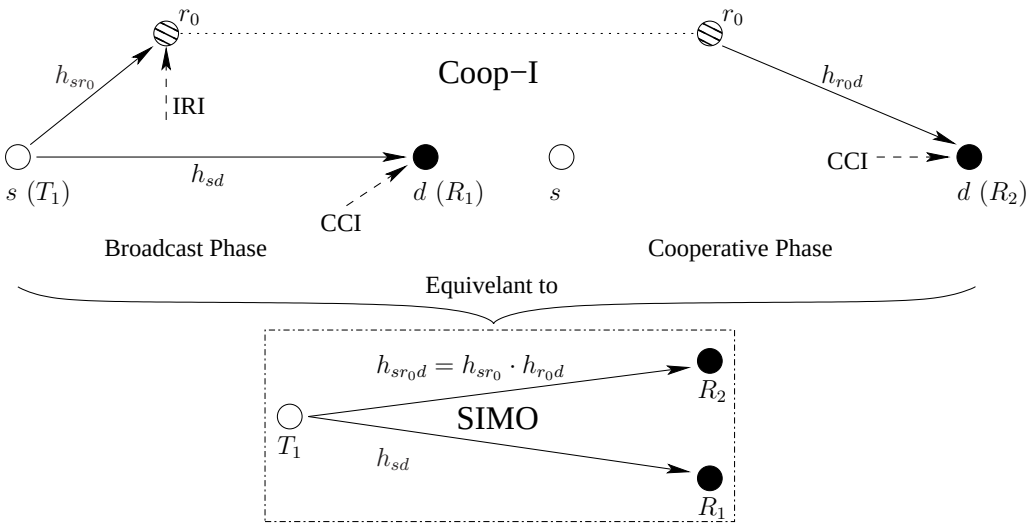

Figure 3.13: Mimic the AF based half-duplex three-terminal cooperative network "Coop-I" by a single-input-twin-output SIMO system.

where the conditional covariance matrix $\mathbf{\Psi}$ is given by

$$\mathbf{\Psi} = \overline{\mathbf{S}} \left(\mathbf{\Phi}_{sd} + \mathbf{\Phi}_{sr_0d} \right) \overline{\mathbf{S}}^H + \mathbf{\Psi}_{\mathbf{n}_s^l} + \mathbf{\Psi}_{\mathbf{n}_{r_0}^{l+1}}. \tag{3.61}$$

Let us define $\beta_1 = \frac{T_s}{T_s+T_r}$ and $\beta_2 = \frac{T_r}{T_s+T_r}$, which was introduced for evaluating the effect of the source- and relay- transmission duration ratio of a conventional single-relay aided two-phase cooperative network, as detailed in [24]. Apparently, the AF based sub-network Coop-I has the inherent relationship of $\beta_1 = \beta_2 = \beta = 0.5$. Then, according to [112] and [114], the capacity of Coop-I can be readily formulated as[6]

$$C_{\text{Coop-I}}^{\text{AF}} = \frac{\beta}{T_b} I\left(\overline{\mathbf{S}}\,; \overline{\mathbf{Z}}\right) = \frac{\beta}{T_b} \left[H\left(\overline{\mathbf{Z}}\right) - H\left(\overline{\mathbf{Z}}|\overline{\mathbf{S}}\right) \right], \tag{3.62}$$

where the conditional entropy $H\left(\overline{\mathbf{Z}}|\overline{\mathbf{S}}\right)$ can be calculated in a closed form as

$$\begin{aligned} H\left(\overline{\mathbf{Z}}|\overline{\mathbf{S}}\right) &= -\int \Pr\left(\overline{\mathbf{Z}}, \overline{\mathbf{S}}\right) \ln\left[\Pr\left(\overline{\mathbf{Z}}|\overline{\mathbf{S}}\right)\right] \mathrm{d}\overline{\mathbf{Z}} \mathrm{d}\overline{\mathbf{S}} \\ &= \log_2 \left\{ \mathrm{e}^{T_b} \cdot \left[\det\left(\pi \mathbf{\Psi}\right)\right]^{N_R} \right\}. \end{aligned} \tag{3.63}$$

However, the entropy $H\left(\overline{\mathbf{Z}}\right)$ cannot be evaluated in a closed form. A practical approach to its numerical evaluation is constituted by the following Monte-Carlo integration

$$\begin{aligned} H\left(\overline{\mathbf{Z}}\right) &= -\mathcal{E}\left\{ \log_2\left[\Pr\left(\overline{\mathbf{Z}}\right)\right] \right\} \\ &= -\mathcal{E}\left\{ \log_2 \left[\frac{1}{M_c^{T_b}} \sum_{\overline{\mathbf{S}}' \in \chi} \frac{\exp\left[-\mathrm{tr}\left(\overline{\mathbf{Z}}^H \mathbf{\Psi}^{-1} \overline{\mathbf{Z}}\right)\right]}{\left[\det\left(\pi \mathbf{\Psi}\right)\right]^{N_R}} \right] \right\}. \end{aligned} \tag{3.64}$$

[6] As stated in the early of Section 3.2.1, specific time-selective block-fading Rayleigh channels defined in [108] are assumed for the capacity derivation.

Since each element of the T_b-component differentially encoded signal vector $\mathbf{S}^l$ is chosen independently from an M_c-point constellation set $\mathcal{M}_c$ with equal probabilities, the number of all hypothetically transmitted symbol matrices $\overline{\mathbf{S}}'$ equals to $M_c^{T_b}$ and χ in (3.64) represents the set of all hypothetical values of $\overline{\mathbf{S}}'$.

Now, we are ready to calculate the value of $C^{\mathrm{AF}}_{\text{Coop-I}}$. Then, we can simply attain the capacity of the sub-network Coop-II following a similar process. According to (3.53), the noncoherent DCMC capacity of the AF based SRAN becomes available.

3.2.3 Capacity Performance and Analysis

Let us define $\theta = \frac{D_{sr_i}}{D_{r_i d}}$, and assume that $D_{r_0 r_1}$ equals to the relatively smaller value between D_{sr_i} and $D_{r_i d}$. Based on the symmetrical structure of the proposed SRAN assumed in Section 3.2.1, the exact proportions of D_{sr_i}, $D_{r_i d}$, D_{sd} and $D_{r_0 r_1}$ associated with different θ values are summarized in Table 3.2, where the shortest distance is always normalized to unity. Employing the normalized

θ	D_{sr_i}	$D_{r_i d}$	D_{sd}	$D_{r_0 r_1}$
$1/3$	1	3	3.824	1
$1/2$	1	2	2.802	1
1.0	1	1	1.732	1
2.0	2	1	2.802	1
3.0	3	1	3.824	1

Table 3.2: Distance proportions with respect to θ

distance list of Table 3.2, the path-loss gain associated with a certain θ may be obtained according to [107].

A cooperative-user-selection scheme is employed, where the effect of the RN's position is considered. Then, we do not employ any sophisticated power-allocation scheme. We simply equally share the total power between the SN and RN, which directly leads to $P_s = P_{r_0} = P_{r_1} = \frac{1}{2} P_{\text{total}}$. The corresponding simulation results of $C^{\mathrm{AF}}_{\text{Successive}}$ as evaluated from (3.53), (3.62), (3.63) as well as (3.64) are displayed in Figure 3.14, where the following RN positions expressed in terms of $\theta \in \left\{3.0, 2.0, 1.0, \frac{1}{2}, \frac{1}{3}\right\}$ were considered and the number of interfering users was fixed to $M = 0$. Observe in Figure 3.14 that the capacity of the SN's uplink employing the AF based SRAN exceeds that of the conventional SL DT structure, when appointing RNs sufficiently close to the SN. By contrast, it results in a degraded capacity compared to the conventional direct transmission structure, when appointing RNs close to the DN. In our particular case, appointing the RNs at the position of $\theta = \frac{1}{2}$ is seen to be the best strategy in Figure 3.14, which slightly improves the capacity $C^{\mathrm{AF}}_{\text{Successive}}$ compared to the scenarios of $\theta = \frac{1}{3}$ and $\theta = 1.0$. The capacity of the conventional single-relay aided two-phase AF based cooperative DS-CDMA uplink having $\theta = \frac{1}{2}$ is also portrayed in Fig-

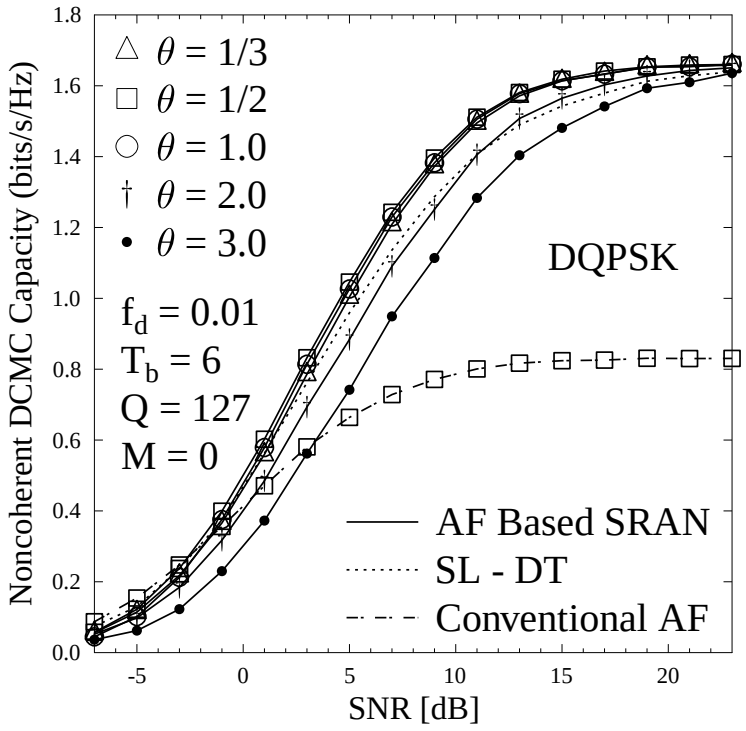

Figure 3.14: The effect of the geographic position of the RN on $C^{\mathrm{AF}}_{\mathrm{Successive}}$, as evaluated from (3.53), (3.62), (3.63) and (3.64), where a normalized Doppler frequency of $f_d = 0.01$ is assumed.

ure 3.14, which is significantly exceeded by that of its AF based SRAN counterpart.

In our next investigation we fixed the position of RNs to $\theta = \frac{1}{2}$ and focussed our attention on the detrimental effects of having an increased number of interfering users M. Specifically, the values of $M \in \{0, 32, 64\}$ are considered for modelling the scenarios of zero, moderate and heavy MAI, respectively. The relevant simulation results displayed in Figure 3.15 demonstrate that the capacity of the AF based SRAN always exceeds that of the direct transmission system, regardless of the number of interfering users. It is more intriguing to find that the capacity advantage of the AF based SRAN increases with respect to the conventional direct transmission system, when the MAI becomes stronger. This implies that in contrast to the conventional DS-CDMA uplink, the cooperative DS-CDMA uplink will exhibit more substantial advantages in high-load situations. Furthermore, it is expected that if we adjust the amplification factor $f_{AM_{r_i}}$ with the aid of accurate power-control instead of equally splitting the power between the SN and RN, the AF based capacity may be further improved, as also reported in [27,106]. This benefit may indeed be anticipated, since having a reduced SN and RN transmit power results in reduced MAI in comparison to the direct transmission scenario.

Additionally, the effect of the coefficient λ involved in (3.57) is investigated in Figure 3.16. As stated in Section 3.2.2, the coefficient λ characterises the effect of the MAI imposed on the RN r_i. Hence it is naturally avoided in the scenario having no interfering users, i.e. for $M = 0$.

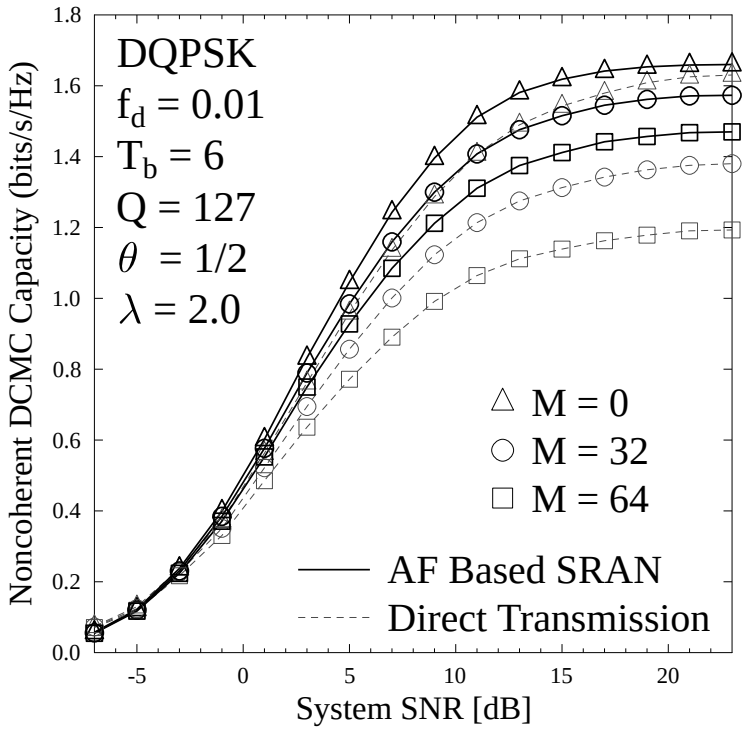

Figure 3.15: The noncoherent DCMC capacity $C^{\mathrm{AF}}_{\mathrm{Successive}}$ in zero, moderate and heavy MAI scenarios, as evaluated from (3.53), (3.62), (3.63) and (3.64), where a normalized Doppler frequency of $f_d = 0.01$ is assumed.

Accordingly, we opt for $M = 32$ in Figure 3.16 for the sake of characterising the effect of λ. Nevertheless, we observe in Figure 3.16 that fortunately the effect of different λ values on the noncoherent DCMC capacity of $C^{\mathrm{AF}}_{\mathrm{Successive}}$ is almost negligible for the AF based SRAN.

3.3 Successive DF Relaying Aided Multi-User DS-CDMA Uplink and its DCMC Capacity

As stated in Section 3.1, in this section, we will replace the AF protocol of our system proposed in Section 3.2 by the DF protocol for the sake of achieving a potentially better BER performance. The realistic multi-user scenario considered takes into account the successive relaying induced interferences. More explicitly, a successive DF relaying aided multi-user DS-CDMA uplink architecture is conceived. Most of the assumptions made in Section 3.2, such as the network topology, the relaying-induced path-loss reduction effect, the power-allocation as well as the channel model remain the same here.

For the sake of designing an energy-efficient communication system, the soft-decision-based MSDSD algorithm of Section 2.5 is advocated instead of its hard-decision-based counterpart. However, as analysed in Section 2.6, the SISO-MSDSD algorithm of Section 2.5 [55] was still con-

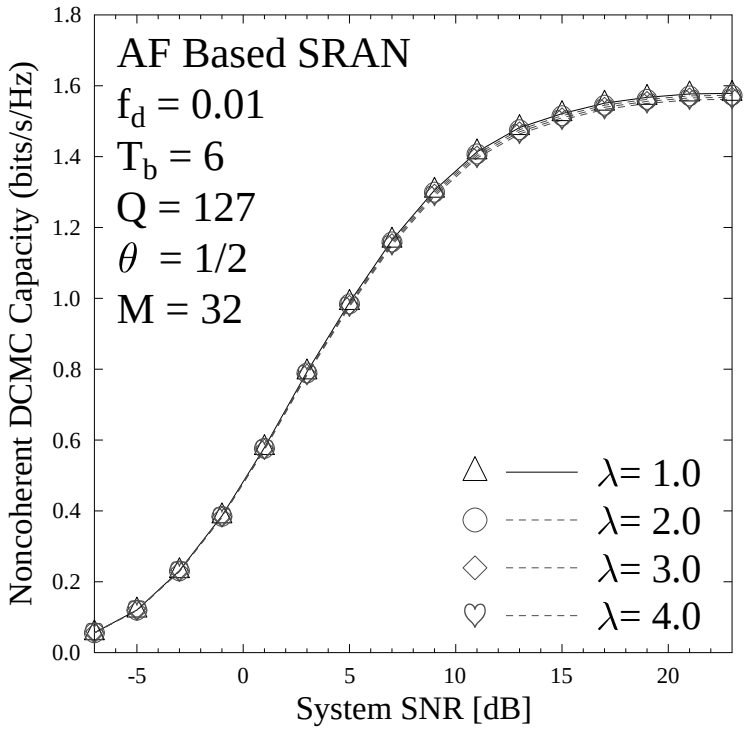

Figure 3.16: Effect of the λ value on the noncoherent DCMC capacity of $C^{\mathrm{AF}}_{\mathrm{Successive}}$.

strained to the family of single-link direct-transmission based systems. Its associated multiple-path version had not been considered. Against this background, in order to adapt the SISO-MSDSD algorithm of Section 2.5 [55] to the DF based SRAN, we specifically devise a relay-aided SISO-MSDSD decoder in this section, which is constituted by an amalgamate of our relay-aided MSDSD of Section 3.1.2 [79] and of the SISO-MSDSD of Section 2.5 [55]. Consequently, the transceiver of the proposed DF based SRAN is designed, which leads to the sophisticated relay-aided SISO-MSDSD assisted three-stage iterative-detection-based transceiver architecture of Section 3.3.3.

In more detail, the content of this section is organised as follows. The system model is described in Section 3.3.1. Section 3.3.2 derives the noncoherent DCMC capacity of the DF based SRAN. The SRAN's capacity characteristics are also provided. Then, in Section 3.3.3, we design a practical transceiver architecture for realizing the proposed DF based SRAN, where the associated complexity is also characterized. Finally, the robustness and throughput of the system is investigated in Section 3.3.4.

3.3.1 DF Based SRAN Model

As indicated at the beginning of Section 3.3, the network's topology illustrated in Figure 3.9 is still valid for the DF based system model. Consequently, both the MAI and the successive relaying induced interferences, namely the "CCI" and "IRI" contributions are also taken into account in our DF based system. Furthermore, the relaying-related path-loss reduction effects and the

power-allocation as well as the channel model are also assumed to be the same as those defined in Section 3.2.1. Hence, for the sake of avoiding repetitions, we refer to Section 3.2.1 for the relevant details of our DF based system model. All the notations given in Section 3.2.1 will retain their original definitions in this section.

The DS-CDMA based interference suppression regime introduced in Section 3.2.1.2 is also valid for the DF based SRAN. In more detail, at the SN s, the modulated symbols $S^l[k]$ are alternately spread by the spreading sequences of $\mathbf{C}_0$ and $\mathbf{C}_1$ from frame to frame ($l = 0, 1, \ldots$). At the RN r_i, the received signals are firstly despread by $\mathbf{C}_i^T$ in the listening mode of RN r_i and then decoded, re-encoded, as well as re-modulated. In the consecutive transmit mode of RN r_i, the re-modulated symbols $\tilde{S}^l[k]$ are always spread by $\mathbf{C}_i$, which are then forwarded to the DN. Again, this spreading scheme is the same to that depicted in Figure 3.10, where only the decoding, re-encoding and re-modulating process is omitted. Thus, the spreading scheme also guarantees that the two different components of the signal received at the DN, namely those that correspond to the SNs transmitted signal and to the RNs forwarded signal, respectively, are always spread by different PN sequences.

When employing the DF protocol, the despread signal of the $(l-1)^{st}$ frame at RN r_i associated with $S^{l-1}[k]$ is given by

$$y_{r_i}^{l-1}[k] = \sqrt{G_{sr_i}} h_{sr_i}^{l-1}[k] \sqrt{P_s} S^{l-1}[k] + \gamma_{\bar{i}i} \sqrt{G_{r_{\bar{i}}r_i}} h_{r_{\bar{i}}r_i}^{l-1}[k] \sqrt{P_{r_i}} R_{\bar{i}}^{l-1}[k] + \sum_{m=1}^{M} \gamma_{mi} \sqrt{G_{s_m r_i}} h_{s_m r_i}^{l-1}[k] \sqrt{P_{s_m}} S_{s_m}^{l-1}[k] + n_{r_i}^{l-1}[k], \tag{3.65}$$

which is similar to (3.43). In order to avoid the typical error-propagation problem of the DF protocol, we ensure that the signals at RN r_i are forwarded only when correctly decoded. Consequently, the signal forwarded by RN r_i is formulated as

$$\mathbf{c}_{r_i}^l[k] = \sqrt{P_{r_i}} \tilde{S}^l[k] \cdot \mathbf{C}_i, \quad \tilde{S}^l[k] = \begin{cases} S^{l-1}[k] & \text{perfect detection} \\ 0 & \text{else.} \end{cases} \tag{3.66}$$

At the DN, the received signal has the exactly same format to (3.41). Hence, when the chip-waveform matched-filter is applied to the waveform of $\mathbf{C}_{\bar{i}}$, the resultant output corresponding to the information bearing symbol $S^l[k]$ is given by

$$z_s^l[k] = \sqrt{G_{sd}} h_{sd}^l[k] \sqrt{P_s} S^l[k] + I_{r_i d}^l[k] + I_{s^M d}^l[k] + n_d^l[k], \tag{3.67}$$

where the definitions of the terms of $I_{r_i d}^l[k]$, $I_{s^M d}^l[k]$ and $n_d^l[k]$ are similar to that in (3.50), and their variances are identical to that in (3.50). Similarly, another despread signal extracted from the signal received at the DN but corresponding to the information-bearing symbol $S^{l-1}[k]$ may be formulated as

$$z_{r_i}^l[k] = \sqrt{G_{r_i d}} h_{r_i d}^l[k] \sqrt{P_{r_i}} \tilde{S}^l[k] + I_{sd}^l[k] + I_{s^M d}^l[k] + n_d^l[k]. \tag{3.68}$$

Similarly, the terms of $I_{sd}^l[k]$, $I_{s^M d}^l[k]$ and $n_d^l[k]$ involved in (3.68) are defined similarly to that in (3.51), and their variances are identical to that in (3.51).

3.3.2 Noncoherent DCMC Capacity of the DF Based SRAN in Multi-User DS-CDMA Uplink

Our decomposition of the SRAN illustrated in Figure 3.12 is valid both for the AF or DF protocol. This implies that the decomposition of the SRAN illustrated in Figure 3.12 remains valid for the DF based system model depicted in Section 3.3.1. Hence, in the spirit of Section 3.2.2, the NC DCMC capacity of the DF-based SRAN is also constituted by the sum of the capacities of the pair of sub-networks Coop-I and Coop-II, which is formulated as

$$C^{\mathrm{DF}}_{\mathrm{Successive}} = C^{\mathrm{DF}}_{\text{Coop-I}} + C^{\mathrm{DF}}_{\text{Coop-II}}, \tag{3.69}$$

where the sub-networks Coop-I and Coop-II of Section 3.2.2 now rely on the DF protocol.

As stated in Section 3.2.1, based on the i.i.d assumption of the channel, in this capacity analysis section, we can focus our attention on a single transmission block, which is randomly extracted from a transmission frame and happen to experience a complete fading block. In more details, in the broadcast interval of sub-network Coop-I, presented by solid lines in the even phase of Figure 3.10, the source signal block $\mathbf{S}^l = \left[S^l[k+1], S^l[k+2], \cdots, S^l[k+T_b]\right]^T$ is broadcast, which is received and further despread to the signal blocks $\mathbf{y}^l_{r_0} = \left[y^l_{r_0}[k+1], y^l_{r_0}[k+2], \cdots, y^l_{r_0}[k+T_b]\right]^T$ associated with (3.65) and $\mathbf{z}^l_s = \left[z^l_s[k+1], z^l_s[k+2], \cdots, z^l_s[k+T_b]\right]^T$ associated with (3.67), at RN r_0 and DN, respectively. Then, during the consecutive multiple-access interval, presented by the solid line in the odd phase, the hypothetical source signal block $\tilde{\mathbf{S}}^{l+1} = \left[\tilde{S}^{l+1}[k+1], \tilde{S}^{l+1}[k+2], \cdots, \tilde{S}^{l+1}[k+T_b]\right]^T$ generated by RN r_0 and associated with (3.66) is received at the DN, which is despread to signal block $\mathbf{z}^{l+1}_{r_0} = \left[z^{l+1}_{r_0}[k+1], z^{l+1}_{r_0}[k+2], \cdots, z^{l+1}_{r_0}[k+T_b]\right]^T$ associated with (3.68). Hence, based on the upper and lower bounds on the capacity of a half-duplex relaying system provided in [24] and on the fact that the SN remains silent during the odd phase, we can obtain the upper and lower bounds for sub-network Coop-I as

$$C^{\mathrm{DF}}_{\text{Coop-I}} \leq \min\left\{\beta_1 I\left(\mathbf{S}^l; \mathbf{z}^l_s, \mathbf{y}^l_{r_0}\right), \beta_1 I\left(\mathbf{S}^l; \mathbf{z}^l_s\right) + \beta_2 I\left(\tilde{\mathbf{S}}^{l+1}; \mathbf{z}^{l+1}_{r_0}\right)\right\}, \tag{3.70}$$

$$C^{\mathrm{DF}}_{\text{Coop-I}} \geq \min\left\{\beta_1 I\left(\mathbf{S}^l; \mathbf{y}^l_{r_0}\right), \beta_1 I\left(\mathbf{S}^l; \mathbf{z}^l_s\right) + \beta_2 I\left(\tilde{\mathbf{S}}^{l+1}; \mathbf{z}^{l+1}_{r_0}\right)\right\}. \tag{3.71}$$

Furthermore, in order for the RN r_0 to detect the received signal correctly and thus to avoid the potential error propagation problem, the actual source transmission rate, namely $R^{\mathrm{DF}}_{\text{Coop-I}}$, cannot exceed the noncoherent DCMC capacity of the Source-to-Relay link. Hence we obtain another constraint on the error-free-relaying-based capacity as

$$R^{\mathrm{DF}}_{\text{Coop-I}} \leq \beta_1 I\left(\mathbf{S}^l; \mathbf{y}^l_{r_0}\right). \tag{3.72}$$

Accordingly, based on (3.70), (3.71) and (3.72), the error-free-relaying-based noncoherent DCMC capacity of sub-network Coop-I is given by

$$C^{\mathrm{DF}}_{\text{Coop-I}} = \min\left\{\beta_1 I\left(\mathbf{S}^l; \mathbf{y}^l_{r_0}\right), \beta_1 I\left(\mathbf{S}^l; \mathbf{z}^l_s\right) + \beta_2 I\left(\tilde{\mathbf{S}}^{l+1}; \mathbf{z}^{l+1}_{r_0}\right)\right\}. \tag{3.73}$$

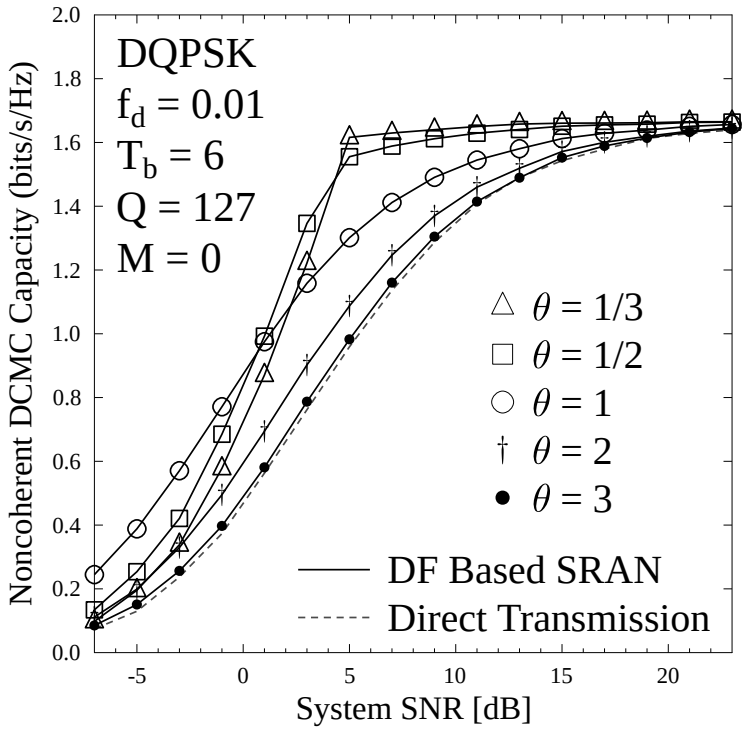

Figure 3.17: The effect of the geographic position of the RN on $C^{\mathrm{DF}}_{\mathrm{Successive}}$, as evaluated from (3.69), (3.73) and (3.74).

The covariance matrices associated with $I\left(\mathbf{S}^l;\mathbf{y}^l_{r_0}\right)$, $I\left(\mathbf{S}^l;\mathbf{z}^l_s\right)$ and $I\left(\tilde{\mathbf{S}}^{l+1};\mathbf{z}^{l+1}_{r_0}\right)$ are represented by $\mathbf{\Psi}_{sr_0}$, $\mathbf{\Psi}_{sd}$ and $\mathbf{\Psi}_{r_0d}$, respectively. Since the covariance matrix of the despread signals is the crucial element engaged in evaluating the noncoherent DCMC capacity, we formulate them explicitly as

$$\begin{aligned}
\mathbf{\Psi}_{sr_0} &= PG_{sr_0}\overline{\mathbf{S}}\mathcal{E}\left\{\mathbf{h}_{sr_0}\mathbf{h}^H_{sr_0}\right\}\overline{\mathbf{S}}^H + \left\{\left[\frac{G_{r_1r_0}}{Q^2}+\frac{\lambda M}{3Q}\right]P+\sigma^2\right\}\mathbf{I}_{T_b},\\
\mathbf{\Psi}_{sd} &= PG_{sd}\overline{\mathbf{S}}\mathcal{E}\left\{\mathbf{h}_{sd}\mathbf{h}^H_{sd}\right\}\overline{\mathbf{S}}^H + \left\{\left[\frac{G_{r_1d}}{Q^2}+\frac{M}{3Q}\right]P+\sigma^2\right\}\mathbf{I}_{T_b},\\
\mathbf{\Psi}_{r_0d} &= PG_{r_0d}\overline{\mathbf{S}}\mathcal{E}\left\{\mathbf{h}_{r_0d}\mathbf{h}^H_{r_0d}\right\}\overline{\mathbf{S}}^H + \left\{\left[\frac{G_{sd}}{Q^2}+\frac{M}{3Q}\right]P+\sigma^2\right\}\mathbf{I}_{T_b},
\end{aligned} \tag{3.74}$$

where the interference components are treated as noise contaminating the desired signal having the equivalent power. The $\mathbf{h}_{sr_0}$ and $\mathbf{h}_{r_0d}$ denote the fading coefficient vectors corresponding to SR_0 link and R_0D link, respectively. We have that $\overline{\mathbf{S}} = \mathrm{diag}\{\mathbf{S}^l\}$

After obtaining the relevant covariance matrices, the noncoherent DCMC capacity of sub-network Coop-I can be attained by implementing a similar process according to (3.62), (3.63) and (3.64). According to the symmetry between sub-network Coop-I and Coop-II, we may argue that the noncoherent DCMC capacity solution of sub-network Coop-II is also available. Hence the evaluation of the noncoherent DCMC capacity of the DF based SRAN is deemed completed. Moreover, no code-rate-optimization was considered here for the sake of simplifying the analysis. Hence we equally split the time between the broadcast and cooperation phases, which directly leads

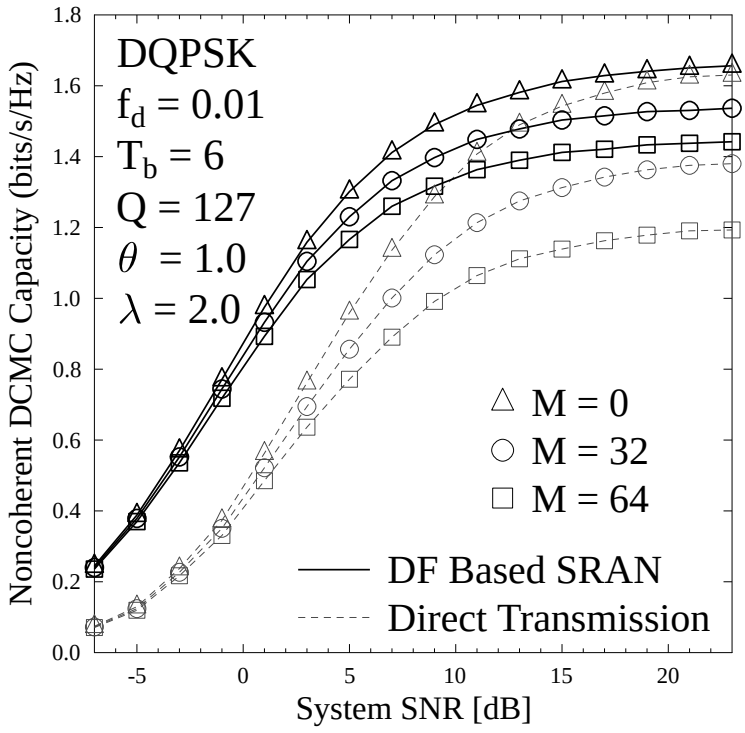

Figure 3.18: The noncoherent DCMC capacity $C^{\mathrm{DF}}_{\mathrm{Successive}}$ in zero, moderate and heavy MAI scenarios, as evaluated from (3.69), (3.73) and (3.74).

to $\beta_1 = \beta_2 = 0.5$, when calculating (3.73).

Our performance results and the associated discussions related to the NC DCMC capacity of the successive DF relaying aided multi-user DS-CDMA uplink are provided below. Similar to Section 3.2.3, a cooperative-user-selection scheme is employed, where the effect of the RN's position is also considered. Consequently, the parameter θ defined in Section 3.2.3 is employed here again for quantifying the exact proportions of D_{sr_i},D_{r_id}, D_{sd} and $D_{r_0r_1}$. In order to compare the DF SRAN capacity to the capacity of the AF based system characterised in Section 3.2.3, the geometric factors characterising the node-positions in this section are those specified in Table 3.2, again.

The attainable capacity $C^{\mathrm{DF}}_{\mathrm{Successive}}$ associated with different RN positions is characterized in Figure 3.17. This demonstrates that appointing RNs, which roam closer to the SN - rather than to the DN - in the DF based SRAN provides a higher capacity. To expound a little further, in the low SNR region (< 1dB), the DF based system appointing RNs at the position of $\theta = 1.0$ achieves the highest capacity. The phenomenon noted in Section 3.2.3, namely that the capacity gain achieved by replacing the direct transmission structure with the SRAN increases upon increasing the number of interfering users remains valid, when considering the DF based SRAN, as demonstrated by Figure 3.18. Furthermore, upon comparing Figure 3.14 to Figure 3.17, we observe that the DF based SRAN appointing appropriate RNs outperforms AF based SRAN, especially at low SNRs, i.e. in the low-throughput region. Hence our objective introduced at the beginning of Section 3.3, namely that of improving the system's energy efficiency and/or bandwidth efficiency by replacing

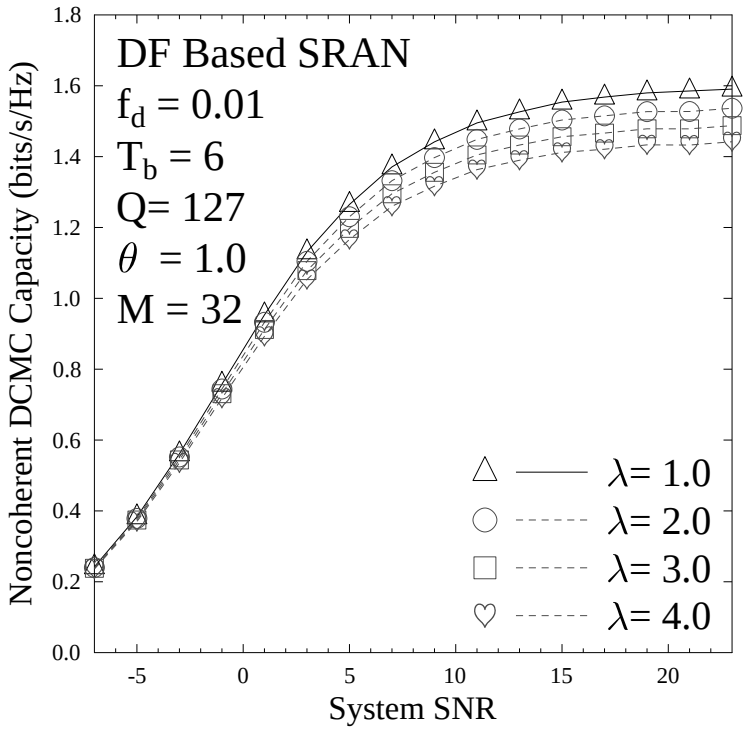

Figure 3.19: Impact of the value of λ on the NC DCMC capacity of $C^{\mathrm{DF}}_{\mathrm{Successive}}$

the AF protocol by the DF protocol has indeed been achieved.

Similar to Section 3.2.3, the effect of the coefficient λ involved in (3.74) is investigated in Figure 3.19. As stated in Section 3.2.3, the number of interfering users is fixed to $M = 32$ for characterising the impact of the parameter λ. Upon comparing Figure 3.16 to Figure 3.19, we observe that the NC DCMC capacity of the DF based SRAN is more sensitive to the value of λ.

3.3.3 Relay-Aided SISO-MSDSD Assisted Three-Stage Iterative Decoder

Let us now develop the proposed DF based SRAN further for the sake of creating a soft-decision-based iterative detection scheme for the sake of significantly improving its energy efficiency. Consequently, we design a three-stage iterative detection based transceiver architecture, leading to our "relay-aided SISO-MSDSD" architecture. Based on the analysis provided in Section 3.3.2, we simply assume that two relays are selected, which employ DF relaying and roam close to the mid-way position between the SN and DN, where we have $D_{sr_i} = D_{r_id}, \theta = 1.0$. In this system design part, a low MAI scenario is assumed for the sake of concentrating on the specific properties of SRANs. Furthermore, we consider a more realistic scenario in this section, where all the channels are assumed to be conventional narrowband correlated time-selective Rayleigh fading channels. Finally, the complexity property of the proposed transceiver, especially of the proposed relay-aided SISO-MSDSD algorithm is characterized at the end of this section.

3.3.3.1 Transceiver Design for the Source Node and Relay Node

The transceiver architecture specifically designed for our DF based SRAN is portrayed in Figure 3.20. At the SN, we use a conventional differential modulator (DM), such as DQPSK depicted at the top right corner of Figure 3.20, which is further combined with a unity-rate-code (URC) encoder in order to create a two-stage inner code. The URC model has an infinite impulse response (IIR) due to its recursive encoder structure, consequently the EXIT curve of the URC aided inner decoder is capable of approaching the point of perfect convergence at $(1.0, 1.0)$ in the EXIT chart, which is a necessary condition for near-capacity operation [7, 81], and for eliminating the potential error floor phenomenon. Therefore, the receiver of the RN is capable of near-perfectly detecting the information bits $\hat{u}_1$ bore in the signals received from the SN, at as low SNR values as possible. Furthermore, a conventional half-rate RSC is employed as the outer code. Hence a three-stage RSC-URC-DM source encoder is created.

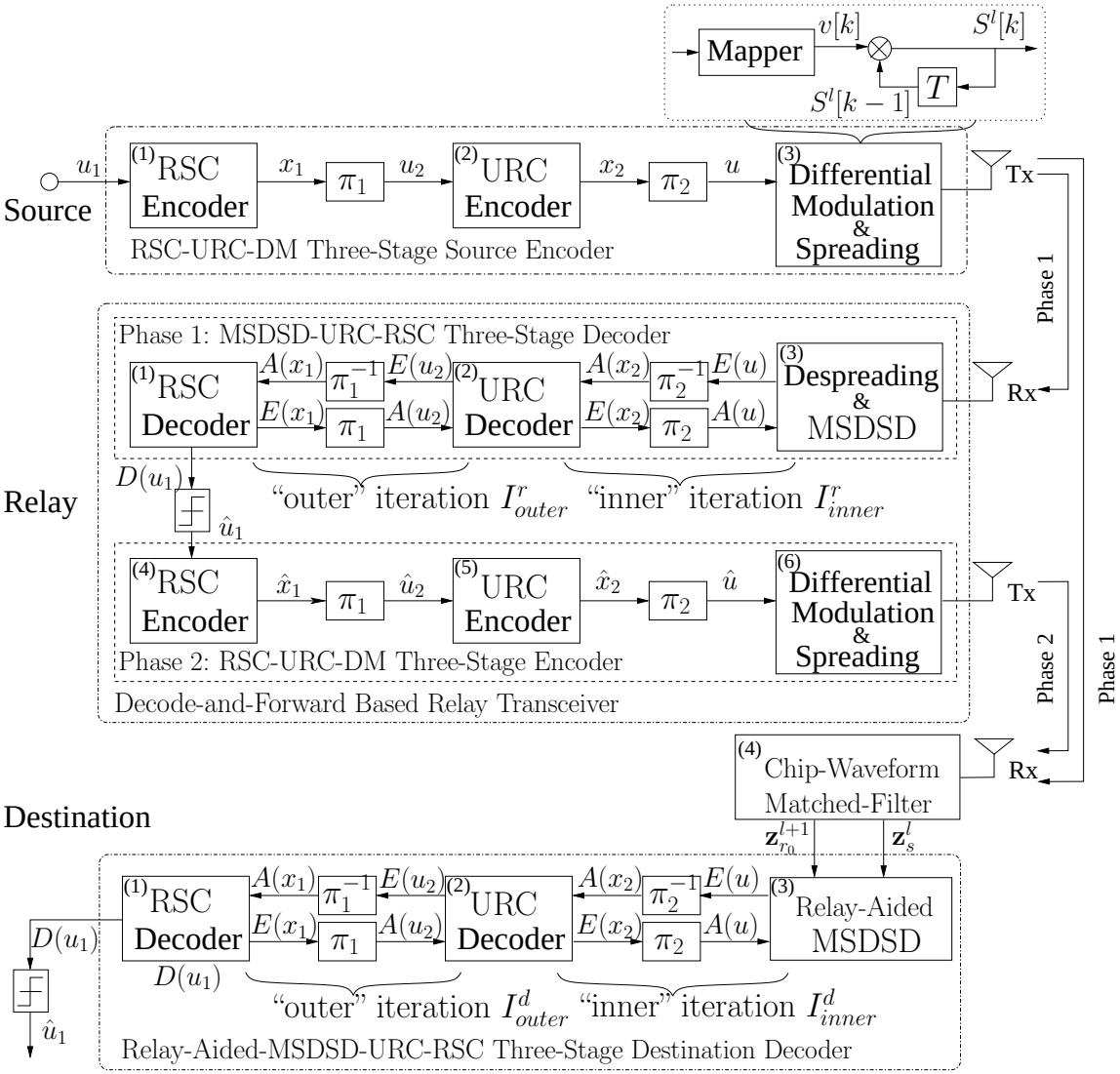

Figure 3.20: Schematic of the proposed transceiver in our DF based SRAN.

The corresponding URC decoder assisted three-stage receiver proposed for the relay is also portrayed in Figure 3.20. In more detail, the RN's receiver consists of three stages, namely the conventional single-path SISO-MSDSD [55] based soft decoder, the URC decoder and the RSC decoder. The *extrinsic* information and *a priori* information, represented by $E(\cdot)$ and $A(\cdot)$ respectively, are interleaved and iteratively exchanged within the two-stage inner decoder I^r_{inner} times, before the result is further exchanged between the inner and outer decoders I^r_{outer} times. The motivation of employing this three-stage concatenated decoder architecture is to improve the convergence behavior of the iterative decoder with the aid of the URC decoder, as detailed in [7, 81]. As a benefit, the error propagation problem of the DF scheme is avoided. Since the proposed SISO-MSDSD decoder will be employed at the DN, where we have to ensure that its multiple input signal streams are corresponding to the same differentially modulated symbols. The RN's transmitter is designed to be identical to the three-stage RSC-URC-DM encoder of the SN. Hence, observe at the RN in Figure 3.20 that if the estimates $\hat{u}_1$ are correctly generated by the RN's receiver, the differentially modulated symbols produced by the RN's transmitter will be the same as $S^l[k]$.

3.3.3.2 Relay-Aided SISO-MSDSD and Transceiver Design for the DN

Before introducing the DN's receiver design, we first clarify the proposed relay-aided SISO-MSDSD algorithm. As stated in Section 2.5 of Chapter 2, the SISO-MSDSD algorithm advocated by Pauli *et al.* in [55] was invoked for iterative decoding in the direct transmission system, which was then further developed for our cooperative network by incorporating the principle of relay-aided MSDSD [79]. The resultant modified SISO-MSDSD algorithm is consequently termed as the "relay-aided SISO-MSDSD". This was achieved by developing a sophisticated sphere detection scheme, which is capable of simultaneously dealing with multiple soft-input information streams, where the streams are associated with the same modulated symbols. Instead of processing a single received signal stream, our relay-aided SISO-MSDSD evaluates the *a posteriori* LLR of the μ^{th} bit $u[\mu]$ by simultaneously processing U received signal streams represented by $\{\mathbf{z}_u\}_{u=1}^{U}$ as follows

$$L\left(u[\mu]\right) = \ln \frac{\Pr\left(u[\mu]=b|\{\mathbf{z}_u\}_{u=1,2,\cdots,U}\right)}{\Pr\left(u[\mu]=\bar{b}|\{\mathbf{z}_u\}_{u=1,2,\cdots,U}\right)}, \;\; b \in \{0,1\}, \tag{3.75}$$

where $\bar{b}$ is the complement of b.

As described in Section 3.3.2, the despread signal streams of $\mathbf{z}_s^l$ and $\mathbf{z}_{r_0}^{l+1}$ generated at the DN correspond to the same SN's transmitted signal stream $\mathbf{S}^l$. Upon substituting them into (3.75) as $\{\mathbf{z}_u\}_{u=1,2}$, (3.75) can be rewritten with the aid of Bayes' theorem as

$$\begin{aligned} L\left(u[\mu]\right) &= \ln \frac{\Pr\left(u[\mu]=b|\mathbf{z}_s^l,\mathbf{z}_{r_0}^{l+1}\right)}{\Pr\left(u[\mu]=\bar{b}|\mathbf{z}_s^l,\mathbf{z}_{r_0}^{l+1}\right)} \\ &= \ln \frac{\sum_{\mathbf{V}\in\chi_{:u[\mu]=b}} \Pr\left(\mathbf{z}_s^l|\mathbf{V}\right)\Pr\left(\mathbf{z}_{r_0}^{l+1}|\mathbf{V}\right)\Pr(\mathbf{V})}{\sum_{\mathbf{V}\in\chi_{:u[\mu]=\bar{b}}} \Pr\left(\mathbf{z}_s^l|\mathbf{V}\right)\Pr\left(\mathbf{z}_{r_0}^{l+1}|\mathbf{V}\right)\Pr(\mathbf{V})}, \end{aligned} \tag{3.76}$$

where the information symbol vector $\mathbf{V}$ consists of (T_b-1) QPSK symbols. The relationship of the symbol-vector $\mathbf{V}$ and $\mathbf{S}^l$ becomes explicit in the model seen at the top-right corner of Figure 3.20. Their relationship is also formulated in (2.1). Furthermore, $\chi_{:u[\mu]=b}$ represents the set of $\frac{M_c^{T_b-1}}{2}$ number of legitimate transmitted vectors $\mathbf{v}$, whose μ^{th} bit is constrained to $u[\mu]=b$, and similarly, $\chi_{:u[\mu]=\bar{b}}$ is defined as the set corresponding to $u[\mu]=\bar{b}$.

Similar to (2.63), we can arrive at

$$\begin{aligned}\Pr\left(\mathbf{z}_s^l|\mathbf{V}\right) &\propto \exp\left\{-\|\mathbf{U}^s\mathbf{S}^l\|^2\right\},\\ \Pr\left(\mathbf{z}_{r_0}^{l+1}|\mathbf{V}\right) &\propto \exp\left\{-\|\mathbf{U}^{r_0}\mathbf{S}^l\|^2\right\}.\end{aligned} \tag{3.77}$$

Hence, based on (3.76), (3.77) and invoking the "sum-max" approximation as well as replacing $\mathbf{S}^l$ by the simplified notation of $\mathbf{S}$, the *a posteriori* LLR of $u[\mu]$ is further approximated by

$$\begin{aligned}L\left(u[\mu]\right) \approx\ & \ln\frac{\max_{\mathbf{V}\in\chi_{:u[\mu]=b}}\exp\{-\|\mathbf{U}^s\mathbf{S}\|^2-\|\mathbf{U}^{r_0}\mathbf{S}\|^2+\ln\Pr(\mathbf{V})\}}{\max_{\mathbf{V}\in\chi_{:u[\mu]=\bar{b}}}\exp\{-\|\mathbf{U}^s\mathbf{S}\|^2-\|\mathbf{U}^{r_0}\mathbf{S}\|^2+\ln\Pr(\mathbf{V})\}}\\ =\ & -\underbrace{\left(\|\mathbf{U}^s\hat{\mathbf{S}}_{\text{MAP}}^b\|^2+\|\mathbf{U}^{r_0}\hat{\mathbf{S}}_{\text{MAP}}^b\|^2-\ln\Pr\left(\hat{\mathbf{V}}_{\text{MAP}}^b\right)\right)}_{\text{MAP-MSDSD}\in\chi_{:\text{u}[\mu]=\text{b}}}\\ & +\underbrace{\left(\|\mathbf{U}^s\hat{\mathbf{S}}_{\text{MAP}}^{\bar{b}}\|^2+\|\mathbf{U}^{r_0}\hat{\mathbf{S}}_{\text{MAP}}^{\bar{b}}\|^2-\ln\Pr\left(\hat{\mathbf{V}}_{\text{MAP}}^{\bar{b}}\right)\right)}_{\text{MAP-MSDSD}\in\chi_{:\text{u}[\mu]=\bar{\text{b}}}},\end{aligned} \tag{3.78}$$

where $\mathbf{U}^s$ can be attained by $\mathbf{U}^s \triangleq (\mathbf{F}\text{diag}\{\mathbf{z}_s^l\})^*$, with $\mathbf{F}$ being an upper-triangular matrix. In more detail, the upper-triangular matrix $\mathbf{F}$ relates to the covariance matrix $\mathbf{\Psi}_{sd}$ in (3.74) and can be obtained according to the interpretations found below (3.16). Explicitly, $\mathbf{U}^{r_0}$ may be calculated by a similar method, where $\mathbf{F}$ is related this time to the covariance matrix $\mathbf{\Psi}_{r_0d}$ of (3.74).

Observe that (3.78) is similar to (2.73) of Chapter 2, apart from the difference that (3.78) has the additional component of $\|\mathbf{U}^{r_0}\mathbf{S}\|^2$, which is related to the Relay-to-Destination transmissions. Hence, the minimization of the term $\{\|\mathbf{U}^s\mathbf{S}\|^2+\|\mathbf{U}^{r_0}\mathbf{S}\|^2-\ln\Pr(\mathbf{V})\}$ in (3.78) may be achieved with the aid of the multiple-path MSDSD algorithm of Section 2.4. The principle of finding the optimum symbol vector $\mathbf{S}$ is described in Section 3.1.2. The evaluation of the *a posteriori* LLR of $u[\mu]$ in (3.78) may be summarized as follows:

1. Let $\hat{\mathbf{S}}_{\text{MAP}}$ denote one of the legitimate differentially encoded DQPSK symbol vectors $\mathbf{S}$, which minimizes the term $\{\|\mathbf{U}^s\mathbf{S}\|^2+\|\mathbf{U}^{r_0}\mathbf{S}\|^2-\ln\Pr(\mathbf{V})\}$ involved in the numerator of (3.78). Then $\hat{\mathbf{V}}_{\text{MAP}}$ represents the corresponding QPSK symbol vector, which is uniquely identified by $\hat{\mathbf{S}}_{\text{MAP}}$. The symbol vector $\hat{\mathbf{S}}_{\text{MAP}}$ may be attained by implementing a specific sphere detection algorithm, which is an amalgam of the MAP-MSDSD algorithm described in Section 2.5.1 and of the Relay-Aided MSDSD algorithm described in Section 3.1.2. In more detail, its associated accumulated squared length accounting for the entire vector may

be derived from (2.68) and (3.21), leading to

$$d_1^2 = \sum_{i=1}^{N-1} \left(\left| \sum_{j=i}^{N} \mathbf{U}_{i,j}^{s} \hat{S}[j] \right|^2 + \left| \sum_{j=i}^{N} \mathbf{U}_{i,j}^{r_0} \hat{S}[j] \right|^2 - \ln\left(\Pr\left(V[i]\right)\right) \right) + |\mathbf{U}_{N,N}^{s}|^2 + |\mathbf{U}_{N,N}^{r_0}|^2. \tag{3.79}$$

2. Employ $\hat{\mathbf{V}}_{\mathrm{MAP}}$ as $\hat{\mathbf{V}}_{\mathrm{MAP}}^{b}$ and $\hat{\mathbf{S}}_{\mathrm{MAP}}$ as $\hat{\mathbf{S}}_{\mathrm{MAP}}^{b}$. Correspondingly, the detected value of the μ^{th} bit of $\hat{\mathbf{V}}_{\mathrm{MAP}}$ is assigned to the variable b in (3.78). As a Result, the reduced-size search space of $\chi_{:u[\mu]=\bar{b}}$ is determined.

3. Implement the constrained MAP-MSDSD algorithm based on (3.79), whose search space is reduced to $\chi_{:u[\mu]=\bar{b}}$. Correspondingly, the associated $\hat{\mathbf{V}}_{\mathrm{MAP}}^{\bar{b}}$ and $\hat{\mathbf{S}}_{\mathrm{MAP}}^{\bar{b}}$ is obtained.

4. Substituting the resultant vectors $\hat{\mathbf{V}}_{\mathrm{MAP}}^{b}$, $\hat{\mathbf{S}}_{\mathrm{MAP}}^{b}$, $\hat{\mathbf{V}}_{\mathrm{MAP}}^{\bar{b}}$ and $\hat{\mathbf{S}}_{\mathrm{MAP}}^{\bar{b}}$ into (3.78), the *a posteriori* LLR of $u[\mu]$ is obtained.

As seen in Figure 3.20, the resultant relay-aided SISO-MSDSD decoder is employed as the first stage of the iterative receiver at the DN, which is then further amalgamated with the URC decoder in order to form a two-stage inner decoder for appropriately complementing the SN's and RN's transmitter architecture. Then, a recursive systematic convolutional code (RSC) decoder is concatenated with the relay-aided-SISO-MSDSD-URC two-stage inner decoder for creating the DN's three-stage decoder seen in Figure 3.20.

3.3.3.3 Complexity of the Proposed Transceiver

Our complexity comparison between the single-path SISO-MSDSD decoder advocated in [55] and the proposed relay-aided SISO-MSDSD decoder is provided in Figure 3.21. In the spirit of [55], the average number of real-valued multiplication operations (RMO) required for generating a single soft-output during the SISO-MSDSD detection once per iteration is employed here as our complexity measure. If a correlated block-fading period of $T_b = 6$, and a normalized Doppler frequency of $f_d = 0.01$ are assumed, the SNR values of 6.05 dB and 2.12 dB represent the corresponding "turbo-cliff" points for the single-path SISO-MSDSD assisted system and for the relay-aided SISO-MSDSD assisted system, respectively. We will return to these issues later in the context of Figure 3.23. For the sake of a fair comparison, we ensured that both the conventional single-path SISO-MSDSD decoder and the relay-aided SISO-MSDSD decoder operated near their associated "turbo-cliff" points. Then we varied the *a priori* mutual information of the two different SISO-MSDSD decoders and recorded the associated number of required for producing a single soft-output once per iteration. Observe in Figure 3.21 that the proposed relay-aided SISO-MSDSD decoder approximately doubles the complexity compared to the single-path SISO-MSDSD decoder, which is valid right across the entire *a priori* mutual information region considered. The remaining components of the DN's receiver are similar to those of the RN, hence they affect the overall complexity in a similar way.

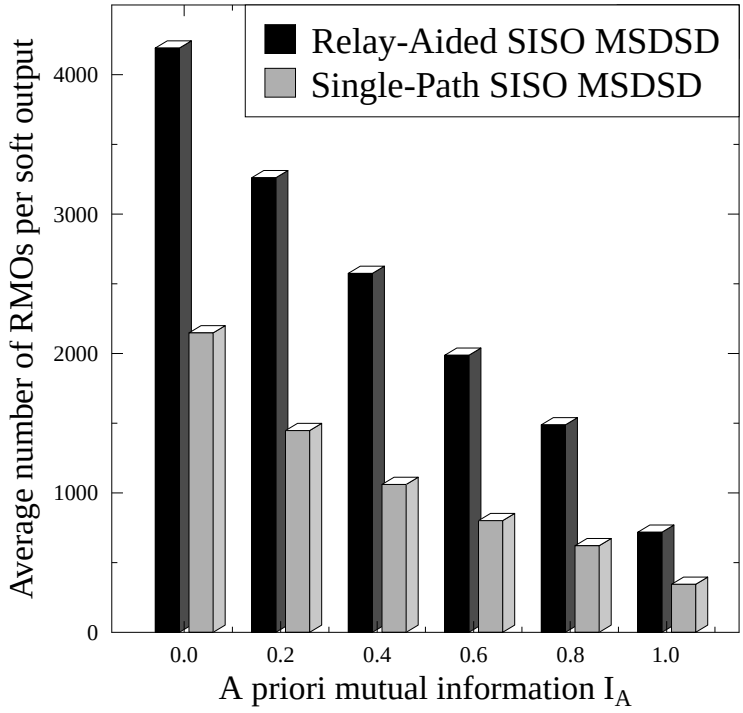

Figure 3.21: Complexity comparison between the relay-aided SISO-MSDSD decoder and the conventional single-path SISO-MSDSD decoder at different a priori mutual information values.

When designing an iterative decoding aided cooperative system, the distributed turbo coding scheme advocated in [64, 115] is attractive, since it benefits from the iterative information exchange between the direct and relayed versions of the same codeword, which experience uncorrelated fading. Naturally, the improved system performance is achieved at the cost of increasing the complexity imposed by employing an extra iteration stage.

By contrast, the proposed relay-aided SISO-MSDSD algorithm constitutes a realistic method of maintaining a low complexity, where the combination of the information provided by the direct and relayed signal streams, namely by $\mathbf{z}_s^l$ and $\mathbf{z}_{r_0}^{l+1}$ is achieved without an extra iteration stage. More explicitly, in a cooperative network, where the distributed turbo coding principle is employed by invoking the single-path SISO-MSDSD [55] algorithm, as in [109], each input signal stream is first individually processed by a single-path SISO-MSDSD aided turbo decoder within the inner iterative stage of [109, (Figure 7)]. Then the resultant information is passed on to the outer iterative stage, and typically at least two iterations are carried out in order to exchange information between the different input signal streams. Hence, based on our complexity comparisons shown in Figure 3.21, it is reasonable to argue that our three-stage relay-aided-SISO-MSDSD-URC-RSC decoder is capable of halving the system complexity imposed by the conventional single-path SISO-MSDSD aided distributed turbo decoder.

3.3.4 Performance of Transceiver's Robustness, Throughput and Complexity

3.3.4.1 Investigation of the Transceiver's Robustness

Channel Model	Time-Selective Block-Fading Channel
Path-Loss Exponent	$\alpha = 3$
Correlated Fading Block Length	$T_b = 6$
Normalized Doppler Frequency	$f_d = 0.01$
PN sequence	Gold sequence: $Q = 127$
Channel Coding	RSC Code
Code Memory Length	$\nu = 6$
Code Rate	$R_c = 0.5$
Modulation	DQPSK
MSDSD Observation Window Size	$N_{wind} = 6$
Inner Iterations of DN's Decoder	$I^d_{inner} = 2$
Outer Iterations of DN's Decoder	$I^d_{outer} = 9$
Relay Position in AF Based SRAN	$\theta = \frac{1}{2}$,
	$G_{sr_i} = \left(\frac{1.0}{0.357}\right)^3$, $G_{r_i d} = \left(\frac{1.0}{0.714}\right)^3$
Relay Position in DF Based SRAN	$\theta = 1.0$,
	$G_{sr_i} = G_{r_i d} = \left(\frac{1.0}{0.577}\right)^3$
Overall Bandwidth efficiency	$\eta = 0.8333$ bits/s/Hz

Table 3.3: SYSTEM PARAMETERS

Let us now investigate the robustness of the three-stage relay-aided-SISO-MSDSD-URC-RSC decoder depicted in Figure 3.20 in the terms of its BER performance. We commence by identifying the "turbo-cliff" SNR with the aid of extrinsic information transfer (EXIT) Charts as detailed in [7]. Both the relevant EXIT-chart and BER results of our AF/DF based SRAN are shown in Figures 3.22 and 3.23, respectively, when using the system parameters summarized in Table 3.3.

The MSDSD scheme requires the symbols of a decision-block to be correlated. By contrast, we have to eliminate the fading-induced correlations among symbols for the sake of achieving efficient iterative decoding, which is attained by using an interleaver frame length corresponding to 480×10^3 differentially modulated symbols. The *adaptive-window-duration* based scheme proposed for the SISO-MSDSD algorithm in [55] is capable of reducing the system's complexity, but all the systems involved in our comparisons, such as the conventional direct transmission based system, and the AF or DF based SRANs are capable of directly adopting it. Hence, regardless whether or not we opt for employing the *adaptive-window-duration* based scheme, this would not affect the preference order of the different systems. Accordingly, we fixed the observation window size of the SISO-MSDSD algorithm to $N_{wind} = 6$ for all the systems. Furthermore, in order to guarantee the fairness of our

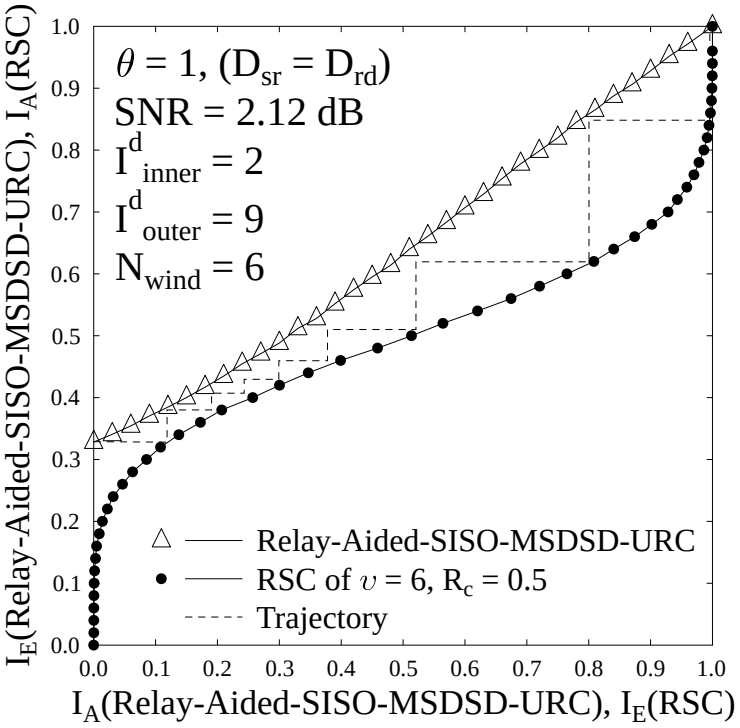

Figure 3.22: The EXIT characteristic of our proposed three-stage relay-aided-SISO-MSDSD-URC-RSC destination receiver.

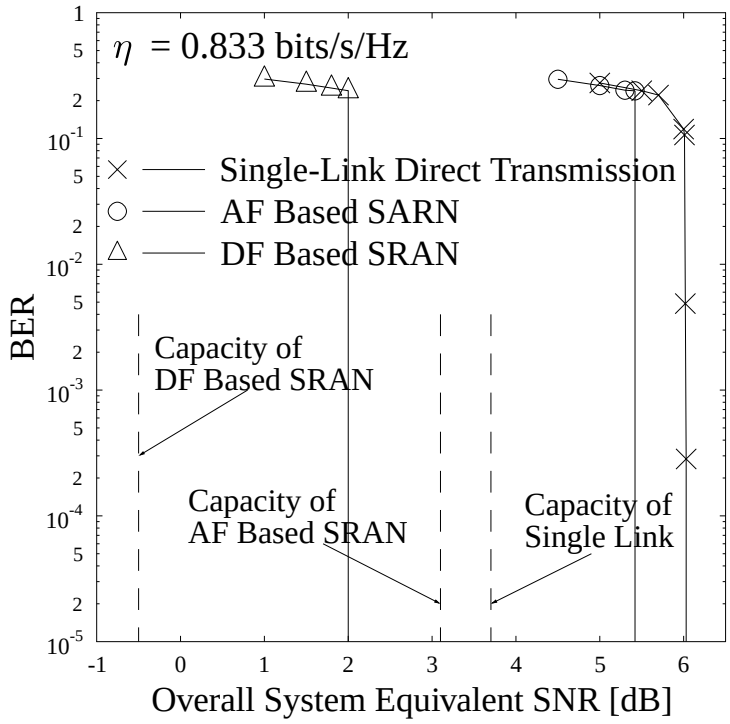

Figure 3.23: The comparison of BER performances among different systems.

comparisons among all the systems considered, the overall transmit power P_{total} is equally shared between the SN and RN transmitters, which equals to the overall power of the direct transmission based system.

Observe in Figure 3.22 that an open tunnel exists between the EXIT curves of the two-stage inner relay-aided-SISO-MSDSD-URC decoder and the outer RSC decoder, when the overall equivalent SNR value[7] reaches 2.12 dB. Furthermore, the associated Monte-Carlo simulation based decoding trajectory relying on a frame length of $L = 960 \times 10^3$ bits closely matches the EXIT curves. Correspondingly, an infinitesimally low BER is expected beyond the SNR $= 2.12$ dB point. This is further evidenced in Figure 3.23. The capacity of the proposed DF based SRAN is also characterized in Figure 3.23, which can be directly attained from Figure 3.17. In our case, the corresponding bandwidth efficiency is $\eta \approx R_c \times \log_2 M_c \times \frac{T_b-1}{T_b} = 0.8333$ bit/s/Hz. Hence, the proposed transceiver architecture of Figure 3.20 attains a performance within 2.6 dB from the capacity of the DF based SRAN. This 2.6 dB discrepancy may be further reduced for example with the aid of an irregular outer code, as detailed for example in [81].

To elaborate a little further, observe in Figure 3.23 that an approximately 3.9 dB power reduction is achieved by the proposed DF scheme in comparison to the classic direct transmission regime. By contrast, its corresponding AF based counterpart attains a more modest power reduction of about 0.5 dB, which is attained at a lower complexity than that of the DF arrangement.

3.3.4.2 Verification of the NC DCMC Capacity Derived for the DF Based SRAN

Having designed the transceiver architecture of Section 3.3.3, we are now in the position to evaluate the simulation based NC DCMC capacity of the DF based SRAN with the aid of EXIT-Chart analysis. This allows us to verify the correctness of our derivation of the NC DCMC capacity presented in Section 3.3.2 by comparing the theoretical and the simulation based noncoherent DCMC capacity of the DF based SRAN. More explicitly, the theoretical capacity was plotted from (3.69), (3.73) and (3.74) derived in Section 3.3.2, while the simulation based capacity was evaluated by exploiting the fact that the area under the inner receiver component's EXIT-curve determines the system's achievable capacity.

For the DF based SRAN having $\theta = 1.0$, owing to the similarity between the Source-to-Relay link and Relay-to-Destination link, we observe that $I\left(\mathbf{S}^l; \mathbf{y}_{r_0}^l\right) \approx I\left(\tilde{\mathbf{S}}^{l+1}; \mathbf{z}_{r_0}^{l+1}\right)$, which is satisfied throughout the entire SNR region considered. Hence we can further arrive at that

$$I\left(\mathbf{S}^l; \mathbf{y}_{r_0}^l\right) < I\left(\mathbf{S}^l; \mathbf{z}_s^l\right) + I\left(\tilde{\mathbf{S}}^{l+1}; \mathbf{z}_{r_0}^{l+1}\right), \tag{3.80}$$

Hence, according to (3.69) and (3.73) in Section 3.3.2, the capacity of the DF based SRAN having

[7] Here the terminology of "equivalent SNR" is defined as the radio of the transmit power with respect to the receiver's noise, which is measured at physically different points.

$\theta = 1.0$ is actually given by

$$C_{\text{Successive}}^{\text{DF}} = I\left(\mathbf{S}^l; \mathbf{y}_{r_0}^l\right), \tag{3.81}$$

which implies that in this specific case, the capacity of the SRAN is limited by the capacity of the Source-to-Relay link.

Observe in Figure 3.20 that the two-stage single-path-SISO-MSDSD-URC inner decoder may be regarded as the optimum differential detector, which is capable of approaching the maximum transmission rate for a specific differentially encoded modulation scheme [109]. According to the above-mentioned area properties of the EXIT charts [116], the area $\mathcal{A}$ under the bit-based EXIT chart curve of the two-stage single-path-SISO-MSDSD-URC inner decoder approximately equals to the maximum achievable coding rate of the outer channel encoder. Provided that there is an open EXIT-tunnel leading to the $(1, 1)$ point of the EXIT-chart, the system is capable of guaranteeing near-error-free transmissions. Hence, the maximum achievable near-error-free transmission rate of our source-to-relay transceiver portrayed in the "Relay" block of Figure 3.20 may be expressed as

$$R_{\max} = \left(\frac{N_{wind} - 1}{N_{wind}} \log_2 M_c\right) \cdot \mathcal{A} \quad \text{bits/s/Hz}, \tag{3.82}$$

and on condition of having $N_{wind} = T_b$, $R_{\max}$ should get close to the capacity of the Source-to-Relay link, or to the capacity of the entire DF based SRAN having $\theta = 1.0$ according to (3.81). The ratio of $\frac{N_{wind}-1}{N_{wind}}$ accounts for the modest rate-loss imposed by the inclusion of a known reference symbol in the classic differentially encoded signalling process [109].

The EXIT chart curves of the two-stage single-path-SISO-MSDSD-URC inner decoder used at the RN associated with different SNR values were shown in Figure 3.24, where the above-mentioned conventional narrowband time-selective Rayleigh fading channel was assumed in conjunction with $N_{wind} = 6$. Explicitly, after evaluating the area $\mathcal{A}$ under each EXIT chart curve[8] portrayed in Figure 3.24 of this response, we can evaluate the simulation-based maximum achievable near-error-free transmission rate of the DF based SRAN having $\theta = 1.0$ according to (3.82) of this response. The maximum achievable near-error-free transmission rate and the theoretical NC DCMC capacity were compared in Figure 3.25 of this response. The maximum achievable rate of the DF based SRAN having $\theta = 1.0$ almost coincides with its theoretical NC DCMC capacity, confirming the validity of our capacity formulae derived in Section 3.3.2.

3.3.4.3 Throughput versus Complexity

Based on the results shown in Figure 3.7, it may be anticipated that the energy efficiency of our noncoherent detection aided system architecture of Figure 3.20 will be improved by increasing the observation window size of the multiple-symbol differential detection scheme employed. Equiv-

[8]The EXIT chart curves corresponding to SNRs ranging from -7 to 23 dB in steps of 2 dB were obtained. However, if we simultaneously plot all of them in Figure 3.24 of this response, it becomes hard to identify every curve. Hence we only provided some of them in Figure 3.24.

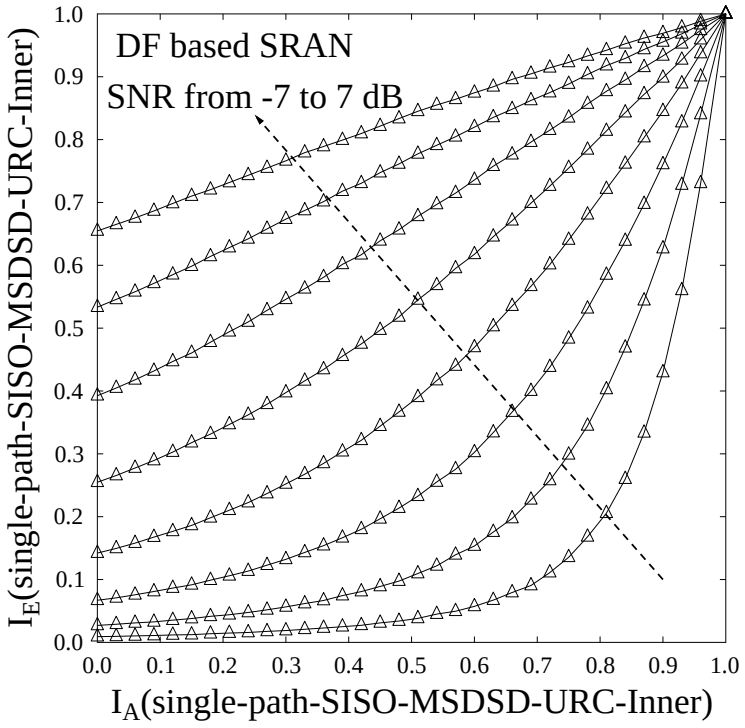

Figure 3.24: EXIT chart curves of the two-stage single-path-SISO-MSDSD-URC inner decoder at the RN, where the SNR increasing scale is 2 dB.

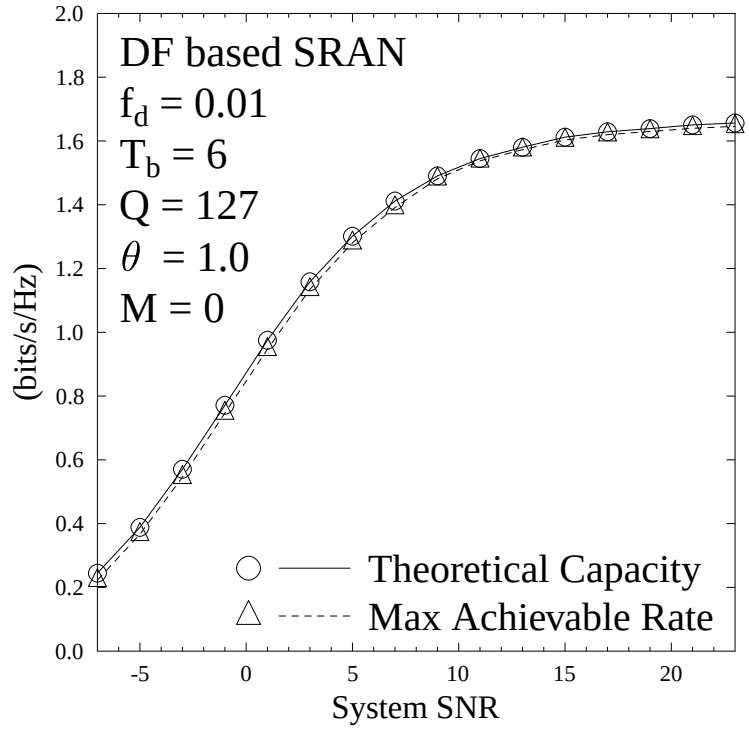

Figure 3.25: Comparison between the simulation based result and the theoretical result, where the theoretical capacity curve was directly abstracted from Figure 3.17, and the maximum achievable rate was evaluated according to (3.82).

alently, if we fix the transmit power, the system's bandwidth efficiency will also benefit from increasing the observation window size. However, this improvement of the bandwidth efficiency is achieved at the cost of imposing an increased complexity on the system, especially on the multiple-symbol differential detection aided decoder, as observed for example in Figure 3.8. Hence we compare the system's complexity imposed by employing different observation window sizes N_{wind} in the context of our transceiver architecture of Figure 3.20 proposed in Section 3.3.3. Naturally, the total complexity can be evaluated as

$$\mathcal{C}_{\text{total}} \triangleq \mathcal{I}_{\text{iter}} \times \mathcal{E}\left(\mathcal{C}_{\text{per}-\text{iter}}\right), \tag{3.83}$$

for different inner codes, where $\mathcal{I}_{\text{iter}}$ represents the number of iterations within the open tunnel between the inner and outer decoder's EXIT curve required for approaching the point of perfect convergence at $(1.0, 1.0)$ in the EXIT chart, while $\mathcal{E}(\mathcal{C}_{\text{per}-\text{iter}})$ is the average system complexity imposed during a single iteration.

As described in [116], the EXIT curve of the optimum outer code, which is capable of attaining the maximum achievable throughput should perfectly match the EXIT curve of the inner codes, namely that of the demodulator. Consequently, an extremely narrow open tunnel will occur between the outer and inner code's EXIT curve. As a penalty, a high $\mathcal{I}_{\text{iter}}$ value is required. Hence we may readily assume that optimum outer codes matched to different inner codes having different observation window sizes require a similar value of $\mathcal{I}_{\text{iter}}$. Consequently, instead of comparing $\mathcal{C}_{\text{total}}$, we may directly use $\mathcal{E}(\mathcal{C}_{\text{per}-\text{iter}})$ for our complexity comparisons, where the proportionality of the complexity associated with different observation window sizes remains. Such optimum outer codes may be designed, for example using irregular convolutional codes, where only the coding rates of the individual constituent sub-codes are different. Hence only the complexity imposed by the relay-aided SISO-MSDSD decoder has to be involved in the complexity comparison.

Based on the above analysis, we first fix the observation window size. Then we gradually increase the *a priori* mutual information of the relay-aided SISO-MSDSD decoder from 0.0 to 1.0 by a step-size of 0.02 and employ the average of all the recorded RMO per bit values associated with each of the iterations as an approximation of $\mathcal{E}(\mathcal{C}_{\text{per}-\text{iter}})$. Meanwhile, the associated maximum achievable throughput can be obtained according to (3.82). After implementing this approximation process for each N_{wind} value considered, the trade-off between the maximum achievable throughput and the complexity imposed is visualized in Figure 3.26, where different SNR values are considered. In Figure 3.26, the path-loss gain of G_{sr_i} is assigned to be 8, which is different to that specified in Table 3.3.

3.4 Chapter Summary

In order to recover the 50% throughput loss incurred by the conventional half-duplex three-terminal cooperative network, we invoked the advanced successive relaying protocol of Section 1.2.4. How-

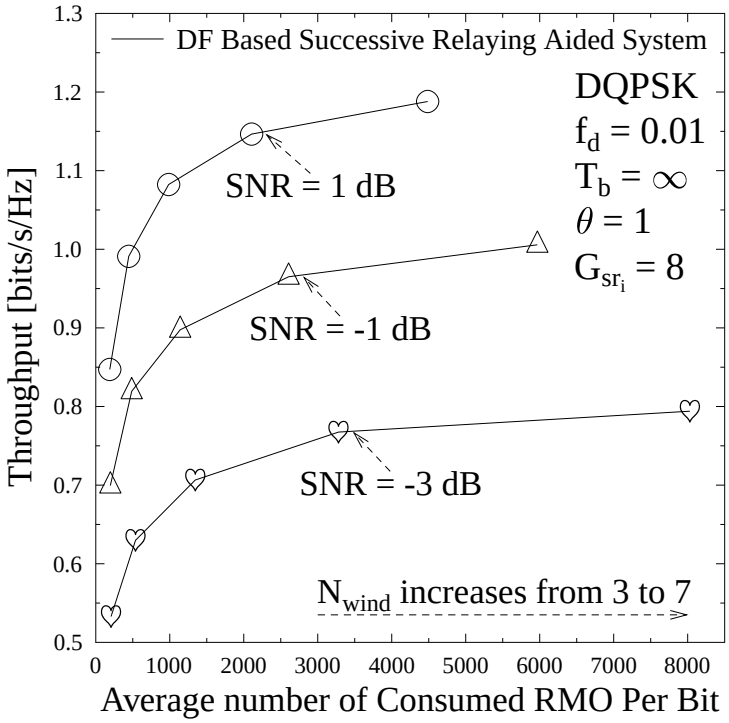

Figure 3.26: The trade-off between the maximum achievable throughput and the complexity per bit, where various values of N_{wind} are investigated.

ever, simultaneously, the successive relaying imposes increased interferences, namely CCI and IRI on the system. For the sake of efficiently solving the interference problem, we employ one of the classic multiple access techniques, namely DS-CDMA as our interference suppression scheme. Consequently, the SRAN is embedded in the DS-CDMA uplink for assisting the cell-edge users, as portrayed in Figure 3.2. In the basic prototype system of Figure 3.2, only the CCI is considered in the context of a single-user scenario. For the sake of maintaining a low complexity at the RN, in Section 3.1, the AF protocol was invoked. Then, in Section 3.2, we further developed our prototype by extending the single-user scenario to the multi-user scenario and additionally, we also considered the effects of the IRI. In this scenario, we derived the theoretical performance bounds in Section 3.2.2. Consequently, the noncoherent DCMC capacity of the successive AF relaying aided multi-user DS-CDMA uplink was evaluated. Finally, for the sake of improving the energy efficiency, in Section 3.3, we replace the AF protocol employed in the system architecture of Figure 3.10 by the DF protocol. The NC DCMC capacity of the DF based SRAN was investigated in Section 3.3.2. It is demonstrated in Figure 3.23 that the DF based SRAN indeed outperforms its AF based counterpart.

However, a large number of relays may be involved in the cooperative system considered. Furthermore, it may be unrealistic to expect that in addition to relaying, the relays could further afford the power-hungry channel estimation for the SR links in support of coherent detection. Hence in Section 3.1.2 we devised the so-called relay-aided MSDSD algorithm. Furthermore,

in Section 3.3.3 the hard-decision-based relay-aided MSDSD was further developed to its soft-decision-based counterpart, resulting in the relay-aided SISO-MSDSD scheme. Correspondingly, the sophisticated three-stage iterative-detection based transceiver architecture of Figure 3.20 was designed for the proposed system, which exhibited a remarkable energy efficiency.

However, according to the preconditions of employing the DS-CDMA technique for controlling the successive relaying induced interferences, as stated in Section 3.1, we have to find a sufficient number of idle users and satisfy that $U_{\mathrm{ACT}} + U_{\mathrm{RN}} < U_{\mathrm{Threshold}}$ for the sake of avoiding any requirement of extra channel resources. Nevertheless, the proposed SRAN aided cooperative DS-CDMA solution may still lead to a potential user-load reduction for the CDMA uplink. In order to obviate above-mentioned disadvantages, while suppressing the successive relaying induced interferences without relying on any CSI, we proposed a novel adaptive Newton algorithm based multiple-symbol differential interference suppression (MS-DIS) scheme, which is detailed in the next chapter.

Chapter 4

Differential Interference Suppression Aided Noncoherent Successive Relaying

As stated in Section 1.1, conventional single-relay aided two-phase cooperative networks employing coherent detection algorithms incur a significant throughput loss of 50%. Furthermore, we pointed out in Section 3.1 that it is hard to expect that in addition to the task of relaying, the RN would dedicate further precious resources to the estimation of the SR channel in support of coherent detection, which would consume extra energy expended in power-hungry channel estimation. Accordingly, in order to circumvent these problems, we proposed the noncoherent successive relaying regime of Chapter 3. A crucial challenge in this context is that of suppressing the successive relaying induced interference, despite dispensing with channel state information (CSI). In Chapter 3, we tackled this challenge by directly exploiting the DS-CDMA multiple access philosophy. However, as stated in Section 3.4, employing DS-CDMA technology for suppressing the successive relaying induced interference may lead to a potential user-load reduction of the CDMA system owing to the limited number of available spreading codes. Furthermore, the preconditions of employing the proposed SRAN aided cooperative DS-CDMA also constrains the application of the regimes proposed in Section 3.1, Section 3.2 and Section 3.3.

Additionally, the interference problems of SRANs had also been considered in [45, 46]. Regretfully, the interference suppression schemes advocated in these contributions were all based on the assumption that the receiver perfectly knows the CSI of all the links involved. Hence, the implementation of interference suppression for the SRAN remains a challenge, when employing noncoherent detection.

Attractively, the differential interference suppression (DIS) philosophy was discussed in [117] and it was then further developed in [118], where a novel amalgam of the adaptive modified Newton algorithm of [119] and of SISO-MSDSD was created. Inspired by these achievements, in Section 4.1 and Section 4.2, we conceive successive relaying induced interference suppression for

employment at the destination, which is achieved despite dispensing with CSI by incorporating the multiple-symbol differential interference suppression (MS-DIS) into SRANs. Consequently, a new adaptive MS-DIS filter and MSDSD decoder assisted channel-code-aided three-stage turbo decoder is designed for the DN's receiver in Section 4.3. In Section 4.5, we demonstrate that our proposed transceiver is capable of efficiently suppressing the interference by imposing as little as 2% training overhead, despite experiencing severe time-selective Rayleigh fading. As we will demonstrate in Section 4.6, implementing the MS-DIS regime at the RNs in a similar manner to that at the DN is also capable of suppressing the inter-relay interference. Hence suppressing the successive relaying induced interference without requiring any extra orthogonal channel resources, while dispensing with CSI becomes feasible.

The rest of this chapter is organised as follows. Our system model is portrayed in Section 4.1. In Section 4.2, the relevant concepts involved in the adaptive MS-DIS scheme are introduced. We design the architecture of the transceiver in Section 4.3. The noncoherent Discrete-input Continuous-output Memoryless Channel (DCMC) capacity of our proposed system is derived in Section 4.4, while the performance of the proposed transceiver is characterized in Section 4.5. Finally, we conclude in Section 4.6.

4.1 Simplified System Model

A realistic multi-user successive relaying aided network is illustrated in Figure 3.9. However, as stated at the beginning of this chapter, suppressing the successive relaying induced interference without requiring any extra orthogonal channel resources and dispensing with CSI is a challenging task. In order to tackle this problem, we simplify the system model depicted in Figure 3.9 and concentrate our attention only on a simple SRAN, which consists of four terminals, i.e. a SN s, two RNs r_0, r_1, and a DN d.

The classic transmission procedure of the SRAN is illustrated in Figure 4.1, where three consecutive phases are exhibited. Typically, in the even phase, the Mobile Station (MS) s broadcasts its information stream, while the activated relay r_0 listens to s and another activated relay r_1 decodes, re-encodes as well as forwards the signals received from s during the most recent phase. In the consecutive odd phase, s continues to broadcast its next information stream, but the roles of the relays r_0 and r_1 alternate. In contrast to the SRAN portrayed in Figure 3.10 of Section 3.2.1, here, we assume that the resource allocation activates carefully selected relays that are sufficiently far apart. Hence the interference between the relays, i.e. the IRI may be tentatively ignored. Only the four terminals of a SRAN are considered in the scenario investigated in this chapter, which implies that the MAI is intrinsically avoided. Accordingly, only the CCI at the DN d is explicitly presented in Figure 4.1.

We assume that all the channels involved in the transmissions are narrowband time-selective

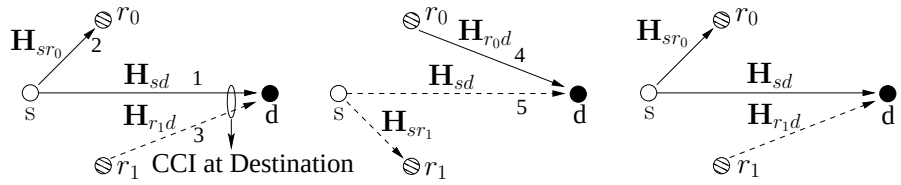

(a) Even Phase (or Frame) (b) Odd Phase (or Frame) (c) Even Phase (or Frame)

Figure 4.1: Transmission processes of SRAN, different typical phases are shown.

Rayleigh fading channels and the notation $\mathbf{H}_{ab}, (a, b) \in \{s, r_0, r_1, d\}$ represents the channel impulse response (CIR) matrix spanning from entity a to b. Furthermore, the relay-aided path-loss reduction [107, 120] induced in Section 3.2.1 is also considered here. Accordingly, the path-loss gain of the Source-to-Relay (SR_i) link and Relay-to-Destination (R_iD) link with respect to the Source-to-Destination (SD) link are introduced here as $G_{sr_i} = \{\frac{D_{sd}}{D_{sr_i}}\}^{\alpha}$ and $G_{r_id} = \{\frac{D_{sd}}{D_{r_id}}\}^{\alpha}$, respectively, where D_{ab} represents the distance between a and b, while α is the path-loss exponent. More specifically, the value of α is fixed to 3 here to model a typical urban area. The transmit power of the node a is represented as $P_a, a \in \{s, r_0, r_1\}$.

Then we assume that N_T transmit antennas are used both at s, as well as at r_i, while N_R receive antennas are employed at d. Due to the limited size and complexity of the handset, we fix $N_T = 1$. Furthermore, the classic frame-by-frame based transmission having a frame length of L routinely adopted in realistic communication networks is employed here.

The realistic transceiver architecture designed for each node involved in the SRAN is portrayed in Figure 4.3. For the sake of relating Figure 4.1 to Figure 4.3, the same transmissions are numbered by the same indices in the two figures. For example, since the transmission from the SN to the DN during the "(a) Even Phase" in Figure 4.1 corresponds to the transmission from the SN's transmit antenna to the receive antennae of the "Even Phase Multiple-Symbol DIS Filter" in Figure 4.3, both of them are labelled by the index 1. Observe in Figure 4.1 that transmission-3 and transmission-5 will contaminate the DN's signals received due to transmission-1 and transmission-4, respectively. In order to mitigate this co-channel interference (CCI), the MS-DIS filter is employed at the input of the DN's receiver. The principle of the MS-DIS filter and the details conceiving other components involved in Figure 4.3 will be provided during our forthcoming discourse.

The system model corresponding to Figure 4.1 may be constructed for the k^{th} symbol duration of the l^{th} frame as

$$\mathbf{Y}^l[k] = \sqrt{G_{sd}}\sqrt{P_s}\mathbf{S}^l[k]\mathbf{H}^l_{sd}[k] + \sqrt{G_{r_id}}\sqrt{P_{r_i}}\mathbf{C}^l_{r_i}[k]\mathbf{H}^l_{r_id}[k] + \mathbf{W}^l[k], \tag{4.1}$$

where we have $\mathbf{Y}^l[k] \in \mathbb{C}^{1\times N_R}$, $\mathbf{S}^l[k] \in \mathbb{C}^{1\times N_T}$, $\mathbf{C}^l_i[k] \in \mathbb{C}^{1\times N_T}$, $\mathbf{H}^l_{ab}[k] \in \mathbb{C}^{N_T\times N_R}$, while $\mathbf{W}^l[k] \in \mathbb{C}^{1\times N_R}$ denotes the k^{th} received signal matrix at the DN, the SN's broadcast symbol matrix, the RN's forwarded symbol matrix and the associated CIR matrix as well as the AWGN matrix obeying a distribution of $\mathcal{CN}(0, N_0)$, respectively. The notation i is calculated as $i =$

$\mathrm{mod}\big[(l+1),2\big]$ and $l=0,1,\cdots$.

In order to invoke the MS-DIS regime of [118] and to further combine it with the SISO-MSDSD algorithm [55], it is necessary to extend the symbol-by-symbol based system model characterized by (4.1) to its multiple-symbol based version. We split the DN's L received signals of a frame into J signal blocks, where each signal block consists of N_{wind} consecutively received $\mathbf{Y}^l[k]$ contributions. Accordingly, the n^{th} signal block matrix received during the l^{th} frame may be readily formulated as

$$\underline{\mathbf{Y}}^l[n]=\sqrt{G_{sd}}\sqrt{P_s}\underline{\mathbf{S}}^l[n]\underline{\mathbf{H}}^l_{sd}[n]+\sqrt{G_{r_id}}\sqrt{P_{r_i}}\underline{\mathbf{C}}^l_{r_i}[n]\underline{\mathbf{H}}^l_{r_id}[n]+\underline{\mathbf{W}}^l[n], \tag{4.2}$$

where $\underline{\mathbf{Y}}^l[n]$ obeys the form of

$$\underline{\mathbf{Y}}^l[n]=\begin{bmatrix}\mathbf{Y}^l[L\cdot l+(N_{wind}-1)\cdot n]\\ \vdots\\ \mathbf{Y}^l[L\cdot l+(N_{wind}-1)\cdot (n+1)]\end{bmatrix}. \tag{4.3}$$

In order to detail our signalling arrangement more explicitly, we create Figure 4.2, where the frame index l and the signal block length N_{wind} are fixed to 0 and 4, respectively. Observe at Figure 4.2 that, the last element of $\underline{\mathbf{Y}}^l[n]$ will become the first element of $\underline{\mathbf{Y}}^l[n+1]$. This overlap between the two adjacent signal blocks is required by the MSDSD algorithm [55].

Then the CIR block $\underline{H}^l_{ab}[n]$ as well as the AWGN block $\underline{W}^l[n]$ given in (4.2) are constructed by vertically stacking the associated $\mathbf{H}^l_{ab}[k]$ and $\mathbf{W}^l[k]$ given in (4.1) in a form similar to (4.3), respectively. Let us define an new matrix operator, namely $T_D(\cdot)$. Similar to (2.42), let $\mathbf{B}$ denote a vector consisting of N_{wind} N_T-element sub-vectors $\mathbf{B}_n$, which can be rewritten as

$$\mathbf{B}=[\mathbf{B}_1,\mathbf{B}_2,\ldots,\mathbf{B}_{N_{\mathrm{wind}}}], \tag{4.4}$$

where we have $\mathbf{B}_n=[b_1,b_2,\ldots,b_{N_T}]$. When the transformation operator $T_D(\cdot)$ is applied to $\mathbf{B}$, it yields

$$T_D(\mathbf{B})=\begin{bmatrix}\mathbf{B}_1 & 0 & \cdots & 0\\ 0 & \mathbf{B}_2 & \cdots & 0\\ \vdots & \vdots & \ddots & \vdots\\ 0 & 0 & \cdots & \mathbf{B}_{N_{\mathrm{wind}}}\end{bmatrix}_{N_{\mathrm{wind}}\times N_{\mathrm{wind}}N_T}. \tag{4.5}$$

Correspondingly, the n^{th} SN's transmitted symbol block received during the l^{th} frame and formulated in (4.2) is given by $\underline{\mathbf{S}}^l[n]=T_D\Big(\big[\mathbf{S}^l[L\cdot l+(N_{\mathrm{wind}}-1)\cdot n],\cdots,\mathbf{S}^l[L\cdot l+(N_{\mathrm{wind}}-1)\cdot(n+1)]\big]\Big)$. An M_c-ary differential encoding scheme is employed here, hence we have $\mathbf{S}^l[k+1]=\mathbf{S}^l[k]\mathbf{V}^l[k]$. Since N_T is fixed to 1, both $\mathbf{S}^l[k]$ and $\mathbf{V}^l[k]$ are actually single-element vectors in our scenario and $\underline{\mathbf{S}}^l[n]$ is uniquely and unambiguously determined by the length-$(N_{\mathrm{wind}}-1)$ information symbol block matrix $\underline{\mathbf{V}}^l[n]=\big[\mathbf{V}^l[L\cdot l+(N_{\mathrm{wind}}-1)\cdot n],\cdots,\mathbf{V}^l[L\cdot l+(N_{\mathrm{wind}}-1)\cdot(n+1)-1]\big]^T$.

Similarly, the n^{th} RN's forwarded symbol block in (4.2) is given by $\underline{\mathbf{C}}^l_{r_i}[n]=T_D\Big(\big[\mathbf{C}^l_{r_i}[L\cdot l+(N_{\mathrm{wind}}-1)\cdot n],\cdots,\mathbf{C}^l_{r_i}[L\cdot l+(N_{\mathrm{wind}}-1)\cdot(n+1)]\big]\Big)$. The decode-and-forward (DF)

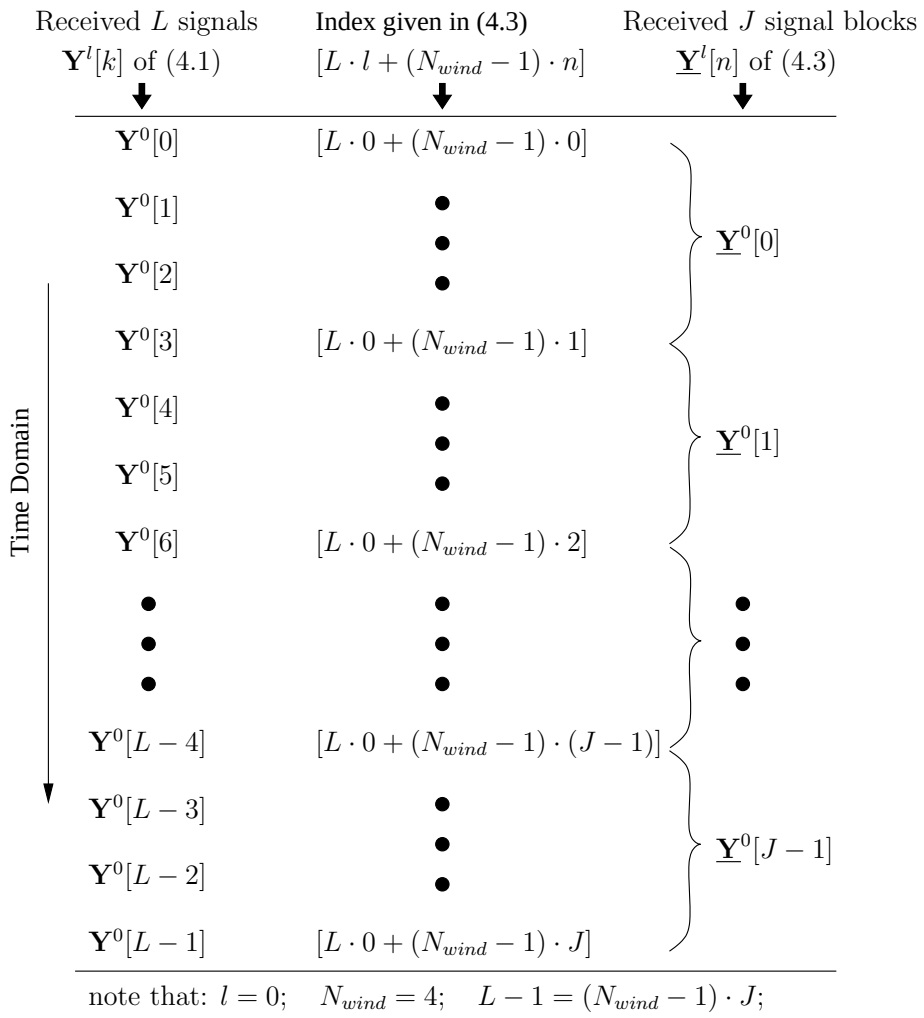

Figure 4.2: The signalling arrangement of a single frame.

relaying protocol is employed at the RN. If the RN perfectly detects the received information bits and re-encodes, as well as re-modulates them in the same way as the SN, we arrive at

$$\underline{\mathbf{C}}^l_{r_i}[n] = \underline{\mathbf{S}}^{l-1}[n]. \tag{4.6}$$

4.2 Adaptive Multiple-Symbol Based Differential Interference Suppression

According to (4.2), it is apparent that the transmitted signals of the SN and RN always interfere with each other at the DN. Hence noncoherent detection cannot be directly applied at the DN, before an interference suppression stage is invoked at the input of the DN's receiver. When we want to detect the signal received from the SN, the first term of (4.2) becomes the desired signal component, while the remaining terms represent the interference-plus-noise component. This partitioning of

the received signal block matrix $\underline{\mathbf{Y}}^l[n]$ is detailed as

$$\underline{\mathbf{Y}}^l[n] = \underbrace{\sqrt{G_{sd}}\sqrt{P_s}\underline{\mathbf{S}}^l[n]\underline{\mathbf{H}}^l_{sd}[n]}_{\text{desired component: } \underline{\mathbf{Y}}^l_g[n]} + \underbrace{\sqrt{G_{r_id}}\sqrt{P_{r_i}}\underline{\mathbf{C}}^l_{r_i}[n]\underline{\mathbf{H}}^l_{r_id}[n] + \underline{\mathbf{W}}^l[n]}_{\text{interference-plus-noise component}} \tag{4.7}$$

Hence our goal is to extract the information pertaining to the desired signal component $\underline{\mathbf{Y}}^l_g[n]$ from the complete received signal block matrix $\underline{\mathbf{Y}}^l[n]$, while suppressing the interference-plus-noise component. The adaptive MS-DIS technique of [118] is capable of realizing our objective and consequently it is invoked at the input of the DN's receiver, as we will detail in Section 4.3 with reference to Figure 4.3.

4.2.1 Maximum Signal-to-Interference-Plus-Noise Ratio Criterion

In order to detect the N_{wind}-element differentially encoded symbol block $\underline{\mathbf{S}}^l[n]$ carried by $\underline{\mathbf{Y}}^l_g[n]$, the received signal block matrix $\underline{\mathbf{Y}}^l[n]$ is passed through an adaptive filter having the coefficient vector $\boldsymbol{f}_g \in \mathbb{C}^{N_R \times 1}$. The filter output is given by

$$\mathbf{y}^l_g[n] = \underline{\mathbf{Y}}^l[n]\boldsymbol{f}_g. \tag{4.8}$$

According to [117], the signal-to-interference-plus-noise-ratio (SINR) is defined as the ratio between the power of the desired filter output component $\underline{\mathbf{Y}}^l_g[n]\boldsymbol{f}_g$ and the power of the interference-plus-noise component $(\underline{\mathbf{Y}}^l[n] - \underline{\mathbf{Y}}^l_g[n])\boldsymbol{f}_g$. Hence, based on the maximum SINR (MSINR) criterion, our goal becomes that of finding a coefficient vector $\boldsymbol{f}_g$, which is capable of maximising the filter's output SINR. The decision rule of the optimum $\boldsymbol{f}_g$ is formulated as

$$\hat{\boldsymbol{f}}_g = \max_{\boldsymbol{f}_g} \frac{\boldsymbol{f}_g^H(\mathbf{R}_{rr} - \mathbf{R}_{ee})\boldsymbol{f}_g}{\boldsymbol{f}_g^H\mathbf{R}_{ee}\boldsymbol{f}_g} = \max_{\boldsymbol{f}_g} \frac{\boldsymbol{f}_g^H\mathbf{R}_{rr}\boldsymbol{f}_g}{\boldsymbol{f}_g^H\mathbf{R}_{ee}\boldsymbol{f}_g}, \tag{4.9}$$

where the correlation matrix of the entire received signal block and of the interference-plus-noise component are defined by

$$\begin{aligned}
\mathbf{R}_{rr} &\triangleq \mathcal{E}\{\underline{\mathbf{Y}}^{l\,H}[n]\underline{\mathbf{Y}}^l[n]\} \\
&= G_{sd}P_s\mathcal{E}\left\{\underline{\mathbf{H}}^{l\,H}_{sd}[n]\underline{\mathbf{H}}^l_{sd}[n]\right\} + G_{r_id}P_{r_i}\mathcal{E}\left\{\underline{\mathbf{H}}^{l\,H}_{r_id}[n]\underline{\mathbf{H}}^l_{r_id}[n]\right\} + N_{\text{wind}}N_0\mathbf{I}_{N_R}, \qquad (4.10)\\
\mathbf{R}_{ee} &\triangleq \mathcal{E}\{(\underline{\mathbf{Y}}^l[n] - \underline{\mathbf{Y}}^l_g[n])^H(\underline{\mathbf{Y}}^l[n] - \underline{\mathbf{Y}}^l_g[n])\} \\
&= G_{r_id}P_{r_i}\mathcal{E}\left\{\underline{\mathbf{H}}^{l\,H}_{r_id}[n]\underline{\mathbf{H}}^l_{r_id}[n]\right\} + N_{\text{wind}}N_0\mathbf{I}_{N_R}, \qquad (4.11)
\end{aligned}$$

respectively. Then $\mathbf{I}_{N_R}$ represents an identity matrix having $(N_R \times N_R)$ elements. Furthermore, $\mathcal{E}\{\cdot\}$ and $[\cdot]^H$ denote the statistical expectation and the Hermitian transposition, respectively.

It was shown in [121] that the optimization problem of (4.9) leads to the generalized eigenvalue problem, which is formulated as

$$\mathbf{R}_{rr}\boldsymbol{f}_g = \lambda\mathbf{R}_{ee}\boldsymbol{f}_g. \tag{4.12}$$

4.2.2 Adaptive Modified Newton Algorithm

According to (4.10), (4.11) and (4.12), each CIR block matrix $\underline{\mathbf{H}}_{ab}^{l}[n]$ has to be known by the DN's receiver for the sake of determining each associated coefficients vector $\boldsymbol{f}_g$, which inherently leads to the employment of coherent detection. Then, even through the receiver already acquired the CIR block matrix $\underline{\mathbf{H}}_{ab}^{l}[n]$, we have to utilize the singular-value decomposition (SVD) [122] to implement the generalized eigen-decomposition for finding the optimum $\boldsymbol{f}_g$, which usually imposes a high computational complexity.

Alternatively, instead of obtaining the precise correlation matrices $\mathbf{R}_{rr}$ and $\mathbf{R}_{ee}$, we can recursively approximate them and update the sub-optimum coefficient vector $\boldsymbol{f}_g[n]$ on a block-by-block basis according to the adaptive modified Newton algorithm, which was shown in [119] to have a fast convergence and an excellent tracking capability.

Similar to [117, (11)], by exploiting the differential encoding principle, the multiple-symbol-based error signal block matrix $\underline{\mathbf{E}}_{g}^{l}[n]$ may be expressed as

$$\underline{\mathbf{E}}_{g}^{l}[n] = \sqrt{\frac{1}{2}} \left(\underline{\mathbf{Y}}^{l}[n] - \underline{\hat{\mathbf{V}}}_{g}^{l}[n] \cdot \underline{\mathbf{Y}}^{l}[\overleftarrow{n}^{(1)}] \right), \tag{4.13}$$

which may be used to approximate the interference-plus-noise component of (4.7). The operation "$\cdot$" denotes the submatrix-wise multiplication between two matrices. Then the specific block index $\overleftarrow{n}^{(m)}$ represents the n^{th} signal block, which was shifted backwards by m symbol durations. Furthermore, we have $\underline{\hat{\mathbf{V}}}_{g}^{l}[n] = \left[\hat{\mathbf{V}}^{l}[L \cdot l + (N_{wind} - 1) \cdot n - 1] \ , \ \underline{\hat{\mathbf{V}}}^{l}[n]^{T} \right]^{T}$, which becomes known to the DN's receiver in the training model of the adaptive filter or is actually substituted by the previous decisions in the decision-directed model of the adaptive filter. The normalization factor $\sqrt{1/2}$ is compensated according to [117].

Example 4.1: A specific example of the product $\left(\underline{\hat{\mathbf{V}}}_{g}^{l}[n] \cdot \underline{\mathbf{Y}}^{l}[\overleftarrow{n}^{(1)}] \right)$ given in (4.13) is provided below for: $l = 0$, $n = 1$, $N_{\text{wind}} = 4$, $N_R = 4$.

Observe in Figure 4.2 and (4.2), for $l = 0$, $n = 1$, $N_{\text{wind}} = 4$ and $N_R = 4$, that the associated signal block matrix received at the DN may be formulated as

$$\underline{\mathbf{Y}}^{l}[n] = \underline{\mathbf{Y}}^{0}[1] = \begin{bmatrix} \mathbf{Y}^{0}[3] \\ \mathbf{Y}^{0}[4] \\ \mathbf{Y}^{0}[5] \\ \mathbf{Y}^{0}[6] \end{bmatrix} = \begin{bmatrix} \mathbf{Y}_{1}^{0}[3] & \mathbf{Y}_{2}^{0}[3] & \mathbf{Y}_{3}^{0}[3] & \mathbf{Y}_{4}^{0}[3] \\ \mathbf{Y}_{1}^{0}[4] & \mathbf{Y}_{2}^{0}[4] & \mathbf{Y}_{3}^{0}[4] & \mathbf{Y}_{4}^{0}[4] \\ \mathbf{Y}_{1}^{0}[5] & \mathbf{Y}_{2}^{0}[5] & \mathbf{Y}_{3}^{0}[5] & \mathbf{Y}_{4}^{0}[5] \\ \mathbf{Y}_{1}^{0}[6] & \mathbf{Y}_{2}^{0}[6] & \mathbf{Y}_{3}^{0}[6] & \mathbf{Y}_{4}^{0}[6] \end{bmatrix}_{N_{\text{wind}} \times N_R}, \tag{4.14}$$

where the signal vector $\mathbf{Y}^{l}[k]$ received at the DN during the k^{th} symbol duration of the l^{th} frame as formulated in (4.1) may be rewritten as $\mathbf{Y}^{l}[k] = \left[\mathbf{Y}_{1}^{l}[k], \mathbf{Y}_{2}^{l}[k], \cdots, \mathbf{Y}_{N_R}^{l}[k] \right]$. For example, we have $\mathbf{Y}^{0}[3] = \left[\mathbf{Y}_{1}^{0}[3], \mathbf{Y}_{2}^{0}[3], \cdots, \mathbf{Y}_{4}^{0}[3] \right]$ in (4.14).

Consequently, after shifting the signal block matrix $\underline{\mathbf{Y}}^{l}[n]$ of (4.14) backwards by a single

symbol duration, the associated signal block matrix is given by

$$\underline{\mathbf{Y}}^l[\overleftarrow{n}^{(1)}] = \underline{\mathbf{Y}}^0[\overleftarrow{1}^{(1)}] = \begin{bmatrix} \mathbf{Y}^0[2] \\ \mathbf{Y}^0[3] \\ \mathbf{Y}^0[4] \\ \mathbf{Y}^0[5] \end{bmatrix} = \begin{bmatrix} \mathbf{Y}_1^0[2] & \mathbf{Y}_2^0[2] & \mathbf{Y}_3^0[2] & \mathbf{Y}_4^0[2] \\ \mathbf{Y}_1^0[3] & \mathbf{Y}_2^0[3] & \mathbf{Y}_3^0[3] & \mathbf{Y}_4^0[3] \\ \mathbf{Y}_1^0[4] & \mathbf{Y}_2^0[4] & \mathbf{Y}_3^0[4] & \mathbf{Y}_4^0[4] \\ \mathbf{Y}_1^0[5] & \mathbf{Y}_2^0[5] & \mathbf{Y}_3^0[5] & \mathbf{Y}_4^0[5] \end{bmatrix}_{N_{\text{wind}} \times N_R}. \tag{4.15}$$

Then, as introduced in (4.13), the associated estimated information symbol block matrix $\underline{\hat{\mathbf{V}}}_g^l[n]$ may be formulated as

$$\underline{\hat{\mathbf{V}}}_g^l[n] = \underline{\hat{\mathbf{V}}}_g^0[1] = \begin{bmatrix} \hat{\mathbf{V}}^0[2] \\ \hat{\mathbf{V}}^0[3] \\ \hat{\mathbf{V}}^0[4] \\ \hat{\mathbf{V}}^0[5] \end{bmatrix}. \tag{4.16}$$

With the aid of (4.15) and (4.16) as well as considering our specific case of $l = 0$, $n = 1$, $N_{\text{wind}} = 4$ and $N_R = 4$, the product of $\left(\underline{\hat{\mathbf{V}}}_g^l[n] \cdot \underline{\mathbf{Y}}^l[\overleftarrow{n}^{(1)}]\right)$ involved in (4.13) is expressed as

$$\begin{aligned} \underline{\hat{\mathbf{V}}}_g^l[n] \cdot \underline{\mathbf{Y}}^l[\overleftarrow{n}^{(1)}] &= \begin{bmatrix} \hat{\mathbf{V}}^0[2] \\ \hat{\mathbf{V}}^0[3] \\ \hat{\mathbf{V}}^0[4] \\ \hat{\mathbf{V}}^0[5] \end{bmatrix} \cdot \begin{bmatrix} \mathbf{Y}_1^0[2] & \mathbf{Y}_2^0[2] & \mathbf{Y}_3^0[2] & \mathbf{Y}_4^0[2] \\ \mathbf{Y}_1^0[3] & \mathbf{Y}_2^0[3] & \mathbf{Y}_3^0[3] & \mathbf{Y}_4^0[3] \\ \mathbf{Y}_1^0[4] & \mathbf{Y}_2^0[4] & \mathbf{Y}_3^0[4] & \mathbf{Y}_4^0[4] \\ \mathbf{Y}_1^0[5] & \mathbf{Y}_2^0[5] & \mathbf{Y}_3^0[5] & \mathbf{Y}_4^0[5] \end{bmatrix} \\ &= \begin{bmatrix} \hat{\mathbf{V}}^0[2]\mathbf{Y}_1^0[2] & \hat{\mathbf{V}}^0[2]\mathbf{Y}_2^0[2] & \hat{\mathbf{V}}^0[2]\mathbf{Y}_3^0[2] & \hat{\mathbf{V}}^0[2]\mathbf{Y}_4^0[2] \\ \hat{\mathbf{V}}^0[3]\mathbf{Y}_1^0[3] & \hat{\mathbf{V}}^0[3]\mathbf{Y}_2^0[3] & \hat{\mathbf{V}}^0[3]\mathbf{Y}_3^0[3] & \hat{\mathbf{V}}^0[3]\mathbf{Y}_4^0[3] \\ \hat{\mathbf{V}}^0[4]\mathbf{Y}_1^0[4] & \hat{\mathbf{V}}^0[4]\mathbf{Y}_2^0[4] & \hat{\mathbf{V}}^0[4]\mathbf{Y}_3^0[4] & \hat{\mathbf{V}}^0[4]\mathbf{Y}_4^0[4] \\ \hat{\mathbf{V}}^0[5]\mathbf{Y}_1^0[5] & \hat{\mathbf{V}}^0[5]\mathbf{Y}_2^0[5] & \hat{\mathbf{V}}^0[5]\mathbf{Y}_3^0[5] & \hat{\mathbf{V}}^0[5]\mathbf{Y}_4^0[5] \end{bmatrix}. \end{aligned} \tag{4.17}$$

Based on (4.13), the correlation matrices $\mathbf{R}_{rr}$ and $\mathbf{R}_{ee}$ may be recursively estimated for the n^{th} length - N_{wind} signal block in the same way as in [119, (28-29)] without any knowledge of the CSI as follows

$$\mathbf{R}_{rr}[n] = \beta \mathbf{R}_{rr}[n-1] + (1-\beta)\underline{\mathbf{Y}}^{l\,H}[n]\underline{\mathbf{Y}}^l[n], \tag{4.18}$$

$$\mathbf{R}_{ee}[n] = \mu \mathbf{R}_{ee}[n-1] + (1-\mu)\underline{\mathbf{E}}_g^{l\,H}[n]\underline{\mathbf{E}}_g^l[n], \tag{4.19}$$

where $0 < \beta, \mu < 1$ are the forgetting factors.

Based on (4.18) and (4.19), the adaptive modified Newton algorithm is derived in [119]. For

convenience, we summarize the major steps as follows [119]

$$\begin{aligned}
\mathbf{P}[n] &= \frac{1}{\mu}\mathbf{P}[n-1]\left(\mathbf{I}_{N_R} - \frac{\underline{\mathbf{E}}_g^{l\,H}[n]\underline{\mathbf{E}}_g^{l}[n]\mathbf{P}[n-1]}{\mathrm{tr}\left(\mu\mathbf{I} + \underline{\mathbf{E}}_g^{l}[n]\mathbf{P}[n-1]\underline{\mathbf{E}}_g^{l\,H}[n]\right)}\right), \\
\mathbf{c}[n] &= \underline{\mathbf{Y}}^{l}[n]\boldsymbol{f}_g[n-1], \\
\mathbf{r}[n] &= \beta\mathbf{r}[n-1] + (1-\beta)\underline{\mathbf{Y}}^{l\,H}[n]\mathbf{c}[n], \\
d[n] &= \beta d[n-1] + (1-\beta)\mathbf{c}^H[n]\mathbf{c}[n], \\
\tilde{\boldsymbol{f}}_g[n] &= \frac{\mathbf{r}[n]}{d[n]}, \\
\boldsymbol{f}_g[n] &= \frac{2\mathbf{P}[n]\tilde{\boldsymbol{f}}_g[n]}{1+\tilde{\boldsymbol{f}}_g^H[n]\mathbf{P}[n]\tilde{\boldsymbol{f}}_g[n]},
\end{aligned} \tag{4.20}$$

where the initialization of the relevant parameters is implemented as: set $\mathbf{P}[0] = \mu_1\mathbf{I}_{N_R}$, $\boldsymbol{f}_g[0] = \mathbf{r}[0] = \mu_2[1,1,\cdots,1]^T$ and $d[0] = \mu_3$, where $\mu_i (i = 1,2,3)$ are appropriate positive values. The appropriate adaptive filter coefficient vector $\boldsymbol{f}_g[n]$ associated with the desired component of the n^{th} received signal block matrix can be acquired by recursively implementing the procedure of (4.20). Consequently, the suppression of the interference-plus-noise component dispensing with CSI becomes possible.

4.2.3 Relay-Aided SISO-MSDSD

As stated in Section 2.5, the SISO-MSDSD algorithm advocated by Pauli *et al.* in [55] is appropriate for the noncoherent detection based iterative decoding scheme in a direct transmission scenario. However, the application of the SISO-MSDSD algorithm of Section 2.5 in multiple access systems had not been considered in [55]. The further development of the SISO-MSDSD algorithm for simultaneously detecting multiple input signal streams was outlined in [80, 99], where the multiple input signal streams were expected to belong to the same modulated symbol alphabet. This condition is indeed usually satisfied in the specific family of cooperative networks, where the same channel coding and modulation schemes are adopted both at the SN and at the RNs. Hence a modified SISO-MSDSD algorithm, namely the relay-aided SISO-MSDSD of Section 3.3.3.2, had to be conceived for our cooperative network.

The proposed relay-aided SISO-MSDSD algorithm evaluates the *a posteriori* log-likelihood ratios (LLR) of the η^{th} bit $u[\eta]$ conditioned on U received signal streams represented by $\{\mathbf{y}_u\}_{u=1,2,\cdots,U}$ as follows

$$L\left(u[\eta]\right) = \ln\frac{\Pr\left(u[\eta]=b|\{\mathbf{y}_u\}_{u=1,2,\ldots,U}\right)}{\Pr\left(u[\eta]=\bar{b}|\{\mathbf{y}_u\}_{u=1,2,\ldots,U}\right)}, \quad b\in\{0,1\}, \tag{4.21}$$

where $\bar{b}$ is the complement of the bit b.

The adaptive filter coefficient vector $\boldsymbol{f}_g[n]$ conditioned for extracting the differentially encoded symbols pertaining to the SN broadcast signals is specifically referred to as $\boldsymbol{f}_s[n]$. Correspondingly, $\boldsymbol{f}_g[n]$ adjusted for extracting the differentially encoded symbols pertaining to the RN's forwarded

signals is denoted by $\boldsymbol{f}_{r_i}[n]$. Assuming the validity of (4.6) and substituting (4.6) into (4.2), the two received signal blocks having the same block index n but two different frame indices of l and $(l+1)$ can be further formulated as

$$\begin{aligned}\underline{\mathbf{Y}}^{l}[n] &= \sqrt{G_{sd}}\sqrt{P_s}\underline{\mathbf{S}}^{l}[n]\underline{\mathbf{H}}^{l}_{sd}[n] + \underline{\mathbf{I}}^{l}[n] + \underline{\mathbf{W}}^{l}[n], \\ \underline{\mathbf{Y}}^{l+1}[n] &= \sqrt{G_{r_id}}\sqrt{P_{r_i}}\underline{\mathbf{S}}^{l}[n]\underline{\mathbf{H}}^{l+1}_{r_id}[n] + \underline{\mathbf{I}}^{l+1}[n] + \underline{\mathbf{W}}^{l+1}[n],\end{aligned} \tag{4.22}$$

where $\underline{\mathbf{I}}^{l}[n]$ or $\underline{\mathbf{I}}^{l+1}[n]$ represents the associated interference component.

After $\underline{\mathbf{Y}}^{l}[n]$ and $\underline{\mathbf{Y}}^{l+1}[n]$ are passed through the adaptive filter and multiplied by $\boldsymbol{f}_s[n]$ and $\boldsymbol{f}_{r_i}[n]$, respectively, the filter outputs are given by

$$\begin{aligned}\mathbf{y}^{l}_{s}[n] &= \underline{\mathbf{Y}}^{l}[n]\boldsymbol{f}_s[n] \\ \mathbf{y}^{l+1}_{r_i}[n] &= \underline{\mathbf{Y}}^{l+1}[n]\boldsymbol{f}_{r_i}[n].\end{aligned} \tag{4.23}$$

Both $\mathbf{y}^{l}_{s}[n]$ and $\mathbf{y}^{l+1}_{r_i}[n]$ correspond to the differentially encoded symbol block $\underline{\mathbf{S}}^{l}[n]$. Hence we substitute them into (4.21) as $\{\mathbf{y}_u\}_{u=1,2}$, and (4.21) may be rewritten with the aid of Bayes' theorem as

$$\begin{aligned}L_u[\eta] &= \ln\frac{\Pr\left(u[\eta]=b|\mathbf{y}^{l}_{s}[n],\mathbf{y}^{l+1}_{r_i}[n]\right)}{\Pr\left(u[\eta]=\bar{b}|\mathbf{y}^{l}_{s}[n],\mathbf{y}^{l+1}_{r_i}[n]\right)} \\ &= \ln\frac{\sum_{\underline{\mathbf{V}}^{l}[n]\in\chi_{:u[\eta]=b}}\Pr\left(\mathbf{y}^{l}_{s}[n]|\underline{\mathbf{V}}^{l}[n]\right)\Pr\left(\mathbf{y}^{l+1}_{r_i}[n]|\underline{\mathbf{V}}^{l}[n]\right)\Pr(\underline{\mathbf{V}}^{l}[n])}{\sum_{\underline{\mathbf{V}}^{l}[n]\in\chi_{:u[\eta]=\bar{b}}}\Pr\left(\mathbf{y}^{l}_{s}[n]|\underline{\mathbf{V}}^{l}[n]\right)\Pr\left(\mathbf{y}^{l+1}_{r_i}[n]|\underline{\mathbf{V}}^{l}[n]\right)\Pr(\underline{\mathbf{V}}^{l}[n])},\end{aligned} \tag{4.24}$$

where $\chi_{:u[\eta]=b}$ denotes the set of $\frac{M_c^{(N_{wind}-1)}}{2}$ legitimate transmitted symbol blocks $\underline{\mathbf{V}}^{l}[n]$, whose η^{th} bit is constrained to $u[\eta]=b$. Similarly, $\chi_{:u[\eta]=\bar{b}}$ is defined as the set corresponding to $u[\eta]=\bar{b}$. Explicitly, this division of the entire set of $\underline{\mathbf{V}}^{l}[n]$ is similar to that portrayed in (3.76) of Section 3.3.3.

The optimum hypothesis of $\underline{\mathbf{V}}^{l}[n]$ can be attained by the ML detector and the corresponding performance is approached by the sphere detection algorithm, which significantly reduces the detection complexity and completes the calculation of $L\left(u[\eta]\right)$ in (4.24). In more detail, the evaluation of $L\left(u[\eta]\right)$ in (4.24) can be realized according to the process introduced in Section 3.3.3.2.

4.3 Transceiver Design and Analysis

An appropriate practical transceiver is required now to implement the state-of-the-art techniques introduced in Section 4.2, which efficiently organizes the collaboration amongst all functional blocks.

4.3.1 Architecture Design and Analysis

We specifically design a transceiver for the proposed DF aided SRAN, whose architecture is portrayed at Figure 4.3. In order to significantly enhance the error correction capability of the decoder,

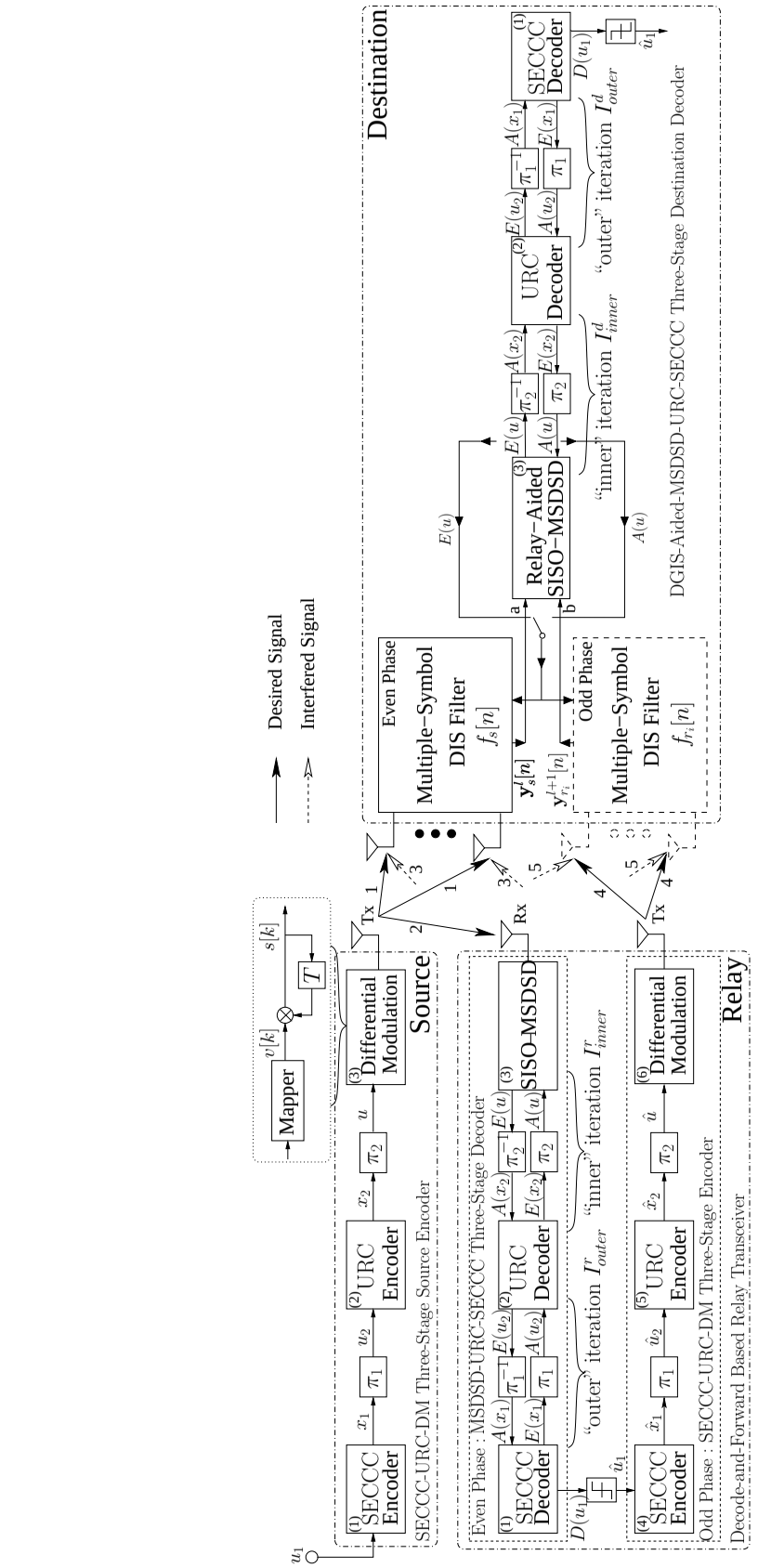

Figure 4.3: The architecture of our proposed MS-DIS plus MSDSD assisted SECCC aided three-stage turbo transceiver.

channel coding is invoked as an essential part of contemporary communication systems. The classic convolutional code (CC) and recursive systematic convolutional (RSC) code constitute some of the most frequently employed schemes [55, 118]. Moreover, since it was demonstrated in [123] that self-concatenated convolutional codes (SECCC) [124] are capable of outperforming state-of-the-art benchmarks, a SECCC encoder is employed as the outer code at the SN. Then, the SECCC is combined with a DM, which is further amalgamated with a unity-rate-code (URC) in order to create a two-stage inner code. Consequently, a three-stage SECCC-URC-DM source encoder was conceived.

Since it is unrealistic to expect that in addition to relaying, the RN could also estimate the channel SR_i, employing noncoherent detection dispensing with channel estimation at the RN seems to be more practical. Then the transmissions spanning the SR_i link are similar to direct transmissions. Hence the single-path SISO-MSDSD scheme of [55], which was also introduced in Section 2.5 may be adopted as the first component decoder of the RN's receiver. Then the SISO-MSDSD soft decoder is further amalgamated with the URC decoder to create a two-stage MSDSD-URC inner decoder. In line with the SN's transmitter, the SECCC decoder is employed as the outer decoder of the RN's receiver. Consequently, a three-stage concatenated iterative decoder is used as the RN's receiver, as seen in the "Relay" block of Figure 4.3. Our motivation with the employment of this three-stage - rather than classic two-stage - concatenated architecture is to improve the attainable convergence behaviour of the iterative decoder with the aid of the URC decoder, as first proposed in [125] and detailed in [126]. Since the URC model has an infinite impulse response (IIR) as a benefit of its recursive encoder structure, it is capable of meritoriously reshaping the EXIT curve of the two-stage MSDSD-URC inner decoder to approach the point of perfect convergence at $(1, 1)$ in the EXIT chart, which implies that an infinitesimally low error probability is attained. This characteristic of the URC model is also introduced in Section 3.3.3.1. Consequently, a potentially critical impediment of the DF protocol - namely its error propagation - may be avoided and (4.6) is satisfied. The transmitter of the RN may be designed to obey exactly the same architecture as that of the SN. Furthermore, the notations $E(\cdot)$ and $A(\cdot)$ denote the *extrinsic* information and *a priori* information, respectively, which are iteratively interleaved and exchanged I^r_{inner} times within the MSDSD-URC inner code and then passed on to the SECCC outer code. The resultant signal will be further iteratively interleaved and exchanged I^r_{outer} times between the MSDSD-URC inner code and the SECCC outer code. Apparently, the proposed transceiver structure for the SN and RN is quite similar to that depicted in Figure 3.20. The difference is that in this section we replace the RSC code of Figure 3.20 by the SECCC code of Figure 4.3.

At the DN, we have to consider the interference problem as introduced in Section 4.2. Then, we always obtain two replicas of the same SN's codeword, as analysed in Section 4.2.3. Hence, in contrast to the RN's receiver, the MS-DIS filter is employed at the DN to carry out adaptive interference suppression. Meanwhile, instead of using a single-path SISO-MSDSD decoder, the more sophisticated Relay-Aided SISO-MSDSD decoder introduced in Section 3.3.3 is employed at

the DN to carry out the joint detection of the two input signal streams corresponding to the same codeword. To elaborate a little further, we observe the "Destination" block in Figure 4.3, while still focusing on the detection of the information pertaining to the SN's broadcast signals during the even-indexed transmission phase (transmission-1 of Figure 4.3). Then the even-phase MS-DIS filter should aim for suppressing the interference imposed by the RN's forwarded signal component (labelled by transmission-3 in Figure 4.3). This is realized by adaptively updating the filter coefficient vector $\boldsymbol{f}_s[n]$ of (4.23) according to the adaptive modified Newton algorithm detailed in (4.20) of Section 4.2.2. Consequently, one of the expected filter outputs $\mathbf{y}_s^l[n]$ of (4.23) is generated. This even-phase MS-DIS filter should be activated during the even-phase. Then, another replica of the differentially encoded symbol block $\underline{\mathbf{S}}^l[n]$ of (4.7) pertains to the RN's forwarded signal block having the block index n and frame index $(l+1)$ (transmission-4 of Figure 4.3). Hence, the odd-phase MS-DIS filter will be activated in the consecutive odd-phase to generate $\mathbf{y}_{r_i}^{l+1}[n]$ of (4.23) by updating the filter coefficient vector $\boldsymbol{f}_{r_i}[n]$. In order to improve the readability, we would like to point out that actually, only one antenna array and one MS-DIS filter are activated at the beginning of the DN's action. The dual antenna arrays seen in Figure 4.3 and a pair of MS-DIS filters are used for emphasizing the distinctive nature of the even and odd phases. Hence the antenna array and the MS-DIS filter corresponding to the odd phase are represented by dashed lines. Then, we concatenate the MS-DIS filter with the Relay-Aided SISO-MSDSD decoder and substitute $\mathbf{y}_s^l[n]$ and $\mathbf{y}_{r_i}^{l+1}[n]$ into (4.21) as $\{\mathbf{y}_u\}_{u=1,2}$. As seen in Figure 4.3, both the soft output of the Relay-Aided SISO-MSDSD decoder at the DN and that of the SISO-MSDSD decoder at the RN correspond to the same coded bit stream "u". Hence the remaining architectural features of our DN's receiver seen in Figure 4.3 are arranged in the same way according to the corresponding part of the RN's receiver.

4.3.2 Turbo Equalization Based Decoding Regime

The turbo equalization philosophy originally proposed in [127] and detailed in [128] combines the equalization technique with the iterative detection process, where the equalization process is activated during each and every iteration of the turbo receiver. As a benefit of the gradually increased reliability of the feedback decisions, the performance of the equalizer may be significantly improved upon increasing the number of iterations. According to the turbo equalization principle, the MS-DIS filter will process the same received signal frame again with the aid of the most recent feedback decisions in each and every inner iteration of the two-stage MSDSD-URC inner code. As proposed in [118], the soft-symbol-decision-directed feedback philosophy is adopted and the coefficient vector $\boldsymbol{f}_g[n]$ is updated on a block-by-block basis to reduce the complexity imposed. For the sake of training the adaptive equalizer, a training sequence constituted by legitimate differentially encoded symbols known by the DN is periodically transmitted by the SN according to a certain training overhead. Hence, in the training mode, the MS-DIS filter exploits the knowledge of the training symbols to adapt its coefficient vector. Naturally, we may argue that these training symbols

can also be utilized for estimating the CSI and consequently coherent detection becomes feasible. Nevertheless, it will be demonstrated in Section 4.5 that the training overhead required by our proposed system is low, which would fail to facilitate the Nyquist-sampling based channel estimation of the channels considered at realistic Doppler frequencies. Then, in the decision-directed mode of the MS-DIS filter, both the *extrinsic* information provided by the relay-aided MSDSD decoder and the *a priori* information provided by the URC decoder may be utilized as the soft decision feedback for updating the coefficient vector. Hence, a supplemental information quantity comparison between the *extrinsic* information and the *a priori* information is needed, so that the higher of the two may be exploited.

In more detail, during the first inner iteration, i.e for $I^d_{\text{inner}} = 1, I^d_{\text{outer}} = 1$, the MS-DIS filter first invokes the current coefficient vector for suppressing the interference and then updates its coefficient vector based on the current feedback decisions. This implies that the coefficient vector generated during the n^{th} block is actually utilized during the $(n+1)^{th}$ block. Furthermore, in this iteration, the switch shown in Figure 4.3 should be set to point "a", since the *a priori* information provided by the URC decoder equals to zero.

During the consecutive iterations, the MS-DIS filter will first update its coefficient vector based on the feedback decisions generated during the most recent iteration and then utilizes the updated coefficient vector to suppress the interference. This implies that the coefficient vector updated in the n^{th} block is immediately exploited within the same block. Then, the switch will oscillate between the points "a" and "b".

Example 4.2: Signal processing of the MS-DIS plus MSDSD assisted three-stage turbo transceiver of Figure 4.3, where the turbo equalization philosophy of Section 4.3.2 is adopted.

Here, let us focus our attention on detecting the differentially encoded symbol block $\underline{\mathbf{S}}^l[n]$. According to the partitioning of the received signal block matrix $\underline{\mathbf{Y}}^l[n]$, which was formulated in (4.7), the transmission via the SD link in the n^{th} observation window of the l^{th} frame contributes the desired signal component, which can be extracted by using the adaptive filter coefficient vector $\boldsymbol{f}_s[n]$. As stated in Section 4.2.3, $\underline{\mathbf{S}}^l[n]$ is also carried by the signal block matrix $\underline{\mathbf{Y}}^{l+1}[n]$ received at the DN, as formulated in (4.22). The transmission via the RD link in the n^{th} observation window of the $(l+1)^{st}$ frame contributes the desired signal component, which can be extracted by using another adaptive filter coefficient vector $\boldsymbol{f}_{r_i}[n]$.

Consequently, the operations implemented during the first iteration of the turbo equalization based MS-DIS plus MSDSD assisted three-stage turbo transceiver are detailed as follows[1]:

Step-①: We directly employ the adaptive filter coefficient vector of the preceding observation window, namely $\boldsymbol{f}_s[n-1]$ for filtering the received signal block matrix $\underline{\mathbf{Y}}^l[n]$. Similar to (4.23), the associated output of the "Even Phase Multiple-Symbol DIS filter" as illustrated

[1]We focus our attention on the decision-directed mode of the MS-DIS filter.

at the right hand side of Figure 4.3 is given by

$$\hat{\mathbf{y}}_s^l[n] = \underline{\mathbf{Y}}^l[n]\boldsymbol{f}_s[n-1]. \tag{4.25}$$

Similarly, we can obtain the output of the "Odd Phase Multiple-Symbol DIS filter", namely $\hat{\mathbf{y}}_{r_i}^{l+1}[n]$[2].

Step-②: We substitute $\hat{\mathbf{y}}_s^l[n]$ and $\hat{\mathbf{y}}_{r_i}^{l+1}[n]$ into (4.24). Consequently, the relay-aided SISO-MSDSD algorithm introduced in Section 3.3.3.2 is executed. Based on the *extrinsic* information $E\{u\}$ provided by the relay-aided SISO-MSDSD decoder, as shown at the right hand side of Figure 4.3, we obtain the estimate of the associated information symbol block, i.e. $\underline{\hat{\mathbf{V}}}_g^l[n]$, which is involved in (4.13)[3]. We represent this operation by its pseudo code, namely by "$\underline{\hat{\mathbf{V}}}_g^l[n] = \text{Generate\_}\underline{\hat{\mathbf{V}}}_g^l\Big(E\{u\}\Big)$".

Step-③: Upon substituting $\underline{\hat{\mathbf{V}}}_g^l[n]$ obtained during Step-② into (4.13), we obtain the multiple-symbol-based error signal block matrix $\underline{\mathbf{E}}_g^l[n]$. We represent this operation by the following pseudo code "$\underline{\mathbf{E}}_g^l[n] = \text{Calculate\_}\underline{\mathbf{E}}_g^l\left(\underline{\mathbf{Y}}^l[n], \underline{\mathbf{Y}}^l[\overleftarrow{n}^{(1)}], \underline{\hat{\mathbf{V}}}_g^l[n]\right)$".

Step-④: We substitute $\underline{\mathbf{E}}_g^l[n]$ obtained during Step-③ and the parameters associated with the preceding observation window, which includes $\boldsymbol{f}_s[n-1], \mathbf{P}[n-1], \mathbf{r}[n-1], d[n-1]$, as well as $\underline{\mathbf{Y}}^l[n]$, which is associated with the current observation window into (4.20). After implementing the adaptive modified Newton algorithm formulated in (4.20), we obtain the updated adaptive filter coefficient vector $\boldsymbol{f}_s[n]$. We represent this operation by the pseudo code of "$\boldsymbol{f}_s[n] = \text{Update\_}\boldsymbol{f}_s\Big(\underline{\mathbf{E}}_g^l[n], \boldsymbol{f}_s[n-1], \mathbf{P}[n-1], \mathbf{r}[n-1], d[n-1], \underline{\mathbf{Y}}^l[n]\Big)$".

Step-⑤: We move forward to the next observation window, i.e. $n = n+1$. Correspondingly, the MS-DIS filter update process as well as the relay-aided SISO-MSDSD detection process implemented during Step-① to Step-④ are repeated again.

The above-mentioned MS-DIS filter's periodic update process as well as the relay-aided SISO-MSDSD decoding process implemented in the first iteration of the three-stage turbo transceiver of Figure 4.3 is also illustrated in Figure 4.4.

As illustrated in Figure 4.4, once all the observation windows have been processed, the three-stage turbo transceiver of Figure 4.3 will launch its next decoding iteration. Accordingly, I_{outer}^d in Figure 4.3 will be increased from $I_{\text{outer}}^d = 1$ to $I_{\text{outer}}^d = 2$. As stated early in this section, when we have $I_{\text{outer}}^d \geq 2$, the MS-DIS filter's periodic update process is slightly different from that involved during the first iteration, where we firstly update the MS-DIS filter's coefficient vector and then invoke it for suppressing the interference. Loosely speaking, this might be interpreted as changing the flowchart order shown in Figure 4.4 to "Step-③ → Step-④ → Step-⑤ → Step-① → Step-②".

[2]In fact, the processes of updating the coefficient vector $\boldsymbol{f}_{r_i}[n]$ and of generating $\hat{\mathbf{y}}_{r_i}^{l+1}[n]$ obey the same mechanism as that of $\boldsymbol{f}_s[n]$ and of $\hat{\mathbf{y}}_s^l[n]$. Hence, in our ensuing discourse, we only exemplify the update of $\boldsymbol{f}_s[n]$ and assume that the update of $\boldsymbol{f}_{r_i}[n]$ and the generation of $\hat{\mathbf{y}}_{r_i}^{l+1}[n]$ have been appropriately completed.

[3]The soft-symbol-decision-direct (SSDD) regime proposed in [118] is employed for generating $\underline{\hat{\mathbf{V}}}_g^l[n]$.

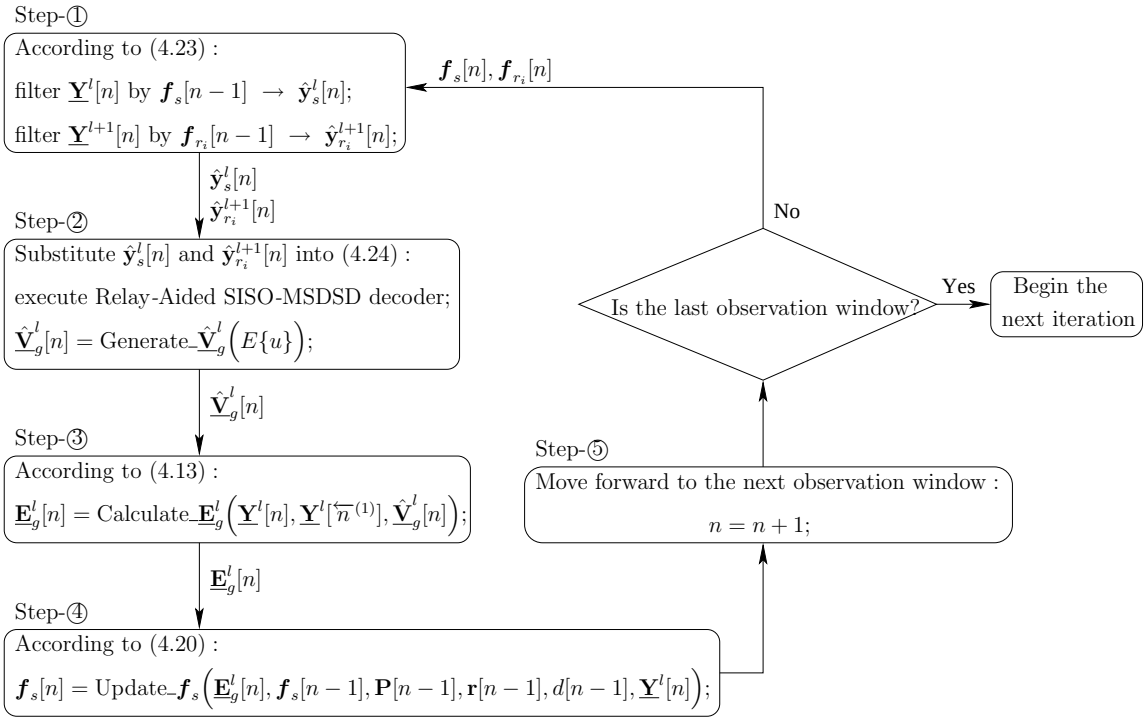

Figure 4.4: Flowchart of the MS-DIS filter's periodic update process implemented during the first iteration of the three-stage turbo transceiver of Figure 4.3, where the relay-aided SISO-MSDSD decoding is simultaneously completed within Step-②.

4.4 NC DCMC Capacity of the Multiple-Antenna Aided DF Based SRAN

In this contribution, we conceive an interference suppression aided DF based SRAN, where a MS-DSD based noncoherent detection scheme is employed. Hence the noncoherent DCMC capacity of the DF based SRAN can be utilized as a benchmark to assess the performance of the transceiver portrayed in Figure 4.3. However, in contrast to the capacity derivation process provided in Section 3.3.2, we encounter a different scenario in this section, where the impact of the interferences may be ignored, which is an explicit benefit of employing the MS-DIS filter and that of removing the interfering users' signal. Another difference is that instead of a single antenna, multiple antennas are employed by the DN's receiver, which may significantly improve the capacity of the SD and RD links. Hence we cannot directly utilize the results acquired in Section 3.3.2. Accordingly, we would like to derive the NC DCMC capacity again in the context of the system structure illustrated in Figure 4.3. Furthermore, the capacity derivation process of this section hinges on the assumptions related to the DN's receiver employed in Section 4.5.

The decomposition of the SRAN illustrated in Figure 3.12 remains valid for the new context of this chapter. In more detail, the transmissions represented by the solid lines in the "(a) Even Phase"

and "(b) Odd Phase" (labelled by "1", "2", "4") of Figure 4.1 constitute a conventional single-relay aided two-phase cooperative network, namely Coop-I. Similarly, the transmissions represented by the dashed lines in the "(b) Odd Phase" and "(c) Even Phase" of Figure 4.1 constitute another one, namely Coop-II. According to the decomposition philosophy introduced in Section 3.2.2 or in Section 3.3.2, we can readily derive the upper and lower bounds on the noncoherent DCMC capacity of our SRAN illustrated in Figure 4.3 as

$$\left\{C_{\text{Coop-I}}^{\text{DF-Upper}} + C_{\text{Coop-II}}^{\text{DF-Upper}}\right\} \geq C_{\text{Successive}}^{\text{DF}} \geq \left\{C_{\text{Coop-I}}^{\text{DF-Lower}} + C_{\text{Coop-II}}^{\text{DF-Lower}}\right\}, \tag{4.26}$$

where the notations $C_{\text{Coop-I}}^{\text{DF-Upper}}$ and $C_{\text{Coop-I}}^{\text{DF-Lower}}$ represent the upper and lower bounds on the noncoherent DCMC capacity of the sub-network "Coop-I", respectively. The capacities $C_{\text{Coop-II}}^{\text{DF-Upper}}$ and $C_{\text{Coop-II}}^{\text{DF-Lower}}$ are defined in a similar way.

Firstly, we concentrate on the sub-network Coop-I. Based on the analysis provided in [24] and on the fact that the SN remains silent during the cooperative phase, we can obtain the upper and lower bounds for the sub-network Coop-I as

$$C_{\text{Coop-I}}^{\text{DF-Upper}} = \min\left\{\frac{\theta_1}{T_b} I\left(\underline{\mathbf{S}}^l[n]; \underline{\mathbf{Y}}^l[n], \underline{\mathbf{Z}}_{r_0}^l[n]\right), \frac{\theta_1}{T_b} I\left(\underline{\mathbf{S}}^l[n]; \underline{\mathbf{Y}}^l[n]\right) + \frac{\theta_2}{T_b} I\left(\underline{\mathbf{C}}_{r_0}^{l+1}[n]; \underline{\mathbf{Y}}^{l+1}[n]\right)\right\}, \tag{4.27}$$

$$C_{\text{Coop-I}}^{\text{DF-Lower}} = \min\left\{\frac{\theta_1}{T_b} I\left(\underline{\mathbf{S}}^l[n]; \underline{\mathbf{Z}}_{r_0}^l[n]\right), \frac{\theta_1}{T_b} I\left(\underline{\mathbf{S}}^l[n]; \underline{\mathbf{Y}}^l[n]\right) + \frac{\theta_2}{T_b} I\left(\underline{\mathbf{C}}_{r_0}^{l+1}[n]; \underline{\mathbf{Y}}^{l+1}[n]\right)\right\}, \tag{4.28}$$

where $\underline{\mathbf{Z}}_{r_0}^l[n]$ represents the n^{th} signal block received at the RN r_0 during the l^{th} frame, which consists of N_{wind} consecutively received signals of the RN. Moreover, $\underline{\mathbf{Y}}^l[n]$ and $\underline{\mathbf{Y}}^{l+1}[n]$ are defined in (4.22), and $\underline{\mathbf{C}}_{r_0}^{l+1}[n]$ is defined in (4.2), where θ_1 and θ_2 are introduced to represent the relative lengths of the broadcast duration and the cooperative duration of sub-network Coop-I, respectively, when their sum is normalized to unity. In contrast to the single antenna aided conventional three-stage receiver of the RN, the DN's receiver has multiple antennas and the novel architecture shown in Figure 4.3, which now becomes our focus. In order to concentrate on the DN's characteristics, we stipulate the idealized simplifying assumption that the relays always achieve perfect detection[4], which implies that

$$\theta_1 I\left(\underline{\mathbf{S}}^l[n]; \underline{\mathbf{Z}}_{r_0}^l[n]\right) \geq \theta_1 I\left(\underline{\mathbf{S}}^l[n]; \underline{\mathbf{Y}}^l[n]\right) + \theta_2 I\left(\underline{\mathbf{C}}_{r_0}^{l+1}[n]; \underline{\mathbf{Y}}^{l+1}[n]\right). \tag{4.29}$$

According to (4.6), and substituting (4.29) into (4.27), (4.28), we arrive at

$$C_{\text{Coop-I}}^{\text{DF-Upper}} = C_{\text{Coop-I}}^{\text{DF-Lower}} = \frac{\theta_1}{T_b} I\left(\underline{\mathbf{S}}^l[n]; \underline{\mathbf{Y}}^l[n]\right) + \frac{\theta_2}{T_b} I\left(\underline{\mathbf{S}}^l[n]; \underline{\mathbf{Y}}^{l+1}[n]\right), \tag{4.30}$$

which implies that, owing to the assumption formulated in (4.29), the upper and lower bounds on the capacity of the sub-network Coop-I converge. According to the symmetry between the

[4]Such idealized assumption will be adopted in the forthcoming simulation part for the sake of concentrating on the DN's characteristics. Hence, in order to relate the capacity analysis here to our simulation results, we have to maintain consistency between the theoretical and simulation part of this chapter.

sub-networks Coop-I and Coop-II, it may be readily seen that the upper and lower bounds on the capacity of the sub-network Coop-II also converge. Hence, (4.26) eventually transforms to

$$C_{\text{Successive}}^{\text{DF}} = C_{\text{Coop-I}}^{\text{DF-Upper}} + C_{\text{Coop-II}}^{\text{DF-Upper}} = C_{\text{Coop-I}}^{\text{DF-Lower}} + C_{\text{Coop-II}}^{\text{DF-Lower}}. \tag{4.31}$$

Then, according to [113], the probability density function of $\underline{\mathbf{Y}}^l[n]$ conditioned on $\underline{\mathbf{S}}^l[n]$ is expressed as [5]

$$\Pr(\underline{\mathbf{Y}}|\underline{\mathbf{S}}) = \frac{\exp\left[-\text{tr}\left(\underline{\mathbf{Y}}^H \mathbf{\Psi}^{-1} \underline{\mathbf{Y}}\right)\right]}{\left[\pi^{T_b N_T} \det(\mathbf{\Psi})\right]^{N_R}}. \tag{4.32}$$

Based on the assumption that the interference components in (4.22) are perfectly eliminated with the aid of an adaptive interference cancellation technique, such as our MS-DIS, the conditional covariance matrix $\mathbf{\Psi}$ may be calculated as

$$\begin{aligned} \mathbf{\Psi} &= \mathcal{E}\left\{\underline{\mathbf{Y}}\underline{\mathbf{Y}}^H|\underline{\mathbf{S}}\right\} \\ &= P_s G_{sd} \underline{\mathbf{S}} \mathcal{E}\left\{\underline{\mathbf{H}}_{sd} \underline{\mathbf{H}}_{sd}{}^H\right\} \underline{\mathbf{S}}^H + N_R N_0 \mathbf{I}_{N_{\text{wind}}}. \end{aligned} \tag{4.33}$$

Similar to the capacity derivation processes demonstrated in Section 3.2.2 and in Section 3.3.2 as well as in [24, 129], the first mutual information component on the right hand side of (4.30) can be attained with the aid of the following process

$$\begin{aligned} I(\underline{\mathbf{S}}; \underline{\mathbf{Y}}) &= H\left(\underline{\mathbf{Y}}\right) - H\left(\underline{\mathbf{Y}}|\underline{\mathbf{S}}\right); \\ H\left(\underline{\mathbf{Y}}|\underline{\mathbf{S}}\right) &= \log_2\left\{\mathrm{e}^{T_b} \cdot \left[\det\left(\pi\mathbf{\Psi}\right)\right]^{N_R}\right\}; \\ H\left(\underline{\mathbf{Y}}\right) &= -\mathcal{E}\left\{\log_2\left[\sum_{\underline{\mathbf{S}}' \in \chi} \frac{\exp\left[-\text{tr}\left(\underline{\mathbf{Y}}^H \mathbf{\Psi}^{-1} \underline{\mathbf{Y}}\right)\right]}{M_c^{T_b}\left[\det\left(\pi\mathbf{\Psi}\right)\right]^{N_R}}\right]\right\}. \end{aligned} \tag{4.34}$$

Similarly, the second mutual information component on the right hand side of (4.30) can be attained by implementing the above process, where the DN's received signal block $\underline{\mathbf{Y}}^{l+1}[n]$ is involved this time and $\mathbf{\Psi}$ has to be modified to

$$\mathbf{\Psi} = P_{r_0} G_{r_0 d} \underline{\mathbf{S}} \mathcal{E}\left\{\underline{\mathbf{H}}_{r_0 d} \underline{\mathbf{H}}_{r_0 d}{}^H\right\} \underline{\mathbf{S}}^H + N_R N_0 \mathbf{I}_{N_{\text{wind}}}. \tag{4.35}$$

According to (4.30), (4.34), (4.33) and (4.35), the noncoherent DCMC capacity bounds $C_{\text{coop-I}}^{\text{DF-Upper}}$ and $C_{\text{coop-I}}^{\text{DF-Lower}}$ of the sub-network Coop-I can now be derived. Then, we can simply attain $C_{\text{coop-II}}^{\text{DF-Upper}}$ and $C_{\text{coop-II}}^{\text{DF-Lower}}$ following a similar process. As a result, the noncoherent DCMC capacity $C_{\text{successive}}^{\text{DF}}$ of the DF based SRAN given by (4.31) becomes available. Assuming that we have $D_{sr_i} = \frac{1}{2}$ and $\theta_1 = \theta_2 = \frac{1}{2}$, as well as that $N_R = 4$ antennas are employed by the DN's receiver, the associated $C_{\text{successive}}^{\text{DF}}$ capacity is portrayed in Figure 4.5. In fact, the resultant capacity $C_{\text{successive}}^{\text{DF}}$ as evaluated from (4.31), (4.30), (4.34), (4.33) and (4.35) is equivalent to the cooperative phase capacity of the DF based SRAN, where the potential 50% capacity loss of the DF based SRAN imposed by the section of the broadcast phase is eliminated owing to the assumption that the relays always achieve perfect detection, as formulated in (4.29).

[5] In order to simplify the equations, the signal block index n and the frame index l were omitted from now on.

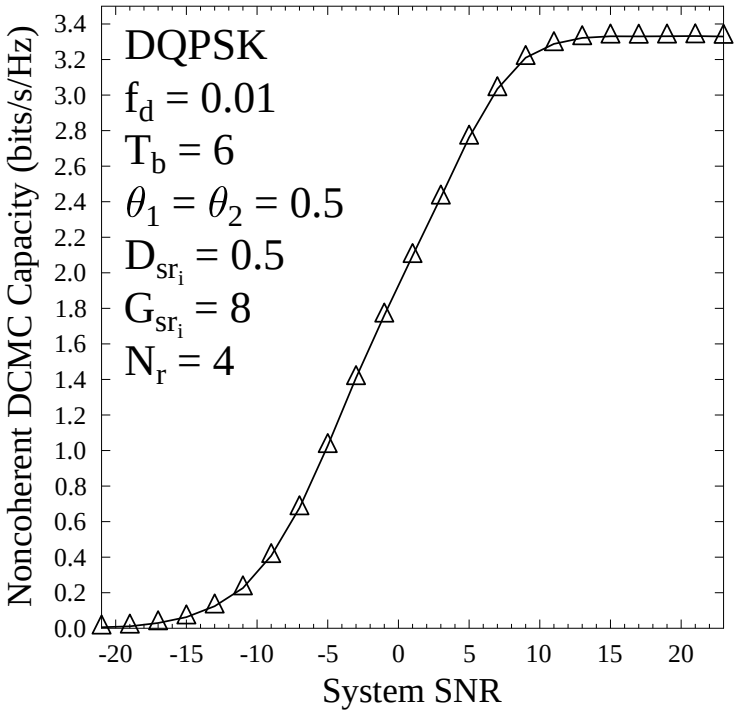

Figure 4.5: The capacity of the cooperative phase in the DF based SRAN, where the relative lengths of the broadcast duration and the cooperative duration are fixed to $\theta_1 = 0.5$ and $\theta_2 = 0.5$, respectively. The result is based on the schematic of Figure 4.3 and the system parameters of Table 4.1.

4.5 EXIT Chart Aided Simulation Results and Discussions

Let us now report on our experiments, including the EXIT chart analysis of the SECCC outer code, the effects of the forgetting factors (β, μ), as well as the error correction capability of both the RN's and the DN's receiver. The EXIT chart based analysis method is extensively employed during our experiments. The major system parameters adopted in our simulations are summarized in Table 4.1. Furthermore, the system parameters involved in some particular experiments will be specifically interpreted, if they happen to be different from the default values provided in Table 4.1.

4.5.1 EXIT Chart Analysis of SECCC

The EXIT curve of the SECCC outer code had been portrayed in [123], where the effects of diverse memory lengths ν and coding rates R_c were characterized. The impact of the puncturing rate p and of the number of inner iterations I_{SECCC} is characterized in Figure 4.6 as an extension of [123], where the EXIT curve of a classic RSC code having the same memory length and coding rate is provided as a benchmark.

Channel Model	Time-Selective Rayleigh Fading Channel
Path-Loss Exponent	$\alpha = 3$
Normalized Doppler Frequency	$f_d = 0.01$
Relay Position	$D_{sr_i} = \frac{1}{2}$; $G_{sr_i} = G_{r_i d} = 8$
Channel Coding	SECCC
Memory Length of SECCC	$\nu = 6$
Puncture Rate of SECCC	$p = 0.5$
Iteration Number of SECCC	$I_{\text{SECCC}} = 2$
Code Rate of SECCC	$R_c = 0.5$
Interleaver Length	$L = 144000$ bits
Modulation	DQPSK
MSDSD Observation Window Size	$N_{\text{wind}} = 6$
Inner Iterations of DN's Decoder	$I^d_{\text{inner}} = 2$
Outer Iterations of DN's Decoder	$I^d_{\text{outer}} = 9$
Overall Bandwidth efficiency	$\eta \approx R_c \cdot \log_2 M_c \cdot \frac{T_b - 1}{T_b}$ $= 0.833$ bits/s/Hz
Optimum Forgetting Factor	$\beta = 0.995; \mu = 0.30$
Training Overhead	2%
Initialization of MS-DIS Filter	$\mu_1 = 0.01; \mu_2 = \frac{1}{\sqrt{\|\boldsymbol{f}_g[n]\|^2_F}}; \mu_3 = 1$
Antenna Configuration	$N_T = 1$; $N_R = 4$

Table 4.1: SYSTEM PARAMETERS

Observe in Figure 4.6a that increasing the number of inner iterations between the two virtual component RSC decoders of the SECCC is capable of slightly improving the EXIT curve of the SECCC at the cost of imposing an increased complexity. Furthermore, it is shown in Figure 4.6b that the optimum puncturing rate of the puncturer in the SECCC may be $1/2$ rather than $1/3, 1/4$, since the former results in an improved EXIT performance. Based on these results we conclude that $I_{\text{SECCC}} = 2$ and $p = 1/2$ constitute a competitive choice.

4.5.2 Optimization of the Forgetting Factors

The specific choice of the forgetting factors (β, μ) invoked in Section 4.2.2 significantly influences the performance of the adaptive modified Newton algorithm, as mentioned in [119]. Hence finding the optimum forgetting factors associated with a specific scenario is required. It was shown in [130] and introduced again in Section 3.3.4.2 that the area under the bit-based EXIT curve of the inner code approximates the maximum achievable coding rate of the outer channel code, while guaranteeing near-error-free communication. Hence we can utilize the EXIT curves of the MS-DIS

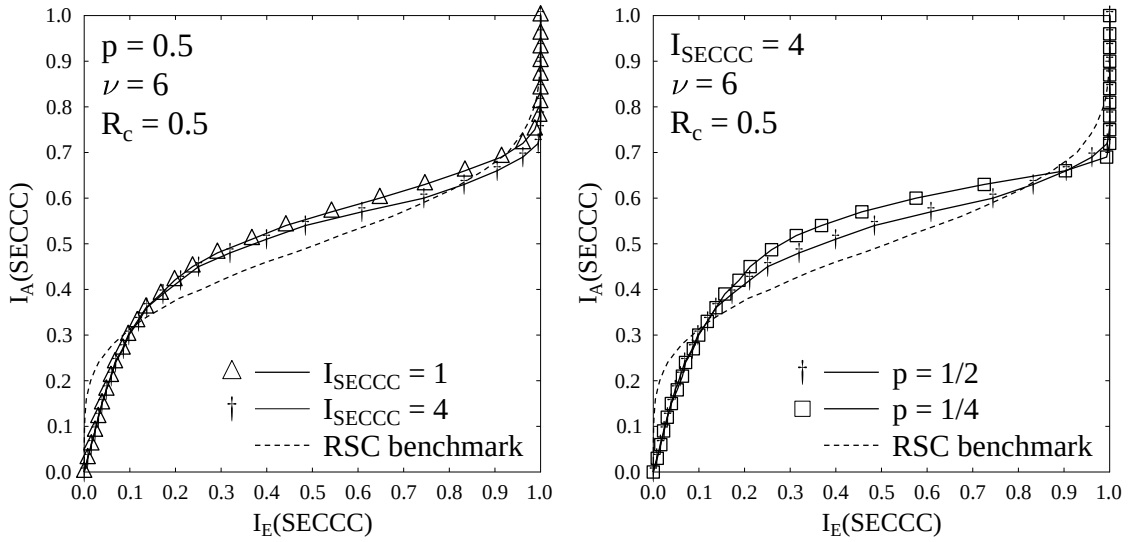

(a) Effects of the inner iterations

(b) Effects of the puncture rates

Figure 4.6: The EXIT characteristic of the SECCC outer code for different number of inner iterations and puncturing rates. The associated parameters are explicitly shown in these diagrams.

aided MSDSD-URC inner codes having different forgetting factor values for the optimization of the forgetting factors. According to the above analysis, the EXIT curve assisted optimization of the forgetting factors is supported by the relevant results shown in Figure 4.7, where the DN relied on $N_R = 4$ and a normalized Doppler frequency of $f_d = 0.01$ was assumed.

The forgetting factors involved in the MS-DIS filters of the even and odd phases are represented by (β_0, μ_0) and (β_1, μ_1), respectively. Due to the particular transmission regime of the SRAN, if a differentially encoded symbol block $\underline{\mathbf{S}}^l[n]$ is broadcast by the SN in the even phase, then it will be forwarded by the RN in the consecutive odd phase. This implies that the roles of the signal components received by the DN from the SN and RN are reversed in the consecutive even and odd phases in terms of the desired component and the interference-plus-noise component. Hence, according to the functions of the forgetting factors β and μ described by (4.18) and (4.19), it may be readily inferred that the values of (β_0, μ_0) and (β_1, μ_1) should also obey a reversed relationship, in order to realize a reasonable collaboration between the even-phase MS-DIS filter and odd-phase MS-DIS filter. This statement is verified by Figure 4.7a, where the EXIT curves corresponding to the forgetting factors satisfying $(\beta_1, \mu_1) = (\beta_0, \mu_0)$ are shifted further down compared to the forgetting factors obeying $(\beta_1, \mu_1) = (\mu_0, \beta_0)$.

After confirming the optimization rule that (β_1, μ_1) should be equal to (μ_0, β_0), a deeper search conceived for finding the optimum forgetting factors with respect to our specific scenario may be invoked and the relevant results are displayed in Figure 4.7b. Observe in Figure 4.7b that the area under the EXIT curve of the MS-DIS aided MSDSD-URC inner code was consistently increased upon reducing the associated value of μ_0. However, the improvement achieved by shifting the EXIT

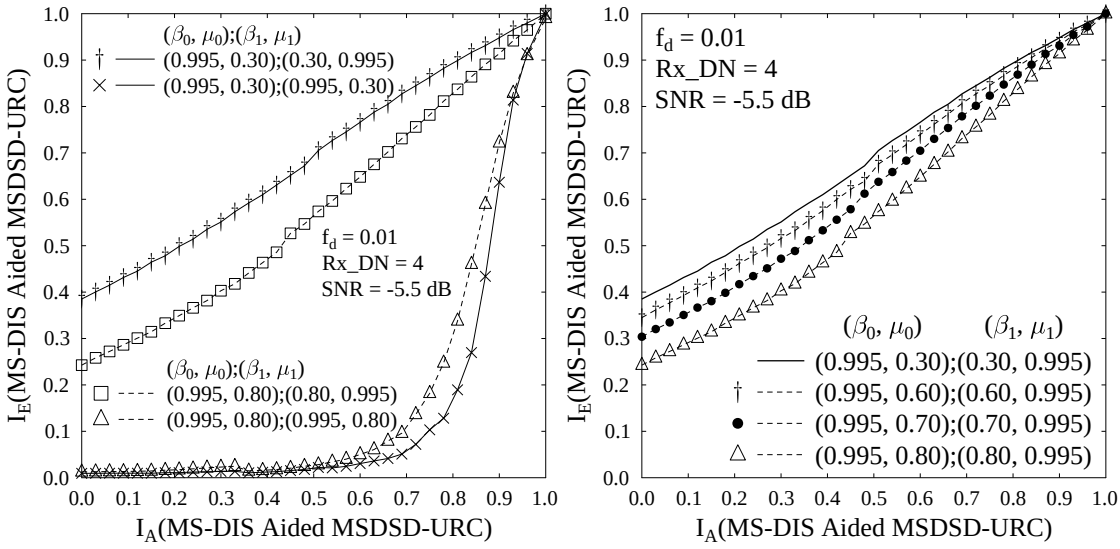

(a) Forgetting factor comparison-I (b) Forgetting factor comparison-II

Figure 4.7: EXIT-curve-assisted forgetting factor optimization. The results are based on the schematic of Figure 4.3 and the system parameters of Table 4.1.

curve upwards upon reducing the value of μ_0 became rather negligible for $\mu_0 < 0.30$. Based on our detailed investigations not included here[6], the forgetting factors $(\beta_0, \mu_0) = (0.995, 0.30)$ were deemed as the best choice and were hence employed for the actual MS-DIS filter in our specific scenario.

4.5.3 Error Correction Performance at the DN

Again, the BS (DN) is capable of supporting a more sophisticated, but higher-complexity architecture than the relays. Accordingly, the number of BS receiver antennas is fixed to $N_R = 4$ for enhancing its error correction capability with the aid of its increased spatial diversity gain. Then, in order to concentrate on the DN's characteristics, the idealized simplifying assumption invoked in Section 4.4, namely that the relays always achieve perfect detection is adopted again. Consequently, our capacity analysis and simulation results provided in Section 4.4 can be utilized here[7]. Based on this assumption, the EXIT chart and the BER vs SNR performance of the proposed BS receiver are portrayed in Figure 4.8 and Figure 4.9, respectively.

When appropriately configuring the SECCC code [123] and the forgetting factors, the Monte-Carlo simulation based EXIT-trajectory of the MS-DIS aided MSDSD-URC-SECCC BS receiver is capable of approaching the point of perfect convergence at $(1, 1)$ in Figure 4.8 after $I^d_{\text{outer}} = 9$ outer iterations, when the SNR is as low as -5.5dB. It is verified again in Figure 4.9 that our transceiver is capable of reliably operating at -5.5dB, where the BER is shown to rapidly drop

[6]The simulation results recorded for higher β_0 values result in improved EXIT characteristics are omitted from Figure 4.7b.

[7]This idealized simplifying assumption will be eliminated in the Section 4.5.4.

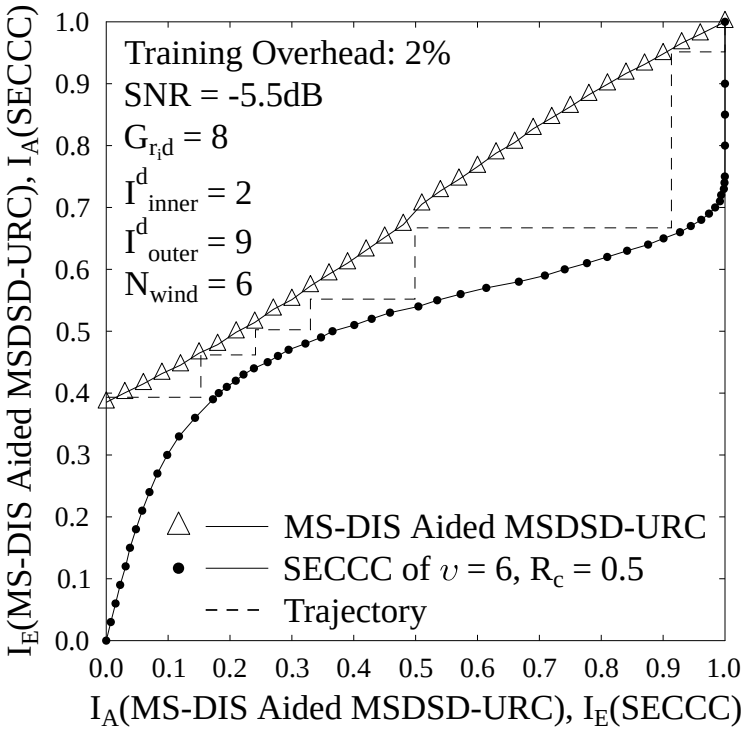

Figure 4.8: The EXIT characteristics of our proposed BS receiver. The results are based on the schematic of Figure 4.3 and the system parameters of Table 4.1.

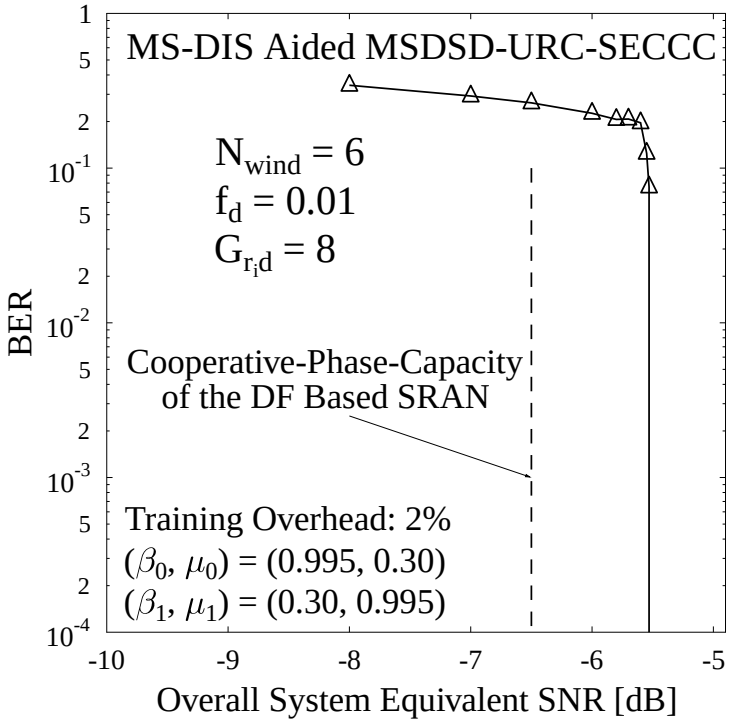

Figure 4.9: The BER vs SNR performance of the BS receiver, corresponding to Figure 4.8. The results are based on the schematic of Figure 4.3 and the system parameters of Table 4.1.

to an infinitesimally low value. Moreover, the corresponding capacity results of Figure 4.5 can be directly applied to Figure 4.9 as a benchmark, since the same system parameters are used. It is demonstrated in Figure 4.9 that the proposed BS receiver of Figure 4.3 attains a performance within about 1.0 dB of the DF based SRAN's capacity. A 2% training overhead is required for adapting the MS-DIS filter in the time-selective fading channel associated with a normalized Doppler frequency of $f_d = 0.01$.

4.5.4 Error Correction Performance at the RN

The idealized simplifying assumption made in Section 4.5.3, namely that the relay perfectly decodes the SN's transmitted signals is verified with the aid of Figure 4.10. Owing to the compact

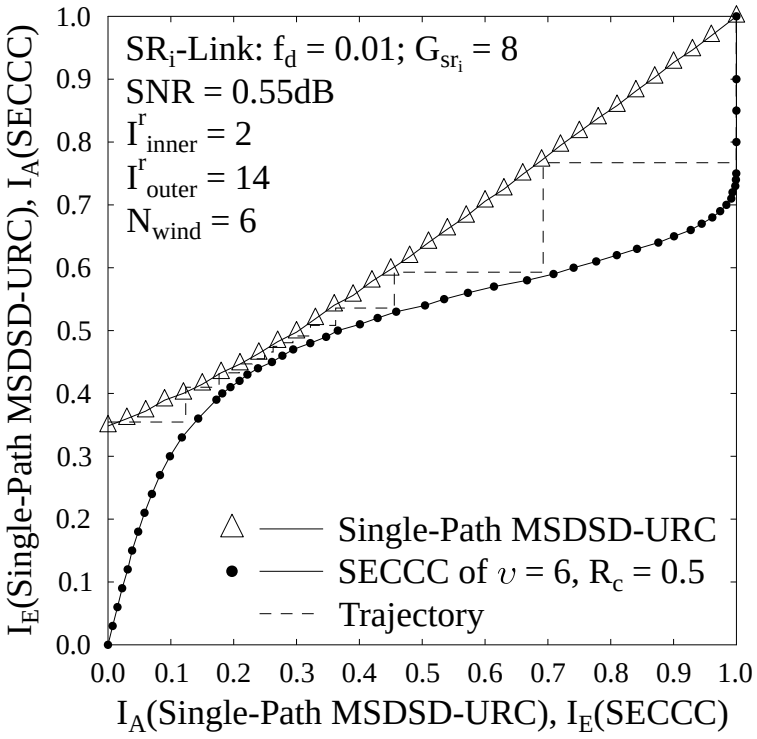

Figure 4.10: EXIT chart characteristics at the RN. The results are based on the schematic of Figure 4.3 and the system parameters of Table 4.1.

dimensions of the mobile, the number of relay receiver antennas is fixed to $N_r = 1$. Observe in Figure 4.10 that the SNR value has to be above 0.55dB in order to allow the decoding trajectory of the proposed single-path MSDSD-URC-SECCC relay decoder to approach the point of perfect convergence at $(1, 1)$ in the EXIT Chart, even when assuming that the RN does not incur any interference. This implies that the error correction capability of our BS receiver may be significantly impaired by the potential error propagation encountered at the RN. Hence the system operating in a realistic interference-infested scenario is unable to exhibit an infinitesimally low BER at SNRs below -5.5dB. However, the error correction capability of the RN receiver can be improved by in-

troducing the cooperative-user-selection scheme of [21], or by sophisticated power-allocation and code-rate-optimization schemes [81], which will be addressed in our future research.

4.6 Chapter Summary

A novel adaptive Newton algorithm based MS-DIS filter was incorporated in the SRAN for the sake of suppressing the successive relaying induced interference without requiring any extra orthogonal channel resource. The carefully designed MS-DIS aided MSDSD-URC-SECCC BS receiver exhibited a powerful error correction capability and a vanishingly low BER for SNR values above -5.5dB, while requiring as low as 2% training overhead. These contributions improved the practicality of our low-complexity noncoherent detection based SRAN.

However, as revealed in Section 4.5.4, the relay receiver's poor error correction capability will significantly erode the powerful error correction ability achieved at the DN's receiver owing to the error propagation problem. Hence the RN's receiver constrains the attainable BER performance of the whole system illustrated in Figure 4.3. A straightforward remedy might be to dedicate more system resources to the RN for the sake of striking a better balance between the achievable error correction capabilities of the RN and DN. Hence the employment of sophisticated power-allocation and code-rate-optimization schemes may be promising for our further research.

Recall that we simply ignored the impact of the IRI in Section 4.1. However, based on the specific design of our MS-DIS filter and on the design of the DN's receiver detailed in Sections 4.2 and 4.3, the IRI may also be suppressed by employing the proposed MS-DIS filter at the RN in a similar manner to the interference suppression process introduced in Section 4.3, albeit this requires multiple antennas at the RN. Hence, instead of mobile users, more complex fixed relay stations are required for acting as the RN in the system proposed in Figure 4.3. As a benefit of employing multiple-antennas at the RN, the limitation of the poor error correction capability of the RN reported in Section 4.5.4 may also be solved.

Chapter 5

Generalized Adaptive Network Coded Noncoherent Successive Relaying

In Chapter 4, we discussed the potential of suppressing the successive relaying induced interference, whilst dispensing with both the CSI and with any extra orthogonal channel resource. This ambitious goal was achieved with the aid of the proposed adaptive MS-DIS filter shown in Figure 4.3. Albeit in Section 4.3 we focussed our efforts on suppressing the CCI interference with the aid of the MS-DIS filter at the DN , we may readily anticipate that as a benefit of the general nature of the proposed MS-DIS regime, the IRI and MAI interference may also be mitigated by invoking the MS-DIS filter. However, employing the MS-DIS regime introduced in Section 4.2 for mitigating the interference incurred in the SRAN will lead to a fairly complex system architecture relying on sophisticated signal processing. Hence it may not be the best strategy to opt for the differential interference suppression aided SRAN [131] in the context of low-complexity noncoherent successive relaying. Hence let us return to the DS-CDMA multiple access assisted SRAN introduced in Chapter 3.

In this context the multi-user DS-CDMA uplink of Figure 3.9 is considered. However, in Figure 3.9 only two relay nodes were employed for improving the communication quality of the cell-edge users, whilst in recent years the research of cooperative networks has further evolved to multi-user, multi-relay scenarios, where beneficial relay-selection and power-allocation techniques as well as user-collaboration regimes were conceived. As reported in [17, 132–134], the performance of the entire network, especially its diversity-multiplexing trade-off (DMT) can be further improved by allowing more users and relays to join in the cooperation. Motivated by these trends, we will further extend our investigations to a multi-user multi-relay scenario. Hence, we propose efficient network coding solutions for efficiently organizing the multiple nodes of a large-scale wireless network.

The network coding concepts [135–137] were originally proposed for increasing the maximum

achievable throughput of a network by invoking simple coding schemes in the intermediate routers. Since the behaviour of the intermediate network coding relays is similar to the relay nodes in the DF aided cooperative network, cross-layer network coding techniques were applied to the physical-layer of cooperative schemes in [11,38,42,138–143] for the sake of reducing BER, while enhancing the energy efficiency and/or the bandwidth efficiency. More particularly, the network coding concepts were also extended to two-way relay systems [39,40,43,144,145], since the intermediate relay node of a two-way relaying system inherently relies on the network coding philosophy. Furthermore, the theoretical bound of the bit error probability of network coding was discussed in [146], whilst the delay optimization problem of a cross-layer network coding technique was analysed in [147].

However, as indicated in [41, 139, 148], the hostile nature and dynamically evolving topology of the wireless network may significantly erode the attainable performance gain of the network coding strategy. In order to combat this problem, the concept of "matching code-on-graph with network-on-graph" technique was proposed by Bao and Li in [41], where the network topology was transformed to a bipartite graph of low-density-parity-check (LDPC) codes, or LDPC-like codes. This transformation activates an LDPC code to serve as the cross-layer network code, and demonstrates remarkable flexibility in adapting to both network topology changes and to link failures. Similarly, based on [42, 142], Rebelatto *et al.* employed an attractive class of linear block codes as the cross-layer network code in [149], and transformed the problem of maximizing the cooperative diversity order to the design of a linear block code defined over the finite Galois Field GF(q). In a more practical approach, Hausl *et al.* [150] devised an energy-efficient joint network-channel coding (JNCC) scheme for network coded cooperation. Compared to the separate network and forward error correction (FEC) coding scheme employed in [149], a further coding gain can be achieved with the aid of JNCC. Similarly, Nguyen *et al.* also advocated the joint network-channel coding philosophy in [151, 152], where the family of more sophisticated irregular convolutional codes was employed as their channel coding scheme. Accordingly, a near capacity performance was achieved in [151, 152]. For the convenience of the reader, we summarize the above-mentioned history of network coding in Table 5.1.

However, all the practical systems proposed in [41, 42, 142, 149, 150] for implementing network coded cooperation incur a 50% half-duplex relaying-induced throughput loss, since a practical transceiver cannot transmit and receive simultaneously. This simply halves the bandwidth efficiency. Then, as emphasized in Sections 3.1 and 4.1, it is unrealistic to expect that in addition to the task of relaying, the relays could altruistically afford the complex and power-hungry task of channel estimation in support of coherent detection. Hence, the SRAN employing relay-aided SISO-MSDSD algorithm and introduced in Section 3.3 becomes a possible solution for recovering the 50% throughput loss, whilst avoiding power-hungry channel estimation.

Against this background, in Section 5.1, we extend the concept of "matching code-on-graph with network-on-graph" [41] to arbitrary channel coding schemes and conceive the required new

Year	Authors	Contributions
2000	Ahlswede *et al.* [135]	Originally proposed the network coding concept for increasing the throughput of a network by invoking simple coding schemes in the intermediate routers. The maximum-flow capacity bound was derived, the linear space based and algebraic frameworks were proposed.
2003	Li *et al.* [136]	
	Koetter and Medard [137]	
2006	Hausl and Hagenauer [39]	The network coding concept found its way in two-way relay systems.
2007	Popovski and Yomo [40]	
2008	Bao and Li [41]	The network coding technique becomes capable of adapting to both link failures and network topology changes. LDPC codes were employed as the cross-layer network code.
2010	Xiao and Skoglund [42]	The diversity network code (DNC) concept was proposed, which also adapts to both link failures and network topology changes. Nonbinary linear block (NBLB) codes were employed as the cross-layer network code.
2012	Rebelatto *et al.* [149]	Transfer the problem of maximizing the diversity order of an NBLB coded network coding regime to the design of the generator matrix of the NBLB code.
	Nguyen *et al.* [151]	Sophisticated channel coding schemes were employed to collaborate with the network coding layer for achieving a near-capacity performance when considering a noncoherent detection based scenario.
2013	Nguyen *et al.* [152]	Again, a near-capacity performance was achieved with the aid of JNCC philosophy, where the investigation was extended to coherent detection based scenarios.
	Li *et al.* [153]	The generalized form of adaptive network coding (ANC) was proposed.

Table 5.1: Contributions to the development of network coding.

signal processing and transmission arrangements in support of this extension. Consequently, a generalized adaptive network coding (GANC) scheme is proposed for multi-user, multi-relay scenarios. Then, in Section 5.2, we intrinsically amalgamate the successive relaying protocol with the GANC philosophy to conceive a new GANC aided SRAN based DS-CDMA system concept. As a result, the typical 50% half-duplex relaying-induced throughput loss is converted to a potential user-load reduction for the CDMA system, since the interference of the relays is avoided by invoking a pair of low-correlation spreading codes. Correspondingly, a generalized iterative detection based three-stage transceiver architecture is created for the proposed GANC aided SRAN in Section 5.3, which efficiently detects the information bits of different users. Finally, our simulation results and discussions are provided in Section 5.4.

5.1 Basic Model of GANC Aided Cooperation

As stated in the preface of this chapter, it is beneficial to jointly treat the transmissions of multiple users relying on multiple relays. Hence, in contrast to the scenario introduced in Section 3.2, which was also portrayed in Figure 3.9, we commence by defining the "source group" and "relay group" concepts in the context of our cooperative network. In more detail, consider the uplink of a multiuser DS-CDMA system, where a number of actively communicating Mobile Stations (MS) may roam close to the edge of the DS-CDMA cell. In order to improve the communication quality, some of them, labelled as the Source Nodes (SN) in Figure 5.1, namely "$s_1, \cdots, s_N$" may invoke GANC aided cooperation by relying on the idle users roaming relatively close to the Base Station (BS), namely the Destination Node (DN) d as their Relay Nodes (RN). Consequently, a GANC aided cooperative network is created. In the GANC aided cooperative network, the RNs, namely "$a_1, \cdots, a_M$" have to negotiate with each other and align their behaviours in support of the GANC scheme. Hence the M RNs actually create a relaying group, which we refer to as "relay group A".

The path-loss reduction achieved by the reduced transmission distance experienced in conventional cooperative systems is exploited here again. As detailed in [107] and similar to our arguments in Section 3.2.1 as well as in Section 4.1, when considering the n^{th} SN s_n and m^{th} RN a_m, the average path-loss reductions of the Source-to-Relay (SR) link and Relay-to-Destination (RD) link with respect to the Source-to-Destination (SD) link are given by $G_{s_n a_m} = \left(\frac{D_{s_n d}}{D_{s_n a_m}}\right)^{\alpha}$ and $G_{a_m d} = \left(\frac{D_{s_n d}}{D_{a_m d}}\right)^{\alpha}$, respectively, where the notation $D_{ij}, i, j \in \{s_n, a_m, d\}$ represents the distance from node i to node j. Throughout this chapter, the path-loss exponent is fixed to $\alpha = 3$ for modelling an urban area. Then we assume that all the channels involved in the GANC aided cooperative network are conventional narrowband time-selective Rayleigh fading channels. In more detail, the fading coefficients $h_{ij}[k], i, j \in \{s_n, a_m, d\}$ of the channel between node i and node j fluctuate according to the associated normalized Doppler frequency f_{ij}. Furthermore, we assume having $(W + N)$ users in the CDMA system, namely the N desired users plus W interfering users. Let $\mathcal{P}_i$ denote the average transmit power of the node $i, i \in \{s_n, s_w, a_m\}$.

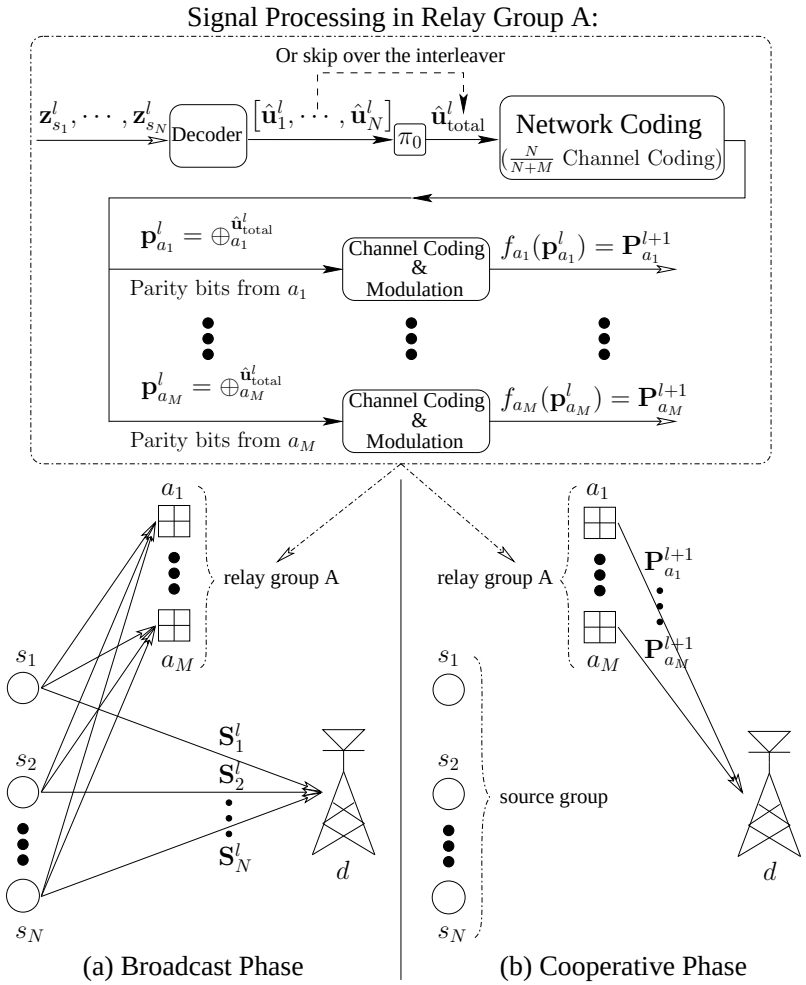

Figure 5.1: Basic framework of the proposed GANC aided cooperative network: signal processing and transmission arrangement. This scheme is a further evolved version of the conventional single-relay aided half-duplex cooperative network portrayed in Figure 1.2.

As detailed in the preface of this chapter, allowing arbitrary channel coding schemes to serve as the cross-layer network code, while remaining adaptive to both network topology changes and to link failures is an important advantage of our GANC regime. Hence, as an important design example, the nonbinary linear block (NBLB) codes representing a typical class of channel codes are employed as our cross-layer network code. The resultant nonbinary linear block (NBLB) coded GANC regime is similar to the diversity network coding (DNC) regime of [42] or to the generalized distributed network coding (GDNC) regime of [149]. Nevertheless, we will demonstrate in the ensuing subsections that compared to the existing regimes of [42, 149], our scheme is capable of achieving the same diversity order, but our solution in terms of adjusting the trade-off between the achievable throughput and the attainable diversity gain has a high flexibility. Moreover, our scheme will additionally benefit from a reduced propagation distance. As another design example, recursive systematic convolutional (RSC) codes invoked as our cross-layer network code are also

analysed. We will reveal that the resultant RSC coded GANC regime is also capable of adapting to both network topology changes and to link failures, while striking the same compromise between the achievable throughput and the attainable diversity gain as its nonbinary linear block coded counterpart.

5.1.1 Transmission Arrangement

In the proposed GANC aided cooperative network, we segment the source transmissions into identical-length transmission frames of K symbols. This implies that the signal frame $\mathbf{S}_n^l$ transmitted from the n^{th} SN during the l^{th} frame is given by

$$\mathbf{S}_n^l = \left[S_n^l[1], S_n^l[2], \cdots, S_n^l[K]\right]^T, \tag{5.1}$$

where $S_n^l[k]$ represents the k^{th} symbol in $\mathbf{S}_n^l$. The associated information-bit stream carried by $\mathbf{S}_n^l$ is represented by $\mathbf{u}_n^l$. Specifically, in the NBLB coded GANC regime, we further divide $\mathbf{S}_n^l$ into T_1 identical-length signal blocks in the form of $\mathbf{S}_n^l = \left[\mathbf{S}_n^l\{1\}, \mathbf{S}_n^l\{2\}, \cdots, \mathbf{S}_n^l\{T_1\}\right]$. The resultant information-bit stream $\mathbf{u}_n^l$ is simultaneously split into T_1 identical-length information-bit packets in the form of $\mathbf{u}_n^l = \left[\mathbf{u}_n^l\{1\}, \mathbf{u}_n^l\{2\}, \cdots, \mathbf{u}_n^l\{T_1\}\right]$, where an information-bit packet $\mathbf{u}_n^l\{t_1\}$ has b bits. The time required for transmitting a signal block $\mathbf{S}_n^l\{t_1\}$ is treated as a standard time slot, namely T_{Slot}.

The network coding algorithm can be realized with the aid of decoding, re-encoding, as well as re-modulation in the DF based RN. Similar to [41, 42, 142, 149], the proposed GANC aided cooperative network also employs the DF protocol.

Observe during the "(a) Broadcast Phase" of Figure 5.1 that, the N SNs $\{s_n\}_{n=1}^N$ simultaneously broadcast N signal frames $\{\mathbf{S}_n^l\}_{n=1}^N$ during the broadcast phase, whose time duration is $T_{\text{Broadcast}}$. Meanwhile, every RN of the relay group A seen in Figure 5.1 switches to listening mode in order to receive $\{\mathbf{S}_n^l\}_{n=1}^N$. When ignoring the interference imposed by the interfering users, i.e. assuming $W = 0$, we obtain the k^{th} received signal of the l^{th} frame at the RN a_m as[1]

$$\mathbf{y}_{a_m}^l[k] = \sum_{n=1}^{N} \sqrt{G_{s_n a_m}} h_{s_n a_m}^l[k] \sqrt{\mathcal{P}_{s_n}} S_n^l[k] \mathbf{C}_{s_n} + \mathbf{n}_{a_m}^l[k], \tag{5.2}$$

where $\mathbf{C}_{s_n}$ represents the user-specific pseudo-noise (PN) sequence employed by the n^{th} SN s_n of the DS-CDMA system. The spread AWGN vector $\mathbf{n}_{a_m}^l[k]$ obeys $\mathcal{E}\{\mathbf{n}_{a_m}^l[k] {\mathbf{n}_{a_m}^l}^H[k]\} = \frac{1}{Q}\sigma^2 \mathbf{I}_Q$, where Q is the spreading factor of $\mathbf{C}_{s_n}$, while $\mathbf{I}_Q$ is the identity matrix having a dimension of Q. Then the RN a_m decodes $\mathbf{y}_{a_m}^l$, and re-encodes, as well as re-modulates the detected bits according to our specific signal processing scheme, which will be described in Section 5.1.2. Consequently,

[1]Since it is difficult to realize perfect synchronization among the users, we assume an asynchronous multiuser CDMA system. By contrast, we assume that perfect synchronization is achieved within the GANC aided cooperative network based on the fact that the total number of its component nodes will remain relatively small.

the signal frame $\mathbf{P}_{a_m}^{l+1}$, which will be forwarded by the RN a_m in the consecutive cooperative phase is prepared. In the same broadcast phase, the k^{th} received signal of the l^{th} frame at the DN d is given by

$$\mathbf{y}_d^l[k] = \sum_{n=1}^{N} \sqrt{G_{s_n d}} h_{s_n d}^l[k] \sqrt{\mathcal{P}_{s_n}} S_n^l[k] \mathbf{C}_{s_n} + \mathbf{n}_d^l[k]. \tag{5.3}$$

The overall transmissions during the broadcast phase are overlapped in the same duration of $T_{\text{Broadcast}}$, but separated by different PN sequences.

During the consecutive cooperative phase, whose time duration is $T_{\text{Cooperative}}$, all of the N SNs remain silent. Meanwhile, all of the M RNs of the relay group A switch to their transmission mode, where the signal frames $\{\mathbf{P}_{a_m}^{l+1}\}_{m=1}^{M}$ are simultaneously forwarded to the DN. The associated k^{th} received signal of the $(l+1)^{st}$ frame at the DN is given by

$$\mathbf{y}_d^{l+1}[k] = \sum_{m=1}^{M} \sqrt{G_{a_m d}} h_{a_m d}^{l+1}[k] \sqrt{\mathcal{P}_{a_m}} P_{a_m}^{l+1}[k] \mathbf{C}_{a_m} + \mathbf{n}_d^{l+1}[k], \tag{5.4}$$

where we have $\mathbf{P}_{a_m}^{l+1} = \left[P_{a_m}^{l+1}[1], P_{a_m}^{l+1}[2], \cdots, P_{a_m}^{l+1}[K]\right]^T$. The PN sequence $\mathbf{C}_{a_m}$ is employed by the RN a_m to spread its forwarded signals $P_{a_m}^{l+1}[k]$. Similar to the broadcast phase, the overall transmissions during the cooperative phase are overlapped in the same duration of $T_{\text{Cooperative}}$, but separated by the PN sequences assigned to the M idle users in the DS-CDMA uplink, i.e. to the M RNs of relay group A. When employing the NBLB coded GANC regime, we further divide $\mathbf{P}_{a_m}^{l+1}$ into T_2 identical-length signal blocks in the form of $\mathbf{P}_{a_m}^{l+1} = \left[\mathbf{P}_{a_m}^{l+1}\{1\}, \mathbf{P}_{a_m}^{l+1}\{2\}, \cdots, \mathbf{P}_{a_m}^{l+1}\{T_2\}\right]$. Consequently, the parity-bit stream $\mathbf{p}_{a_m}^l$ carried by $\mathbf{P}_{a_m}^{l+1}$ is simultaneously split into T_2 identical-length parity-bit packets in the form of $\mathbf{p}_{a_m}^l = \left[\mathbf{p}_{a_m}^l\{1\}, \mathbf{p}_{a_m}^l\{2\}, \cdots, \mathbf{p}_{a_m}^l\{T_2\}\right]$, where a parity-bit packet $\mathbf{p}_{a_m}^l\{t_2\}$ has b bits.

The transmission arrangement during the broadcast phase and that during the cooperative phase will be alternately activated during the consecutive transmission frames. Throughput this chapter, the broadcast phase and cooperative phase always have the same time duration, i.e. we have $T_{\text{Broadcast}} = T_{\text{Cooperative}}; T_1 = T_2$.

5.1.2 Signal Processing at the Relay Group A

Observe at the top block of Figure 5.1 that specifically designed signal processing is implemented at the relay group A in order to realize the GANC scheme. When considering a single RN a_m, relying on the DS-CDMA principle [97], after applying the chip-waveform matched-filter to the waveform of $\mathbf{C}_{s_n}$, the received signal $\mathbf{y}_{a_m}^l[k]$ of (5.2) is despread to yield

$$z_{s_n}^l[k] = \sqrt{G_{s_n a_m}} h_{s_n a_m}^l[k] \sqrt{\mathcal{P}_{s_n}} S_n^l[k] + I_{s^{\text{Part}} a_m}^l[k] + n_{a_m}^l[k], \tag{5.5}$$

where the signal component contributed by the n^{th} SN s_n is retained, while the multiple access interference (MAI) $I_{s^{\text{Part}} a_m}^l[k]$ imposed by the other $(N-1)$ SNs is suppressed, which is formulated

as

$$I^l_{s^{\text{Part}}a_m}[k] = \sum_{i=1,\neq n}^{N} \sqrt{G_{s_i a_m}} h^l_{s_i a_m}[k] \sqrt{\mathcal{P}_{s_i}} S^l_i[k] \gamma_{s_i s_n}, \tag{5.6}$$

where $\gamma_{s_i s_n}$ represents the cross-correlation (CCL) between $\mathbf{C}_{s_i}$ and $\mathbf{C}_{s_n}$. Consequently, multiple despread signal frames $\{\mathbf{z}^l_{s_n}\}_{n=1}^N$ are generated at the RN a_m, where we have $\mathbf{z}^l_{s_n} = \left[z^l_{s_n}[1], z^l_{s_n}[2], \cdots, z^l_{s_n}[K]\right]^T$.

After forwarding the despread signal frame $\mathbf{z}^l_{s_n}$ to the decoder of a_m, the estimate $\hat{\mathbf{u}}^l_n$ of the original information-bit stream $\mathbf{u}^l_n$ is generated. Specifically, when employing the RSC code as our cross-layer network code, the RN activated should be capable of perfectly detecting all the SN's information-bit streams $\{\mathbf{u}^l_n\}_{n=1}^N$, which is a necessary requirement of the RSC coded GANC. For satisfying this requirement, we have to appropriately construct the source group and relay group A. Let $\mathcal{R}$ denote the entire RN resource pool, which consists of the idle users roaming between the SNs and DN. The specific RNs, which perfectly decoded the information-bit stream $\mathbf{u}^l_n$ transmitted by the SN s_n, are selected from $\mathcal{R}$ for the sake of constructing the subset $\mathcal{R}_{s_n}$. Consequently, when the source group is constituted by $\{s_n\}_{n=1}^N$, where the maximum relay group set in the RSC coded GANC is given by $\{\mathcal{R}_{s_1} \cap \mathcal{R}_{s_2} \cap \cdots \cap \mathcal{R}_{s_N}\}$, which implies that we should set "$\text{relay gourp A} \subseteq \{\mathcal{R}_{s_1} \cap \mathcal{R}_{s_2} \cap \cdots \cap \mathcal{R}_{s_N}\}$".

During the network coding stage, the N SNs create a source group, while the M RNs form the relay group A. Inspired by the "matching code-on-graph with network-on-graph" concept of [41], our basic regime conceived for the proposed GANC consists of three steps:

(1) Assign the ratio of the source group size[2] and the relay group size to the coding rate R_{code} of the cross-layer network code, which is formulated as

$$R_{\text{code}} = \frac{N \cdot T_1}{N \cdot T_1 + M \cdot T_2} = \frac{N}{N+M}. \tag{5.7}$$

(2) Specify the generator matrix of the cross-layer network code.

(3) Distribute the parity bits $\mathbf{p}^l_{\text{total}}$ generated by the GANC scheme among the M RNs.

When employing the NBLB codes as our cross-layer network code, we consecutively concatenate each estimated information-bit stream $\hat{\mathbf{u}}^l_n$ for the sake of constructing the entire input of the cross-layer network code encoder - $\hat{\mathbf{u}}^l_{\text{total}}$. This process is represented by the dashed arrow at the top of Figure 5.1. Hence we have $\hat{\mathbf{u}}^l_{\text{total}} = \left[\hat{\mathbf{u}}^l_1, \hat{\mathbf{u}}^l_2, \cdots, \hat{\mathbf{u}}^l_N\right]$. For the NBLB coded GANC, the basic signal processing framework of relay group A depicted at the top of Figure 5.1 is further detailed in Figure 5.2, which may be formulated as

$$\left[\mathbf{u}^l_{\text{total}}, \mathbf{p}^l_{\text{total}}\right] = \hat{\mathbf{u}}^l_{\text{total}} \cdot \mathbf{G}, \tag{5.8}$$

[2]The size of the source group is given by the number of SNs included in the source group. A similar definition is stipulated for the relay group size.

where $\mathbf{G} = [\alpha \mid \beta]$ is the systematic generator matrix of a nonbinary linear block code, which serves as our cross-layer network code. The specific part of $\mathbf{G}$, which is denoted by α is an NT_1-dimensional identity matrix. Then we have $\beta \in \mathbb{C}^{NT_1 \times MT_2}$. Since the entire input $\hat{\mathbf{u}}^l_{\text{total}}$ in (5.8) consists of NT_1 information-bit packets and because we have $T_1 = T_2$, the dimension of $\mathbf{G}$ is in line with the cross-layer coding rate given in (5.7).

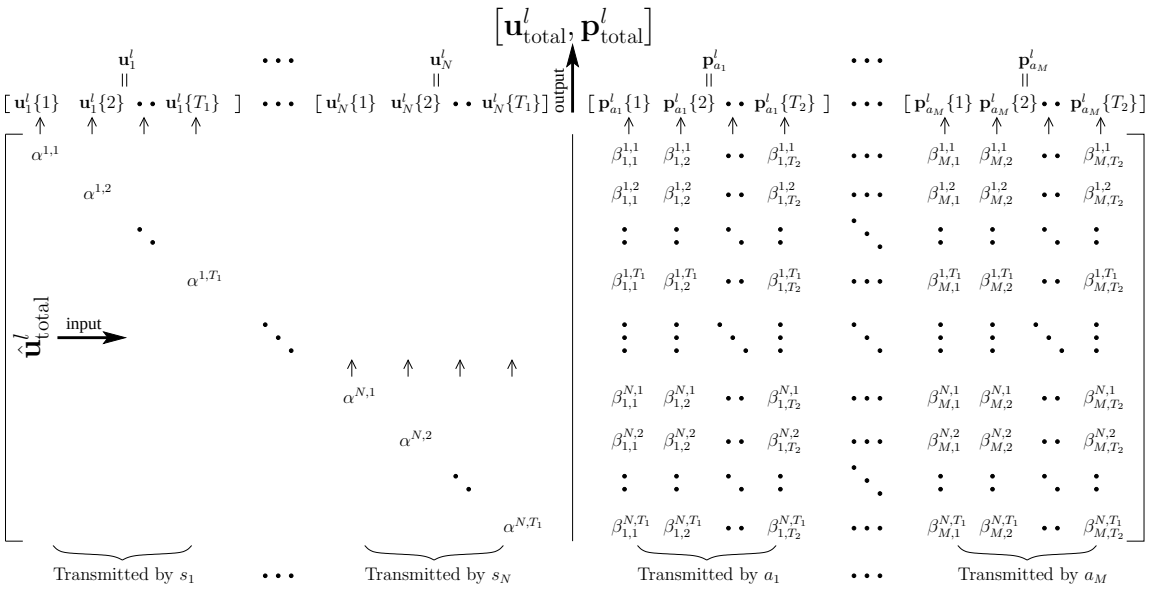

Figure 5.2: Illustration of the systematic generator matrix and the network coding process engaged in the NBLB coded GANC.

Observe in Figure 5.2 that a parity-bit packet $\mathbf{p}^l_{a_m}\{t_2\}$, which is generated by RN a_m during the broadcast phase, is given by

$$\mathbf{p}^l_{a_m}\{t_2\} = \sum_{n=1}^{N} \sum_{t_1=1}^{T_1} \beta^{n,t_1}_{m,t_2} \hat{\mathbf{u}}^l_n\{t_1\}, \tag{5.9}$$

which will be forwarded to DN d in the t_2^{th} time slot during the consecutive cooperative phase. For the sake of adapting to link failures, if we have $\hat{\mathbf{u}}^l_n\{t_1\} \neq \mathbf{u}^l_n\{t_1\}$ in the RN a_m, the corresponding coding coefficients $\{\beta^{n,t_1}_{m,t_2}\}^{T_2}_{t_2=1}$ in Figure 5.2 are fixed to zero value. Hence all the parity-bit packets $\{\mathbf{p}^l_{a_m}\{t_2\}\}^{T_2}_{t_2=1}$ generated at the RN a_m are irrelevant to $\hat{\mathbf{u}}^l_n\{t_1\}$, because we discard this corrupted data. Let $\mathcal{D}_{n,t_1}$ denote the specific set of RNs, which succeed in correctly decoding $\mathbf{u}^l_n\{t_1\}$ during the broadcast phase. Correspondingly, the number of RNs contained in the set $\mathcal{D}_{n,t_1}$ is denoted by $|\mathcal{D}_{n,t_1}|$. Let $\mathcal{D}_{n,t_1}(I)$ denote the set of all information-bit packets correctly decoded by the RNs in the set $\mathcal{D}_{n,t_1}$ during the broadcast phase, including $\mathbf{u}^l_n\{t_1\}$ itself. Similarly, the number of information-bit packets contained in the set $\mathcal{D}_{n,t_1}(I)$ is denoted by $|\mathcal{D}_{n,t_1}(I)|$. According to [42, 137], the generator matrix $\mathbf{G}$ seen in Figure 5.2 should allow us to recover the entire information-bit packet set $\mathcal{D}_{n,t_1}(I)$ from any correctly decoded $|\mathcal{D}_{n,t_1}(I)|$ packets[3] at the DN for the sake

[3]This $|\mathcal{D}_{n,t_1}(I)|$ packets should belong to the packet set, which is related to the information-bit packet set $\mathcal{D}_{n,t_1}(I)$ and consists of $|\mathcal{D}_{n,t_1}(I)| + |\mathcal{D}_{n,t_1}|T_2$ packets received at the DN d.

of maximizing the diversity order of the NBLB coded GANC. The generator matrix construction method introduced in [149] satisfies this requirement, hence it may be employed for specifying the coefficients β_{m,t_2}^{n,t_1} in (5.9).

Observe at the DN that, the systematic part of the whole network codeword, i.e. the $\mathbf{u}_{\text{total}}^l$ part of $\left[\mathbf{u}_{\text{total}}^l, \mathbf{p}_{\text{total}}^l\right]$, is gleaned from the Source-to-Destination transmissions during the broadcast phase, while, the remaining parity part $\mathbf{p}_{\text{total}}^l = \left[\mathbf{p}_{a_1}^l, \mathbf{p}_{a_2}^l, \cdots, \mathbf{p}_{a_M}^l\right]$ is gleaned from the Relay-to-Destination transmissions during the cooperative phase. Hence the DN may first individually decode every $\mathbf{u}_n^l\{t_1\}$ and $\mathbf{p}_{a_m}^l\{t_2\}$ vectors, and then jointly decodes $\{\{\mathbf{u}_n^l\{t_1\}\}_{t_1=1}^{T_1}\}_{n=1}^{N}$ based on the structure of the cross-layer network code illustrated in Figure 5.2.

Example 5.1: Example of the NBLB coded GANC scheme using the parameters of $N = 2, M = 2, T_1 = T_2 = 2$.

The generalized transmission arrangement and signal processing of the GANC aid cooperative network were introduced in Sections 5.1.1 and 5.1.2, respectively. Here we would like to demonstrate how we exploit these generalized schemes for supporting a specific multi-user multi-relay cooperative network in the proposed GANC aided scenario.

Consequently, a NBLB coded GANC aided cooperative system consisting of two SNs, namely s_1 and s_2, and of a pair of RNs, namely a_1 and a_2, as well as of a common DN, namely d, is illustrated in Figure 5.3. This regime may be regarded as a specific instantiation of the generalized network coded cooperative scenario characterized in Figure 5.1, where the cross-layer network code is contributed by NBLB codes, the source group size is fixed to $N = 2$, while the relay group size is fixed to $M = 2$. Furthermore, both its broadcast phase and its cooperative phase are fixed to two time slot durations, i.e. we have $T_1 = T_2 = 2$. Observe in Figure 5.3 that during the phase "(a) Broadcast time slot 1", s_1 broadcasts its first information-bit packet, namely $\mathbf{u}_1\{1\}$. Then, during the second time slot of the broadcast phase, s_1 broadcasts another information-bit packet, namely $\mathbf{u}_1\{2\}$. Accordingly, the information-bit stream transmitted by s_1 is given by $\mathbf{u}_1 = \left[\mathbf{u}_1\{1\}, \mathbf{u}_1\{2\}\right]$[4]. Similarly, the information-bit stream transmitted by s_2 is given by $\mathbf{u}_2 = \left[\mathbf{u}_2\{1\}, \mathbf{u}_2\{2\}\right]$. According to the signal processing strategy introduced in Section 5.1.2, we then concatenate the information-bit streams $\mathbf{u}_1$ and $\mathbf{u}_2$ for the sake of constructing the combined input of the cross-layer network code encoder - $\mathbf{u}_{\text{total}}$, which is hence given by

$$\mathbf{u}_{\text{total}} = \Big[\mathbf{u}_1\{1\}, \mathbf{u}_1\{2\}, \mathbf{u}_2\{1\}, \mathbf{u}_2\{2\}\Big]. \tag{5.10}$$

According to the first step of our basic regime conceived in Section 5.1.2 for the proposed GANC, namely to (5.7), a rate $4/8$ NBLB code is appropriate for employment as the cross-layer network code for the network portrayed in Figure 5.3.

[4]In order to simplify our notations, the superscripts used for representing the frame index are omitted in Example 5.1.

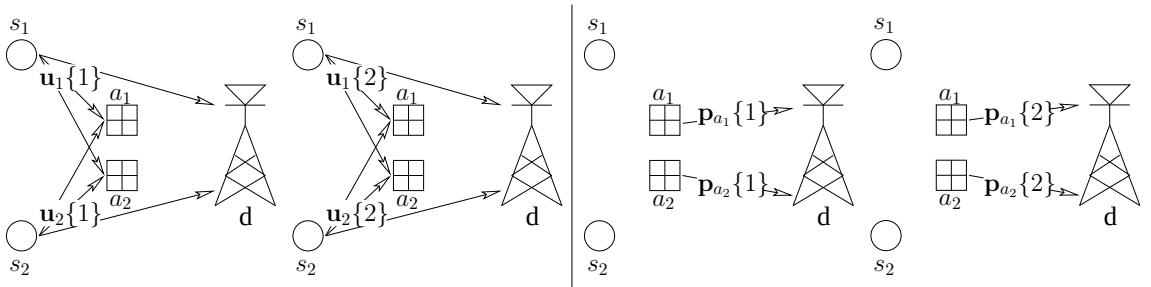

(a) Broadcast time slot 1 : $t_1 = 1$ (b) Broadcast time slot 2 : $t_1 = 2$ (c) Cooperative time slot 1 : $t_2 = 1$ (d) Cooperative time slot 2 : $t_2 = 2$

Figure 5.3: A NBLB coded GANC aided cooperative system having $N = 2, M = 2, T_1 = T_2 = 2$, where all the SR transmissions are assumed to be perfectly detected at the RNs. Explicitly, this is a specific instantiation of the generalized network coded cooperative scenario characterized in Figure 5.1. The associated network topology may be encapsulated into a NBLB code's generator matrix as shown in (5.11). Moreover, the parity-bit packets $\mathbf{p}_{a_1}\{1\}$, $\mathbf{p}_{a_1}\{2\}$, $\mathbf{p}_{a_2}\{1\}$ and $\mathbf{p}_{a_2}\{2\}$ are constructed according to (5.13), (5.14), (5.15) and (5.16), respectively.

Then, according to the second step of our basic regime conceived in Section 5.1.2 for the proposed GANC, we proceed by specifying the generator matrix of the rate $4/8$ NBLB code. Based on the network topology portrayed in Figure 5.3, as well as on the code construction principle proposed in [42] and in Section 5.1.2, the generator matrix may be specified as below[5]

$$\mathbf{G} = \mathbf{G}\left[\alpha|\beta\right] = \left[\begin{array}{cccc|cccc} 1 & 0 & 0 & 0 & 3 & 7 & 3 & 6 \\ 0 & 1 & 0 & 0 & 5 & 7 & 7 & 4 \\ 0 & 0 & 1 & 0 & 2 & 4 & 6 & 1 \\ 0 & 0 & 0 & 1 & 5 & 5 & 3 & 2 \end{array}\right]. \tag{5.11}$$

The above-mentioned two steps of our basic regime conceived in Section 5.1.2 for realizing the proposed GANC - namely determining the coding rate and specifying the generator matrix of the cross-layer NBLB code - actually obey the concept of "matching code-on-graph with network-on-graph", which was proposed by Bao and Li in [41]. Hence these two steps are equivalent to converting the network topology portrayed in Figure 5.3 into the generator matrix of a NBLB code given in (5.11).

In more detail, each DN-oriented link portrayed in Figure 5.3 is transformed to a specific column of the generator matrix $\mathbf{G}\left[\alpha|\beta\right]$ given in (5.11). In order to indicate this linkage, we would like to present the transmit node and the transmit phase of a DN-oriented link portrayed in Figure 5.3 right below its associated coefficient column of (5.11). Consequently, the generator matrix $\mathbf{G}\left[\alpha|\beta\right]$ given in (5.11) is further detailed in Figure 5.4.

For example, observe in Figure 5.3 that the $s_1 \rightarrow d$ link of the processing phase of $t_1 = 2$

[5]The generator matrix $\mathbf{G}$ given in (5.11) is based on Section V of [154], which was beneficially constructed, because it achieves the largest possible minimum Hamming distance over the finite Galois Field GF(8).

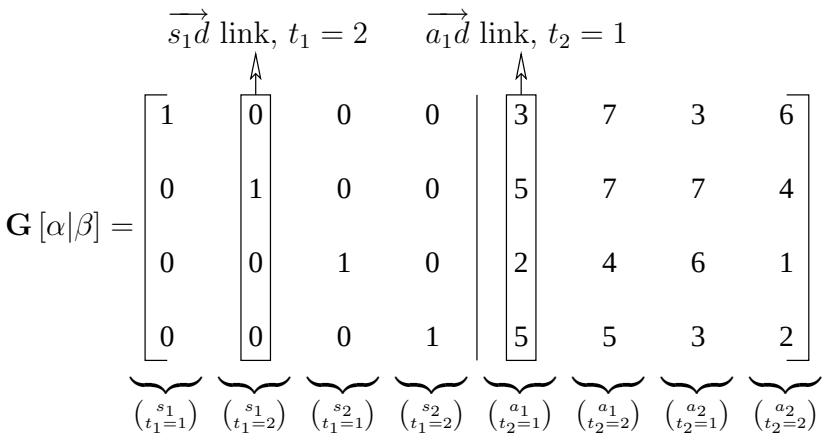

Figure 5.4: Relating the DN-oriented links portrayed in Figure 5.3 to the columns of the generator matrix $\mathbf{G}\,[\alpha|\beta]$ given in (5.11). The notation below a coefficient column, e.g. $\binom{s_1}{t_1=2}$ below the second column indicates that the second column is related to the DN-oriented link transmitted from SN s_1 to DN d during the processing phase of $t_1 = 2$ in Figure 5.3. This diagram reveals the physical meaning of the generator matrix $\mathbf{G}\,[\alpha|\beta]$ of (5.11) in more depth.

is related to the second column of the generator matrix $\mathbf{G}\,[\alpha|\beta]$ shown in Figure 5.4, which is the coefficient column $[0\ 1\ 0\ 0]^T$. In order to explicitly indicate this linkage, the transmit node and the transmit phase of the associated link are presented below the second column in Figure 5.4 as $\binom{s_1}{t_1=2}$. Since only the information-bit packet $\mathbf{u}_1\{2\}$ is involved in the $s_1 \rightarrow d$ link during the processing phase of $t_1 = 2$, only the second element of the associated coefficient vector $[0\ 1\ 0\ 0]^T$ is set to be non-zero. Similarly, the $a_1 \rightarrow d$ link during the processing phase of $t_2 = 1$ portrayed in Figure 5.3 is related to the fifth column of the generator matrix $\mathbf{G}\,[\alpha|\beta]$ shown in Figure 5.4. Hence, as shown in Figure 5.4, the notation $\binom{a_1}{t_2=1}$ is labelled below the fifth column. Now, all the information-bit packets $\mathbf{u}_1\{1\}$, $\mathbf{u}_1\{2\}$, $\mathbf{u}_2\{1\}$, $\mathbf{u}_2\{2\}$ are involved in the $a_1 \rightarrow d$ link during the processing phase of $t_2 = 1$. Correspondingly, all the elements of the coefficient vector $[3\ 5\ 2\ 5]^T$ are set to be non-zero.

Recall by considering the specific partitioning of the generator matrix $\mathbf{G}$ discussed right below (5.8) as well as by observing Figure 5.4 again that in general, all the SD links during the broadcast phases are related to the α part of $\mathbf{G}\,[\alpha|\beta]$, while all the RD links during the cooperative phases are related to the β part.

Furthermore, each SR link portrayed in Figure 5.3 is transformed to a specific element of the β part in the generator matrix $\mathbf{G}\,[\alpha|\beta]$ given in (5.11). Similar to Figure 5.4, in order to indicate this linkage, we present the transmit node and transmit phase as well as the receive node of a SR link as the row index and column index of its associated element in the generator matrix $\mathbf{G}\,[\alpha|\beta]$ of Figure 5.5. For example, observe in Figure 5.5 that the element $\boxed{3}$ has the row index of $\binom{s_1}{t_1=1}$ and the column index of a_1. This implies that the SR link of $s_1 \rightarrow a_1$

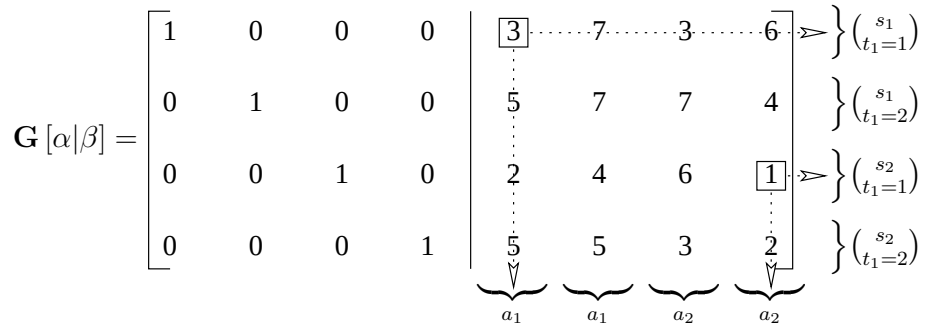

Figure 5.5: Relating the SR links portrayed in Figure 5.3 to the elements in the β part of the generator matrix $\mathbf{G}[\alpha|\beta]$ given in (5.11). The transmit node and transmit phase of a SR link are presented as the row index of the associated element, while the receive node of the same SR link is presented as the column index of the associated element. Similar to Figure 5.4, this diagram is used to reveal the physical meaning of the generator matrix $\mathbf{G}[\alpha|\beta]$ given in (5.11) in more depth.

during $t_1 = 1$ is related to the element $\boxed{3}$. Observe in Figure 5.5 again that the element $\boxed{1}$ has the row index of $\binom{s_2}{t_1=1}$ and the column index of a_2. Similarly, this implies that the SR link of $s_2 \rightarrow a_2$ during $t_1 = 1$ is related to the element $\boxed{1}$.

Hence, the linkage between each propagation link involved in Figure 5.3 and its associated coefficients in the generator matrix $\mathbf{G}[\alpha|\beta]$ of (5.11) has explicitly been portrayed in Figures 5.4 and 5.5.

Then, upon substituting (5.10) and (5.11) into (5.8), the entire network's codeword employed by the specific cooperative system shown in Figure 5.3 may be formulated as [6]

$$\begin{aligned}\mathbf{c} &= \mathbf{u}_{\text{total}} \times \mathbf{G} \\ &= \Big[\mathbf{u}_1\{1\}, \mathbf{u}_1\{2\}, \mathbf{u}_2\{1\}, \mathbf{u}_2\{2\}\Big] \times \left[\begin{array}{cccc|cccc} 1 & 0 & 0 & 0 & 3 & 7 & 3 & 6 \\ 0 & 1 & 0 & 0 & 5 & 7 & 7 & 4 \\ 0 & 0 & 1 & 0 & 2 & 4 & 6 & 1 \\ 0 & 0 & 0 & 1 & 5 & 5 & 3 & 2 \end{array}\right] \\ &= \Big[\mathbf{u}_1\{1\}, \mathbf{u}_1\{2\}, \mathbf{u}_2\{1\}, \mathbf{u}_2\{2\}, \mathbf{p}_{a_1}\{1\}, \mathbf{p}_{a_1}\{2\}, \mathbf{p}_{a_2}\{1\}, \mathbf{p}_{a_2}\{2\}\Big], \end{aligned} \tag{5.12}$$

where the parity-bit packets are given by

$$\mathbf{p}_{a_1}\{1\} = 3\mathbf{u}_1\{1\} + 5\mathbf{u}_1\{2\} + 2\mathbf{u}_2\{1\} + 5\mathbf{u}_2\{2\}, \tag{5.13}$$

$$\mathbf{p}_{a_1}\{2\} = 7\mathbf{u}_1\{1\} + 7\mathbf{u}_1\{2\} + 4\mathbf{u}_2\{1\} + 5\mathbf{u}_2\{2\}, \tag{5.14}$$

$$\mathbf{p}_{a_2}\{1\} = 3\mathbf{u}_1\{1\} + 7\mathbf{u}_1\{2\} + 6\mathbf{u}_2\{1\} + 3\mathbf{u}_2\{2\}, \tag{5.15}$$

$$\mathbf{p}_{a_2}\{2\} = 6\mathbf{u}_1\{1\} + 4\mathbf{u}_1\{2\} + 1\mathbf{u}_2\{1\} + 2\mathbf{u}_2\{2\}. \tag{5.16}$$

[6] The notation "$\times$" in (5.12) represents matrix multiplication.

Finally, after specifying the generator matrix, according to the third step of our basic regime conceived in Section 5.1.2 for the proposed GANC, we will distribute all the parity-bits of the network codeword $\mathbf{c}$, which was generated according to (5.12) between the RNs a_1 and a_2. This may be simply achieved by simply exploiting the specific behaviour of the RNs during the cooperative phase according to $(5.13)\sim(5.16)$. In more detail, during the phase "(c) Cooperative time slot 1" of Figure 5.3, the RN a_1 will be responsible for creating the parity-bit packet $\mathbf{p}_{a_1}\{1\}$ and for forwarding it to the DN d. Hence, during the processing phase "(c) Cooperative time slot 1", a_1 amplifies the information-bit packets $\mathbf{u}_1\{1\}$, $\mathbf{u}_1\{2\}$, $\mathbf{u}_2\{1\}$, $\mathbf{u}_2\{2\}$, which are detected during the preceding broadcast phases, and then composes them according to (5.13). Consequently, the parity-bit packet $\mathbf{p}_{a_1}\{1\}$ is obtained. Similarly, after appropriately amplifying the information-bit packets $\mathbf{u}_1\{1\}$, $\mathbf{u}_1\{2\}$, $\mathbf{u}_2\{1\}$, $\mathbf{u}_2\{2\}$ detected during the preceding broadcast phases, and then composing them according to (5.16), the parity-bit packet $\mathbf{p}_{a_2}\{2\}$ will be created at the RN a_2, which will then be further forwarded to the DN during the second cooperative time slot of Figure 5.3.

Example 5.2: Adapting the NBLB coded GANC aided cooperative system portrayed in Figure 5.3 to link failures.

As stated in Section 5.1, a significant advantage of the proposed GANC aided cooperative system is that it is capable of adapting to link failures. Here, in order to exemplify this benefit, we impose some link failures on the NBLB coded GANC aided cooperative system portrayed in Figure 5.3. Consequently, the network topology of Figure 5.3 is modified to that of Figure 5.6, where the $s_1 \rightarrow a_1$ link is assumed to incur link failure events during "(a) Broadcast time slot 1", while the $s_2 \rightarrow a_2$ link during the processing phase of "(b) Broadcast time slot 2" is also assumed to incur link failure events.

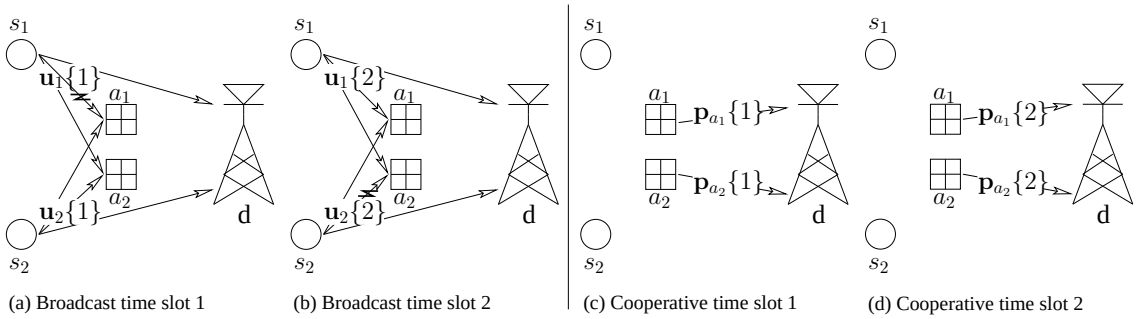

(a) Broadcast time slot 1 (b) Broadcast time slot 2 (c) Cooperative time slot 1 (d) Cooperative time slot 2

Figure 5.6: Changing the link states of the NBLB coded GANC aided cooperative system shown in Figure 5.3, where we assume that link failures occur in the $s_1 \rightarrow a_1$ link during "(a) Broadcast time slot 1" and in the $s_2 \rightarrow a_2$ link during "(b) Broadcast time slot 2". The zigzags indicate the link failure events.

According to the relationship between the generator matrix of the NBLB code and the cooperative network considered in Example 5.1, the $s_1 \rightarrow a_1$ link of "(a) Broadcast time slot 1"

$$\mathbf{G}\left[\alpha|\beta\right] = \left[\begin{array}{cccc|cccc} 1 & 0 & 0 & 0 & \boxed{0} & \boxed{0} & 3 & 6 \\ 0 & 1 & 0 & 0 & 5 & 7 & 7 & 4 \\ 0 & 0 & 1 & 0 & 2 & 4 & 6 & 1 \\ 0 & 0 & 0 & 1 & 5 & 5 & \boxed{0} & \boxed{0} \\ & & & & \underbrace{\quad}_{a_1} & \underbrace{\quad}_{a_1} & \underbrace{\quad}_{a_2} & \underbrace{\quad}_{a_2} \end{array}\right] \begin{array}{l} \left.\begin{array}{l}\\\\\end{array}\right\}\binom{s_1}{t_1=1} \\ \left.\begin{array}{l}\\\\\end{array}\right\}\binom{s_1}{t_1=2} \\ \left.\begin{array}{l}\\\\\end{array}\right\}\binom{s_2}{t_1=1} \\ \left.\begin{array}{l}\\\\\end{array}\right\}\binom{s_2}{t_1=2} \end{array}$$

Figure 5.7: According to Figure 5.5, the elements labelled by the dashed boxes in this diagram are related to the $s_1 \rightarrow a_1$ link during "(a) Broadcast time slot 1" of Figure 5.6, while the elements labelled by the solid boxes in this diagram are related to the $s_2 \rightarrow a_2$ link during "(b) Broadcast time slot 2" of Figure 5.6. Since these two SR links incur link failures in Figure 5.6, the values of their associated elements in the generator matrix $\mathbf{G}\left[\alpha|\beta\right]$ will be replaced by zeros. Consequently, the generator matrix given in (5.11) is updated to that shown in this diagram for adapting to the network topology change observed by comparing Figure 5.3 and Figure 5.6.

and the $s_2 \rightarrow a_2$ link of "(b) Broadcast time slot 2" seen in Figure 5.6 correspond to specific elements of the generator matrix $\mathbf{G}$ given in (5.11), which are explicitly indicated by the dashed and solid boxes in Figure 5.7, respectively. Owing to the link failures, the values of these elements are modified.

According to the method of implementing (5.9), the elements of the NBLB code's generator matrix $\mathbf{G}$, which are associated with the failed links have to be fixed to zero values. Hence, as shown in Figure 5.7 indeed, the elements indicated by boxes were set to zeros. Correspondingly, Equations (5.13) and (5.14) are rewritten as

$$\mathbf{p}_{a_1}\{1\} = 0\hat{\mathbf{u}}_1\{1\} + 5\mathbf{u}_1\{2\} + 2\mathbf{u}_2\{1\} + 5\mathbf{u}_2\{2\}, \tag{5.17}$$

$$\mathbf{p}_{a_1}\{2\} = 0\hat{\mathbf{u}}_1\{1\} + 7\mathbf{u}_1\{2\} + 4\mathbf{u}_2\{1\} + 5\mathbf{u}_2\{2\}. \tag{5.18}$$

Explicitly, now the parity-bit packets $\mathbf{p}_{a_1}\{1\}$ in (5.17) and $\mathbf{p}_{a_1}\{2\}$ in (5.18) become irrelevant to the corrupted data $\hat{\mathbf{u}}_1\{1\}$. Similarly, the parity-bit packets $\mathbf{p}_{a_2}\{1\}$ and $\mathbf{p}_{a_2}\{2\}$ generated at the RN a_2 of Figure 5.6 become irrelevant to the corrupted data $\hat{\mathbf{u}}_2\{2\}$ received at the RN a_2.

As a benefit of the above-mentioned mechanism, the NBLB coded GANC aided cooperative network becomes capable of adapting to link failures.

Then, in the RSC coded GANC, we generate $\hat{\mathbf{u}}_n^l = \mathbf{u}_n^l, n \in \{1, 2, \cdots, N\}$ at every RN as a benefit of our relay group selection strategy introduced at the beginning of this subsection. Similar to the NBLB coded GANC, at the RN we concatenate every detected $\mathbf{u}_n^l$ for creating a single

information-bit stream in the form of $\left[\mathbf{u}_1^l, \mathbf{u}_2^l, \cdots, \mathbf{u}_N^l\right]$. However, for the sake of eliminating the ensuing fading-induced correlation among the symbols of the signal frames $\mathbf{S}_n^l$ and $\mathbf{P}_{a_m}^{l+1}$, the combined detected information-bit stream $\left[\mathbf{u}_1^l, \mathbf{u}_2^l, \cdots, \mathbf{u}_N^l\right]$ is further interleaved. This operation is represented by the notation "π_0" in Figure 5.1. Hence the entire input of the cross-layer network code becomes $\mathbf{u}_{\text{total}}^l = \text{Interleaver}\left(\left[\mathbf{u}_1^l, \mathbf{u}_2^l, \cdots, \mathbf{u}_N^l\right]\right)$, which consists of NT_1b bits. According to the first step of the proposed basic GANC regime, a $\left(\frac{N}{N+M}\right)$-rate RSC code is employed at the RN as the cross-layer network code. Naturally, its generator polynomials should aim for maximizing the RSC code's free distance d_{free}, because maximizing the free distance of the $\left(\frac{N}{N+M}\right)$-rate RSC code is equivalent to maximizing the diversity order of the associated GANC aided cooperative network, which will be revealed in Section 5.1.3.

After fixing the cross-layer network code, the overall signal processing carried out in relay group A for the RSC coded GANC is further detailed in Figure 5.8. The resultant network codeword $\mathbf{c}$ may be formulated as

$$\mathbf{c} = \left[\mathbf{u}_{\text{total}}^l, \mathbf{p}_{\text{total}}^l\right] = \mathbf{u}_{\text{total}}^l \cdot \mathbf{G} = \mathbf{u}_{\text{total}}^l \cdot [\,\mathbf{I} \mid \mathbf{P}\,], \tag{5.19}$$

where $\mathbf{G}$ is the systematic generator matrix of the $\left(\frac{N}{N+M}\right)$-rate RSC code, while $\mathbf{I}$ is an NT_1b-dimensional identity matrix, and $\mathbf{P} \in \mathbb{C}^{NT_1b \times MT_2b}$. Since $\mathbf{u}_{\text{total}}^l$ consists of NT_1b bits, according to the coding rate of $\left(\frac{N}{N+M}\right)$ and bearing in mind that we have $T_1 = T_2$, $\mathbf{p}_{\text{total}}^l$ will consist of MT_2b bits, which is further split into M parity-bit streams $\{\mathbf{p}_{a_m}^l\}_{m=1}^M$, where every parity-bit stream $\mathbf{p}_{a_m}^l$ consists of T_2b bits.

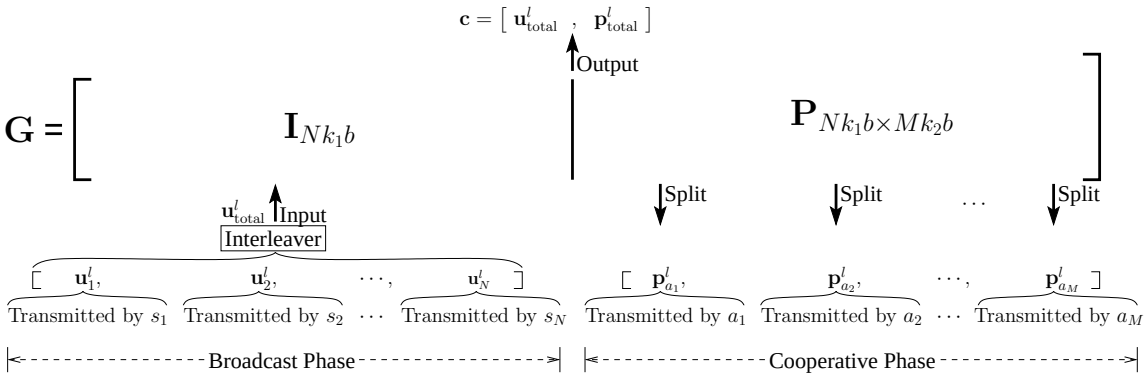

Figure 5.8: Illustration of the network coding process engaged in the RSC coded GANC.

The network encoding process represented by (5.19) and the ensuing partitioning of $\mathbf{p}_{\text{total}}^l$, i.e. we consecutively split $\mathbf{p}_{\text{total}}^l$ into M parity-bit streams $\{\mathbf{p}_{a_m}^l\}_{m=1}^M$, are implemented at every RN of relay group A. Hence we obtain $\mathbf{p}_{\text{total}}^l = \left[\mathbf{p}_{a_1}^l, \mathbf{p}_{a_2}^l, \cdots, \mathbf{p}_{a_M}^l\right]$ at every RN. According to the third step of the proposed basic GANC regime outlined in this section, the RN a_1 may be only responsible for the transmission of the parity-bit stream $\mathbf{p}_{a_1}^l$. Hence $\mathbf{p}_{a_1}^l$ is extracted from $\mathbf{p}_{\text{total}}^l$, and re-encoded, as well as re-modulated for creating the signal frame $\mathbf{P}_{a_1}^{l+1}$ at the RN a_1, which will

be further forwarded from the RN a_1 to the DN d during the cooperative phase. Similar operations will be carried out in all the other RNs $a_m, m = 2, 3, \cdots, M$. This allocation of the parity part of the network codeword $\mathbf{c}$ is also illustrated at the lower right corner of Figure 5.8.

5.1.3 Advantages of GANC Aided Cooperation

Based on the similarity of our proposed solution to [149], the diversity order derivation of the generalized dynamic-network codes (GDNC) provided in [149, Section V] can be applied for evaluating the achievable diversity order of our NBLB coded GANC. Consequently, we may arrive at

$$D_{\mathrm{GANC}} = (M - |\mathcal{D}_{n,t_1}|) + |\mathcal{D}_{n,t_1}|T_2 + 1, \tag{5.20}$$

where D_{GANC} represents the diversity order of the proposed NBLB coded GANC, and we have $|\mathcal{D}_{n,t_1}| \in [0, M]$. Hence the range of the diversity order D_{GANC} is limited to

$$M + 1 \leq D_{\mathrm{GANC}} \leq MT_2 + 1. \tag{5.21}$$

According to (5.20), the diversity order of the proposed NBLB coded GANC is almost the same as that of the DNC regime proposed in [42] or that of the GDNC scheme proposed in [149]. The only difference is that the minimum value of $|\mathcal{D}_{n,t_1}|$ equals to 1 in the DNC or GDNC regime, since the SN continues to serve as the RN in [42, 149], whilst, it drops to 0 in our system, since we employ other idle users as our RNs.

Let us now analyse the diversity order of the RSC coded GANC. Let $\{\mathbf{c}_1, \mathbf{c}_2, \cdots, \mathbf{c}_{\mathcal{M}}\}$ represent the set of all the legitimate network codewords generated from (5.19). Since the input information-bit stream $\mathbf{u}^l_{\mathrm{total}}$ of the RSC code exploited in (5.19) has NT_1b bits, the total number of all the legitimate network codewords is $\mathcal{M} = 2^{NT_1b}$. Then, let $\mathbf{c}_i(k)$ denote the k^{th} bit of network codeword $\mathbf{c}_i$, where we have $k \in \{1, 2, \cdots, NT_1b + MT_2b\}$. According to [59, Chapter 3], when experiencing an i.i.d $\mathcal{CN}(0, 1)$ Rayleigh fading channel, the upper bound of the overall probability of erroneously decoding the network codeword $\mathbf{c}$ in (5.19) is given by

$$P_{\mathrm{outage}} \leq \frac{4^{d_{\mathrm{free}}}}{\mathcal{M}} \sum_{i \neq j} \frac{1}{\delta_{ij}} \mathrm{SNR}^{-d_{\mathrm{free}}} \leq \frac{4^{d_{\mathrm{free}}}\,(\mathcal{M} - 1)}{\min_{i \neq j} \delta_{ij}} \mathrm{SNR}^{-d_{\mathrm{free}}}, \tag{5.22}$$

where δ_{ij} is the squared product distance between $\mathbf{c}_i$ and $\mathbf{c}_j$, which is evaluated as

$$\delta_{ij} = \prod_{k=1}^{NT_1b+MT_2b} |\mathbf{c}_i(k) - \mathbf{c}_j(k)|^2. \tag{5.23}$$

As stated in [155] and in [156, Section III], the free distance of a systematic convolutional code is upper bounded by the minimum distance of the associated best linear block code. When considering the Singleton bound [110, Chapter 7], the achievable free distance d_{free} is given by

$$d_{\mathrm{free}} = (NT_1b + MT_2b) - (NT_1b) + 1 = MT_2b + 1. \tag{5.24}$$

In order to represent the upper bound of P_{outage} in a block-based form, after substituting (5.24) into (5.22), we arrive at

$$\begin{aligned} P_{\text{outage}} &\leq \frac{4^{2(MT_2b+1)}\left(\mathcal{M}-1\right)}{\min_{i\neq j}\delta_{ij}}\left[\left(\frac{1}{4\text{SNR}}\right)^{b}\right]^{MT_2+\frac{1}{b}} \\ &\leq \frac{4^{2(MT_2b+1)}\left(\mathcal{M}-1\right)}{\min_{i\neq j}\delta_{ij}}\left(P_e\right)^{MT_2+\frac{1}{b}}, \end{aligned} \tag{5.25}$$

where P_e is the outage probability of a signal block (i.e. of an information-bit packet), which has the same definition as that given in [42, (2)]. Based on (5.25), the block based diversity order of our RSC coded GANC is given by

$$D_{\text{GANC}} = MT_2 + \frac{1}{b} \approx MT_2 + 1. \tag{5.26}$$

Hence, observe from (5.21) that, if perfect detection is achieved at every RN pertaining to the relay group A[7], the RSC coded GANC becomes capable of achieving the same diversity order as the NBLB coded GANC, or the DNC of [42], or the GDNC of [149].

Then, the average throughput of the whole system may be quantified by the ratio of the total number of transmitted information bits divided by the number of orthogonal time slots and codes required, which is similar to the concept of the overall rate defined in [149, (14)]. In line with [41, 42, 149], we also assume that every node in our GANC aided cooperative network transmits its messages at the same rate of X bits/s. Therefore, according to the transmission arrangement illustrated in Figure 5.1 and bearing in mind that we have $T_{\text{Broadcast}} = T_{\text{Cooperative}}$, the average throughput of our GANC aided cooperative network is given by

$$\mathcal{T}_{\text{ave}} = \frac{\overbrace{N \cdot T_{\text{Broadcast}} \cdot X}^{\text{Transmitted Information}}}{\underbrace{N \cdot T_{\text{Broadcast}} + M \cdot T_{\text{Cooperative}}}_{\text{Required Orthogonal Channels}}} = \frac{N}{N+M} \cdot X \quad \text{bits/s}. \tag{5.27}$$

Recall that in the ANCC regime of [41], the throughput $\mathcal{T}_{\text{ave}}$ is inherently constrained to $\frac{1}{2}$, since each SN will also serve as a RN during the cooperative phase, while in the DNC regime of [42] and GDNC regime of [149] different $\mathcal{T}_{\text{ave}}$ values can be achieved by varying the broadcast phase to cooperative phase duration. By contrast, based on (5.21), (5.26), and (5.27), our GANC aided cooperative network is capable of striking an arbitrary trade-off between the attainable diversity gain and the achievable throughput by appropriately adjusting the relay group size (or source group size). Since there may be an abundant supply of RN candidates constituted by the idle mobile users in the DS-CDMA uplink for constructing the relay group A, it is entirely unproblematic to allow nodes to join or disjoin the source group or the relay group A. Hence the technique of adjusting the diversity order and/or throughput facilitated by our GANC regime exhibits a high flexibility.

Furthermore, the precondition of employing the cooperative network in support of the cell-edge users of our DS-CDMA system is adopted here again, which was detailed in Section 3.1.

[7]For the NBLB coded GANC, it means that $|\mathcal{D}_{n,t_1}|$ in (5.20) equals to M.

Correspondingly, the RNs relied upon in our GANC regime are selected from the set of idle users of the DS-CDMA system. Hence we may argue that the user-specific PN sequence $\mathbf{C}_{a_m}$ assigned to the RN a_m may be readily exploited by our GANC aided cooperative network. Therefore we may observe that the GANC aided cooperative network only requires $T_{\text{Cooperative}}$ orthogonal time slots during the cooperative phase. Consequently, the average throughput $\mathcal{T}_{\text{ave}}$ in (5.27) becomes

$$\mathcal{T}_{\text{ave}} = \frac{N \cdot T_{\text{Broadcast}} \cdot X}{N \cdot T_{\text{Broadcast}} + T_{\text{Cooperative}}} = \frac{N}{N+1} \cdot X \quad \text{bits/s.} \tag{5.28}$$

As a result, the previously mentioned trade-off between the attainable diversity gain and achievable throughput may also be interpreted as a trade-off between the achievable transmission integrity of our GANC aided cooperative network and the potential user-load reduction of the DS-CDMA system.

Based on the analysis of the two typical applications of the proposed GANC regime employing NBLB codes and RSC codes as the cross-layer network code, respectively, it may be concluded that for a moderate network size, where the RNs are capable of affording a relatively high detection complexity, the RSC coded GANC scheme is preferred. By contrast, the NBLB coded GANC scheme will be preferred for large networks, especially when the RNs have different error correction capability. In more depth, it also reveals that the basic framework of our GANC aided cooperative network depicted in Figure 5.1 is capable of accommodating arbitrary channel coding schemes as our cross-layer network code, while retaining its adaptivity to both network topology changes and to link failures. Alternatively, the solutions of [41] and [149] may be treated as two specific realizations of our proposed GANC algorithm. Compared to the existing advanced network coding schemes of [41, 42, 149], our GANC aided cooperative network achieves a beneficial trade-off between the attainable diversity gain and the achievable throughput. Furthermore, our GANC aided cooperative network further benefits from the path-loss reduction achieved in the Source-to-Relay and Relay-to-Destination links, which will be demonstrated in Section 5.4.

5.2 Incorporation of Successive Relaying

As stated in Section 5.1.3, although the PN sequence $\mathbf{C}_{a_m}$ may be readily available for relaying, the proposed GANC aided regime still incurs a relative throughput loss of at least $\frac{1}{N+1}$, as the result of obeying the basic half-duplex three-terminal cooperative network arrangement. Hence, in order to recover the throughput loss, we amalgamated the successive relaying regime proposed in [43, 44] and in Section 1.2.4 as well as in Section 3.1 with our GANC aided cooperative scheme.

The DF based SRAN was introduced and analysed in Section 3.3, but for convenience, we highlight it briefly again in this section. The DF based SRAN regime is portrayed in Figure 5.9, where the SN s_1 employs two relays, namely a_1 and b_1 to alternately assist its Up Link (UL) transmissions. In more detail, in Phase 0 of Figure 5.9, s_1 broadcasts its information stream, while a_1 listens to s_1 and b_1 remains silent. Then, in Phase 1 of Figure 5.9, s_1 continues to broadcast its

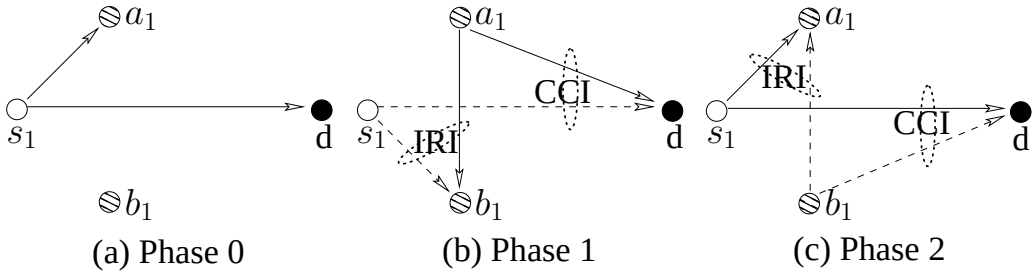

Figure 5.9: The framework of a typical SRAN

next information stream, while a_1 decodes, re-encodes and forwards the signals received from s_1 during Phase 0 and b_1 listens to s_1. By contrast, in Phase 2 of Figure 5.9, s_1 broadcasts its third information stream, but the roles of a_1 and b_1 are reversed. In the future phases, the transmission scheduling of Phase 1 and 2 portrayed in Figure 5.9 are repeated.

As emphasized in Sections 3.2 and Section 3.3, a critical problem of the SRAN is the successive relaying-induced inference imposed both on the RN and on the DN [44, 46], which constitute the inter-relay interference (IRI) and the co-channel interference (CCI), respectively. Observe in Figure 5.9 that the IRI arises due to the fact that the signal forwarded by one of the two RNs will contaminate the reception of the signal broadcast by the SN at the other RN. By contrast, the CCI arises due to the fact that the signal forwarded by the RN and that broadcast by SN may simultaneously arrive at the DN, where these signals will interfere with each other.

By adding another relay group, namely "relay group B" to the basic model of our GANC aided cooperation portrayed in Figure 5.1, as well as simultaneously replacing the previous transmission arrangement described in Section 5.1.1 by the successive relaying regime, we arrive at the GANC aided SRAN seen in Figure 5.10. Particularly, the transmission arrangements of the first and last phases in the SRAN are different from the other phases, as also seen in [102, Figure 1]. Nevertheless, when the total number of transmission phases in the SRAN is sufficently high, we may use the transmission arrangements of two typical phases, e.g. Phases 1 and 2 of Figure 5.9 to summarize the entire transmission arrangement of the SRAN, where the slight inaccuracies incurred during the first and last phases are ignored. In fact, this approximation has also been adopted during the decomposition process of the SRAN detailed in Section 3.2.2. Accordingly, the entire transmission arrangement of the GANC aided SRAN is summarized in the form of two typical phases, namely the "Even Phase" and "Odd Phase" of Figure 5.10.

Observe in Figure 5.10 that the relay group B consists of E RNs, namely "$b_1, \cdots, b_E$", which also uses the same signal processing as that detailed in Section 5.1.2 for relay group A. Consequently, when relay group B listens to the source group during the odd phase of Figure 5.10, each RN b_e generates its transmission frame $\mathbf{P}_{b_e}^l = \left[P_{b_e}^l[1], \cdots, P_{b_e}^l[K]\right]^T$, which carries the parity-bit stream $\mathbf{p}_{b_e}^l$. Then, the RN b_e forwards the signal frame $\mathbf{P}_{b_e}^l$ to the DN during the even phase. Similar to [43, 44], we assume that the GANC aided SRAN constituted by the source group, the relay

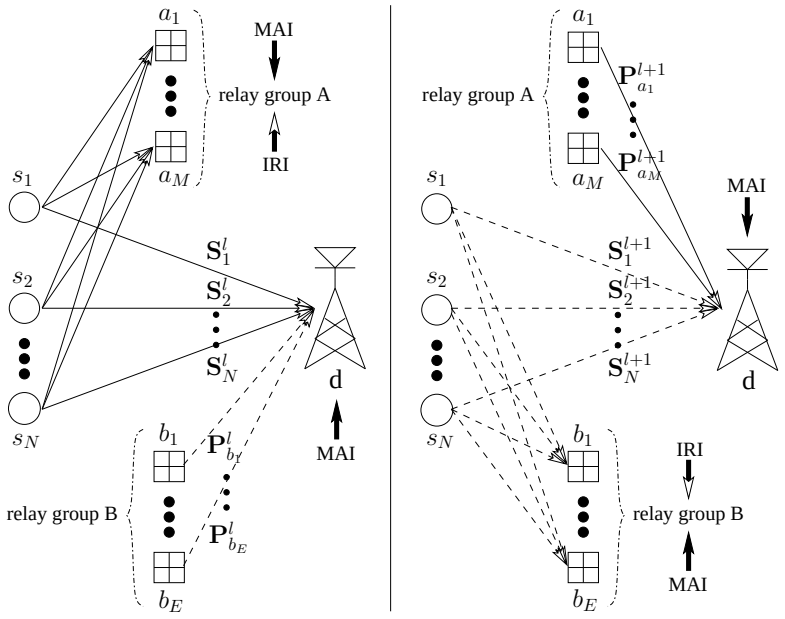

(a) Even Phase (b) Odd Phase

Figure 5.10: Schematic of the GANC aided SRAN

groups A and B, as well as the common DN d portrayed in Figure 5.10 are perfectly aligned in the time-domain by forming a synchronous system. Hence the k^{th} signal of the l^{th} frame received at the DN during the even phase of the GANC aided SRAN is given by

$$\mathbf{y}_d^l[k] = \sum_{n=1}^{N} \sqrt{G_{s_n d}} h_{s_n d}^l[k] \sqrt{\mathcal{P}_{s_n}} S_n^l[k] \mathbf{C}_{s_n} + \sum_{e=1}^{E} \sqrt{G_{b_e d}} h_{b_e d}^l[k] \sqrt{\mathcal{P}_{b_e}} P_{b_e}^l[k] \mathbf{C}_{b_e} + \sum_{w=1}^{W} \sqrt{G_{s_w d}} h_{s_w d}^l[k] \sqrt{\mathcal{P}_{s_w}} S_w^l[k] \mathbf{C}_{s_w} + \mathbf{n}_d^l[k], \tag{5.29}$$

where we have $l = 0, 2, 4, \cdots$. Then the k^{th} signal of the $(l+1)^{st}$ frame received at the DN in the consecutive odd phase of the GANC aided SRAN is given by

$$\mathbf{y}_d^{l+1}[k] = \sum_{n=1}^{N} \sqrt{G_{s_n d}} h_{s_n d}^{l+1}[k] \sqrt{\mathcal{P}_{s_n}} S_n^{l+1}[k] \mathbf{C}_{s_n} + \sum_{m=1}^{M} \sqrt{G_{a_m d}} h_{a_m d}^{l+1}[k] \sqrt{\mathcal{P}_{a_m}} P_{a_m}^{l+1}[k] \mathbf{C}_{a_m} + \sum_{w=1}^{W} \sqrt{G_{s_w d}} h_{s_w d}^{l+1}[k] \sqrt{\mathcal{P}_{s_w}} S_w^{l+1}[k] \mathbf{C}_{s_w} + \mathbf{n}_d^{l+1}[k]. \tag{5.30}$$

According to the signal processing stipulated in Section 5.1.2 and to the transmission arrangement of the GANC aided SRAN portrayed in Figure 5.10, the N signal frames $\{\mathbf{S}_n^l\}_{n=1}^N$ broadcast by the source group in the l^{th} frame (the even phase of Figure 5.10) and the M signal frames $\{\mathbf{P}_{a_m}^{l+1}\}_{m=1}^M$ forwarded by the relay group A in the $(l+1)^{st}$ frame (the odd phase of Figure 5.10) correspond to the information part and parity-bit part of the cross-layer network code output in the relay group A, respectively. Hence the receiver at the DN should collect these two types of signal frames in order to jointly detect the original information-bit streams $\{\mathbf{u}_n^l\}_{n=1}^N$. However, according to (5.29), the

information-bearing symbols $\{S_n^l[k]\}_{n=1}^N$ contaminate each other and are further contaminated by the other signal components of $\mathbf{y}_d^l[k]$, which impose CCI and MAI. The symbols $\{P_{a_m}^{l+1}[k]\}_{m=1}^M$ in (5.30) incur a similar interference problem. Fortunately, as a benefit of operating our GANC aided SRAN in the context of a DS-CDMA system, we may exploit the DS-CDMA philosophy to retain the desired component in $\mathbf{y}_d^l[k]$ (or $\mathbf{y}_d^{l+1}[k]$), while suppressing the interference components. Explicitly, it is similar to the interference suppression strategy implemented in Section 3.1, Section 3.2 and Section 3.3.

In more detail, similar to the operations involved in (5.5), when the chip-waveform matched-filter of the DN is matched to the waveform of $\mathbf{C}_{s_n}$, the symbol $S_n^l[k]$ directly transmitted by the SN s_n will contribute the main component of the despread signal $\mathbf{y}_d^l[k]$, while the other components of (5.29) - including all the other information bearing symbols $\{S_i^l[k]\}_{i=1,\neq n}^N$ - become the interference components. The associated output of the chip-waveform matched-filter is given by

$$z_{s_n}^l[k] = \sqrt{G_{s_n d}} h_{s_n d}^l[k] \sqrt{\mathcal{P}_{s_n}} S_n^l[k] + I_{s^{\mathrm{Part}}d}^l[k] + I_{b^{\mathrm{All}}d}^l[k] + I_{\mathrm{MAI}}^l[k] + n_d^l[k], \tag{5.31}$$

where we have

$$\begin{aligned} I_{s^{\mathrm{Part}}d}^l[k] &= \sum_{i=1,\neq n}^{N} \sqrt{G_{s_i d}} h_{s_i d}^l[k] \sqrt{\mathcal{P}_{s_i}} S_i^l[k] \gamma_{s_i s_n}, \\ I_{b^{\mathrm{All}}d}^l[k] &= \sum_{e=1}^{E} \sqrt{G_{b_e d}} h_{b_e d}^l[k] \sqrt{\mathcal{P}_{b_e}} P_{b_e}^l[k] \gamma_{b_e s_n}, \\ I_{\mathrm{MAI}}^l[k] &= \sum_{w=1}^{W} \sqrt{G_{s_w d}} h_{s_w d}^l[k] \sqrt{\mathcal{P}_{s_w}} S_w^l[k] \gamma_{s_w s_n}. \end{aligned} \tag{5.32}$$

Similarly to the definition given in (3.44), the CCL between the PN sequences $\mathbf{C}_i$ and $\mathbf{C}_j$ is commonly represented by $\gamma_{ij}, i, j \in \{s_n, a_m, b_e, s_w\}$. We employ the Gold sequence set having a spreading factor of Q. Then, we specifically assign the PN sequences in order to guarantee that the CCL between any two nodes in the GANC aided SRAN constituted by the source group and the relay groups A as well as B is $-1/Q$. Let us define the transmit power of the SN s_n in a conventional SL DT based DS-CDMA uplink as $\mathcal{P}_{s_n}^{\mathrm{DT}}$. For the sake of a fair comparison, we assume that the overall transmit power of the system employing the proposed GANC aided SRAN and that of the system operating without a GANC aided SRAN are identical, which implies that

$$\sum_{n=1}^{N} \mathcal{P}_{s_n} + \sum_{e=1}^{E} \mathcal{P}_{b_e} = \sum_{n=1}^{N} \mathcal{P}_{s_n} + \sum_{m=1}^{M} \mathcal{P}_{a_m} = N \cdot \mathcal{P}_{s_n}^{\mathrm{DT}}, \tag{5.33}$$

where $\mathcal{P}_{s_n}$, $\mathcal{P}_{b_e}$ and $\mathcal{P}_{a_m}$ represent the transmit powers of the SN s_n, the RN b_e and the RN a_m in the GANC aided SRAN, respectively. In this chapter, the system's equivalent SNR is defined as $\mathrm{SNR} = 10\log_{10}\left(\frac{\mathcal{P}_{s_n}^{DT}}{N_0}\right)$, where N_0 represents the receiver's noise. In the ensuing Section 5.4, we will manage the transmit signal power of the SNs and RNs according to (5.33).

Furthermore, we also assume that the DS-CDMA based GANC aided SRAN benefits from perfect power control. Hence, as observed at the DN d of Figure 5.10, all the received signals

transmitted by the different users i.e. $\{s_n\}_{n=1}^{N}$ and $\{s_w\}_{w=1}^{W}$ should have the same signal power of $\mathcal{P}_s$. Based on our previous assumption of having perfect synchronisation within the GANC aided SRAN, the variances of the variables $I^l_{s^{\text{Part}}d}[k]$ and $I^l_{b^{\text{All}}d}[k]$ may be evaluated as

$$\mathbf{Var}\left[I^l_{s^{\text{Part}}d}\right] = (N-1)\frac{\mathcal{P}_s}{Q^2}; \mathbf{Var}\left[I^l_{b^{\text{All}}d}\right] = \sum_{e=1}^{E}\frac{G_{b_e d}\mathcal{P}_{b_e}}{Q^2}. \tag{5.34}$$

However, it is challenging to maintain perfect synchronisation across the entire DS-CDMA system, especially when considering the UL of a high-load scenario. Hence we assume that the transmissions $\{s_w\}_{w=1}^{W}$ of the W interfering users are asynchronous with the transmissions $\{s_n\}_{n=1}^{N}$ of the N desired users. Consequently, we encounter a similar power calculation problem to that discussed in Section 3.2.1.3. By exploiting the same principle based on the central limit theorem [110], the summation of W independent random variables may be modelled by the Gaussian distribution. Hence the component $I^l_{\text{MAI}}[k]$ in (5.31) may be approximated by a Gaussian variable. In line with [97, 157], by exploiting the Standard Gaussian Approximation method [111] derived by Pursley, the variance of the MAI in an asynchronous DS-CDMA system experiencing Rayleigh fading channels i.e. $I^l_{\text{MAI}}[k]$ may be approximated by

$$\mathbf{Var}\left[I^l_{\text{MAI}}\right] \approx \frac{1}{3Q}\sum_{w=1}^{W}\left(G_{s_w d}\mathcal{P}_{s_w}\right) = W\frac{\mathcal{P}_s}{3Q}. \tag{5.35}$$

As stated before, in order to detect the original information-bit streams $\{\mathbf{u}^l_n\}_{n=1}^{N}$, we also have to extract every symbol $P^{l+1}_{a_m}[k]$ from the received signal $\mathbf{y}^{l+1}_d[k]$ at the DN. Hence, similar to the operations invoked for generating $z^l_{s_n}[k]$ of (5.31), we match the chip-waveform matched-filter to the waveform of $\mathbf{C}_{a_m}$ of the $(l+1)^{st}$ frame. Then, we input the received signal $\mathbf{y}^{l+1}_d[k]$ to the chip-matched filter. The associated output is given by

$$z^{l+1}_{a_m}[k] = \sqrt{G_{a_m d}}h^{l+1}_{a_m d}[k]\sqrt{\mathcal{P}_{a_m}}P^{l+1}_{a_m}[k] + I^{l+1}_{a^{\text{Part}}d}[k] + I^{l+1}_{s^{\text{All}}d}[k] + I^{l+1}_{\text{MAI}}[k] + n^{l+1}_d[k], \tag{5.36}$$

where we have

$$\begin{aligned}
I^{l+1}_{a^{\text{Part}}d}[k] &= \sum_{j=1,\neq m}^{M}\sqrt{G_{a_j d}}h^{l+1}_{a_j d}[k]\sqrt{\mathcal{P}_{a_j}}P^{l+1}_{a_j}[k]\gamma_{a_j a_m},\\
I^{l+1}_{s^{\text{All}}d}[k] &= \sum_{n=1}^{N}\sqrt{G_{s_n d}}h^{l+1}_{s_n d}[k]\sqrt{\mathcal{P}_{s_n}}S^{l+1}_n[k]\gamma_{s_n a_m},\\
I^{l+1}_{\text{MAI}}[k] &= \sum_{w=1}^{W}\sqrt{G_{s_w d}}h^{l+1}_{s_w d}[k]\sqrt{\mathcal{P}_{s_w}}S^{l+1}_w[k]\gamma_{s_w a_m}.
\end{aligned} \tag{5.37}$$

Similar to the derivations of (5.34) and (5.35), the variances of the interference components $I^{l+1}_{a^{\text{Part}}d}[k]$, $I^{l+1}_{s^{\text{All}}d}[k]$ and $I^{l+1}_{\text{MAI}}[k]$ in (5.36) may be evaluated as

$$\mathbf{Var}\left[I^{l+1}_{a^{\text{Part}}d}\right] = \sum_{j=1,\neq m}^{M}\frac{G_{a_j d}\mathcal{P}_{a_j}}{Q^2}, \mathbf{Var}\left[I^{l+1}_{s^{\text{All}}d}\right] = N\frac{\mathcal{P}_s}{Q^2}, \mathbf{Var}\left[I^{l+1}_{\text{MAI}}\right] = W\frac{\mathcal{P}_s}{3Q}. \tag{5.38}$$

According to (5.31) and (5.36), the estimates $\{z_{s_n}^l[k]\}_{n=1}^N$ of the information-bearing symbols $\{S_n^l[k]\}_{n=1}^N$ and the estimates $\{z_{a_m}^{l+1}[k]\}_{m=1}^M$ of the parity-bit bearing symbols $\{P_{a_m}^{l+1}[k]\}_{m=1}^M$ become available for the decoding of the cross-layer network code. Furthermore, according to the symmetry of the GANC aided SRAN, the despread signals $\{z_{s_n}^{l+1}[k]\}_{n=1}^N$ and $\{z_{b_e}^{l+2}[k]\}_{e=1}^E$ - which correspond to the information part and parity part of the cross-layer code codeword - will be exploited by the cross-layer network code decoder for detecting the original information-bit streams[8] $\{\mathbf{u}_n^{l+1}\}_{n=1}^N$. This process is similar to that specified by (5.29), (5.30), (5.31) and (5.36).

Furthermore, recall our arguments from Section 5.1.3, namely that the PN sequences used by the RNs are readily available for our GANC aided SRAN, because they have already been assigned to the inactive users appointed as RNs. From this perspective, the average throughput $\mathcal{T}_{\text{ave}}$ of the GANC aided SRAN is capable of approaching X bits/s, which represents the fact that in our GANC aided SRAN, the SNs are allowed to continuously broadcast their information-bit streams, namely during both the broadcast and cooperative phases. In order to visualize the throughput improvement achieved by our GANC aided SRAN, the average throughputs of different network coding regimes are compared in Figure 5.11, where all the benchmarkers maintain the same diversity order for the sake of a fair comparison. In more detail, from the top to the bottom, the surfaces portrayed in Figure 5.11 correspond to the average throughputs achieved by our GANC aided SRAN, by our GANC assisted basic cooperative network, by the GDNC regime of [149] and by the DNC regime of [42], respectively. Then, the relay groups A and B are independent of each other, which implies that the size of the relay group B and the channel code used as the cross-layer network code of relay group B can be different from that of relay group A. This indicates the convenient flexibility of the proposed GANC aided SRAN, again.

5.3 Noncoherent Iterative Detection Based Transceiver Designed for the GANC Aided SRAN

Having introduced our GANC aided SRAN, we now need an appropriate practical transceiver. Since employing nonbinary liner block codes as the cross-layer network code had also been discussed in the context of other network coding regimes [41,42,149], we would like to dedicate more attention to our RSC code based GANC regime both in this transceiver design section and in the ensuing simulation section. Hence we designed the noncoherent iterative detection aided architecture of Figure 5.12. Without loss of generality, in Figure 5.12, we assume that the size of the source group is $N = 3$. The relay groups A and B have the same size of $M = E = 2$ and employ the same cross-layer network code.

As indicated in Section 5.2, $\{\mathbf{u}_n^l\}_{n=1}^N$ is broadcast during the l^{th} frame, which is related to the

[8]The information-bit streams $\{\mathbf{u}_n^{l+1}\}_{n=1}^N$ are broadcast in the $(l+1)^{st}$ frame and are represented by the dashed lines in the odd phase of Figure 5.10.

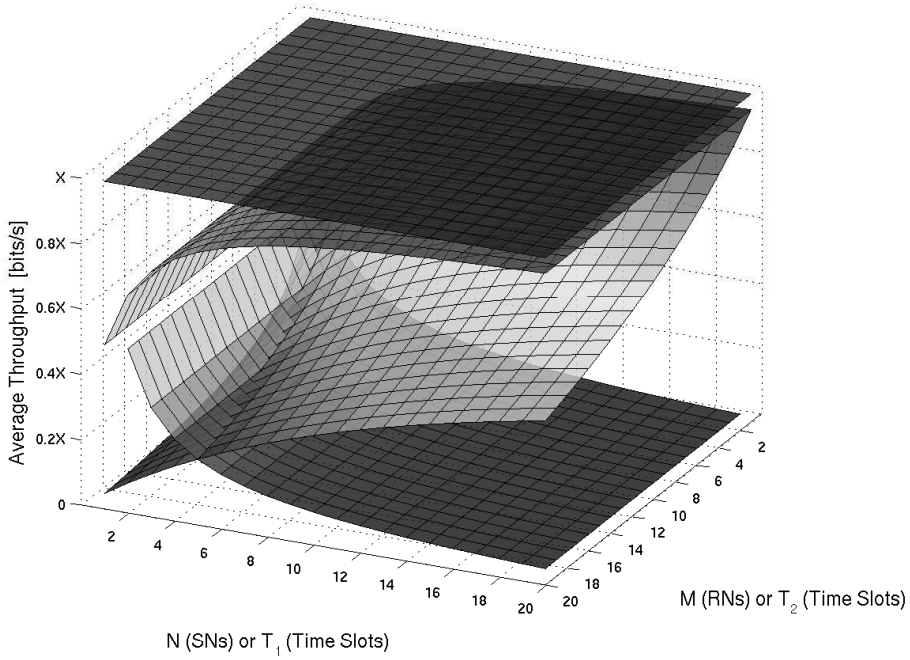

Figure 5.11: The average throughput comparison of different network coding regimes. In more detail, from the top to the bottom, the surfaces correspond to the average throughputs achieved by our GANC aided SRAN of Figure 5.10, by our GANC assisted basic cooperative network of Figure 5.1, by the GDNC regime of [149] and by the DNC regime of [42], respectively.

solid lines during the even phase of Figure 5.10. We collect the despread signals $\{z_{s_n}^{l}\}_{n=1}^{N}$ and $\{z_{a_m}^{l+1}\}_{m=1}^{M}$ in order to invoke cross-layer network code decoding at the DN d during the $(l+1)^{st}$ frame. Similarly, $\{\mathbf{u}_n^{l+1}\}_{n=1}^{N}$ is broadcast during the $(l+1)^{st}$ frame, which is related to the dashed lines in the odd phase of Figure 5.10. We collect the despread signals $\{z_{s_n}^{l+1}\}_{n=1}^{N}$ and $\{z_{b_e}^{l+2}\}_{e=1}^{E}$ for the sake of detecting $\{\mathbf{u}_n^{l+1}\}_{n=1}^{N}$ at the DN d during the $(l+2)^{nd}$ frame. Given the similarity of the above mentioned information-bit streams $\{\mathbf{u}_n^{l}\}_{n=1}^{N}$ and $\{\mathbf{u}_n^{l+1}\}_{n=1}^{N}$ at the DN d, we restrict our discussion to the detection of $\{\mathbf{u}_n^{l}\}_{n=1}^{N}$ in Figure 5.12. Furthermore, for simplicity, the superscript l is omitted from now on.

Then, given the above-mentioned similarity, most of the principles adopted in our previous transceiver designs, such as these in Figure 3.20, or in Figure 4.3, may be inherited in this section.

5.3.1 Source Node Architecture

In order to significantly enhance the error correction capability of the decoder, channel coding is invoked as an essential part of contemporary communication systems. Hence the classic RSC code having a coding rate of $R_{\text{code}} = \frac{1}{2}$ is employed at each SN s_n for encoding the original

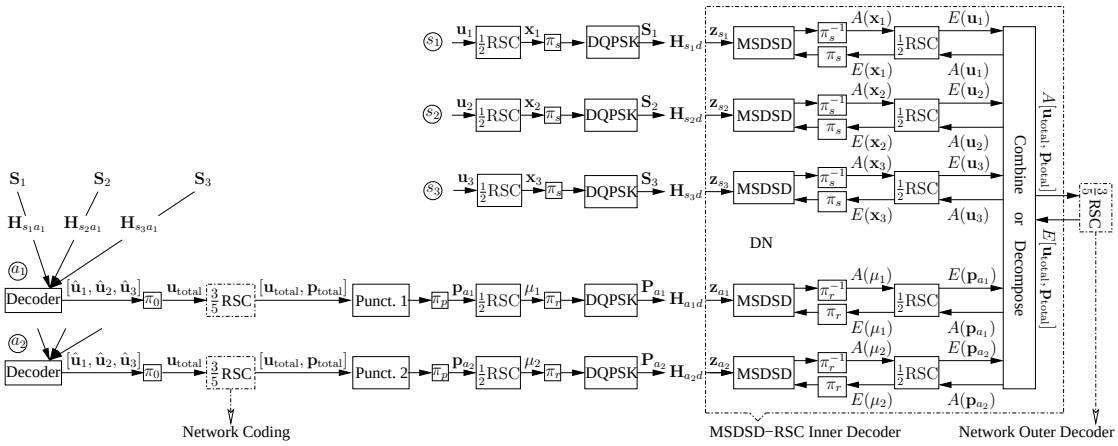

Figure 5.12: The architecture of the noncoherent iterative detection assisted GANC aided SRAN. This transceiver architecture is designed for practically implementing the proposed GANC aided SRAN portrayed in Figure 5.10, when the source group size is fixed to $N = 3$ and the relay group size is fixed to $M = 2$. Furthermore, similar to our previous transceiver designs seen in Figures 3.20 and 4.3, the three-stage iterative detection architecture is employed here again.

information-bit stream $\mathbf{u}_n$[9]. In addition to the complex task of relaying, the RNs have to afford the power-hungry estimation of SR channels in support of coherent detection. Furthermore, the overhead of channel estimation also reduces the system's bandwidth efficiency. Hence, for the sake of obviating the extra energy and bandwidth consumption imposed by employing coherent detection, a differentially-encoded QPSK (DQPSK) modulator is amalgamated with a half-rate RSC channel encoder for generating the signal frame $\mathbf{S}_n$, which dispenses with pilot-based channel estimation[10].

5.3.2 Relay Node Architecture

As stated in Section 2.5, the SISO-MSDSD algorithm was devised by Pauli *et al.* [55] in support of soft-decision-aided iterative detection schemes in the context of noncoherent detection based communication systems. As a state-of-the-art noncoherent detection technique, it strikes an attractive trade-off between the BER performance attained and the complexity imposed. Hence the SISO-MSDSD scheme may be adopted as the first component decoder of the RN's receiver in Figure 5.12. Then, in line with the SN's transmitter, the half-rate RSC decoder is adopted as the second component decoder of the RN's receiver. Consequently, a two-stage MSDSD-RSC decoder

[9]The choice of the channel coding rate is independent of the design of the network coding layer. If a high error correction capability is desired, we may further reduce the coding rate of the channel code at the cost of reducing the system's throughput, and vice versa.

[10]Although perfect channel-estimation (CE) aided coherent detection typically outperforms its noncoherent counterpart by about 3 dB, for a realistic practical CE, the difference becomes less substantial.

is created for detecting the information-bit streams $\{\mathbf{u}_n\}_{n=1}^{N}$ at each RN a_m, which is illustrated in Figure 5.13. For simplifying the illustration of our entire transceiver architecture, we simply label

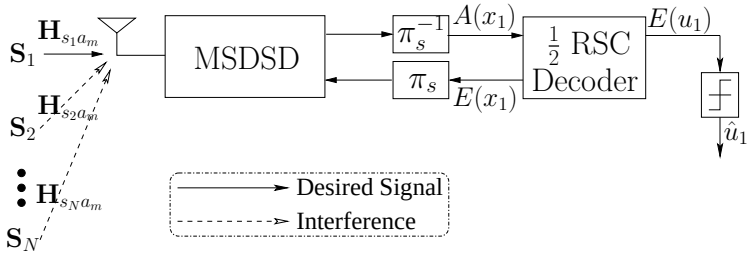

Figure 5.13: The architecture of the RN's decoder. In line with the SN's two-stage transmitter shown in Figure 5.12, a two-stage iterative detection architecture is devised for the RN's receiver, where the SISO-MSDSD decoder introduced in Section 2.5 is employed as the inner decoder.

the RN's two-stage MSDSD-RSC decoder as "Decoder" at the left of Figure 5.12.

In the spirit of GANC, arbitrary channel codes can serve as the cross-layer network code. However, employing LDPC codes and linear block codes for cross-layer network code was proposed in [41] and [149], respectively. In our low-complexity system, we opt for the conventional RSC code as our cross-layer network code and demonstrate that this low-complexity RSC code is capable of achieving a high performance. According to the first signal processing step stipulated in Section 5.1.2 that ***assign the ratio of the source group size and the relay group size to the coding rate*** R_{code} ***of the cross-layer network code***, the coding rate of the cross-layer network code scheme should be $R_{\text{code}} = \frac{3}{5}$ at both a_1 and a_2. As the second step, we concatenate a half-rate RSC code with a $\frac{5}{6}$-rate puncturer, where the octally represented generator polynomials and the constraint lengths of the half-rate RSC code are $(5, 7)$ and 3, respectively. As the third step, a_1 extracts half the bits from the entire set of parity-bits $\mathbf{p}_{\text{total}}$ as its parity-bit stream $\mathbf{p}_{a_1}$. Similarly, a_2 extracts the remaining parity-bits of $\mathbf{p}_{\text{total}}$ in order to create its parity-bit stream $\mathbf{p}_{a_2}$. Two punctures, namely "Punct.1" and "Punct.2" of Figure 5.12 are employed for the appropriate partitioning of the bit stream $\mathbf{p}_{\text{total}}$. Furthermore, two interleavers, namely "π_0" and "π_p" of Figure 5.12 are employed for eliminating the potential fading-induced correlation, as stated in Section 5.1.2.

The same transmitter may be employed at the RNs a_1 and a_2 as at the SN, in order to generate, as well as to modulate the parity-bit streams $\mathbf{p}_{a_1}$ and $\mathbf{p}_{a_2}$ for the sake of creating the transmitted signal frames of $\mathbf{P}_{a_1}$ and $\mathbf{P}_{a_2}$, respectively.

5.3.3 Destination Node Architecture

For appropriately complementing the SN's and RN's transmitter architecture, five two-stage MSDSD-RSC decoders are employed at the DN, which were introduced in Section 5.3.2. They individually detect the information bit streams $\{\mathbf{u}_n\}_{n=1}^{N}$ and the parity-bit streams $\{\mathbf{p}_{a_m}\}_{m=1}^{M}$ based on both

the despread signal frames $\{\mathbf{z}_{s_n}\}_{n=1}^{N}$ and $\{\mathbf{z}_{a_m}\}_{m=1}^{M}$ as well as on the information fed back by the cross-layer network code decoder of Figure 5.12. The *extrinsic* information and *a priori* information, represented by $E(\cdot)$ and $A(\cdot)$ respectively, are interleaved and iteratively exchanged I_{inner}^{d} times within the two-stage MSDSD-RSC decoder seen at the right of Figure 5.12.

As a benefit of the network coding process implemented at the RNs, the parity-bit streams $\{\mathbf{p}_{a_m}\}_{m=1}^{M}$ carry redundant bits related to the information-bit streams $\{\mathbf{u}_n\}_{n=1}^{N}$. After appropriately rearranging the *extrinsic* information frames $\{E(\mathbf{u}_n)\}_{n=1}^{N}$ and $\{E(\mathbf{p}_{a_m})\}_{m=1}^{M}$, their combination, namely $A\left[\mathbf{u}_{\text{total}}, \mathbf{p}_{\text{total}}\right]$ becomes capable of providing *a priori* information for the cross-layer network code decoder. Inspired by the JNCC scheme proposed by Hausl *et al.* in [150], we fed back the *extrinsic* information $E\left[\mathbf{u}_{\text{total}}, \mathbf{p}_{\text{total}}\right]$ provided by the cross-layer network code decoder to the five two-stage MSDSD-RSC decoders on the right of Figure 5.12. Naturally, the appropriate decomposition of $E\left[\mathbf{u}_{\text{total}}, \mathbf{p}_{\text{total}}\right]$ is required for mapping $E\left[\mathbf{u}_{\text{total}}, \mathbf{p}_{\text{total}}\right]$ to both $\{A(\mathbf{u}_n)\}_{n=1}^{N}$ and to $\{A(\mathbf{p}_{a_m})\}_{m=1}^{M}$. The five distributed two-stage MSDSD-RSC decoders actually constitute a single composite decoder conceived for cooperation with the cross-layer network code decoder of Figure 5.12. Hence this architecture may be viewed as a three-stage MSDSD-RSC-Network-Code receiver specifically created for the DN, where the composite decoder is constituted by five two-stage MSDSD-RSC decoder branches, acting in unison as the MSDSD-RSC inner decoder, while the cross-layer network code decoder acts as the outer decoder, as shown in Figure 5.12.

Observe at the base station of [150, Fig 4] that there is no FEC decoder for specifically detecting the RN's parity-bits. Hence, after entering the output of the RD link "$\mathbf{y}_{43}$" into the "Network Dec." of [150, Fig 4], the *extrinsic* information of the "Network Dec." can only be fed back to those particular channel decoders, which are used for detecting the SN's information bits. This implies that the redundant information contained in the RD link is utilized only once. However, as a benefit of its reduced propagation distance, the RD link may achieve a higher integrity than the SD link. Hence the original JNCC scheme proposed in [150] only partially benefits from the iterations between the channel code and network code, as well as from the redundancy received via the RD link. Hence, if we directly apply the original JNCC scheme of [150] to our decoder at the DN of Figure 5.10, it would be unable to exploit the *extrinsic* information $E\left[\mathbf{u}_{\text{total}}, \mathbf{p}_{\text{total}}\right]$ provided by the outer network code decoder for updating the *a priori* information $A\left(\mathbf{p}_{a_1}\right)$ and $A\left(\mathbf{p}_{a_2}\right)$ during the outer iterations between the MSDSD-RSC inner decoder and outer network code decoder. The resultant architecture may be referred to as a "partial-iteration" based three-stage MSDSD-RSC-Network-Code decoder. By contrast, the proposed DN's receiver portrayed in Figure 5.12 may be referred to as a "full-iteration" based three-stage MSDSD-RSC-Network-Code decoder, where the *a priori* information $A\left(\mathbf{p}_{a_1}\right)$ and $A\left(\mathbf{p}_{a_2}\right)$ is updated during each outer iteration between the MSDSD-RSC inner decoder and outer network code decoder.

In order to visualize the discrepancy between the "partial-iteration" and "full-iteration" based three-stage MSDSD-RSC-Network-Code decoders, the extrinsic information transfer (EXIT) [116] curves of their MSDSD-RSC inner decoders are compared in Figure 5.14, where the sizes of the

source group and relay group A were modified to $N = 2$ and $M = 2$, respectively[11]. It was shown in [130] that the area under the bit-based EXIT curve of the inner code approximates the maximum achievable coding rate of the outer channel code, while guaranteeing near-error-free communication. Hence the "full-iteration" based three-stage MSDSD-RSC-Network-Code decoder always outperforms its "partial-iteration" based counterpart throughout the entire range of SNR values considered. In more detail, observe in Figure 5.14 that as a detriment of losing the redundant information conveyed by the RD link, the EXIT curves associated with the "partial-iteration" based regime fails to approach the point of perfect convergence at $(1, 1)$ in the EXIT chart, which implies that a BER floor is expected to emerge.

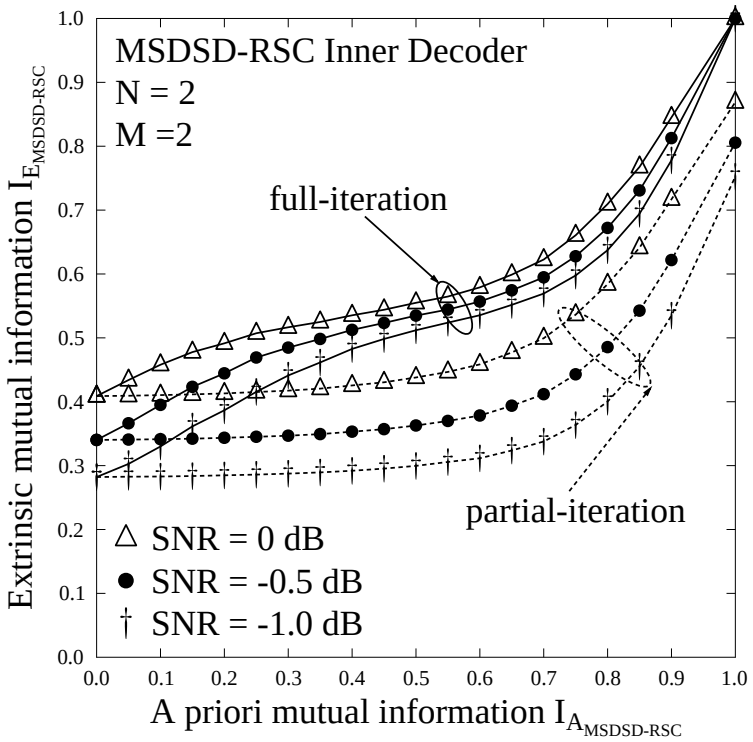

Figure 5.14: EXIT curve comparison between the "partial-iteration" and "full-iteration" based three-stage MSDSD-RSC-Network-Code decoders, where different SNR values are considered. The results are based on the schematic of Figure 5.12. Moreover, the source group size and the relay group size as well as the SNR values are explicitly shown in this diagram. The remaining parameters employed for generating the results are listed in Table 5.2.

By observing the entire transceiver architecture of Figure 5.12, again, we infer that when the size of the source group, or of the relay group A or B changes, we only have to modify the number of two-stage MSDSD-SRC decoder branches involved in the MSDSD-RSC inner decoder at the DN and then appropriately adjust the coding rate of the network code at the RNs and DN. The

[11]The purpose of opting for a different configuration with respect to that illustrated in Figure 5.12 in this simulation is to demonstrate the discrepancy between the two schemes more explicitly.

basic framework of the proposed transceiver still remains valid. Hence the proposed noncoherent "full-iteration" based three-stage transceiver also adapts to the time-variant network topologies.

5.4 Simulation Results and Discussions

In our simulations, we assumed that the component SNs of the source group seen in Figure 5.10 roam in each other's vicinity. Hence the distance between two SNs becomes negligible with respect to that between the SN and DN (or between the SN and RN). Accordingly, the entire source group is treated as a co-located unit, when considering the geometric relationship of the source group, relay group A, relay group B and DN. The same assumption is also applicable to the relay groups A and B. Hence the distances $D_{i,j}, i, j \in \{s_n, a_m, b_e, d\}$ are simplified to $D_{i,j}, i, j \in \{s, a, b, d\}$, where s, a, b, d represent the source group, relay group A, relay group B and DN, respectively. Moreover, we also assume having $M = E = 2$ and that an identical cross-layer network code is employed by the relay groups A and B. For the sake of concentrating our attention on the GANC aided SRAN, we assume having no interfering users i.e. $W = 0$. The main system parameters adopted in our simulations are summarized in Table 5.2.

Channel Model	Time-Selective Rayleigh Fading Channel
Path-Loss Exponent	$\alpha = 3$
Normalized Doppler Frequency	$f_d = 0.01$
Destination Proportion	$D_{sa} : D_{sb} : D_{ad} : D_{bd} : D_{sd}$ $\approx 1 : 1 : 1 : 1 : 1.732$
PN Sequence	Gold sequence: Q = 127
Interfering Users	W = 0
Channel Coding	half-rate RSC
Octal Generator Polynomials	$(5, 7)$
Cross-Layer Network Code	$\frac{N}{N+M}$-rate RSC
Memory Length of RSC	$v = 3$
Modulation Scheme	DQPSK
MSDSD Observation Window Size	$N_{wind} = 6$
Inner Iterations of DN's Decoder	$I^d_{inner} = 2$
Size of Relay Group A (or B)	2

Table 5.2: SYSTEM PARAMETERS

When two SNs constitute the source group of our GANC aided SRAN, the EXIT chart of the proposed three-stage MSDSD-RSC-Network-Code decoder at the DN is seen in Figure 5.15. Observe in Figure 5.15 that an open tunnel exists between the EXIT curves of the MSDSD-RSC inner

decoder and the outer network code decoder of Figure 5.12, when the system's overall equivalent SNR value reaches -0.4 dB. Furthermore, the associated Monte-Carlo simulation based decoding trajectory closely matches the EXIT curves and approaches the point of perfect convergence at $(1, 1)$ in the EXIT chart. Correspondingly, an infinitesimally low BER is expected beyond SNR $= -0.4$ dB. This is further evidenced in Figure 5.17, where the associated BER curve is seen to drop rapidly to an infinitesimally low value.

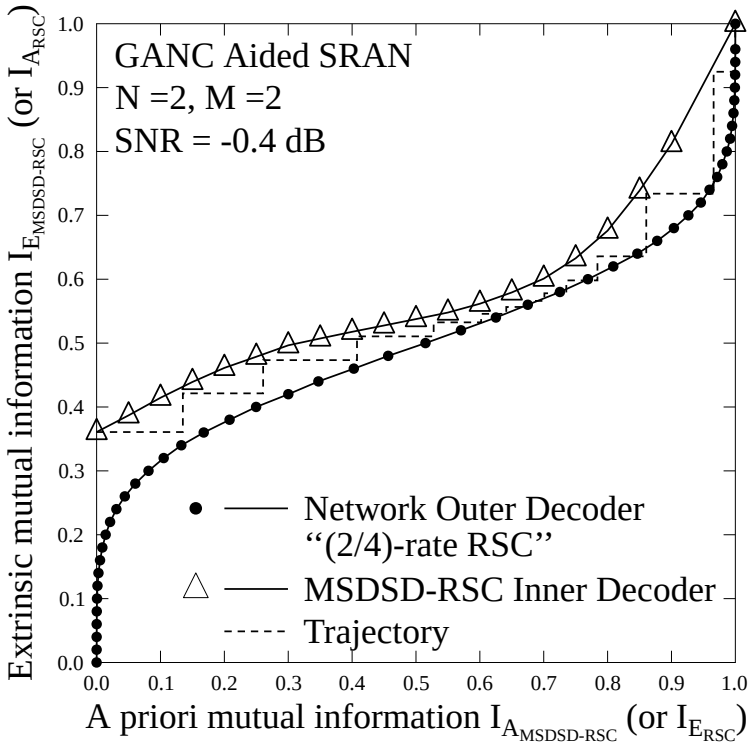

Figure 5.15: The EXIT Chart of the DN's three-stage concatenated iterative decoder seen in Figure 5.12, where a $\frac{2}{4}$-rate RSC code serves as the cross-layer network code. The remaining parameters are listed in Table 5.2

As stated in Section 5.1.3, the ratio of the source group size to the relay group size impacts both the potential user-load reduction of the DS-CDMA system as well as the achievable reliability of our GANC aided SRAN. For the sake of investigating the effect of different source group size to relay group size ratios, we added one more SN to the source group. The associated EXIT chart performance of the proposed three-stage MSDSD-RSC-Network-Code decoder recorded at the DN is shown in Fig 5.16. This time, an open tunnel exists between the EXIT curves of the MSDSD-RSC inner decoder and the outer network code decoder for equivalent SNR values in excess of 2.2 dB. According to (5.7), this observation is in line with the basic philosophy that increasing the ratio of the source group size to the relay group size is equivalent to degrading the coding gain of the cross-layer network code. Nevertheless, the benefit of this is that the potential user-load reduction imposed on the DS-CDMA system is mitigated.

In the spirit of our EXIT-chart analysis, the BER performance of different network topologies

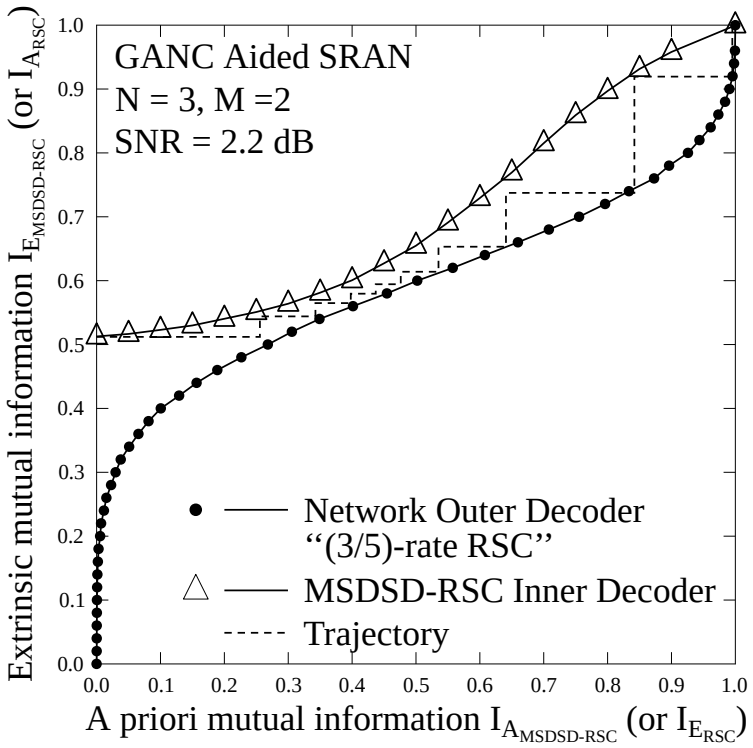

Figure 5.16: The EXIT Chart of the DN's three-stage concatenated iterative decoder seen in Figure 5.12, where a $\frac{3}{5}$-rate RSC code serves as the cross-layer network code. The remaining parameters are listed in Table 5.2

having different source group size to the relay group size ratios is provided in Fig 5.17, where the source group size increased from $N = 2$ to $N = 6$, while the relay group size is fixed to $M = 2$. It is demonstrated in Fig 5.17 again that increasing the source group size to relay group size ratio will degrade the system's BER performance. However, this degradation becomes more negligible, when increasing their ratio. As a benefit of employing the "full-iteration" based three-stage MSDSD-RSC-Network-Code decoder of Figure 5.12, a significant gain of about 10 dB is achieved compared to the simulation results shown in [150, Fig 9] at a target BER of 10^{-3}.

5.4.1 Analysing the Assumption of Achieving Perfect Detection at the RNs

All the simulation results provided in this section are based on the assumption that a perfect detection is achieved at the RN. Firstly, this assumption is supported by our GANC scheme detailed in Section 5.1.3, where the specific RN who cannot perfectly detect all the received SN's information-bit streams will be removed from the relay group. Secondly, as a benefit of the relay-aided path-loss reduction, as well as that of employing a two-stage MSDSD-RSC decoder at the RN, which has a powerful error-correction capability, the FER of the RN rapidly drops to a sufficiently low level. Consequently, we can successfully construct the GANC aided SRAN in the manner proposed in Section 5.3 with a high probability of P_{success}.

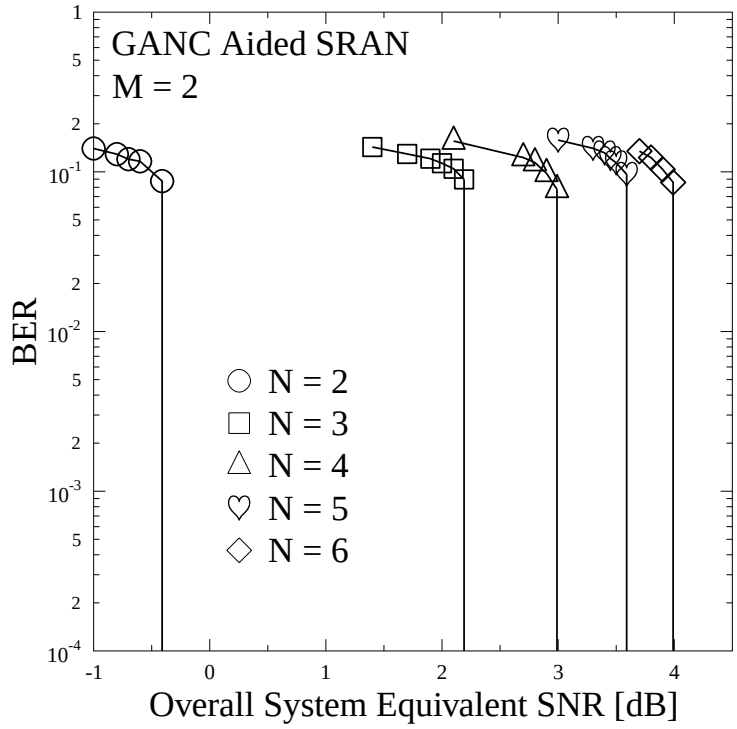

Figure 5.17: The BER vs SNR performance, when considering different network topologies, where the relay group size is fixed to $M = 2$, while the source group size increases from $N = 2$ to $N = 6$. The results are based on the schematic of Figure 5.12. The remaining parameters are listed in Table 5.2.

In more depth, let V represent the number of idle users available in the entire relay node resource pool $\mathcal{R}$. When aiming for a source group size of N and a relay group size of M, we have to select M idle users out of the V candidates as our RNs in order to construct the proposed GANC system, where the RN appointed should perfectly detect all the N source nodes' signal frames. Hence the probability of successfully constructing the GANC regime is identical to the probability that at least M idle users out of V RN candidates satisfy the "perfect detection" requirement, which may be formulated as[12]

$$P_{\text{success}} = \binom{V}{M} \overbrace{\left[(1-P_e)^N\right]^M}^{M \text{ valid candidates}} \overbrace{\left[1-(1-P_e)^N\right]^{V-M}}^{V-M \text{ invalid candidates}} + \binom{V}{M+1} \overbrace{\left[(1-P_e)^N\right]^{M+1}}^{M+1 \text{ valid candidates}} \overbrace{\left[1-(1-P_e)^N\right]^{V-M-1}}^{V-M-1 \text{ invalid candidates}} + \cdots + \overbrace{\left[(1-P_e)^N\right]^V}^{V \text{ valid candidates}}, \tag{5.39}$$

where P_e is the probability of erroneously decoding a signal frame $\mathbf{S}_n^l$. Hence $(1-P_e)^N$ is the probability that a RN perfectly decodes all the N signal frames $\{\mathbf{S}_n^l\}_{n=1}^N$. In practice, P_e equals to the frame error ratio (FER).

[12]For simplicity, we assume that every Source-to-Relay link has the same outage probability.

In Section 5.4, we investigated five different network topologies, which are obtained by specifying the generalized schematic of Figure 5.10, where M was fixed to 2, while N was increased from 2 to 6. In a practical DS-CDMA uplink, it is typically straightforward to find idle users, which are scattered randomly between the SN and DN. Hence it may be reasonable to assume that we have $V = 5$. Based on Eq.(5.39), the probability of successfully constructing our GANC regime associated with the above-mentioned five different network topologies is depicted in Figure 5.18.

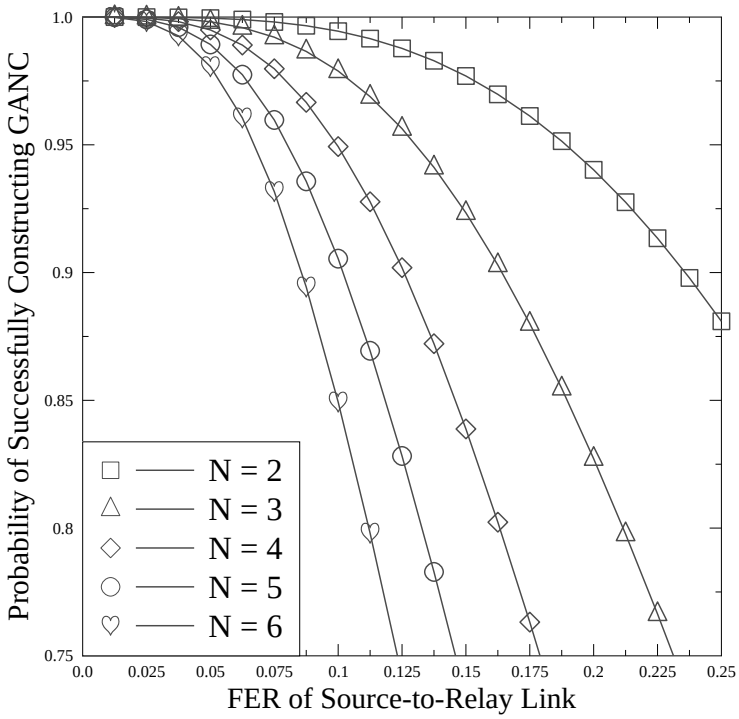

Figure 5.18: Probability of successfully constructing our GANC regime versus the FER of the SR link, where we have $V = 5$, $M = 2$, and N increases from 2 to 6. These P_{success} versus FER curves are pure theoretical results evaluated from (5.39).

From a practical perspective, we may require the probability of $P_{\text{success}} \geq 99.9\%$ as the minimum required probability of successfully constructing an RSC coded GANC system, where the condition of perfect Source-to-Relay transmission is guaranteed. Based on Figure 5.18, the associated FER thresholds are summarized in Table 5.3.

When $V = 5$; $M = 2$, for the sake of achieving $P_{\text{success}} \geq 99.9\%$					
N	2	3	4	5	6
FER (P_e)	≤ 0.07	≤ 0.04	≤ 0.035	≤ 0.025	≤ 0.02

Table 5.3: Associated FER (P_e) thresholds to be satisfied for the sake of achieving $P_{\text{success}} \geq 99.9\%$.

As illustrated in Figure 5.18, the probability of successfully constructing our GANC regime is determined by the FER of the SR link. Hence we focus our attention on the detection process carried out at the RN of Figure 5.13. Then the error correction capability of the two-stage MSDSD-RSC decoder depicted in Figure 5.13 is characterized in Figure 5.19, where a transmission frame consists of 9898 information bits and a single-link direct-transmission based DS-CDMA uplink scenario is considered, where the propagation distance is that of the SD link. Hence the transmit signal power used in Figure 5.19 is similar to $\mathcal{P}_{s_n}^{DT}$ defined in (5.33), which is represented by $\overline{\mathcal{P}_{s_n}^{DT}}$. Assuming that the variance of the noise imposed on the decoder is N_0, the SNR used in Figure 5.19 is defined as $\text{SNR} = 10\log_{10}\left(\frac{\overline{\mathcal{P}_{s_n}^{DT}}}{N_0}\right)$.

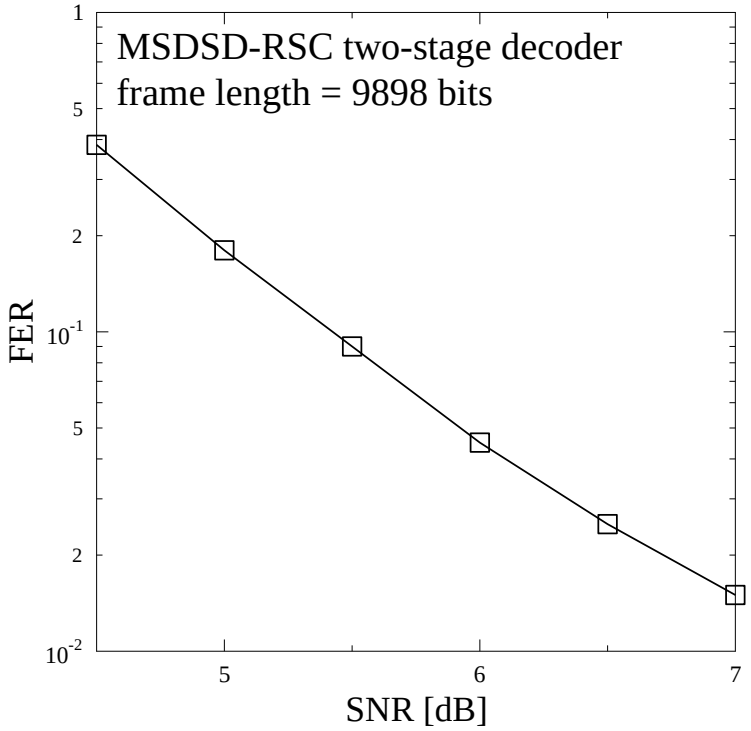

Figure 5.19: Error correction capability of the MSDSD-RSC two-stage decoder in terms of FER versus SNR. The results are based on the schematic of Figure 5.13 and the system parameters of Table 5.5.

Observe in Figure 5.19 that as expected, the FER is determined by the SNR value. Hence Table 5.3 is further extended to Table 5.5. For the sake of a fair comparison, we should set the overall transmit power of the system employing the proposed GANC regime to that of the system operating without the GANC regime. Let us consider the conventional direct-transmission based DS-CDMA uplink, where there are N SNs. Every SN transmits its signals at the same signal power of $\mathcal{P}_{s_n}^{DT}$. Hence the overall transmit power becomes $N \cdot \mathcal{P}_{s_n}^{DT}$. The propagation distance of these transmissions is equal to D_{sd}.

In order to maintain a fixed overall transmit power, when employing the GANC regime, we share the total power of $N \cdot \mathcal{P}_{s_n}^{DT}$ equally amongst $(N + M)$ nodes, i.e. amongst N SNs plus M

Transmission Scenario	Single-Link Direct-Transmission
Propagation Distance	Equal to the distance from SN to DN
PN Sequence	Gold Sequence $Q = 127$
Interfering Users	W = 0
Channel Model	Time-Selective Rayleigh Fading Channel
Normalized Doppler Frequency	$f_d = 0.01$
Channel Coding	half-rate RSC
Octal Generator Polynomials	$(5, 7)$
Memory Length of RSC	$v = 3$
Modulation Scheme	DQPSK
MSDSD Observation Window Size	$N_{wind} = 6$
Iteration Number of RN's Decoder	$I^r_{outer} = 2$
Frame Length	9898 bits

Table 5.4: System parameters used for generating the simulation results of Figure 5.19.

When $V = 5$; $M = 2$, for the sake of achieving $P_{\text{success}} \geq 99.9\%$					
N	2	3	4	5	6
FER (P_e)	≤ 0.07	≤ 0.04	≤ 0.035	≤ 0.025	≤ 0.02
$10\log_{10}\left(\frac{\overline{\mathcal{P}^{DT}_{s_n}}}{N_0}\right)$	≥ 5.6 dB	≥ 6.05 dB	≥ 6.25 dB	≥ 6.5 dB	≥ 6.75 dB

Table 5.5: The thresholds $10\log_{10}\left(\frac{\overline{\mathcal{P}^{DT}_{s_n}}}{N_0}\right)$ required for the sake of achieving $P_{\text{success}} \geq 99.9\%$. This table is an extension of the Table 5.3. Explicitly, observe in Figure 5.19 that every FER value corresponds to a certain SNR value. Hence the FER thresholds given in Table 5.3 are equivalently transformed to their associated $10\log_{10}\left(\frac{\overline{\mathcal{P}^{DT}_{s_n}}}{N_0}\right)$ thresholds in this table.

RNs. Hence the transmit signal power of a SN in the proposed GANC regime becomes $\mathcal{P}_{s_n} = \frac{N}{N+M} \cdot \mathcal{P}_{s_n}^{DT}$. However, as detailed in [107], when observing the RN of the proposed GANC regime, the benefit of the reduced propagation distance with respect to the SD link is equivalent to amplifying $\mathcal{P}_{s_n}$ by a factor of G_{sa}. Alternatively, if we transfer the SR link of the proposed GANC regime to the SD link assumed for generating Figure 5.19, the transmit signal power of the SN, namely $\mathcal{P}_{s_n}$, should be equivalently amplified by a factor of G_{sa}, while the variance of the noise imposed on the receiver remains N_0. Hence we arrive at

$$\begin{aligned} \mathcal{P}_{s_n} \cdot G_{sa} &= \overline{\mathcal{P}_{s_n}^{DT}} \\ \mathcal{P}_{s_n}^{DT} \cdot \frac{N}{N+M} \cdot G_{sa} &= \overline{\mathcal{P}_{s_n}^{DT}}. \end{aligned} \tag{5.40}$$

Accordingly, Table 5.5 is further extended to Table 5.6, where $10\log_{10}\left(\frac{\mathcal{P}_{s_n}^{DT}}{N_0}\right)$ is the system's

When $V = 5$; $M = 2$, for the sake of achieving $P_{\text{success}} \geq 99.9\%$					
N	2	3	4	5	6
FER (P_e)	≤ 0.07	≤ 0.04	≤ 0.035	≤ 0.025	≤ 0.02
$10\log_{10}\left(\frac{\overline{\mathcal{P}_{s_n}^{DT}}}{N_0}\right)$	≥ 5.6 dB	≥ 6.05 dB	≥ 6.25 dB	≥ 6.5 dB	≥ 6.75 dB
$10\log_{10}\left(\frac{\mathcal{P}_{s_n}^{DT}}{N_0}\right)$	≥ 1.44 dB	≥ 1.11 dB	≥ 0.85 dB	≥ 0.81 dB	≥ 0.84 dB

Table 5.6: The thresholds $10\log_{10}\left(\frac{\mathcal{P}_{s_n}^{DT}}{N_0}\right)$ required for the sake of achieving $P_{\text{success}} \geq 99.9\%$. The SNR used in Figure 5.19 or in Table 5.5 is defined as SNR $= 10\log_{10}\left(\frac{\overline{\mathcal{P}_{s_n}^{DT}}}{N_0}\right)$, which is different from the concept of the system's equivalent SNR, that was defined as $10\log_{10}\left(\frac{\mathcal{P}_{s_n}^{DT}}{N_0}\right)$ and employed extensively in Figures 5.14, 5.15, 5.16, 5.17. Hence, according to (5.40), the $10\log_{10}\left(\frac{\overline{\mathcal{P}_{s_n}^{DT}}}{N_0}\right)$ thresholds given in Table 5.5 are equivalently transformed to their associated $10\log_{10}\left(\frac{\mathcal{P}_{s_n}^{DT}}{N_0}\right)$ thresholds in this table.

equivalent SNR extensively employed in Chapter 5, e.g. in Figures 5.14, 5.15, 5.16, 5.17.

Hence, upon comparing Table 5.6 to Figure 5.17, we may conclude that the system's equivalent SNR values, which are seen to be sufficiently high in Figure 5.17 for reducing the system's BER to an infinitesimally low value for the cases of $N = \{3, 4, 5, 6\}$, are also capable of increasing the associated P_{success} values listed in Table 5.6 beyond 99.9%. This implies that for the $N = \{3, 4, 5, 6\}$ scenarios, the perfect detection condition expected at both the RN and at the DN can be simultaneously achieved for the SNR values observed in Figure 5.17. In the case of $N = 2$, we have to increase the SNR value from -0.4 dB to 1.44 dB in order to simultaneously achieve perfect detection at both the RN and at the DN. Therefore the idealized simplifying assumption that we always have perfect SR links, as assumed for generating the results of Figures 5.15 and 5.16

as well as 5.17 is not far from reality and hence may not significantly impair the accuracy of these simulation results.

5.5 Chapter Summary

In this chapter, we proposed a new GANC scheme. Upon intrinsically amalgamating the successive relaying protocol with our GANC aided cooperation, the GANC aided SRAN was created, where the typical 50% half-duplex relaying-induced throughput loss was converted to a potential user-load reduction of the DS-CDMA system. In order to improve the practicality of our investigations, a noncoherent iterative detection based transceiver was devised, which is capable of adapting to rapidly time-variant network topologies. The assumption of perfect detection at the RN will be eliminated in our future research by invoking the soft forwarding technique of [158] in our GANC aided cooperation.

Chapter 6

Conclusions and Future Work

In this concluding chapter, we will formulate overall design guidelines for successive relaying aided systems in Section 6.1, followed by a range of promising research topics in Section 6.2.

6.1 Conclusions and Design Guidelines

In this thesis, we proposed noncoherent successive relaying for multi-user wireless systems, which are capable of significantly improving the system's bandwidth efficiency by mitigating the half-duplex relaying-induced throughput loss. Furthermore, they are capable of circumventing the power-hungry channel estimation process at the cost of the typical 3dB power-loss. Hence, in the spirit of our discourse in Section 1.1, the proposed solutions are capable of striking an attractive compromise amongst the conflicting design factors highlighted in Figure 1.1, namely the **effective throughput**, the **attainable coding gain**, the **bit error ratio achieved** and the **computational complexity imposed**.

For the sake of constructing efficient noncoherent successive relaying (NC-SR) aided multi-user wireless systems, a range of advanced techniques and sophisticated analysis methods were devised, which are summarized below

- *Advanced noncoherent detection algorithms* - the MSDSD algorithm was introduced in Section 2.3, followed by the conception of the SISO-MSDSD algorithm introduced in Section 2.5, the relay-aided MSDSD technique of Section 3.1 and the relay-assisted SISO-MSDSD algorithm of Section 3.3.

- *Three-stage iterative-detection based transceiver design* - the relay-aided SISO-MSDSD assisted three-stage iterative transceiver was designed in Figure 3.20, while our MS-DIS plus our MSDSD assisted SECCC aided three-stage iterative transceiver was created in Figure 4.3, followed by the GANC based JNCC assisted noncoherent three-stage iterative transceiver of

Figure 5.12.

- *Interference suppression techniques* - the DS-CDMA multiple access technique was exploited in Sections 3.2, 3.3, 5.1 and 5.2, while the adaptive MS-DIS technique was invoked in Sections 4.2 and 4.3.

- *Efficient wireless networking* - the GANC scheme was employed in Sections 5.1 and 5.2, while our JNCC scheme was investigated in Section 5.3.

- *DCMC capacity* - the DCMC capacities of the systems considered were derived in Sections 3.2, 3.3 and 4.4.

- *EXIT-chart based analysis* - EXIT-chart based analysis was invoked in Sections 3.3, 4.5 and 5.4.

These salient techniques employed in support of our proposed NC-SR aided multi-user systems are also briefly summarized in Table 6.1.

Advanced Techniques	The Sections Involved
Advanced noncoherent detection algorithms	2.3, 2.5, 3.1 and 3.3
Three-stage iterative-detection based transceiver designs	3.3, 4.3 and 5.3
Interference suppression techniques	3.2, 3.3, 4.2, 4.3, 5.1 and 5.2.
Efficient wireless networking	5.1, 5.2 and 5.3.
DCMC capacity based characterization	3.2, 3.3 and 4.4.
EXIT-chart based analysis	3.3, 4.5 and 5.4.

Table 6.1: Critical techniques in support of our NC-SR aided multi-user wireless systems proposed in this treatise.

6.1.1 Conclusions

- **Chapter 2**: In Chapter 2, we focussed our attention on noncoherent differential multiple-symbol joint detection techniques, commencing with the mathematical principles of the MSDD algorithm in Section 2.2. We demonstrated that it is capable of recovering the performance degradation of the CDD, when experiencing severely time-selective Rayleigh fading associated with a high Doppler frequency. However, its complexity might become excessive in realistic practical applications. Consequently, it was further developed to conceive the MSDSD algorithm, which was detailed in Section 2.3. The MSDSD algorithm strikes an attractive trade-off between the achievable BER performance and the complexity imposed. It was demonstrated in Figure 2.8 that the MSDSD algorithm is capable of shifting the BER

curve towards the NC differential detector's optimum performance bound. Figure 2.9 indicated that the complexity imposed by MSDSD is directly related to the observation window size and to the SNR value. In order to process the multiple-path components received at the destination of the cooperative network, an efficient multiple-path MSDSD algorithm was devised. Its decision rule as well as implementation were detailed in Section 2.4. Quantitatively, it was demonstrated in Figure 2.15 that the multiple-path MSDSD is capable of outperforming the classic single-link based coherent detection at target BERs below 10^{-3} with the aid of a sufficiently wide observation window ($N_{\text{wind}} > 4$) for $f_d = 0.03$. Finally, based on the hard-decision-aided MSDSD, we conceived the soft-decision-assisted SISO-MSDSD in Section 2.5, which constitutes the foundation of our relay-aided SISO-MSDSD algorithm employed throughout Chapter 3.

Naturally, the BER performance improvements of the noncoherent detection schemes introduced in Chapter 2 were achieved at the cost of imposing an increased complexity. Bearing the conflicting design factors of Figure 1.1 in mind, we characterise the trade-off between the power gain attained and the extra complexity imposed. Consequently, the power gain versus complexity of the multiple-path MSDSD is visualized in Figure 6.1. Specifically, according to Figure 6.1, we may conclude that the triple-path MSDSD aided system of Figure 2.14 is capable of striking a better trade-off between the power gain attained and the extra complexity imposed, than the twin-path MSDSD aided system of Figure 2.13.

- **Chapter 3**: In Chapter 3, we proposed a noncoherent successive relaying aided cooperative DS-CDMA system. Specifically, in Section 3.1, the successive AF relaying aided single-user DS-CDMA uplink was conceived as our basic system prototype and then, we devised a new hard-decision-based relay-aided MSDSD algorithm as its noncoherent detection scheme. As a benefit of the diversity gain gleaned, our basic prototype system is capable of reducing the power-dissipation by 8dB at the target BER of 10^{-4} compared to the classic "benchmark-II" of Table 3.1. Consequently, the BER criterion emphasized in Figure 1.1 was improved at the cost of imposing a higher computational complexity on the system. Then, we further developed our prototype system from the single-user scenario to a more realistic multi-user scenario in Section 3.2. In this section, we revealed the noise accumulation problem imposed by the IRI in our system, which was mitigated by a DS-CDMA based interference suppression regime. As a theoretical contribution, the noncoherent DCMC capacity of the AF based SRAN embedded in the multi-user DS-CDMA uplink was derived in Section 3.2.2. The DCMC capacity results of Figure 3.14 indicated that the capacity of the AF based SRAN significantly exceeds that of conventional AF relaying or that of single-link direct-transmission, provided that RNs located at the appropriate positions are appointed. Hence, both the effective throughput and the BER will be improved as a benefit of employing the AF based SRAN. Finally, in Section 3.3, we further developed our basic prototype of Section 3.1 in order to construct the successive DF relaying aided multi-user DS-CDMA uplink for the

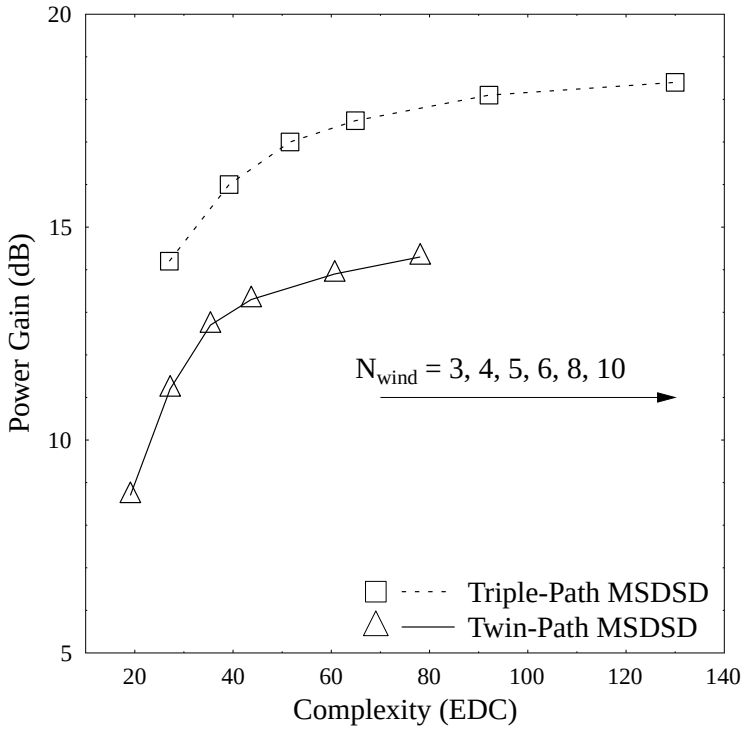

Figure 6.1: Power gain versus complexity for the multiple-path MSDSD, where the normalized Doppler frequency is fixed to $f_d = 0.03$, the target BER is BER $= 10^{-4}$, the SNR required by the single-link MSDSD algorithm having $N_{\text{wind}} = 6$ for approaching the target BER of 10^{-4} is regarded as the benchmark. The results of the "twin-path" system are based on the schematic of Figure 2.13, while the results of the "triple-path" system are based on the schematic of Figure 2.14.

sake of remarkably improving the system's energy efficiency. The noncoherent DCMC capacity of the DF based SRAN embedded in the multi-user DS-CDMA uplink was derived. The related simulation results portrayed in Figure 3.17 revealed that the DF based SRAN outperforms the AF based SRAN, especially in the low-SNR region (SNR $<$ 0dB). In the spirit of improving the system's energy efficiency, the hard-decision-based relay-aided MSDSD was then replaced by a novel soft-decision-based relay-aided SISO-MSDSD algorithm in Section 3.3.3. As a further advance, a relay-aided SISO-MSDSD assisted three-stage iterative transceiver was designed for efficiently implementing the proposed DF based SRAN. Observe in Figure 3.23 that this transceiver architecture attains a performance within about 2.6dB of the DF-based SRAN's capacity.

In Figure 6.2, we quantitatively characterize the compromise between the BER performance attained and the extra complexity imposed by the successive DF relaying aided multi-user DS-CDMA uplink introduced in Section 3.3. As expected, Figure 6.2 demonstrated that the BER was improved upon investing an increased computational complexity in terms of increasing the number of outer iterations. Furthermore, increasing I^d_{outer} to 9 will result in

an infinitesimally low BER, as shown in Figure 3.22.

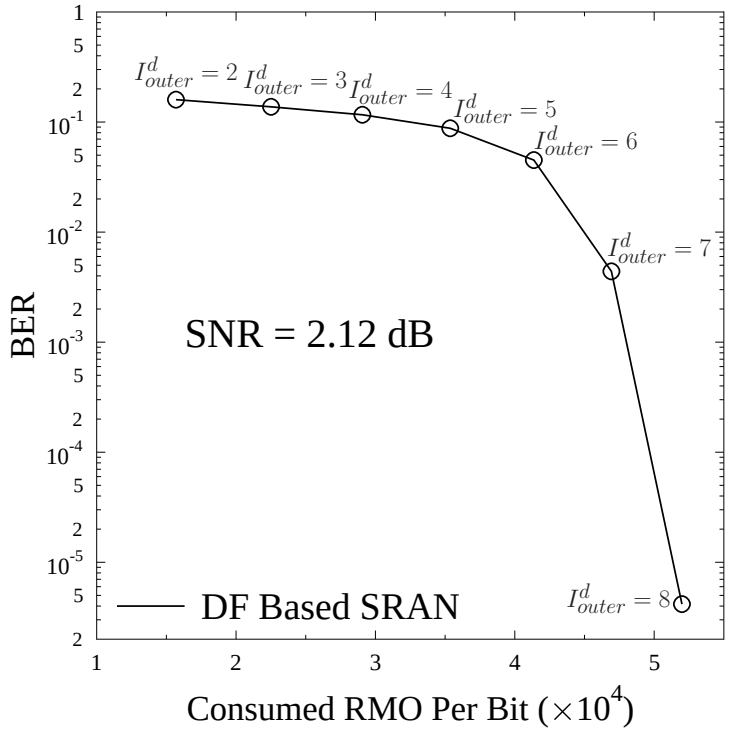

Figure 6.2: The BER performance versus the complexity per bit, where the number of outer iterations of the DN's three-stage turbo decoder seen in Figure 3.20 was increased from $I^d_{outer} = 2$ to $I^d_{outer} = 8$, while the SNR value was fixed to 2.12 dB. The results are based on the schematic of Figure 3.20. The remaining parameters employed for generating the results are listed in Table 3.3.

- **Chapter 4**: Employing the classic DS-CDMA principle relying on link-specific spreading codes is beneficial in terms of suppressing the IRI and CCI incurred in our noncoherent successive relaying aided systems, but this may lead to a potential user-load reduction for the CDMA system. Since each relay-aided link requires two spreading sequences, rather than one. Suppressing the successive relaying induced interferences without requiring any extra orthogonal spreading sequences and without any CSI remains an open challenge at this stage. However, in Chapter 4, we attempted to overcome this challenge with the aid of our novel MS-DIS regime, which is constituted by an amalgam of the adaptive modified Newton algorithm and the SISO-MSDSD algorithm. Our system model was described in Section 4.1, where a DF based SRAN consisting of only four nodes was considered. In Section 4.2, the basic principles of the adaptive MS-DIS regime were discussed. As a further advance, a MS-DIS plus relay-aided SISO-MSDSD assisted three-stage turbo transceiver was designed in Section 4.3, where the adaptive MS-DIS filter of Section 4.2 was employed as the first component of the DN for the sake of suppressing the interference. The noncoherent DCMC capacity of the multiple-antenna aided DF based SRAN was derived in Section 4.4

as a benchmarker for assessing the proposed transceiver's performance. We demonstrated in Section 4.5 that the proposed MS-DIS filter aided transceiver is capable of efficiently suppressing the interference at the expense of imposing as little as 2% training overhead, despite experiencing severely time-selective Rayleigh fading.

- **Chapter 5**: In this chapter we returned to the DS-CDMA assisted noncoherent SRAN of Section 3.3, where a multi-user, multi-relay scenario was considered. In order to efficiently organize the cooperation among the multiple nodes of a large-scale wireless network, we invoked the advanced ANCC regime [41] and further developed it to conceive the GANC of Figure 5.1, which was then incorporated into the noncoherent SRAN of Figure 5.10. More explicitly, in Section 5.1, we devised the GANC regime based on the ANCC and DNC regimes, which allows arbitrary channel coding schemes to serve as the cross-layer network code, while remaining adaptive to both the network's topology changes and to link failures. The associated transmission arrangement, the related signal processing, as well as the major advantages of the NBLB coded GANC and of the RSC coded GANC were detailed in Section 5.1 for two typical instances. Then we incorporated the proposed GANC regime of Figure 5.1 into the successive DF relaying aided multi-user multi-relay DS-CDMA uplink in Section 5.2. Consequently, in Section 5.3, an iterative detection based three-stage transceiver architecture was created for realizing the proposed GANC aided noncoherent SRAN, where the JNCC concept was employed. Again, the proposed transceiver is also capable of adapting to network topology changes. The robustness of the proposed GANC aided noncoherent SRANs having different source group size to relay group size ratios was investigated in Section 5.4 with the aid of the EXIT chart analysis method.

  The power gain versus complexity performance of the GANC aided SRAN is characterised in Figure 6.3. The solid triangle portrayed at the bottom-left corner of Figure 6.3 represents our benchmarker, which is the SNR gain versus complexity performance for a single-link direct-transmission based three-stage SISO-MSDSD-URC-RSC decoder aided system. According to our principle of calculating the SNR gain and the complexity imposed, as introduced in the caption of Figure 6.3, the SNR gain of our benchmarker is equal to 0 dB and it requires only a single SISO-MSDSD decoder. Hence the associated index of our benchmarker in Figure 6.3 should be $(1.0, 0)$, which is marked by the triangle in Figure 6.3. Then, the square portrayed at the right hand side of Figure 6.3 represents the SNR gain versus complexity characteristics of the SRAN shown in Figure 3.20. According to Figure 3.21, the relay-aided SISO-MSDSD decoder employed in Figure 3.20 approximately doubles the complexity of a single-path SISO-MSDSD decoder. Hence the SRAN illustrated in Figure 3.20 may be equivalently regarded as employing two SISO-MSDSD decoders for a single user. Hence its normalized complexity in Figure 6.3 equals to 2. According to Figure 3.23, the SNR gain compared to our benchmarker is $(6.05 - 2.1) = 3.95$ dB, which is marked by the square in Figure 6.3 at the position $(2.0, 3.95)$.

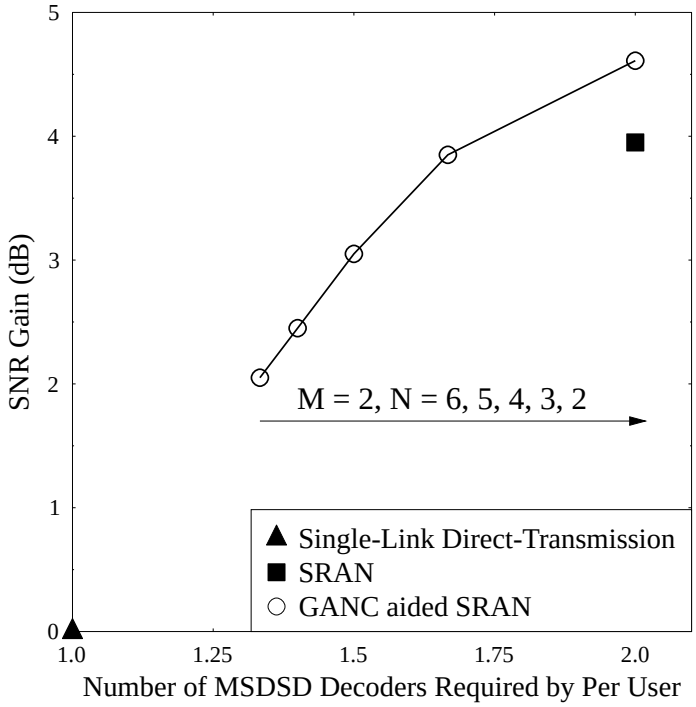

Figure 6.3: SNR gain versus complexity performance for the GANC aided SRAN of Figure 5.10, when considering different network topologies, where the relay group size is fixed to $M = 2$, while the source group size reduces from $N = 6$ to $N = 2$. The SNR required by a single-link direct-transmission based three-stage SISO-MSDSD-URC-RSC decoder aided system for approaching an infinitesimally low BER is used as our benchmarker, which equals to 6.05 dB, as shown in the simulation results of Figure 3.23. Then, as a somewhat unconventional metric, the number of SISO-MSDSD decoders required per user is employed as our metric for characterising the system's complexity. For example, observe in Figure 5.12 that a GANC aided SRAN having $M = 2$, $N = 3$ employs five SISO-MSDSD decoders at the DN in support of $N = 3$ users. Hence the number of SISO-MSDSD decoders required per user is equal to "$\frac{5}{3}$". The associated SNR required by this transceiver for approaching an infinitesimally low BER is 2.2 dB, as shown in Figure 5.17. Hence its SNR or power gain is given by $(6.05 - 2.2) = 3.85$ dB. According to similar principle and based on Figures 3.23, 5.17 as well as on Tables 3.3, 5.2, we arrive at the results shown in this diagram.

Upon comparing the rightmost circle[1] to the solid square in Figure 6.3, we may conclude that combining two DF based SRANs and operating them with the aid of the proposed GANC regime of Figure 5.10 is capable of attaining a power gain of 0.66 dB compared to operating them independently, i.e. without any cooperation with each other, whilst imposing the same complexity on the system. Accordingly, the GANC aided SRAN proposed in Chapter 5 strikes a better trade-off between the robustness attained and the complexity imposed in comparison to the classic SRAN of Figure 3.10 as proposed in Chapter 3. Hence, from the perspective of Figure 1.1, the overall performance of the system may be considered to be further improved.

6.1.2 Design Guidelines

Improving the overall quality of wireless systems in terms of striving for a better compromise amongst the conflicting design factors of Figure 1.1 is the basic motivation of our designs. These efforts led to the design guidelines listed below:

- As a benefit of having a high spatial diversity order, MIMOs improve the throughput and/or robustness of classic single-antenna-aided systems, since they may be able to increase the achievable throughput linearly, rather than logarithmically with the transmit power. Accordingly, it constitutes an important technique in support of the operational 3G or 4G wireless communication standards. Accordingly, in order to achieve a beneficial spatial diversity gain, we may opt for invoking the family of MIMO techniques.

- However, a crucial condition of actually achieving the spatial diversity gain promised by the family of MIMO techniques is that the multiple co-located antenna elements have to be sufficiently far apart for the sake of experiencing independent fading. In order to circumvent this limitation, we can rely on the cooperative communication techniques, where the single-antenna-based mobiles, which are sufficiently far apart may form a VAA.

- However, the conventional three-terminal, two-phase based cooperative systems impose a severe 50% multiplexing loss due to the half-duplex transmit/receive modes of practical contemporary transceivers.

- In order to recover the 50% throughput loss of half-duplex relaying, we may advocate the successive relaying regime of Section 1.2.4. The main idea is to utilize a pair of half-duplex relays for mimicking a full-duplex relay, where the relay's reception and transmission operations occur simultaneously, but they are assigned to different relays.

[1]This corresponds to the GANC aided SRAN having $N = 2$, $M = 2$. As stated in Section 5.4.1, for simultaneously achieving perfect detection at both the RN and at the DN in this GANC aided SRAN, we have to increase the SNR to 1.44 dB, as shown in Table 5.6. The SNR value of 1.44dB is also used for calculating the associated power gain in Figure 6.3.

- On the other hand, in support of a coherent MIMO system having M transmit antennae and N receive antennae, the associated estimation of $(M \times N)$ channels will significantly increase the computational complexity and may dissipate excessive battery-power, whilst imposing a high pilot overhead, especially at high normalized Doppler frequencies.

- Furthermore, it is somewhat unrealistic to expect that in addition to the task of relaying, the relay could altruistically afford the complex and power-hungry channel estimation of the source-to-relay link in support of coherent detection.

- Against this background, in the context of cooperative communication, we may propose the employment of noncoherent detection for the sake of operating without any requirement of channel estimation.

- The CDD of Section 2.1 typically imposes a 3 dB performance loss, which will be significantly aggravated in hostile channels experiencing a high Doppler frequency, where often a high error-floor is exhibited. The MSDD algorithm is capable of mitigating the CDD's performance degradation compared to its coherent counterpart, but this is achieved at the expense of imposing an extremely high computational complexity. As a remedy, the cluster of MSDSD algorithms strikes an attractive trade-off between the BER performance attained and the complexity imposed.

- Given the above-mentioned advantages of successive relaying and the associated MSDSD algorithms, we may beneficially combine them for the sake of constituting an attractive solution, which is capable of circumventing both the 50% throughput loss and the power-hungry channel estimation incurred in conventional half-duplex relaying aided systems. On the other hand, CDMA techniques constitute the basis of the commercial 3G wireless communication systems. Hence, in order to suppress the successive relaying induced interferences, we may additionally invoke the classic DS-CDMA technique, which results in the successive AF relaying aided single-user DS-CDMA uplink advocated in Section 3.1.

- For the sake of characterizing the impact of diverse sources of interference (MUI, CCI, IRI), we may then extend the communication scenario considered to multi-user scenarios. We may use the noncoherent DCMC capacity bound of the resultant successive AF relaying aided multi-user DS-CDMA uplink for quantifying its benefits over its conventional counterparts.

- In contrast to the AF protocol, the DF protocol of Section 1.2.2 may achieve a better BER performance, since it is capable of supporting the employment of sophisticated coding schemes. Another technique of significantly improving the system's energy efficiency is that of using the family of soft-decision-based MSDSD algorithms. However, employing the single-link SISO MSDSD of Section 2.3 and then operating in a classic distributed turbo decoding manner imposes a high complexity. For the sake of mitigating the complexity imposed, we devised the relay-aided SISO MSDSD algorithm of Section 3.3.3.

- The three-stage turbo decoding structure exhibits a powerful error-correction capability. Motivated by this advance, we designed a sophisticated relay-aided SISO-MSDSD assisted three-stage iterative-detection based transceiver architecture for improving the performance of the successive DF relaying aided cooperative multi-user DS-CDMA system.

- The successive relaying induced interference may be mitigated by the classic DS-CDMA technique of Section 3.1, despite dispensing with any CSI. However, this is achieved at the expense of a potential user-load reduction for the CDMA system, since each relaying link requires its own unique spreading sequence, rather than relying on a single spreading code.

- Alternatively, it is possible to suppress the interferences in a noncoherent communication system without requiring any extra unique spreading sequences with the aid of the DIS philosophy of Section 4.2. The resultant MS-DIS scheme created by a novel amalgam of the adaptive modified Newton algorithm and the SISO-MSDSD algorithm constitutes a powerful state-of-the-art DIS regime.

- Consequently, we may employ the MS-DIS filter at the DN. Hence, we in Section 4.2 designed a novel adaptive MS-DIS filter and relay-aided SISO-MSDSD decoder assisted three-stage iterative detection based transceiver architecture for a typical noncoherent DF based SRAN. This powerful transceiver is capable of efficiently suppressing the interference by imposing as little as 2% training overhead, even in the face of severely time-selective Rayleigh fading associated with a high Doppler-frequency.

- The classic DS-CDMA assisted noncoherent successive relaying regime is capable of improving the diversity-multiplexing trade-off by allowing more users and relays to join in the cooperation. Hence this regime is eminently applicable to a multi-user, multi-relay scenario. The cross-layer operation based network coding regime of Section 5.1 is capable of efficiently organizing the cooperation amongst the multiple users and multiple relays of a large-scale wireless network. Against this background, in Section 5.1, we further extended our research to a multi-user multi-relay DS-CDMA uplink and advocated the family of cross-layer network coding regimes.

- In order to counteract the hostile propagation properties and the dynamically varying topology of the wireless network, the concept of ANCC detailed in [41] may be used as a remedy. Furthermore, we generalized the ANCC to our GANC scheme, which allows arbitrary channel coding schemes to serve as the cross-layer network code, while still facilitating a high grade of adaptivity to both network topology changes and to propagation-induced link failures.

- Accordingly, in Section 5.2, we incorporated our GANC philosophy into the successive relaying regime for creating a powerful GANC aided SRAN based DS-CDMA system. In order to efficiently operate this GANC aided SRAN, in Section 5.3, we designed a JNCC

assisted iterative detection based three-stage transceiver, which is also capable of adapting to dynamically fluctuating network topology changes. Hence a large-scale wireless network supporting multiple users with the aid of multiple relays may be created by using the GANC aided SRAN, where the 50% throughput loss of conventional half-duplex relaying may be obviated.

6.2 Future Research

Our research results reported in this thesis have confirmed the benefits of the proposed noncoherent successive relaying technique. After appropriately combining it with the proposed sophisticated techniques, such as the MSDSD algorithm of [53], the network coding scheme advocated in [136, 137], as well as our differential interference suppression technique of [117], the resultant noncoherent successive relaying aided systems are capable of mitigating the half-duplex relaying induced 50% throughput loss, even when dispensing with CSI. Furthermore, the noncoherent successive relaying aided systems also achieve a competitive BER performance, while their complexity may still remain affordable for practical applications.

However, it is still possible to further improve the systems introduced in the previous chapters of this thesis in terms of striking a better compromise amongst the system's complexity, bandwidth/energy efficiency and achievable diversity order, which constitute a range of conflicting design factors, as shown in Figure 1.1. To elaborate a little further, we stipulated some idealized assumptions in order to simplify the relevant analyses. Naturally, it is necessary to dispense with these idealized assumptions in our future research for the sake of improving their grade of realism. Let us hence briefly discuss some of the open problems of noncoherent successive relaying aided systems.

6.2.1 Complexity Reduction for MSDSD Algorithms

As detailed in Chapter 2, the performance of noncoherent detection may be improved at the cost of an increased complexity. The multiple-symbol joint detection concept was conceived in [49, 71] and then, the sphere detection technique was invoked in [53, 55] for multiple-symbol differential detection. However, there is a whole range of further contributions dedicated to the complexity reduction of multiple-symbol joint differential detection. For example, Pun *et al.* [75] conceived the so-called "Fano-multiple symbol differential detection" principle, which imposes a lower complexity than MSDSD [53] in the low-SNR region. Ahmadi *et al.* [159] compared the performance versus complexity trends of the vertical Bell laboratories layered space-time (V-BLAST) aided MSDD to that of the Sphere Decoding aided MSDD regime. Furthermore, Schenk *et al.* [160] investigated a range of different stopping criteria conceived for MSDSD in terms of their achievable complexity reduction. All these investigations indicate that it is possible to further reduce the complexity of the

multiple-symbol differential detection algorithms employed in Chapters 3∼5.

More specifically, it appears promising to invest further research efforts into mitigating the complexity of the MAP-MSDSD algorithm introduced in Section 2.5.1 without eroding its error correction capability. When calculating the *a posteriori* LLRs according to the Max-Log-MAP algorithm [161] or using the Approx-Log-MAP algorithm [162], it appears potentially promising to rely only on the maximum probability metric, rather than on the conventional method of evaluating the probability metric associated with each legitimate symbol and then comparing them in order to find the most likely one. This brute-force method of finding the highest-probability decision-candidate has some redundant operations. If we could directly spot the highest-probability decision-candidate based on the knowledge of the CSI and of the modulation scheme without visiting each constellation point, then the detection complexity would be remarkably reduced. In this context, Xu *et al.* proposed an intelligent algorithm [163, 164] for directly spotting the highest-probability decision-candidate in the context of the MAP soft detection process, where the square-shaped L-ary quadrature amplitude modulation (QAM) modulation scheme was considered. Since the calculation of the *posteriori* LLRs is also involved in the SISO-MSDSD algorithm, this fundamental development of soft detection theory may also be applied to the SISO-MSDSD algorithm of [55] for further mitigating its complexity.

In more detail, according to (2.69), the incremental Euclidean distance of the SISO-MSDSD algorithm, which is imposed by the calculation of the i^{th} hypothetical information symbol $V[i]$, is given by

$$\triangle_i^2 \triangleq \left\{ \left| u_{i,i} a[i+1] V^*[i] + \sum_{l=i+1}^{N} u_{i,l} a[l] \right|^2 - \ln\Big(\Pr(V[i]) \Big) \right\}. \tag{6.1}$$

When implementing the SISO-MSDSD algorithm according to the process proposed in [55], we have to calculate each value of "$u_{i,l} \cdot a[l]$" in (6.1) and then sum them for evaluating $\triangle_i^2$. Once the value of $\triangle_i^2$ associated with each legitimate candidate symbol $V[i]$ was obtained, we arrange all the legitimate candidate symbols $V[i]$ in a increasing order of their associated $\triangle_i^2$ values. However, if we rewrite (6.1) in the spirit of [163, 164], we may find that the incremental Euclidean distance of the different candidate symbols $V[i]$ does have a common part. Hence we only have to calculate their distinctive part in support of the related $\triangle_i^2$-based ordering of all the legitimate information symbols $V[i]$. Consequently, the calculation of $\triangle_i^2$ associated with the different legitimate symbols $V[i]$ may be completed using a more simple process. Since the operations encapsulated in (6.1) will be frequently executed during the SISO-MSDSD decoding process, the complexity reduction contributed by the above-mentioned simplified calculation of $\triangle_i^2$ may significantly reduce the entire complexity of the SISO-MSDSD algorithm. This improved SISO-MSDSD algorithm may also be applied to our systems introduced in Chapters 3, 4, 5 for replacing the conventional SISO-MSDSD algorithm [55]. As a benefit, the SISO-MSDSD aided schemes proposed in these chapters may benefit from a reduced complexity.

6.2.2 Improve Our Iterative Decoders with the Aid of Irregular Codes

In order to achieve a substantially improved BER performance compared to hard-decision-based detection, iterative detection techniques have been extensively employed in our sophisticated transceiver designs, as shown in Figures 3.20 and 4.3 as well as 5.12. For the sake of characterizing our iterative decoders, we invoked the EXIT chart based analysis method of [116]. According to [116], it is beneficial to match the EXIT curve of the outer decoder to that of the inner decoder, while maintaining a narrow but still open tunnel between them. Consequently, a near-capacity performance may be obtained [102, 126, 165–167]. However, observe by inspecting the EXIT chart characteristics shown in Figures 3.22, 4.8, 5.16 that the open tunnels between the EXIT curve of the inner decoder and that of the outer decoder are still relatively wide. Since the area within this open tunnel can be shown to be proportional to the SNR-difference from the capacity, this indicates that further performance improvements may be attained.

In order to improve the EXIT chart characteristics of our iterative decoders proposed in Chapters 3, 4, 5, we may employ irregular convolutional codes (IrCC) as our outer decoder, which was proposed by Tüchler *et al.* in [168]. The IrCC amalgamates a number of component convolutional codes (CC) having different coding rates, each of which encodes an appropriately selected fraction of the input source information-bit stream. Hence, we may appropriately select the component code rates with the aid of EXIT chart analysis [169] and adjust the associated fractions of the source information-bit stream for the sake of shaping the inverted EXIT curve of the composite IrCC for ensuring that it remains close to the EXIT curve of the inner decoder throughout the entire mutual information interval of $[0, 1]$, but they never cross. In this way, the discrepancy between the "turbo-cliff" point and the associated system's capacity exemplified in Figure 3.23 will be further mitigated. Consequently, achieving a near-capacity performance becomes feasible.

6.2.3 Optimising the Resource Allocation for the Proposed SRAN

It was demonstrated in numerous sources [24, 170–173] that an appropriate resource allocation is capable of significantly improving the power efficiency and/or bandwidth efficiency of cooperative communications. One of the most important issues in this research area is that of finding the optimal power allocation (OPA) for a cooperative network, which results in a longer battery recharge-period, whilst imposing a reduced interference. Numerous studies have been conducted for finding the OPA, which may rely on diverse performance criteria. Explicitly, they might be aiming for minimizing the outage probability [27, 174], whilst considering different system configurations associated with either a single relay [175] or with multiple relays [171]. Another important issue of resource allocation is that of finding the optimal rate allocation (ORA) [109, 176]. Accordingly, assigning different transmission rates or equivalently, different transmission durations to the different nodes in a cooperative network according to their near-instantaneous channel conditions may further improve the bandwidth efficiency of the entire system compared to the conventional

rate allocation regime.

For the sake of simplifying our discourse, we consistently assumed that all the component nodes of our SRAN have the same transmission rate and transmit power. Hence the optimization of both the power allocation and of the rate allocation has been excluded. Furthermore, we also assumed that our noncoherent successive relaying aided networks have a symmetric network topology, which is rarely the case in practice.

Hence it is desirable to carry out the investigation of the above-mentioned advanced OPA and ORA regimes in the context of our noncoherent successive relaying aided systems. Since the OPA and ORA have only been considered in the context of conventional half-duplex, two-phase cooperative networks in previous studies, the incorporation of OPA and ORA into successive relaying requires further research attention. Furthermore, in contrast to assuming a symmetric network topology, it is more practical to consider a realistic random network topology, where the two RNs (or relay groups) appointed by our SRAN may have arbitrary geometric positions with respect to the SN and DN.

6.2.4 Designing an Advanced Soft-DF Relaying Regime

The Soft decode and forward (Soft-DF) relaying protocol was proposed in [177], which was then further improved in [178, 179]. It constitutes an advanced relaying regime, which combines the main advantages of both the AF relaying and DF relaying solutions.

In more detail, in contrast to conventional DF relaying, Soft-DF relaying will not lose any of the information received at the relay nodes. Hence the error-propagation problem of the conventional hard-decision-based DF relaying is avoided. This characteristic of the Soft-DF relaying regime is particularly beneficial for our MS-DIS based noncoherent successive relaying system introduced in Chapter 4. As indicated in Section 4.5.4, the MS-DIS based SRAN is prone to the unequal error correction capability of the RN and of the DN. The potentially poor BER performance of the RN will significantly erode the potentially stronger error correction capability of the DN, which is a consequence of the hard-decision-based DF scheme's error propagation problem. As a result, the BER performance of the system shown in Figure 4.3 is limited by the RN's error correction capability. Hence after replacing the conventional DF regime employed in Chapter 4 by the Soft-DF regime, a further BER improvement is expected for this system.

The beneficial characteristics of the Soft-DF relaying regime may also be expected to enhance the overall performance of our RSC coded GANC scheme introduced in Chapter 5. After replacing the conventional DF relaying by the Soft-DF regime relying on our RSC coded GANC aided SRAN, we no longer have to consider whether the received signals have or have not been correctly decoded in the RN, since no hard-decisions are made at the RN. Accordingly, the size of the "relay-group" in the RSC coded GANC aided SRAN will no longer be constrained by the "perfect hard detection" requirement of every component RN. This implies that similar to the NBLB coded GANC regime

of Section 5.1, the improved RSC coded GANC regime also becomes applicable to a large-scale wireless network. As a price to pay, more sophisticated signal processing is required at the RN for appropriately combining the information components obtained from different users. This is a potential challenge in the context of Soft-DF based network coded cooperation.

6.2.5 Invoking a Buffer-Aided Relaying Regime

Assuming that the relay of a cooperative network has a buffer grants the system with an additional operational flexibility in the context of cooperative communications. As a benefit of having buffers, it is no longer necessary for a relay to immediately forward its re-encoded and re-modulated signals right after its reception. Instead, the relay equipped with a buffer can temporarily store the signals received and wait for an opportune moment, until the occurrence of a "good channel" quality for transmission to the destination [180]. Hence the data packets transmitted by the relay are capable of always benefiting from a "good channel", which has a sufficiently high capacity in support of error-free transmissions.

Inspired by the classic concept of relaying with combined a buffer [180], Xia *et al.* conceived a pair of basic system models for buffer-aided relaying, namely the "fixed buffering relay model" as well as the "dynamic buffering relay model" and quantified their capacity in [181]. The relay regularly forwards its data packets at a transmission rate, which is "just" below the instantaneous relay-to-destination channel's capacity [181]. The remaining data packets stored in the relay's buffer will be transmitted during the ensuing transmission phases. However, the basic buffering-aided relay models proposed in [181] failed to fully exploit the flexibility offered by the buffering-assisted relay, since the instants of the source's and the relay's transmissions are fixed. Consequently, Zlatanov *et al.* [182, 183] proposed buffer-aided relaying combined with adaptive link activation, where a decision is made in any given time slot based on the instantaneous CSI of the source-to-relay and the relay-to-destination link, as to whether the source or the relay will be allowed to transmit. In summary, the buffer-aided relaying regime abandons the fixed transmission instants of conventional relaying protocols. As a benefit, it has been demonstrated in [181–184] that buffer-aided relaying achieves significant performance gains compared to conventional relaying operating without a buffer, as long as the associated time-variant delay can be tolerated.

Hence we would like to incorporate the above-mentioned ideas into our successive relaying regime proposed in this thesis. With the aid of a well-designed transmission arrangement, we may be able to simultaneously exploit the benefits of both successive relaying and of buffer-aided relaying. In fact, the max-max relay selection based buffer-aided relaying scheme proposed in [185, 186] may be treated as a potential realization of the above-mentioned buffer-aided successive relaying regime. However, the detrimental effects of successive relaying induced interferences were simply ignored in [185, 186] by assuming perfect interference cancellation, which was an idealized simplifying assumption. Hence, investigating the interference limited buffer-aided successive relaying

regime based on the previous contributions reported in [185, 186] may be a promising topic for our future research.

Glossary

M_c**-DPSK**	M_c-ary differential phase-shift keying
M_c**-PSK**	M_c-ary phase-shift keying
AF	amplify-and-forward
AN	accumulated noise
ANC	adaptive network coding
ARQ	automatic-repeat-request
AWGN	additive white Gaussian noise
BER	bit-error-ratio
CC	convolutional code
CCL	cross-correlation
CDD	conventional differential detection
CDMA	code division multiple access
CIR	channel impulse response
CSI	channel state information
CSS	compare-shift-select
DCMC	discrete-input continuous-output memoryless channel
DF	decode-and-forward
DF-DD	decision-feedback differential detection
DIS	differential interference suppression
DM	differential modulator
DMT	diversity-multiplexing trade-off
DN	destination node
DNC	diversity network code
DS-CDMA	direct-sequence code division multiple access

DT direct-transmission

EDC Euclidean distance calculation
EXIT extrinsic information transfer

Fano-MSDD Fano Multiple-Symbol Differential Detection
FDMA frequency division multiple access
FEC forward error correction

GANC generalized adaptive network coding

IIR infinite impulse response
IrCC irregular convolutional codes

JNCC joint network-channel coding

LDPC low-density-parity-check
LLR log-likelihood ratio

MAI multiple access interference
MAP maximum *a posteriori*
MAP-MSDSD maximum a posteriori multiple-symbol differential sphere detection
MIMO multiple-input multiple-output
ML maximum-likelihood
ML-MSDD maximum-likelihood multiple-symbol differential detection
MS Mobile Station
MS-DIS multiple-symbol differential interference suppression
MSDD multiple-symbol differential detection
MSDSD multiple-symbol differential sphere detection
MUI multi-user interference

NBLB nonbinary linear block code
NC noncoherent
NC-SR noncoherent successive relaying

OFDMA orthogonal frequency division multiple access
OPA optimal power allocation
OR opportunistic relaying

ORA	optimal rate allocation
PDF	probability density function
PN	pseudo-noise
PSA	pilot symbol assisted
QAM	quadrature amplitude modulation
RD	relay-to-destination
RMO	real-valued multiplication operations
RN	relay node
RSC	recursive systematic convolutional code
SC	selection cooperation
SD	source-to-destination
SECCC	self-concatenated convolutional codes
SF	spreading factor
SINR	signal-to-interference-plus-noise-ratio
SISO-MSDSD	soft-input soft-output MSDSD
SL	single-link
SN	source node
SNR	signal-to-noise ratio
Soft-DF	soft decode-and-forward
SR	source-to-relay
SRAN	successive relaying aided network
SVD	singular-value decomposition
TDMA	time division multiple access
URC	unity-rate-code
V-BLAST	vertical Bell laboratories layered space-time
VAA	virtual antenna array

Bibliography

[1] S. M. Alamouti, "A Simple Transmit Diversity Technique for Wireless Communications," *IEEE Journal on Selected Areas in Communications*, vol. 16, pp. 1451–1458, October 1998.

[2] I. E. Telatar, "Capacity of Multi-antenna Gaussian Channels," *European Transactions on Telecommunications*, vol. 10, pp. 585–595, Nov. 1999.

[3] G. Foschini, G. Golden, R. Valenzuela, and P. Wolniansky, "Simplified Processing for High Spectral Efficiency Wireless Communication Employing Multi-Element Arrays," *IEEE Journal on Selected Areas in Communications*, vol. 17, pp. 1841–1852, November 1999.

[4] L. Zheng and D. N. C. Tse, "Diversity and Multiplexing: A Fundamental Tradeoff in Multiple-Antenna Channels," *IEEE Transactions on Information Theory*, vol. 49, pp. 1073–1096, May 2003.

[5] A. J. Paulraj, D. A. Gore, R. U. Nabar, and H. Bölcskei, "An Overview of MIMO Communications - A Key to Gigabit Wireless," *Proceedings of the IEEE*, vol. 92, pp. 198–218, February 2004.

[6] C. Dubuc, D. Starks, T. Creasy, and Y. Hou, "A MIMO-OFDM Prototype for Next-Generation Wireless WANs," *IEEE Communications Magazine*, vol. 42, pp. 82–87, December 2004.

[7] L. Hanzo, O. R. Alamri, M. El-Hajjar, and N. Wu, *Near-Capacity Multi-Functional MIMO Systems: Sphere-Packing, Iterative Detection and Cooperation*, ch. Cooperative Space-Time Block Codes. John Wiley and Sons Ltd, 2009.

[8] E. C. V. der Meulen, "Three-Terminal Communication Channels," *Advanced Applied Probability*, vol. 3, pp. 120–154, 1971.

[9] T. M. Cover and A. A. El Gamal, "Capacity Theorems for the Relay Channel," *IEEE Transactions on Information Theory*, vol. 25, pp. 572–584, Sept 1979.

[10] J. N. Laneman, D. N. C. Tse, and G. W. Wornell, "Cooperative Diversity in Wireless Networks: Efficient Protocols and Outage Behavior," *IEEE Transactions on Information Theory*, vol. 50, pp. 3062–3080, Dec 2004.

[11] J. N. Laneman and G. W. Wornell, "Distributed Space-Time-Coded Protocols for Exploiting Cooperative Diversity in Wireless Networks," *IEEE Transactions on Information Theory*, vol. 49, pp. 2415–2425, Oct 2003.

[12] A. Sendonaris, E. Erkip, and B. Aazhang, "User Cooperation Diversity-Part I: System Description," *IEEE Transactions on Communications*, vol. 51, pp. 1927–1938, November 2003.

[13] A. Sendonaris, E. Erkip, and B. Aazhang, "User Cooperation Diversity-Part II: Implementation Aspects and Performance Analysis," *IEEE Transactions on Communications*, vol. 51, pp. 1939–1948, November 2003.

[14] K. Azarian, H. E. Gamal, and P. Schniter, "On the Achievable Diversity-Multiplexing Tradeoff in Half-Duplex Cooperative Channels," *IEEE Transactions on Information Theory*, vol. 51, pp. 4152–4172, December 2005.

[15] M. Yuksel and E. Erkip, "Multiple-Antenna Cooperative Wireless Systems: A Diversity-Multiplexing Tradeoff Perspective," *IEEE Transactions on Information Theory*, vol. 53, pp. 3371–3393, October 2007.

[16] S. Q. Wei, "Diversity-Multiplexing Tradeoff of Asynchronous Cooperative Diversity in Wireless Networks," *IEEE Transactions on Information Theory*, vol. 53, pp. 4150–4172, November 2007.

[17] C. Wang, Y. J. Fan, J. S. Thompson, and H. V. Poor, "A Comprehensive Study of Repetition-Coded Protocols in Multi-User Multi-Relay Networks," *IEEE Transactions on Wireless Communications*, vol. 8, pp. 4329–4339, August 2009.

[18] A. A. Haghighi and K. Navaie, "Outage Analysis and Diversity-Multiplexing Tradeoff Bounds for Opportunistic Relaying Coded Cooperation and Distributed Space-Time Coding Coded Cooperation," *IEEE Transactions on Wireless Communications*, vol. 9, pp. 1198–1206, March 2010.

[19] A. Bletsas, A. Khisti, D. P. Reed, and A. Lippman, "A Simple Cooperative Diversity Method Based on Network Path Selection," *IEEE Journal on Selected Areas in Communications*, vol. 24, pp. 659–672, March 2006.

[20] A. Bletsas, H. Shin, and M. Z. Win, "Cooperative Communications with Outage-Optimal Opportunistic Relaying," *IEEE Transactions on Wireless Communications*, vol. 6, pp. 3450–3460, September 2007.

[21] E. Beres and R. Adve, "Selection Cooperation in Multi-Source Cooperative Networks," *IEEE Transactions on Wireless Communications*, vol. 7, pp. 118–127, Jan 2008.

[22] D. S. Michalopoulos and G. K. Karagiannidis, "Performance Analysis of Single Relay Selection in Rayleigh Fading," *IEEE Transactions on Wireless Communications*, vol. 7, pp. 3718–3724, October 2008.

[23] W. F. Su and X. Liu, "On Optimum Selection Relaying Protocols in Cooperative Wireless Networks," *IEEE Transactions on Communications*, vol. 58, pp. 52–57, January 2010.

[24] A. Høst-Madsen and J. Zhang, "Capacity Bounds and Power Allocation for Wireless Relay Channels," *IEEE Transactions on Information Theory*, vol. 51, pp. 2020–2040, June 2005.

[25] E. G. Larsson and Y. Cao, "Collaborative Transmit Diversity with Adaptive Radio Resource and Power Allocation," *IEEE Communications Letters*, vol. 9, pp. 511–513, June 2005.

[26] R. Annavajjala, P. C. Cosman, and L. B. Milstein, "Statistical Channel Knowledge-Based Optimum Power Allocation for Relaying Protocols in the High SNR Regime," *IEEE Journal on Selected Areas in Communications*, vol. 25, pp. 292–305, February 2007.

[27] Y. Zhao, R. Adve, and T. J. Lim, "Improving Amplify-and-Forward Relay Networks: Optimal Power Allocation versus Selection," *IEEE Transactions on Wireless Communications*, vol. 6, pp. 3114–3123, Aug 2007.

[28] M. Chen, S. Serbetli, and A. Yener, "Distributed Power Allocation Strategies for Parallel Relay Networks," *IEEE Transactions on Wireless Communications*, vol. 7, pp. 552–561, February 2008.

[29] L. Sankar, Y. B. Liang, N. B. Mandayam, and H. V. Poor, "Fading Multiple Access Relay Channels: Achievable Rates and Opportunistic Scheduling," *IEEE Transactions on Information Theory*, vol. 57, pp. 1911–1931, April 2011.

[30] D. W. K. Ng and R. Schober, "Resource Allocation and Scheduling in Multi-Cell OFDMA Systems with Decode-and-Forward Relaying," *IEEE Transactions on Wireless Communications*, vol. 10, pp. 2246–2258, July 2011.

[31] Y. X. Chen and Q. Zhao, "On the Lifetime of Wireless Sensor Networks," *IEEE Communications Letters*, vol. 9, pp. 976–978, November 2005.

[32] G. Ganesan and Y. Li, "Cooperative Spectrum Sensing in Cognitive Radio, Part I: Two User Networks," *IEEE Transactions on Wireless Communications*, vol. 6, pp. 2204–2213, June 2007.

[33] G. Ganesan and Y. Li, "Cooperative Spectrum Sensing in Cognitive Radio, Part II: Multiuser Networks," *IEEE Transactions on Wireless Communications*, vol. 6, pp. 2214–2222, June 2007.

[34] K. B. Letaief and W. Zhang, "Cooperative Communications for Cognitive Radio Networks," *Proceedings of the IEEE* , vol. 97, pp. 878–893, May 2009.

[35] L. Y. Li, X. W. Zhou, H. B. Xu, Y. Li, D. D. Wan, and A. Soong, "Simplified Relay Selection and Power Allocation in Cooperative Cognitive Radio Systems," *IEEE Transactions on Wireless Communications*, vol. 10, pp. 33–36, January 2011.

[36] M. Pischella and J. C. Belfiore, "Power Control in Distributed Cooperative OFDMA Cellular Networks," *IEEE Transactions on Wireless Communications*, vol. 7, pp. 1900–1906, May 2008.

[37] L. F. Weng and R. D. Murch, "Cooperation Strategies and Resource Allocations in Multiuser OFDMA Systems," *IEEE Transactions on Vehicular Technology*, vol. 58, pp. 2331–2342, June 2009.

[38] T. E. Hunter and A. Nosratinia, "Diversity through Coded Cooperation," *IEEE Transactions on Wireless Communications*, vol. 5, pp. 283–289, February 2006.

[39] C. Hausl and J. Hagenauer, "Iterative Network and Channel Decoding for the Two-Way Relay Channel," in *IEEE Proceedings of International Conference on Communications (ICC)*, vol. 4, pp. 1568–1573, June 2006.

[40] P. Popovski and H. Yomo, "Physical Network Coding in Two-Way Wireless Relay Channels," in *IEEE Proceedings of International Conference on Communications (ICC)*, pp. 707–712, June 2007.

[41] X. Bao and J. Li, "Adaptive Network Coded Cooperation (ANCC) for Wireless Relay Networks: Matching Code-on-Graph with Network-on-Graph," *IEEE Transactions on Wireless Communications*, vol. 7, pp. 574–583, Feb 2008.

[42] M. Xiao and M. Skoglund, "Multiple-User Cooperative Communications Based on Linear Network Coding," *IEEE Transactions on Communications*, vol. 58, pp. 3345–3351, Dec 2010.

[43] B. Rankov and A. Wittneben, "Spectral Efficient Protocols for Half-Duplex Fading Relay Channels," *IEEE Journal on Selected Areas in Communications*, vol. 25, pp. 379–389, February 2007.

[44] Y. J. Fan, C. Wang, J. S. Thompson, and H. V. Poor, "Recovering Multiplexing Loss through Successive Relaying Using Repetition Coding," *IEEE Transactions on Communications*, vol. 6, pp. 4484–4493, December 2007.

[45] C. B. Luo, Y. Gong, and F.-C. Zheng, "Interference Cancellation in Two-Path Successive Relay System with Network Coding," in *PIMRC, 2010 IEEE 21st International Symposium on*, pp. 465–469, Sept. 2010.

[46] C. B. Luo, Y. Gong, and F.-C. Zheng, "Full Interference Cancellation for Two-Path Relay Cooperative Networks," *IEEE Transactions on Vehicular Technology*, vol. 60, pp. 343–347, Jan 2011.

[47] H. Wicaksana, S. H. Ting, C. K. Ho, W. H. Chin, and Y. L. Guan, "AF Two-Path Half Duplex Relaying with Inter-Relay Self Interference Cancellation: Diversity Analysis and its Improvement," *IEEE Transactions on Wireless Communications*, vol. 8, pp. 4720–4729, September 2009.

[48] C. I. Bang and M. H. Lee, "An Analysis of Pilot Symbol Assisted 16 QAM in the Rayleigh Fading Channel," *IEEE Transactions on Consumer Electronics*, vol. 41, pp. 1138–1141, November 1995.

[49] D. Divsalar and M. K. Simon, "Multiple Symbol Differential Detection of MPSK," *IEEE Transactions on Communications*, vol. 38, pp. 300–308, March 1990.

[50] K. Mackenthun, "A Fast Algorithm for Multiple-Symbol Differential Detection of MPSK," *IEEE Transactions on Communications*, vol. 42, pp. 1471–1474, April 1994.

[51] R. Schober, W. H. Gerstacker, and J. B. Huber, "Decision-Feedback Differential Detection of MDPSK for Flat Rayleigh Fading Channels," *IEEE Transactions on Communications*, vol. 47, pp. 1025–1035, July 1999.

[52] O. Damen, H. E. Gamal, and G. Gaire, "On Maximum Likelihood Detection and the Search for the Closest Lattice Point.," *IEEE Transactions on Information Theory*, vol. 49, pp. 2389–2402, October 2003.

[53] L. Lampe, R. Schober, V. Pauli, and C. Windpassinger, "Multiple-Symbol Differential Sphere Decoding," *IEEE Transactions on Communications*, vol. 12, pp. 1981–1985, Dec 2005.

[54] L. Wang and L. Hanzo, "Multiple-Symbol Differential Sphere Detection for the Amplify-and-Forward Cooperative Uplink," in *Proceedings of IEEE 70th Vehicular Technology Conference Fall (VTC2009-Fall)*, pp. 1–5, September 2009.

[55] V. Pauli, L. Lampe, and R. Schober, "Turbo DPSK Using Soft Multiple-Symbol Differential Sphere Decoding," *IEEE Transactions on Information Theory*, vol. 52, pp. 1385–1398, April 2006.

[56] B. Schein and R. Gallager, "The Gaussian Parallel Relay Network," in *Proceedings of IEEE International Symposium on Information Theory (ISIT)*, p. 22, June 2000.

[57] A. B. Carleial, "Multiple-Access Channels with Different Generalized Feedback Signals," *IEEE Transactions on Information Theory*, vol. 28, pp. 841 – 850, Nov 1982.

[58] J. N. Laneman and G. W. Wornell, "Energy-Efficient Antenna Sharing and Relaying for Wireless Networks," in *IEEE Proceedings of Wireless Communications and Networking Conference (WCNC), 2000.*, vol. 1, pp. 7–12, August 2000.

[59] D. Tse and P. Viswanath, *Fundamentals of Wireless Communications*. Cambridge: Cambridge university press, 2005.

[60] A. Sendonaris, E. Erkip, and B. Aazhang, "Increasing Uplink Capacity via User Cooperation Diversity," *in IEEE Proceedings of International Symposium on Information Theory*, p. 156, August 1998.

[61] T. M. Cover and C. S. K. Leung, "An Achievable Rate Region for the Multiple-Access Channel with Feedback," *IEEE Transactions on Information Theory*, vol. 27, pp. 292–298, May 1981.

[62] T. Wang, A. Cano, G. B. Giannakis, and J. N. Laneman, "High-Performance Cooperative Demodulation with Decode-and-Forward Relays," *IEEE Transactions on Communications*, vol. 55, pp. 1427–1438, July 2007.

[63] L. Wang and L. Hanzo, "The Resource-Optimized Differentially Modulated Hybrid AF/DF Cooperative Cellular Uplink Using Multiple-Symbol Differential Sphere Detection," *IEEE Signal Processing Letter*, vol. 16, pp. 965–968, November 2009.

[64] L. K. Kong, S. X. Ng, R. G. Maunder, and L. Hanzo, "Irregular Distributed Space-Time Code Design for Near-Capacity Cooperative Communications," *IEEE Vehicular Technology Conference (VTC)* , vol. 1, pp. 1–6, Sept 2009.

[65] T. Oechtering and A. Sezgin, "A New Cooperative Transmission Scheme Using the Space-Time Delay Code," in *Proceedings of ITG Workshop on Smart Antennas*, pp. 41–48, March 2004.

[66] B. Rankov and A. Wittneben, "Spectral Efficient Signaling for Half-Duplex Relay Channels," in *Conference Record of the Thirty-Ninth Asilomar Conference on Signals, Systems and Computers*, pp. 1066–1071, 2005.

[67] S. Yang and J. C. Belfiore, "On Slotted Amplify-and-Forward Cooperative Diversity Schemes," in *Proceedings of IEEE International Symposium on Information Theory*, pp. 2446–2450, 2006.

[68] S. Yang and J. C. Belfiore, "Towards the Optimal Amplify-and-Forward Cooperative Diversity Scheme," *IEEE Transactions on Information Theory*, vol. 53, pp. 3114–3126, September 2007.

[69] H. V. Trees, "Detection, Estimation and Modulation Theory: Part I," *Wiley*, vol. 6, pp. 98–99, Mar 1968.

[70] D. Divsalar, M. K. Simon, and M. Shahshahani, "The Performance of Trellis-Coded MDPSK with Multiple Symbol Detection," *IEEE Transactions on Communications*, vol. 38, pp. 1391–1403, September 1990.

[71] P. Ho and D. Fung, "Error Performance of Multiple-Symbol Differential Detection of PSK Signals Transmitted Over Correlated Rayleigh Fading Channels," *IEEE Transactions on Communications*, vol. 40, pp. 1566–1569, October 1992.

[72] P. Ho and D. Fung, "Error Performance of Multiple Symbol Differential Detection of PSK Signals Transmitted Over Correlated Rayleigh Fading Channels," in *Proceedings of IEEE International Conference on Communications (ICC)*, pp. 568–574, June 1991.

[73] X. F. Wu and S. G. Sun, "Low Complexity Multisymbol Differential Detection of MDPSK Over Flat Correlated Rayleigh Fading Channels," *Electronics Letters*, vol. 34, pp. 2008–2009, October 1998.

[74] R. Schober, W. H. Gerstacker, and J. B. Huber, "Decision-Feedback Differential Detection of MDPSK for Flat Rayleigh Fading Channels," *IEEE Transactions on Communications*, vol. 47, pp. 1025–1035, July 1999.

[75] P. Pun and P. Ho, "The Performance of Fano-Multiple Symbol Differential Detection," in *IEEE Proceedings of International Conference on Communications (ICC)*, pp. 2516–2521, May 2005.

[76] P. Pun and P. Ho, "Fano Multiple-Symbol Differential Detectors for Differential Unitary Space-Time Modulation," *IEEE Transactions on Communications*, vol. 55, pp. 540–550, March 2007.

[77] R. M. Fano, "A Heuristic Discussion of Probabilistic Decoding ," *IEEE Transactions on Information Theory*, vol. 9, pp. 64–74, April 1963.

[78] L. Wang and L. Hanzo, "The Amplify-and-Forward Cooperative Uplink Using Multiple-Symbol Differential Sphere-Detection," *IEEE Signal Processing Letters*, vol. 16, pp. 913–916, October 2009.

[79] L. Li and L. Hanzo, "Multiple-Symbol Differential Sphere Detection aided Successive Relaying in the Cooperative DS-CDMA Uplink," in *Proceedings of IEEE Wireless Communications and Networking Conference (WCNC)*, pp. 1875–1880, March 2011.

[80] L. Li, L. Wang, and L. Hanzo, "The Capacity of Successive DF Relaying and Using Soft Multiple-Symbol Differential Sphere Detection," in *Proceedings of IEEE Global Telecommunications Conference (GLOBECOM)*, pp. 1–5, December 2011.

[81] L. Hanzo, Y. Akhtman, M. Jiang, and L. Wang, *MIMO-OFDM for LTE, WIFI and WIMAX: Coherent versus Non-Coherent and Cooperative Turbo-Transceivers*. John Wiley, 2010.

[82] W. C. Lindsey and M. K. Simon, *Telecommunication Systems Engineering*. Englewood Cliffs, NJ: Prentice-Hall, 1973.

[83] R. H. Clarke, "A Statistical Theory of Mobile Radio Reception," *Bell System Technical Journal*, vol. 47, pp. 957–1000, July/Aug. 1968.

[84] E. Agrell, T. Eriksson, A. Vardy, and K. Zeger, "Closest Point Search in Lattices," *IEEE Transactions on Information Theory*, vol. 48, pp. 2201–2214, August 2002.

[85] C. Berrou, A. Glavieux, and P. Thitimajshima, "Near Shannon Limit Error-Correcting Coding and Decoding: Turbo-Codes," in *Proceedings of IEEE International Conference on Communications (ICC)*, vol. 2, pp. 1064 –1070, May 1993.

[86] S. L. Goff, A. Glavieux, and C. Berrou, "Turbo-Codes and High Spectral Efficiency Modulation," in *Proceedings of IEEE International Conference on Communications (ICC)*, pp. 645–649, May 1994.

[87] S. Benedetto and G. Montorsi, "Design of Parallel Concatenated Convolutional Codes," *IEEE Transactions on Communications*, vol. 44, pp. 591–600, May 1996.

[88] S. Benedetto and G. Montorsi, "Unveiling Turbo Codes: Some Results on Parallel Concatenated Coding Schemes," *IEEE Transactions on Information Theory*, vol. 42, pp. 409–428, March 1996.

[89] J. Hagenauer, E. Offer, and L. Papke, "Iterative Decoding of Binary Block and Convolutional Codes," *IEEE Transactions on Information Theory*, vol. 42, pp. 429–445, March 1996.

[90] B. Sklar, "A Primer on Turbo Code Concepts," *IEEE Communications Magazine*, pp. 94–102, December 1997.

[91] C. P. Schnorr and H. H. Hörner, "Lattice Basis Reduction: Improved Practical Algorithms and Solving Subset Sum Problems," *Mathematical Programming*, vol. 66, pp. 181–191, 1994.

[92] P. Robertson, "Illuminating the Structure of Code and Decoder of Parallel Concatenated Recursive Systematic (Turbo) Codes," in *Proceedings of IEEE Global Telecommunications Conference (GLOBECOM)*, vol. 3, pp. 1298–1303, November 1994.

[93] N. Seshadri and P. Hoeher, "On Post-Decision Symbol-Reliability Generation," in *Proceedings of IEEE International Conference on Communications (ICC)*, vol. 2, pp. 741–745, May 1993.

[94] G. J. Foschini and M. J. Gans, "On Limits of Wireless Communications in a Fading Environment when Using Multiple Antennas," *Wireless Personal Communications*, vol. 6, pp. 311–335, Mar 1998.

[95] F. Xue and S. Sandhu, "Cooperation in a Half-Duplex Gaussian Diamond Relay Channel," *IEEE Transactions on Information Theory*, vol. 53, pp. 3806–3814, October 2007.

[96] S. H. Won and L. Hanzo, "Initial Synchronisation of Wideband and UWB Direct Sequence Systems: Single- and Multiple-Antenna Aided Solutions," *IEEE Communications Surveys & Tutorials*, vol. 14, pp. 87–108, February 2012.

[97] L. Hanzo, L.-L. Yang, E.-L. Kuan, and K. Yen, *Single and Multi-Carrier DS-CDMA : Multi-User Detection, Space-Time Spreading, Synchronisation and Standards*. John Wiley & Sons, 2005.

[98] L. Li, L. Wang, and L. Hanzo, "Capacity Analysis of the Successive AF Relaying Aided Cooperative DS-CDMA Uplink," in *Proceedings of IEEE Wireless Communications and Networking Conference (WCNC)*, pp. 3057–3062, April 2012.

[99] L. Li, L. Wang, and L. Hanzo, "Successive AF/DF Relaying in the Cooperative DS-CDMA Uplink: Capacity Analysis and Its System Architecture," *IEEE Transactions on Vehicular Technology*, vol. 62, pp. 655–666, Feb. 2013.

[100] L. Wang, L. K. Kong, S. X. Ng, and L. Hanzo, "A Near-Capacity Differentially Encoded Non-Coherent Adaptive Multiple-Symbol-Detection Aided Three-Stage Coded Scheme," in *Proceedings of IEEE Vehicular Technology Conference (VTC) 71st*, pp. 1–5, May 2010.

[101] S. Won, K. Lee, and L. Hanzo, "Initial Code Acquisition in the Cooperative Noncoherent MIMO DS-CDMA Downlink," *IEEE Transactions on Vehicular Technology*, vol. 58, pp. 1387–1395, March 2009.

[102] L. K. Kong, S. X. Ng, R. G. Maunder, and L. Hanzo, "Near-Capacity Cooperative Space-Time Coding Employing Irregular Design and Successive Relaying," *IEEE Transactions on Communications*, vol. 58, pp. 2232–2241, August 2010.

[103] W. Fang, L.-L. Yang, and L. Hanzo, "Single-user Performance of Direct-Sequence Code-Division Multiple-Access Using Relay Diversity and Power Allocation," *IET Communications*, vol. 2, pp. 462–472, 2008.

[104] T. Himsoon, W. Su, and K. J. R. Liu, "Differential Transmission for Amplify-and-Forward Cooperative Communications," *IEEE Signal Processing letters*, vol. 12, pp. 597–600, Sept 2005.

[105] A. Abrardo, "Noncoherent MLSE Detection of M-DPSK for DS-CDMA Wireless Systems," *IEEE Transactions on Vehicular Technology*, vol. 52, pp. 1435–1446, Nov 2003.

[106] Y. W. Ding, J. K. Zhang, and K. M. Wong, "Ergodic Channel Capacity for the Amplify-and-Forward Half-Duplex Cooperative Systems," *IEEE Transactions on Information Theory*, vol. 55, pp. 713–730, February 2009.

[107] T. S. Rappaport, *Wireless Communications: Principles and Practice*. Upper Saddle River, NJ: Prentice-Hall, 1996.

[108] Y. B. Liang and V. V. Veeravalli, "Capacity of Noncoherent Time-Selective Block Rayleigh Flat-Fading Channel," *IEEE International Symposium on Information Theory*, p. 166, 2002.

[109] L. Wang, L. K. Kong, S. X. Ng, and L. Hanzo, "Code-Rate-Optimized Differentially Modulated Near-Capacity Cooperation," *IEEE Transactions on Communications*, vol. 59, pp. 2185–2195, Aug 2011.

[110] J. G. Proakis, *Digital Communications*. Mc-Graw Hill, 3rd ed., 1995.

[111] M. Pursley, "Performance Evaluation for Phase-Coded SSMA Communication - Part I : System Analysis," *IEEE Transactions on Communications*, vol. 25, pp. 795–799, Aug 1977.

[112] T. M. Cover and J. A. Thomas, *Elements of Information Theory*. John Wiley & Sons, 2006.

[113] R. Schober and L. Lampe, "Noncoherent Receivers for Differential Space-Time Modulation," *IEEE Transactions on Communications*, vol. 50, pp. 768–777, May 2002.

[114] R.-R. Chen, R. Koetter, U. Madhow, and D. Agrawal, "Joint Noncoherent Demodulation and Decoding for the Block Fading Channel: A practical Framework for Approaching Shannon Capacity," *IEEE Transactions on Communications*, vol. 10, pp. 1676–1689, October 2003.

[115] B. Zhao and M. C. Valenti, "Distributed Turbo Coded Diversity for Relay Channel," *Electronics Letters*, vol. 39, pp. 786–787, May 2003.

[116] A. Ashikhmin, G. Kramer, and S. ten Brink, "Extrinsic Information Transfer Functions: Model and Erasure Channel Properties," *IEEE Transactions on Information Theory*, vol. 50, pp. 2657–2673, Nov 2004.

[117] S. K. Cheung and R. Schober, "Differential Spatial Multiplexing," *IEEE Transactions on Wireless Communications*, vol. 5, pp. 2127–2135, Aug 2006.

[118] L. Wang and L. Hanzo, "Multiple-Symbol Detection Aided Differential Spatial Division Multiple Access," in *Proceedings of IEEE International Conference on Communications (ICC)*, pp. 1–5, June 2011.

[119] J. Yang, F. Yang, H. S. Xi, and W. Guo, "Robust Adaptive Modified Newton Algorithm for Generalized Eigendecomposition and Its Application," *EURASIP Journal on Advances in Signal Processing*, vol. 2007, pp. 1–10, June 2007.

[120] H. Ochiai, P. Mitran, and V. Tarokh, "Design and Analysis of Collaborative Diversity Protocols for Wireless Sensor Networks," in *VTC 2004-Fall, 2004 IEEE*, vol. 7, pp. 4645–4649, Sept. 2004.

[121] H.-J. Su and E. Geraniotis, "Maximum Signal-to-Noise Ratio Array Processing for Space-Time Coded Systems," *IEEE Transactions on Communications*, vol. 50, pp. 1419–1422, Sept 2002.

[122] S. Haykin, "Adaptive Filter Theory," *3rd ed. Englewood Cliffs, NJ: Prentice -Hall*, 1996.

[123] M. F. Butt, R. Riaz, S. X. Ng, and L. Hanzo, "Near-Capacity Iterative Decoding of Binary Self-Concatenated Codes Using Soft Decision Demapping and 3-D EXIT Charts," *IEEE Transactions on Wireless Communications*, vol. 9, pp. 1608–1616, May 2010.

[124] S. Benedetto, D. Divsalar, G. Montorsi, and F. Pollara, "Self-Concatenated Trellis Coded Modulation with Self-Iterative Decoding," in *GLOBECOM, 1998 IEEE*, vol. 1, pp. 585–591, 1998.

[125] D. Divsalar, S. Dolinar, and F. Pollara, "Serial Concatenated Trellis Coded Modulation with Rate-1 Inner Code," in *GLOBECOM, 2000 IEEE*, vol. 2, pp. 777–782, 2000.

[126] L. Hanzo, R. G. Maunder, J. Wang, and L.-L. Yang, *Near-Capacity Variable-Length Coding: Regular and Exit-Chart Aided Irregular Designs*. John Wiley & Sons, March 2011.

[127] C. Douillard, A. Picart, P. Didier, M. Jezequel, C. Berrou, and A. Glavieux, "Iterative Correction of Intersymbol Interference: Turbo-Equalization," *Euro. Trans. Telecommun.*, vol. 6, pp. 507–511, Sept 1995.

[128] L. Hanzo, T. H. Liew, B. L. Yeap, and R. Y. S. Tee, "Turbo Coding, Turbo Equalisation and Space-Time Coding : EXIT-Chart Aided Near-Capacity Designs for Wireless Channels," *John Wiley & Sons and IEEE Press*, March 2011.

[129] L. Wang, L. K. Kong, S. X. Ng, and L. Hanzo, "To Cooperate or Not: A Capacity Perspective," in *Proceedings of IEEE Vehicular Technology Conference (VTC)*, pp. 1–5, May 2010.

[130] I. Land, S. Huettinger, P. A. Hoeher, and J. B. Huber, "Bounds on Information Combining," *IEEE Transactions on Information Theory*, vol. 51, pp. 612–619, Feb. 2005.

[131] L. Li, L. Wang, and L. Hanzo, "Differential Interference Suppression Aided Three-Stage Concatenated Successive Relaying," *IEEE Transactions on Communications*, vol. 60, pp. 2146–2155, August 2012.

[132] J. Kim, D. S. Michalopoulos, and R. Schober, "Diversity Analysis of Multi-User Multi-Relay Networks," *IEEE Transactions on Wireless Communications*, vol. 10, pp. 2380–2389, July 2011.

[133] S. Chen, W. Wang, and X. Zhang, "Performance Analysis of Multiuser Diversity in Cooperative Multi-Relay Networks under Rayleigh-Fading Channels," *IEEE Transactions on Wireless Communications*, vol. 8, pp. 3415–3419, July 2009.

[134] I. Krikidis, J. S. Thompson, S. McLaughlin, and N. Goertz, "Max-Min Relay Selection for Legacy Amplify-and-Forward Systems with Interference," *IEEE Transactions on Wireless Communications*, vol. 8, pp. 3016–3027, June 2009.

[135] R. Ahlswede, N. Cai, S.-Y. R. Li, and R. W. Yeung, "Network Information Flow," *IEEE Transactions on Information Theory*, vol. 46, pp. 1204–1216, July 2000.

[136] S.-Y. R. Li, R. W. Yeung, and N. Cai, "Linear Network Coding," *IEEE Transactions on Information Theory*, vol. 49, pp. 371–381, Feb. 2003.

[137] R. Koetter and M. Medard, "An Algebraic Approach to Network Coding," *IEEE/ACM Transactions on Networking*, vol. 11, pp. 782–795, Oct 2003.

[138] G. Kramer, M. Gastpar, and P. Gupta, "Cooperative Strategies and Capacity Theorems for Relay Networks," *IEEE Transactions on Information Theory*, vol. 51, pp. 3037–3063, September 2005.

[139] D. H. Woldegebreal and H. Karl, "Multiple-Access Relay Channel with Network Coding and Non-Ideal Source-Relay Channels," in *Wireless Communication Systems, 2007. ISWCS 2007. 4th International Symposium on*, pp. 732–736, Oct. 2007.

[140] L. Xiao, T. Fuja, J. Kliewer, and D. Costello, "A Network Coding Approach to Cooperative Diversity," *IEEE Transactions on Information Theory*, vol. 53, pp. 3714–3722, Oct 2007.

[141] Z. Zhang, "Linear Network Error Correction Codes in Packet Networks," *IEEE Transactions on Information Theory*, vol. 54, pp. 209–218, Jan 2008.

[142] M. Xiao and M. Skoglund, "M-User Cooperative Wireless Communications Based on Nonbinary Network Codes," in *IEEE Information Theory Workshop. ITW 2009*, pp. 316–320, June 2009.

[143] K. Pang, Z. Lin, Y. Li, and B. Vucetic, "Joint Network-Channel Code Design for Real Wireless Relay Networks," in *International Symposium on Turbo Codes and Iterative Information Processing (ISTC)*, pp. 429–433, 2010.

[144] R. Zhang, Y. C. Liang, C. C. Chai, and S. G. Cui, "Optimal Beamforming for Two-Way Multi-Antenna Relay Channel with Analogue Network Coding," *IEEE Journal on Selected Areas in Communications*, vol. 27, pp. 699–712, June 2009.

[145] W. Chen, L. Hanzo, and Z. Cao, "Network Coded Modulation for Two-Way Relaying," in *IEEE Proceedings of Wireless Communications and Networking Conference (WCNC)*, pp. 1765–1770, March 2011.

[146] M. Xiao and T. Aulin, "Optimal Decoding and Performance Analysis of a Noisy Channel Network with Network Coding," *IEEE Transactions on Communications*, vol. 57, pp. 1402–1412, May 2009.

[147] M. Xiao, M. Médard, and T. Aulin, "Cross-Layer Design of Rateless Random Network Codes for Delay Optimization," *IEEE Transactions on Communications*, vol. 59, pp. 3311–3322, December 2011.

[148] X. Bao and J. Li, "An Information Theoretic Analysis for Adaptive-Network-Coded-Cooperation (ANCC) in Wireless Relay Networks," in *IEEE Proceedings of International Symposium on Information Theory*, pp. 2719–2723, 2006.

[149] J. L. Rebelatto, B. F. Uchôa-Filho, Y. Li, and B. Vucetic, "Multiuser Cooperative Diversity Through Network Coding Based on Classical Coding Theory," *IEEE Transactions on Signal Processing*, vol. 60, pp. 916–926, Feb 2012.

[150] C. Hausl and P. Dupraz, "Joint Network-Channel Coding for the Multiple-Access Relay Channel," in *Proceedings of 3rd Annual IEEE Communications Society on Sensor and Ad Hoc Communications and Networks (SECON '06)*, pp. 817 –822, Sept 2006.

[151] H. V. Nguyen, C. Xu, S. X. Ng, and L. Hanzo, " Non-Coherent Near-Capacity Network Coding for Cooperative Multi-User Communications ," *IEEE Transactions on Communications*, vol. 60, pp. 3059–3070, Oct. 2012.

[152] H. V. Nguyen, S. X. Ng, and L. Hanzo, " Irregular Convolution and Unity-Rate Coded Network-Coding for Cooperative Multi-User Communications ," *IEEE Transactions on Wireless Communications*, vol. 12, pp. 1231–1243, March 2013.

[153] L. Li, L. Wang, and L. Hanzo, "Generalized Adaptive Network Coding Aided Successive Relaying for Noncoherent Cooperation," *IEEE Transactions on Communications*, vol. 61, pp. 1750–1763, May 2013.

[154] J. L. Rebelatto, B. F. Uchôa-Filho, Y. Li, and B. Vucetic, "Generalized Distributed Network Coding Based on Nonbinary Linear Block Codes for Multi-User Cooperative Communications," in *Proceedings of IEEE International Symposium on Information Theory (ISIT)*, pp. 943–947, 2010.

[155] J. W. Layland and R. J. McEliece, "An Upper Bound on the Free Distance of a Tree Code," *Jet Propulsion Laboratory, California Institute of Technology, Pasadena, California, Space Programs Summary 37-62*, vol. 3, pp. 63–64, Apr 1970.

[156] J. M. Jensen, "Bounds on the Free Distance of Systematic Convolutional Codes," *IEEE Transactions on Information Theory*, vol. 34, pp. 586–589, May 1988.

[157] J. Cheng and N. C. Beaulieu, "Accurate DS-CDMA Bit-Error Probability Calculation in Rayleigh Fading," *IEEE Transactions on Wireless Communications*, vol. 1, pp. 3–15, Jan 2002.

[158] Y. H. Li, B. Vucetic, T. F. Wong, and M. Dohler, "Distributed Turbo Coding with Soft Information Relaying in Multihop Relay Networks," *IEEE Journal on Selected Areas in Communications*, vol. 24, pp. 2040–2050, Nov. 2006.

[159] M. Ahmadi and A. S. Mehr, "Multiple-Symbol Differential Detection:V-BLAST vs. Sphere Decoding," in *Canadian Conference on Electrical and Computer Engineering (CCECE) 2007*, pp. 333–335, April 2007.

[160] A. Schenk and R. F. H. Fischer, "A Stopping Radius for the Sphere Decoder: Complexity Reduction in Multiple-Symbol Differential Detection," in *International ITG Conference on Source and Channel Coding (SCC) 2010*, pp. 1–6, Jan. 2010.

[161] W. Koch and A. Baier, "Optimum and Sub-Optimum Detection of Coded Data Disturbed by Time-Varying Intersymbol Interference [Applicable to Digital Mobile Radio Receivers]," in *IEEE Proceedings of Global Telecommunications Conference (GLOBECOM)*, vol. 3, pp. 1679–1684, Dec. 1990.

[162] P. Robertson, E. Villebrun, and P. Hoeher, "A Comparison of Optimal and Sub-Optimal MAP Decoding Algorithms Operating in the log Domain," in *IEEE Proceedings of International Conference on Communications (ICC)*, vol. 2, pp. 1009 –1013 vol.2, June 1995.

[163] C. Xu, S. Sugiura, S. X. Ng, and L. Hanzo, "Reduced-Complexity Noncoherently Detected Differential Space-Time Shift Keying," *IEEE Signal Processing Letters*, vol. 18, pp. 153–156, March 2011.

[164] C. Xu, S. Sugiura, S. X. Ng, and L. Hanzo, "Reduced-Complexity Soft-Decision Aided Space-Time Shift Keying," *IEEE Signal Processing Letters*, vol. 18, pp. 547–550, October 2011.

[165] J. Wang, S. X. Ng, A. Wolfgang, L.-L. Yang, S. Chen, and L. Hanzo, "Near-Capacity Three-Stage MMSE Turbo Equalization Using Irregular Convolutional Codes," in *International Symposium on Turbo Codes*, pp. 1–6, April 2006.

[166] R. G. Maunder, J. Wang, S. X. Ng, L.-L. Yang, and L. Hanzo, "On the Performance and Complexity of Irregular Variable Length Codes for Near-Capacity Joint Source and Channel Coding," *IEEE Transactions on Wireless Communications*, vol. 7, pp. 1338–1347, April 2008.

[167] L. Kong, S. X. Ng, R. Y. S. Tee, R. G. Maunder, and L. Hanzo, "Reduced-Complexity Near-Capacity Downlink Iteratively Decoded Generalized Multi-Layer Space-Time Coding Using Irregular Convolutional Codes," *IEEE Transactions on Wireless Communications*, vol. 9, pp. 684–695, Feb. 2010.

[168] M. Tüchler and J. Hagenauer, "EXIT Charts of Irregular Codes," *in Proceedings of Conference on Information Sciences and Systems*, pp. 748–753, Mar. 2002.

[169] S. ten Brink, "Convergence behaviour of iteratively decoded parallel concatenated codes," *IEEE Transactions on Communications*, vol. 49, pp. 1727–1737, October 2001.

[170] A. Reznik, S. Kulkarni, and S. Verdú, "Capacity and Optimal Resource Allocation in the Degraded Gaussian Relay Channel with Multiple Relays," in *Proceedings of 40th Allerton Conference on Communication, Control, and Computing*, Oct. 2002.

[171] A. Reznik, S. R. Kulkarni, and S. Verdú, "Degraded Gaussian Multirelay Channel: Capacity and Optimal Power Allocation," *IEEE Transactions on Information Theory*, vol. 50, pp. 3037–3046, Dec. 2004.

[172] T. Ng and W. Yu, "Joint Optimization of Relay Strategies and Resource Allocations in Cooperative Cellular Networks," *IEEE Journal on Selected Areas in Communications*, vol. 25, pp. 328–339, Feb. 2007.

[173] J. W. Huang, Z. Han, M. Chiang, and H. V. Poor, "Auction-Based Resource Allocation for Cooperative Communications," *IEEE Journal on Selected Areas in Communications*, vol. 26, pp. 1226–1237, Sept. 2008.

[174] M. O. Hasna and M.-S. Alouini, "Optimal Power Allocation for Relayed Transmissions Over Rayleigh-Fading Channels," *IEEE Transactions on Wireless Communications*, vol. 3, pp. 1999–2004, Nov. 2004.

[175] X. Deng and A. M. Haimovich, "Power Allocation for Cooperative Relaying in Wireless Networks," *IEEE Communications Letters*, vol. 9, pp. 994–996, Nov. 2005.

[176] C. Y. Ng, C.-W. Sung, and K. W. Shum, "Rate Allocation for Cooperative Transmission in Parallel Channels," in *IEEE Proceedings of Global Telecommunications Conference (GLOBECOM)*, pp. 3921–3925, 2007.

[177] H. H. Sneesens and L. Vandendorpe, "Soft Decode and Forward Improves Cooperative Communications," in *1st IEEE International Workshop on Computational Advances in Multi-Sensor Adaptive Processing*, pp. 157–160, Dec. 2005.

[178] T. Bui and J. H. Yuan, "A Decode and Forward Cooperation Scheme with Soft Relaying in Wireless Communication," in *IEEE 8th Workshop on Signal Processing Advances in Wireless Communications (SPAWC)*, pp. 1–5, June 2007.

[179] M. A. Karim, T. Yang, J. Yuan, Z. Chen, and I. Land, "A Novel Soft Forwarding Technique for Memoryless Relay Channels Based on Symbol-Wise Mutual Information," *IEEE Communications Letters*, vol. 14, pp. 927–929, October 2010.

[180] K. Navaie and H. Yanikomeroglu, "Induced Cooperative Multi-User Diversity Relaying for Multi-Hop Cellular Networks," in *Proceedings of IEEE 63rd Vehicular Technology Conference (VTC)-Spring*, vol. 2, pp. 658–662, May 2006.

[181] B. Xia, Y. J. Fan, J. S. Thompson, and H. V. Poor, "Buffering in a Three-Node Relay Network," *IEEE Transactions on Wireless Communications*, vol. 7, pp. 4492–4496, Nov. 2008.

[182] N. Zlatanov, R. Schober, and P. Popovski, "Buffer-Aided Relaying with Adaptive Link Selection," *IEEE Journal on Selected Areas in Communications*, vol. 31, Aug. 2013, *(Early Access)*.

[183] N. Zlatanov and R. Schober, "Buffer-Aided Relaying with Adaptive Link Selection - Fixed and Mixed Rate Transmission," *IEEE Transactions on Information Theory*, January 2013, *(Early Access)*.

[184] N. Zlatanov and R. Schober, "Buffer-Aided Half-Duplex Relaying Can Outperform Ideal Full-Duplex Relaying," *IEEE Communications Letters*, vol. 17, pp. 479–482, March 2013.

[185] A. Ikhlef, D. S. Michalopoulos, and R. Schober, "Max-Max Relay Selection for Relays with Buffers," *IEEE Transactions on Wireless Communications*, vol. 11, pp. 1124–1135, March 2012.

[186] A. Ikhlef, J. Kim, and R. Schober, "Mimicking Full-Duplex Relaying Using Half-Duplex Relays with Buffers," *IEEE Transactions on Vehicular Technology*, vol. 61, pp. 3025–3037, Sept. 2012.

Index

Author Index

I

J

K

L

M

N

O

P

R

S

T

U

V

W

X

Y

Z